Addis Ababa University

School of Graduate Studies
Addis Ababa Institute of Technology
School of Civil and Environmental Engineering

By
Ashenafi Yilekal Bogale

A Thesis Submitted to School of Graduate Studies in Partial Fulfillment of the Requirements for Degree of Master of Science
In
Civil Engineering

Advisor
Alemayehu Teferra
Professor of Civil Engineering
Addis Ababa University

November, 2015
Addis Ababa, Ethiopia

Addis Ababa University
School of Graduate Studies
Addis Ababa Institute of Technology
School of Civil and Environmental Engineering

ANALYSIS OF GIDABO EARTH FILL DAM BY INTRODUCING GEOTEXTILE REINFORCEMENT

By
Ashenafi Yilekal Bogale

A Thesis Submitted to School of Graduate Studies in Partial Fulfillment of the Requirements for Degree of Master of Science In Civil Engineering

Approved by Board of Examiners:

Alemayehu Teferra (Prof.) Advisor	_____ Signature	_____ Date
Samuel Tadesse (Dr-Ing) External Examiner	_____ Signature	_____ Date
Asrat Worku (Dr-Ing) Internal Examiner	_____ Signature	_____ Date
Esayas G/Youhannes (Dr) Chairman	_____ Signature	_____ Date

Declaration

I, undersigned declare that this thesis is my original work, has not been presented for a degree in any other universities and that all sources of materials used for this thesis have been duly acknowledged.

Kind regards

Ashenafi Yilekal Bogale

ashnfylkl@yahoo.com

+251 911 542647

Acknowledgement

I praise the almighty GOD for providing me the power and courage to carry out this thesis.

I would like to express my most sincere gratitude to Professor Alemayehu Teferra for his guidance and suggestions throughout the course of this research. My thanks also go to Ameyu T. and Geotechnical Engineering staff for the help that they provided. I also want to thank Dr Atalaye from IGSSA/AAU for his important help given to me.

I am grateful to my friends (class of 2015 regular Geotechnical Engineering students, namely: Abdirshikur K., Belay Z., Beneyam A., Gedion A., Melat B., Mikias W., Wubeshet H., Yemiserach G., Zikreab N.) for their cooperation and harmony.

I would also like to thank my mother Tiguaded Tesfa, my sister Mastewal Y. my brothers Aemero Y. and Abraham Y. for their support and encouragement. Mimmy, I thank you.

Finally, I want to thank to all of my cousins for their support and encouragement throughout this work.

Table of Contents

Table of contents i
List of tables viii
List of figures ix
List of Acronyms xv
Abstract xvi
1 Introduction 1
1.1 Background 1
1.2 Statement of the Problem 2
1.3 Objective of the Study 2
1.3.1 General Objective 2
1.3.2 Specific Objective 2
1.4 Materials and Methods (Methodology) 2
1.5 Scope of the study 3
1.6 The significance of the study 3
1.7 Research Question 3
1.8 Hypothesis 3
1.9 Organization of the thesis 4
2 Literature review 5
2.1 Reinforced Slopes and Embankments 5
2.1.1 Reinforced Soil Technique 5
2.1.2 Fundamentals of limit equilibrium analysis with concentrated lateral loads 6
2.1.3 Factors of Safety for Reinforcing Forces and Soil Strengths 6
2.1.4 Types of Soil Reinforcement 9
2.1.5 Applications of geosynthetics 11
2.1.6 Geotextile Types and Properties 11
2.2 Static Slope Stability Analysis 20
2.2.1 General 20
2.2.2 Conditions of Slope Stability Analysis 21
2.2.3 Rapid (Sudden) Drawdown 23
2.2.4 Earthquake 24

2.3 Dynamic Stability Analysis 24
2.3.1 General 24
2.3.2 Liquefaction Analysis 25
2.3.3 Seismic slope stability analysis 28
3 Project characterization 37
3.1 General 37
3.1.1 Location of the Gidabo Earth Fill Dam 37
3.1.2 General description of the project 39
3.1.3 Topography 39
3.1.4 Climate 39
3.1.5 Vegetation 39
3.1.6 Geology of the area 41
3.1.7 Regional Geology 42
3.1.8 Surface Geological studies 43
3.2 Seismicity of the Project area 44
3.2.1 Regional Seismicity study of Gidabo Irrigation Project 44
3.2.2 Ground acceleration estimation of the area 45
3.3 Embankment type and geometry 46
3.3.1 Embankment type 46
3.3.2 Embankment Geometry/ Cross section/ Zoning 46
3.4 Material parameters used in different analysis 47
3.4.1 General 47
3.4.2 Hydraulic parameters of embankment and foundation materials 47
3.4.3 Shear strength parameters and unit weight 48
3.4.4 Geotextile reinforcement parameters 48
3.4.5 Dynamic material properties 49
4 Material models, material properties and methodology 58
4.1 General 58
4.1.1 Limit equilibrium method 58
4.1.2 Finite element method 58
4.2 Seepage analysis using SEEP/W 60

4.2.1 Introduction 60
4.2.2 Material models and properties 60
4.2.3 Boundary Conditions 61
4.2.4 Analysis Types 62
4.3 Slope stability analysis using SLOPE/W 63
4.3.1 Introduction 63
4.3.2 Material Strength and model 64
4.3.3 Mobilization of reinforcement forces 66
4.4 Stress-deformation modeling with SIGMA/W 67
4.4.1 Applications 67
4.4.2 Material models and properties 67
4.4.3 Boundary conditions 68
4.4.4 Analysis Types 68
4.5 Dynamic modeling with QUAKE/W 69
4.5.1 Introduction 69
4.5.2 Material models and properties 69
5 Analysis results and discussions of Gidabo earth fill dam 74
5.1 Static Stability Analysis 74
5.1.1 Embankment type and geometry 74
5.1.2 Loading condition and minimum factor of safety 74
5.1.3 Model of the Gidabo earth fill dam 76
5.1.4 Downstream slope stability analysis of dam for steady state seepage condition 76
5.2 Dynamic Stability Analysis 118
5.2.1 General 118
5.2.2 Design Earthquake 118
5.2.3 Liquefaction Susceptibility Assessment of Gidabo Dam Materials 121
5.2.4 Finite Element Model 125
5.2.5 Dynamic analysis results 126
5.2.6 Initial In-Situ Stress Analysis 127
5.2.7 Dynamic analysis results and discussions 130
6 Conclusion and recommendation 139

6.1 Conclusions 139
6.1.1 Static analysis 139
6.1.2 Dynamic analysis 140
6.2 Recommendations 140
7 References 141
Appendix A: Earthquake records 147
Appendix B: The 1995 Kobe JMA Record (Japan) dynamic analysis result 150
Appendix C: The 1968 Hachinohe record (Japan) dynamic analysis result 155

List of tables

Table 2.1: Reduction factors for tensile strengths of geotextiles and geogrids for use in Eq.2.5 15
Table 2.2: Pullout Resistance Factors α and F* for use in Eq. 2.7 16
Table 2.3: Tolerable Strains for Reinforced Slopes and Embankments 18
Table 2.4: Results of Pseudostatic analysis of earth dams that failed during earthquakes (Source Seed 1979) 29
Table 3.1: Design peak ground acceleration 45
Table 3.2: Average permeability coefficients used in the analysis (adopted from final design report, (WWDSE, 2009) 47
Table 3.3: Saturated volumetric water content (SVWC) values used in the analysis (taken from Seep/W modeling Engineering book, (Krhan, 2007)) 47
Table 3.4: Shear strength parameters and unit weight to be used in the analysis (adapted from, (WWDSE, 2009)). 48
Table 3.5: Ultimate tensile strength and long term design strength adopted from geosynthetics magazine (IFAI, 2012) 49
Table 3.6: Frictional properties and stiffness of geotextile (Koerner, 2005) 49
Table 3.7: K_{2max} and K_G values based on Eq.3.3 51
Table 4.1: Material models and properties used in seepage analysis using Seep/W 61
Table 4.2: Equations that satisfy static equilibrium 63
Table 4.3: Interslice force characteristics and relationships 63
Table 4.4: Fabric (geotextile) parameters used in the analysis 66
Table 4.5 **:** Linear-elastic properties 68
Table 4.6: Elastic – plastic material properties 68
Table 5.1: As Constructed Geometry data for Gidabo earth fill dam 74
Table 5.2: Minimum factors of Safety (adapted from USBR Design standards Nr 13: embankment dams, static stability analysis) 76
Table 5.3: Summary of factor of safety against reinforcement spacing for downstream slope under steady state condition 91
Table 5.4: Water evacuation time during transient rapid drawdown at 8, 16, 21 and 30 days 92
Table 5.5: Summary of analysis results for sudden drawdown condition for the upstream slope 115
Table 5.6: Earth fill material and foundation excavation saved due to reinforcement and its amount in Ethiopian birr 117
Table 5.7: Stability after Earthquake using Quake/W stress (Slope/W) for El Centro MCE 136
Table 5.8**:** Newmark Deformation Analysis result Using Slope/W for El Centro MCE 136
Table B1: Acceleration response at crest of the dam for KOBE earthquake record 150
Table B3: Newmark Deformation Analysis result Using Slope/W for KOBE_ MCE 154
Table B4: Newmark Deformation Analysis result Using Slope/W for KOBE_ DBE 154
Table C1: Acceleration response at crest of the dam for HACHINOHE earthquake record 155
Table C3: Newmark Deformation Analysis result Using Slope/W for HACHINOHE_ MCE 159
Table C4: Newmark Deformation Analysis result Using Slope/W for HACHINOHE_ DBE 159

List of figures

Fig. 2.1: Details of circular arc slope stability analysis for (c, Φ) shear strength soils (Koerner, 2005) 8
Fig. 2.2: Different types of geosynthetics (Koerner, 2005) 11
Fig. 2.3: Main types of geotextiles (Koerner, 2005) 11
Fig. 2.4: Variation of Tlim and Tall with distance along reinforcement (Duncan, et al., 2005) .. 17
Fig. 2.5: Definition of E_{secant} for geosynthetic reinforcement (Koerner, 2005) 18
Fig. 2.6**:** Variations with time of shear stress, pore pressure, and factor of safety for an embankment on saturated clay. (After Bishop and Bjerrum, 1960.) 22
Fig. 2.7: Liquefaction induced bearing capacity failures of kawagishi- echo apartment buildings following the 1964 Nigata earthquake (courtesy of USGS) 26
Fig. 2.8: Lower San Fernando Dam following failure of upstream slope in the 1971 San Fernando earthquake (Courtesy of EERC, University of California). 27
Fig. 2.9: Forces acting on triangular wedge of soil above planar failure surface in Pseudostatic slope stability analysis (Kramer, 1996) 30
Fig. 2.10: Integration of accelerograms to determine downslope displacements 31
Fig. 2.11: Development of permanent slope displacements for actual earthquake ground motion. (After Wilson and Keefer, 1985) 32
Fig. 2.12: Permanent slope displacements depend on the relationship between the yield acceleration and the maximum acceleration. (a) If the yield acceleration of a slope is greater than the maximum acceleration of a particular ground motion, no displacement will occur. As yield accelerations decrease, as in (b) and (c), slope displacements increase quickly. 33
Fig. 2.13: Initial (dashed) and postliquefaction (solid) configurations of Sardis Dam in Mississippi from TARA-3FL analyses. Note the large strains due to liquefaction in core and thin seam below the upstream shell. 35
Fig. 2.14: (a) Finite-element mesh for analysis of Upper San Fernando Dam with elements determined to have liquefied by Serffet et al. (1976) shaded; (b) positions of original and final meshes (displacements exaggerated by factor of 2) by procedure of Byrne et al. (1992). Note large shear strains in liquefied zones. 36
Fig. 3.1: Location map of Gidabo Irrigation Project 38
Fig. 3.2: General layout of Gidabo earth fill dam and spillway (WWDSE, 2009) 40
Fig. 3.3: Geomorphological map of Gidabo dam site and reservior area 40
Fig. 3.4: Relationship of the Ethiopian rift system of the Main East African Rift system 43
Fig. 3.5: Seismic zoning map of Ethiopia (WWDSE, 2008) 44
Fig. 3.6: Values of K_2 moduli for different soils ((Seed, et al., 1970a) 50
Fig. 3.7: G-Reduction and Dumping ratio Functions for Clay Core 52
Fig. 3.8: G-Reduction and Damping Ratio Functions for Sandy Gravel Shell 52
Fig. 3.9: G-Reduction and Damping Ratio Functions for Compacted Alluvium 52
Fig. 3.10: G-Reduction and Damping Ratio Functions for Sandy Gravel Foundation 52

Fig. 3.11: G-Reduction and Damping Ratio Functions for Transition/filter 52
Fig. 3.12: G-reduction and damping ratio functions for toe drain 52
Fig. 3.13: Gmax functions for various embankment and foundation materials 53
Fig. 3.14: Pore pressure function used for liquefiable material 54
Fig. 3.15: Cyclic number function used for analysis (DeAlba, et al., 1976) 55
Fig. 3.16: Cyclic number function used in the analysis (DeAlba, et al., 1976) (USNRC, 1985) . 56
Fig. 3.17: Kσ correction function used for the analysis 57
Fig. 3.18: Ka Correction factor (Seed, et al., 1990) 57
Fig. 3.19:Ka correction function used for analysis 57
Fig. 4.1: Slice discretization and slice forces in a sliding 58
Fig. 4.2: The enhanced Burland triangle (after Anon., 1999) 59
Fig. 4.3: Slice discretization and slice forces in a sliding mass 64
Fig. 4.4: Linear elastic model 67
Fig. 4.5: Elastic-perfectly plastic constitutive relationship 67
Fig. 4.6: Change in G with each iteration through the earthquake 70
Fig. 4.7: Typical G reduction function 71
Fig. 4.8: A damping ratio function 71
Fig. 4.9: Illustrations of fixed boundary conditions 72
Fig. 5.1: Typical Section Gidabo Earth Fill Dam 75
Fig. 5.2: Model of Gidabo Earth Fill Dam from Slope/W 76
Fig. 5.3: Diagram showing the sequence of analysis followed in this research. 77
Fig. 5.4: Finite element model for seepage analysis (taken from Seep/W) 78
Fig. 5.5: Isopotential lines (total head) contour 78
Fig. 5.6: Pore Water Pressure Contour (kPa) 78
Fig. 5.7: Stability analysis of downstream slope under steady state condition (unreinforced: 2.5H: 1V) 80
Fig. 5.8: Analysis of reinforced downstream slope under steady state condition (2.5H: 1V) 80
Fig. 5.9: Variation of factor of safety with respect to spacing between geotextile layers for steady state condition 81
Fig. 5.10: Stability analysis downstream slope under steady state condition (unreinforced: 81
2.25H: 1V) 81
Fig. 5.11: Stability analysis of reinforced downstream slope under steady state condition (2.25H: 1V) 82
Fig. 5.12: Variation of factor of safety with respect to spacing between geotextile layers for steady state condition 83
Fig. 5.13: Stability analysis downstream slope under steady state condition (unreinforced; 2.0H:1V) 83
Fig. 5.14 : Analysis of reinforced downstream slope under steady state condition (2.0H: 1V) ... 84
Fig. 5.15: Detail C: shows how critical failure surface is intersected by reinforcement (2.0H: 1V) 84

Fig. 5.17: Stability Analysis downstream slope under steady state condition (unreinforced; 1.75H: 1V) 85
Fig. 5.18: Stability analysis of reinforced downstream slope under steady state condition (1.75H:1V) 85
Fig. 5.19: Detail D: shows intersection of critical failure surface and reinforcement (1.75H: 1V) 86
Fig. 5.20: Variation of factor of safety with respect to spacing between geotextile layers for steady state condition 86
Fig. 5.21: Stability Analysis downstream slope under steady state condition(unreinforced; 1.5H:1V) 87
Fig. 5.22: Stability analysis of reinforced downstream slope under steady state condition 87
Fig. 5.23: Detail E; shows the intersection between critical failure surface and reinforcement (1.5H: 1V) 88
Fig. 5.24: Variation of factor of safety with respect to spacing between geotextile layers for steady state condition 88
Fig. 5.25: Stability analysis downstream slope under steady state condition (unreinforced 1.25H:1V) 89
Fig. 5.26: Stability analysis of reinforced downstream slope under steady state condition (1.25H: 1V) 89
Fig. 5.27: Detail F, shows the intersection between critical failure surface and reinforcement (1.25H: 1V) 90
Fig. 5.28: Variation of factor of safety with respect to spacing between geotextile layers for steady state condition 90
Fig. 5.29: Variation of factor of safety with respect to spacing between geotextile layers for steady state condition 91
Fig. 5.30: Hydraulic conductivity function for impervious core 93
Fig. 5.31: Hydraulic conductivity function for gravel shell 94
Fig. 5.32: Hydraulic conductivity function for filter 94
Fig. 5.33: Hydraulic conductivity function for compacted alluvium 95
Fig. 5.34: Hydraulic conductivity function for foundation 95
Fig. 5.35: Volumetric water content function for impervious core 96
Fig. 5.36: Volumetric water content function gravel shell 96
Fig. 5.37: Volumetric water content function for filter 96
Fig. 5.38: Pore water pressure contour used as initial steady state seepage for transient analysis 97
Fig. 5.39: Zero pressure line in steady state analysis 97
Fig. 5.40: Drawdown boundary functions used in transient analysis for various evacuation times 98
Fig. 5.41: Isolines (zero pressure line) for 08 days draw down and 30 days analysis duration 98
Fig. 5.42: Detail N: Isolines (zero pressure lines) for different analysis days 99
Fig. 5.43: Factor of Safety vs. time for sudden drawdown analysis (upstream slope 2.5H: 1V) 100

Fig. 5.44: Stability analysis for 8 days sudden drawdown (9th day) (upstream slope/unreinforced) (2.5H:1V) 101
Fig. 5.46: Stability analysis (on 9th day) (upstream slope/reinforced with 2.0m Geotextile spacing) (2.5H: 1V) 102
Fig. 5.47: Variation of Factor of Safety with spacing of Geotextile (upstream slope, sudden draw down condition_2.5H:1V) 102
Fig. 5.48: Factor of Safety vs. time for sudden drawdown analysis (upstream slope 2.25H: 1V) 103
Fig. 5.51: Stability analysis (on 9th day) (upstream slope/reinforced with 2.4m Geotextile spacing) (2.25H: 1V) 104
Fig. 5.52: Variation of Factor of Safety with spacing of Geotextile (upstream Slope_sudden draw down condition_2.25H:1V) 105
Fig. 5.53: Factor of Safety vs. time for sudden drawdown analysis (upstream slope 2.0H: 1V) 105
Fig. 5.54: Stability analysis for 8 days sudden drawdown (9th day) (upstream slope/unreinforced) (2.0H: 1V) 106
Fig. 5.55: Stability analysis (on 9th day) (upstream slope/reinforced with 1.6m Geotextile spacing) (2.0H: 1V) 106
Fig. 5.56: Stability analysis (on 9th day) (upstream slope/reinforced with 2.0m Geotextile spacing) (2.0H: 1V) 107
Fig. 5.57: Variation of Factor of Safety with spacing of Geotextile (upstream slope_sudden draw down condition_2.0H:1V) 107
Fig. 5.59: Stability analysis for 8 days sudden drawdown (9th day) (upstream slope/unreinforced) (1.75H:1V). 108
Fig. 5.60: Stability analysis (on 9th day) (upstream slope/reinforced with 1.6m Geotextile spacing) (1 109
Fig. 5.61: Stability analysis (on 9th day) (upstream slope/reinforced with 2.0m Geotextile Spacing) 109
Fig. 5.62: Variation of Factor of Safety with spacing of Geotextile (upstream Slope_SDDC_1.75H:1V) 110
Fig. 5.64: Stability analysis for 8 days sudden drawdown (9th day) (upstream slope/unreinforced) (1.5H: 1V) 111
Fig. 5.65: Stability analysis (on 9th day) (upstream slope/reinforced with 1.6m Geotextile Spacing) (1.5H: 1V) 111
Fig. 5.66: Stability analysis (on 9th day) (upstream slope/reinforced with 2.0m Geotextile Spacing) (1.5H: 1V) 112
Fig. 5.67: Variation of Factor of Safety with spacing of Geotextile (upstream slope_sudden draw down condition_1.5H:1V) 112
Fig. 5.69: Stability analysis for 8 days sudden drawdown (9th day) (upstream slope/unreinforced) (1.25H:1V) 113

Fig. 5.70: Stability analysis (on 9th day) (upstream slope/reinforced with 1.6m Geotextile Spacing) (1.25H: 1V)..... 114
Fig. 5.71: Stability analysis (on 9th day) (upstream slope/reinforced with 2.0m Geotextile Spacing) (1.25H: 1V)..... 114
Fig. 5.72: Variation of Factor of Safety with spacing of Geotextile (upstream Slope_sudden draw down condition_1.25H:1V) 115
Fig. 5.73: variation of factor of safety with respect to spacing of geotextile layers (summary) 116
Fig. 5.74: El Centro 1940 a) MCE -Horizontal b) MCE –Vertical..... 119
Fig. 5.75: El Centro 1940 a) DBE -Horizontal b) DBE –Vertical..... 120
Fig.5.76: Relationship between limiting epicentral distance of sites at which liquefaction has been observed and moment magnitude for shallow earthquakes. Deep earthquakes (focal depth > 50 km) have produced liquefaction at greater distances. After (Ambraseys, 1988) 121
Fig. 5.76: Geological profile along the dam axis..... 123
Fig. 5.77: Limits in the particle size gradation curves separating liquefiable and nonliquefiable soils as suggested in 1985 by USNRC (USNRC, 1985). 124
Fig. 5.78: Gradation curves for borrow areas (shell 1, Shell 2, shell 3 and compacted alluvium) 125
Fig. 5.79: Finite element model for dynamic analysis..... 126
Fig. 5.80: Finite Element Model for dynamic Analysis (Impervious Boundary and History Points)..... 126
Fig. 5.81: Total Head Contour from SEEP/W Steady state analysis..... 128
Fig. 5.82: Pore Water Pressure Contour taken from SEEP/W..... 128
Fig. 5.83: Total Vertical Stress at in situ condition 129
Fig. 5.84: Pore Water Pressure Contour for insitu state condition 129
Fig. 5.85: Vertical Effective Stress Contour at in situ condition..... 130
Fig. 5.86: x- acceleration response at dam crest for El Centro (MCE)..... 131
Fig. 5.87: x- acceleration response at dam crest for El Centro (DBE) 131
Fig. 5.88: y- acceleration response at dam crest for El Centro (MCE)..... 131
Fig. 5.89: y- acceleration response at dam crest for El Centro (DBE) 131
Fig. 5.90: Horizontal spectral response at dam crest corresponding to MCE (El Centro) 132
Fig. 5.91: Vertical spectral response at dam crest corresponding to MCE (El Centro)..... 132
Fig. 5.92: Horizontal spectral response at dam crest corresponding to DBE (El Centro)..... 133
Fig. 5.93: Vertical spectral response at dam crest corresponding to DBE (El Centro) 133
Fig. 5.94: Post earthquake stability (upstream slope)..... 134
Fig. 5.95: Post earthquake stability (downstream slope)..... 134
Fig. 5.96 : Post Earthquake deformation 135
Fig. 5.97: Slip surface involving 100 % crest width from Newmark deformation analysis for Elcentro earthquake loading corresponding to MCE 137
Fig. 5.98: Slip surface involving 50 % crest width from Newmark deformation analysis for downstream slope (Elcentro earthquake loading corresponding to MCE)..... 137

Fig. 5.99: Slip surface involving 100 % crest width from Newmark deformation analysis for downstream slope (El Centro earthquake loading corresponding to MCE)..... 137
Fig. 5.100: Slip surface involving 0% crest width from Newmark deformation analysis for downstream slope (El Centro earthquake loading corresponding to MCE)..... 138

List of Acronyms

ATH	Acceleration time history
BC	Boundary condition
CSR	Critical stress ratio
DBE	Design base earthquake
Eq.	Equation
EQL	Equivalent linear
E-W	East - West
FHWA	Federal highway association
G	Dynamic shear modulus
GSD	Grain size distribution
ICOLD	International commission on large dams
IGSSA	Institute of geophysics seismic science and astronomy
$K\sigma$	correction factor for overburden stress
K_a	correction factor for initial static stress
LEA	Limit equilibrium analysis
LEMs	Limit equilibrium method
MCE	Maximum credible earthquake
MERS	Main Ethiopian rift system
NWL	Normal water level
NNE-SSW	North north east – south south west
N	Number of cycles of an eqrthquake
N_L	Number of cycles required to cause liquefaction
PGA	Peak ground acceleration
PWP	Pore water pressure
SDDC	Sudden drawdown condition
USACE	United states association of civil engineers
USBR	United states bureau of reclamation
USCOLD	United states commision on large dams
USNRC	United States national research center
WFB	Wonji fault belt
WWDSE	water works design and supervison enterprise

Abstract

Soil reinforcement is now well established technique for geotechnical applications in most parts of the world. This thesis includes the application of soil reinforcement technique for slope stability of earth fill dams. The dam section designed by WWDSE has been considered for the case study. The slopes of dam are then considered to be reinforced with horizontal layers of geotextile and the percent improvement of factor of safety under static loading has been studied. The statically optimized section has been checked for stability against dynamic loading. The analysis is carried out by state of the art software package, Geo-Slope software. It is found that much steeper slopes may be provided to the earth dams by providing geotextile reinforcing layers. The suitable length of reinforcing layers, spacing between them and offset from the face needs to be determined for the required slopes of dam. The statically optimized section is found to be stable against the earthquake loading. This technique may be particularly useful for high earth dams and may result in lesser construction cost as well as construction time.

KEYWORDS *:* geotextile reinforcement,earth fill dam, reinforced slopes,dynamic analysis, earthquake, Geo-Slope software

1 Introduction

1.1 Background

Amongst innumerable engineering projects, dams construction and their industry involves major challenges. Since more than 100 years ago, construction of embankment dams are more common than other types of dams. The reasons for this common usage are: the method of construction is based on ordinary technology with utilization of cheap raw soil materials, subsurface materials, and does not depend on particular valley shape. Also geometry design of embankment dams depends on borrowed soil materials, subsurface conditions and type of construction. Consequently, feasible design can cause significant reduction on construction time, materials and costs (Hasani, et al., 2013).

Geosynthetics have become well established construction materials for geotechnical and other applications in all over the world. As these products are manufactured relatively in easy way compared to solutions they are providing, the use of these materials becomes very popular to the construction industry. Among others, soil reinforcement is one of most accepted method of geosynthetics technology and this has been used in almost all types of dams and others, like, railways and road projects, both for new construction and rehabilitation purposes (Duncan, et al., 2005).

Embankment dam slopes are reinforced to have strong and economical structure as reinforced slopes gets steep slope and use less material than which have been designed in conventional design procedures.

Gidabo earth fill dam which is under construction in Southern part of Ethiopia has been used for the study. The dam is zoned earth fill dam having a height of 20 meter above the original ground level and founded on around 30m thick sandy gravel foundation material. Around 8 to 10 meter thick fine material has been removed and replaced by compacted alluvium for the shell part and clay material for core section (WWDSE, 2009).

One of the practical issues in dam engineering related to the slope stability of embankment dams; however the importance of such surfaces should be designed more compliance with the principles of an economic point, have enough safety and make sure that slope must be stabled. Stability of dam means maintaining a balance and preventing movement of components of a dam against the static forces. It is observed that the stability of the dam is a relative problem and by changing the ratio of the unbalanced forces to the resistance forces, different degrees of stability can exist. And in dam designing, the stability of slope is measured by safety factor criterion (Ghaffari, 2010). Finite element analyses have great potential for modeling field conditions realistically but they require large amounts of efforts and involve high costs (Duncan, 2005).
Most reference books on soil mechanics include several methods of slope stability analysis. Slope stability problems are commonly analyzed using LEMs of slices. These methods satisfy all

or some of the balance equations (Atkinson, 2007). Duncan gave a detailed description of equilibrium methods of slope stability analysis (Duncan, 2005). These methods include the ordinary method of slices (Fellenius, 1936), Bishop's modified method (Bishop, et al., 1960), Janbu's generalized procedure of slices (Janbu, 1954), Morgenstern and Price's method (Morgenstern, et al., 1965) and Spencer's method (Spencer, 1967).

1.2 Statement of the Problem

Almost all embankment dams in Ethiopia have been designed with conventional way of design which always consumes ample source of borrowed materials. This technique uses large volume of construction material and large area of construction which will lead to uneconomical project and takes a long time of construction. Besides, there are areas where shortage of such construction materials requires special technique to build optimized embankments. Thus, to alleviate these problems, soil reinforcement technique has been used in other areas of the world.

This study will present the analysis of geotextile reinforced earth fill dam and come up with the percent improved in factor of safety as it is compared with unreinforced dam.

1.3 Objective of the Study

1.3.1 General Objective

- To analyze the stability of *Gidabo* earth fill dam by introducing geotextile as reinforcement.

1.3.2 Specific Objective

- To determine factor of safety of the dam for static loading before and after reinforcement.
- To verify the dynamic stability of the dam during earthquake loading for statically optimized reinforced slope.

1.4 Materials and Methods (Methodology)

While carrying out this study, the following methodology has been followed

- Literature review is conducted about reinforcement technique and stability analysis of embankment dam.
- The designed section of Gidabo earth fill dam which is under construction in Southern part of Ethiopia has been considered for the study.
- Geotechnical parameters for the dam are collected from geotechnical investigation and as built construction material reports.

- Geometry and other relevant parameters are collected from the final design report prepared by the design organization, WWDSE.
- Modeling of the dam is carried out using appropriate Geoslope Software.
- Static stability analysis is carried out for different exposure conditions using Seep/W and Slope/W before reinforcement.
- Seep/W, Slope/W, Sigma/W and Quake/W from geostudio is used for the analysis.
- Horizontal layers of geotextile material are introduced in the slope of the dam and modeling and analysis has been carried out.
- Percent increase in factor of safety due to reinforcement has been calculated.
- Dynamic stability analysis is carried out for statically optimized section of the dam.
- Using the advantage of reinforcement, optimized reinforced section is prepared and cost analysis is carried out.
- Finally, conclusion and recommendation are presented based on the analysis results.

1.5 Scope of the study

This thesis has been intended to address the benefit of geotextile reinforcement in embankment dam (earth fill dam) design in Ethiopia.

1.6 The significance of the study

Embankment dams can be constructed using naturally available borrowed material. But, this conventional way of design procedures will give a large volume embankment which will use large area for construction and volume of materials that resulted in uneconomical and take long time of construction. However, if an embankment dam is reinforced, it will have a steep slope even on weak foundation than unreinforced dam. Thus, reinforcement will have advantage of saving a lot of money, decreases construction period so that the project can be utilized early and will be a good solution for areas of shortage of construction materials.

So far, no such works have been done in Ethiopia, thus, this thesis will encourage Ethiopian designers to contemplate an option of designing reinforced embankment dams. Reinforcement technique will also help raising the height of existing dams when there is limited downstream area and still saves considerable money from conventional design slope.

1.7 Research Question

How much does geotextile reinforcement improve factor of safety for stability of earth fill dams?

1.8 Hypothesis

Introducing geotextile reinforcement in earth fill dam slopes will improve the stability factor of safety by significant amount.

1.9 Organization of the thesis

A review of previous works regarding soil reinforcement technique is presented in Chapter 2. Limit equilibrium and finite element method of slope stability analysis concepts which have been approached by different researchers are also included.

The Gidabo earth fill dam site and project area has been described in Chapter 3. Seismicity of the area and considerations used in the analysis are discussed in detail.

Both limit equilibrium and finite element based softwares used for the analysis have been discussed in Chapter 4. In this section, a brief description of different methods, techniques and constitutive models is presented.

Chapter 5 presents the results of analysis of Gidabo earth fill dam by introducing geotextile material as reinforcement. The section includes analysis and discussions for both static and dynamic stability conditions.

Conclusions of the findings of the study are presented in Chapter 6. Valuable recommendations for practical works and for further researches are also provided in this chapter.

2 Literature review

2.1 Reinforced Slopes and Embankments

Soil can resist pressure and shear forces very well, but it is not able to tolerate tensile forces. Reinforced soil is composite material that contains components that can easily stand tensile forces. Nowadays, reinforcing materials are widely used to overcome technical problems. Reinforced soil is used in stabilizing embankment (slope), fill dams, retaining walls, foundation and in-situ slope for increasing the shear resistance of soil layer in different earth structures.

2.1.1 Reinforced Soil Technique

Soil Reinforcement is a technique where tensile elements are placed in soil to improve stability and control deformation. To be effective, the reinforcement must intersect the potential failure surface in the soil mass. Strains in the soil mass generate strains in the reinforcement, which in turn, generate tensile loads in the reinforcement. These tensile loads act to resist soil movements and thus impart additional shear strength. This results in composite soil reinforcement system having significantly greater shear strength than soil mass alone. Reinforced soil is very cost effective technique compared to other construction techniques. Literature clearly established that the reinforced soil technique provides cost effective solution with lesser construction period and higher stability of the completed structure.

A great number of reinforced soil structures, particularly for retaining walls, for railways and highways has been constructed in recent parts and showed successful performance even in the seismic loading condition. It is also recognized that the technology is useful to reinforce and rehabilitate soil structures to have higher stability, rainfall and water flow as well (Sivakumar Babu, et al., 2011). (Zhu, et al., 2009) study the anti-seismic measure of geo grid of high earth rock fill dam, using dynamic elasto-plastic analysis method and suggested installing geogrid in dam slopes to have better performance during strong earthquakes. The adoption of soil reinforcement technology is found to highly efficient in terms of ensuring stability and also very cost effective.

The conventional method of embankment dams to a stable slope for a given height may involve considerable expenses in construction material, construction equipment, construction time and extension to the base area of embankment dam. However, these issues can be minimized using appropriate solutions. One of the solutions to this issue is to make the dam slopes much steeper than obtained by conventional design procedure. The slopes of embankment dam can be made steeper by reinforcing them with suitable reinforcing material. Reinforcement has been used in four distinct types of applications (Duncan, et al., 2005):

- *Reinforced slopes.* Multiple layers of reinforcement at various elevations within fill slopes have been used to increase the factor of safety for slip surfaces that cut through the

reinforcement, making it possible to construct slopes steeper than would be possible without reinforcement.

- *Reinforced embankments on weak foundations.* Reinforcement at the bottom of an embankment on a weak foundation can increase the factor of safety for slip surfaces passing through the embankment, making it possible to construct the embankment higher than would be possible without reinforcement.

- *Reinforced soil walls or mechanically stabilized earth walls.* Several different proprietary systems have been developed for reinforced soil walls, which are used as alternatives to conventional retaining walls.

- *Anchored walls.* Vertical soldier pile walls or slurry trench concrete walls can be ‘‘tied back’’ or anchored at one or more levels to provide vertical support for excavations or fills. Anchored walls have been used in both temporary and permanent applications.

2.1.2 Fundamentals of limit equilibrium analysis with concentrated lateral loads

An important concept that needs to be fully comprehended is that all reinforcement fundamentally is a concentrated point load in a limit equilibrium formulation. The concentrated point loads act on the free body, which is the potential sliding mass, and must therefore be included in the moment and force equilibrium equations.

Reinforced slopes can be analyzed using limit equilibrium procedures by including the reinforcement forces in the analyses as known forces. Zoernberg et al (Zornberg, et al., 1198a) have shown through centrifuge tests that limit equilibrium analyses provide valid indications of factor of safety and failure mechanisms for reinforced slopes. Their analyses, which agreed well with the results of their tests, were performed using peak values of Φ’ rather than the lower critical state friction angle of the backfill soil.

2.1.3 Factors of Safety for Reinforcing Forces and Soil Strengths

Mobilization of reinforcement forces

The effect of reinforcement can conceptually act immediately or develop with some strain. A pre-stressed anchor, for example, acts immediately. The force is induced by the pre-stressing. The force in a geofabric (geotextile), on the other hand, may develop over time during construction and during stress re-distribution upon completion of the construction (Hoek, et al., 1974). In other words, the reinforcement forces are mobilized in response to straining in the same way that the soil strength is mobilized as the soil strains.

Two methods have been used for limit equilibrium analyses of reinforced slopes (Duncan, et al., 2005).

- *Method A.* The reinforcement forces used in the analysis are *allowable* forces and *are not divided* by the factor of safety calculated during the slope stability analysis. Only the soil strength is divided by the factor of safety calculated in the slope stability analysis.

- *Method B.* The reinforcement forces used in the analysis are ultimate forces, and are divided by the factor of safety calculated in the slope stability analysis. Both the reinforcing force and the soil strength are divided by the factor of safety calculated in the slope stability analysis.

When a computer program is used to analyze reinforced slopes, it is essential to understand which of these methods is being used within the program, so that the appropriate measure of reinforcing force (allowable force or ultimate force) can be specified in the input for the analysis.

Method A Equations

If the factor of safety for circular slip surfaces is defined by an equation of the form as Eq. 2.1, the program uses method A, and the reinforcement forces specified in the input should be allowable forces.

$$F = \frac{Shear\ Strength}{Shear\ Stress\ required\ for\ equilibrium - reinforcement\ resistance} \quad (2.1)$$

Method B Equations

If the factor of safety for circular slip surfaces is defined by an equation of the form as Eq. 2.2, the program uses method B, and the reinforcement forces specified in the input should be the unfactored long-term load capacity of the reinforcement.

$$F = \frac{Shear\ strength + reinforcement\ resistance}{Shear\ stress\ required\ for\ equilibrium} \quad (2.2)$$

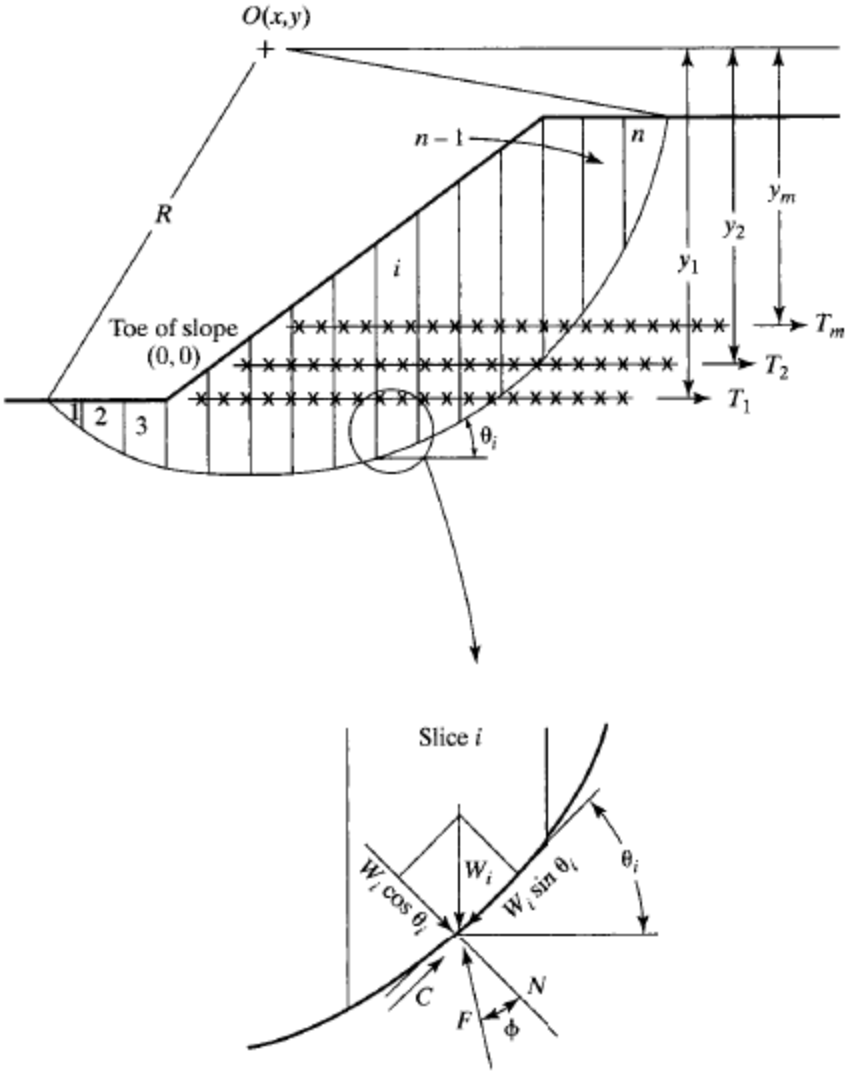

Fig. 2.1: Details of circular arc slope stability analysis for (c, Φ) shear strength soils (Koerner, 2005)

$$FS = \frac{\sum_{i=1}^{n}(N_i \tan \phi + c\Delta l_i)R + \sum_{i=1}^{m} T_i y_i}{\sum_{i=1}^{n}(W_i \sin \theta_i)\, R} \tag{2.3}$$

$$FS = \frac{\sum_{i=1}^{n}\left(N'_i tan\emptyset' + C'\Delta l_i\right)R + \sum_{i=1}^{m} T_i y_i}{\sum_{i=1}^{n}(W'_i sin\theta_i)R} \tag{2.4}$$

FS = Factor of safety
N′i = W′i sinθi
W_i, W'_i = total and effective weight of each slice
θ_i = angle of intersection of horizontal to tangent at center of each slice
R = radius of failure circle
$\emptyset, \emptyset'$ = total and effective angles of shearing resistance, respectively
c, c' = total and effective cohesions, respectively
Ti = allowable geotextile tensile strength
Y_i = moment arm for geotextiles (note that in large deformation situation these moment arms could become equal to R, which is generally a larger value)
n = number of slices
m = number of geotextile layers
Δli = arc length of each slice
N'_I = N_i - $U_i\Delta x_i$,in which
U_i = $h_i\gamma_w$=Pore water pressure
h_i = height of water above base of circle for each slice
γ_w = unit weight of water
Δx_I = width of slice

The use of equation 2.3, the total stress analysis equation, is recommended for embankments where water is not involved or when the soil is at less than saturation conditions. The reason for this is that pore pressure measurement is difficult in low permeability soils. The effective stress analysis (Eq. 2.4) is for conditions where water and saturated soil are involved, conditions typical of earth dams and delta areas involving fine grained cohesive soils (Koerner, 2005).

Geotextile reinforced embankments have been shown to be a practical and expedient in many situations. When reinforced, slope heights and/or angles can be significantly increased over the non-reinforced situation. Design wise, the process involves modifications to limit equilibrium procedures that are within the realm of geotechnical engineering practice and seem to be a rational approach.

2.1.4 Types of Soil Reinforcement

Among others, Geosynthetics are well-known products in soil reinforcement technique. Geosynthetic is a planar product manufactured from polymeric material used with soil, rock, earth, or other geotechnical engineering related material as an integral part of a human made project, structure, or system (ASTM, D4439).

Geosynthetics, which comprise a variety of products, are the following types: Geotextiles, geogrids, geonets, geomembranes, geosythetic clay liners, geopipe, geofoam and geocomposites. Geotextiles are textiles, but they consist of synthetic fibers rather than natural ones such as

cotton, wool, or silk. Thus biodegradation and subsequent short time is not a problem in geotextile. Types of different geosynthetics are shown in Fig. 2.2 (Koerner, 2005).

When synthetic fibers are made into a flexible, porous fabric by standard weaving machinery or are matted together in woven and nonwoven manner, the product known as "Geotextile". Geogrids are plastics formed into a very open netlike configuration. Geotextiles and Geogrids are used usually as reinforcing material for soil improvement. These reinforcing materials are not susceptible to corrosion, have relatively low stiffness and flexible enough to tolerate large deformation. These factors make them to be superior to steel reinforcing materials in soils (Koerner, 2005).

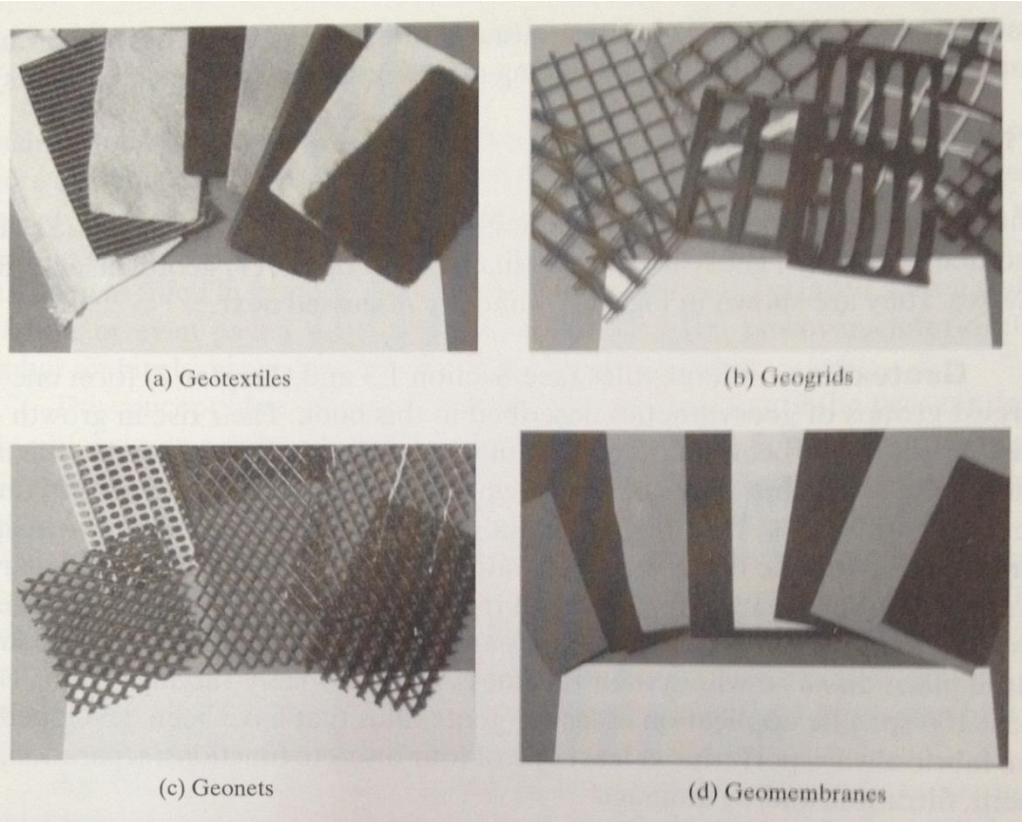

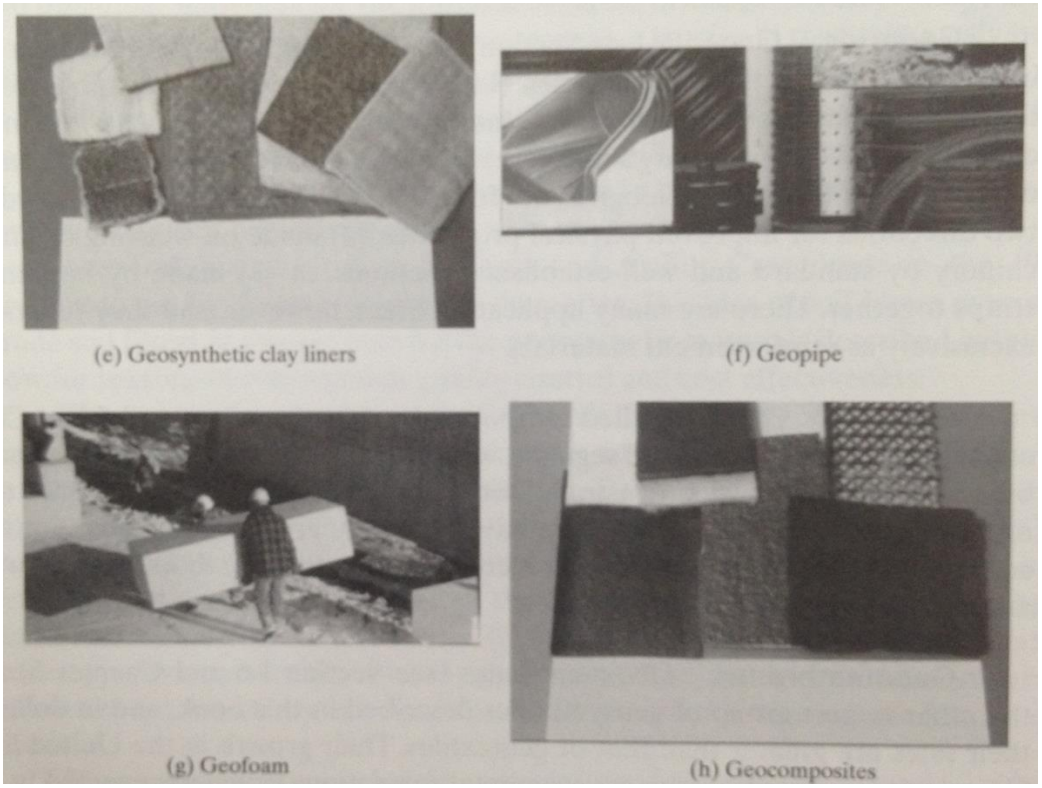

Fig. 2.2: Different types of geosynthetics (Koerner, 2005)

2.1.5 Applications of geosynthetics

Geosynthetics are produced using different types of polymer fiber namely: polypropylene, polyester etc. Use of Geosynthetics is growing in civil engineering activities. Their applications, among others are namely: Reinforcement, Separation, Filtration, Drainage and Sealing.

2.1.6 Geotextile Types and Properties

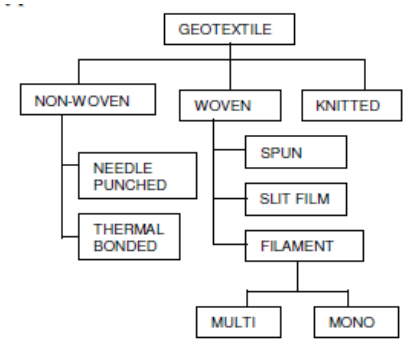

Fig. 2.3: Main types of geotextiles (Koerner, 2005)

2.1.6.1 Materials

Geotextiles are manufactured by weaving polymeric fibers into a fabric or by matting the fibers together to form a continuous nonwoven fabric. Specifically, geotextiles are made from polypropylene, polyester, polyethylene, polyamide (nylon), polyvinylidene chloride, and fiberglass (Koerner, 2005). Polypropylene and polyester are the most used material for the geotextiles. Geotextiles are available in a variety of structures and polymer compositions designed to meet a wide range of applications. It is important all geotextiles be composed of strong, durable, chemical inert polymeric materials that are resistant to the effects of site specific ground conditions, whether, and aging.

2.1.6.2 Woven Geotextiles

In woven constructions, the warp yarns, which run parallel with the length of the geotextiles panel (machine direction), are interlaced with yarns called till or filling yarns, which run perpendicular to the length of the panel (cross direction). Woven construction produces geotextiles with high strengths and moduli in the warp and fill directions and low elongations at rupture. The modulus varies depending on the rate and direction in which the geotextile is loaded. When woven geotextiles are pulled on a bias, the modulus decreases, although the ultimate breaking strength may increase. The construction can be varied so that the finished geotextile has equal or different strengths in the warp and fill directions. Woven construction produces geotextiles with a simple pore structure and narrow range of pore sizes or openings between fibers. Woven geotextiles are commonly plain woven. Woven geotextiles can be composed of monofilaments or multifilament yarns. Generally, woven fabrics exhibit high tensile strength, high modulus and low elongation.

Multifilament woven construction produces the highest strength and modulus of all the constructions but also highest cost. A monofilament variant is the slit-film or ribbon filament woven geotextile. The fibers are thin and flat and made by cutting sheets of plastic into narrow strips. This type of woven geotextile is relatively inexpensive and is used for separation, i.e the prevention of intermixing of two materials such as aggregate and fine-grained soil. Woven geotextiles are stiffer and stronger than nonwoven geotextiles and more useful for reinforced slope applications.

2.1.6.3 Non-Woven Geotextiles

Non-woven geotextiles are formed by a process other than weaving or knitting, and they are generally thicker than woven products. These geotextiles may be made either from continuous filaments or from staple fibers. The fibers are generally oriented randomly within the plane of the geotextile but can be given preferential orientation. In the spun bonding process, filaments are extruded, and laid directly on moving belt to process described below.

- Needle punching: - Bonding: Bonding by needle punching involves pushing many barbed needles through one or several layers of a fiber mat normal to the plane of the geotextile. The process causes the fibers to be mechanically entangled. The resulting geotextile has the appearance of a felt mat.

- Heat bonding: This is done by incorporating fibers of the same polymer type but having different melting points in the mat, or by using hetro filaments, that is, fiber composed of one type of polymer on the inside and covered or sheathed with a polymer having a low melting point.

2.1.6.4 Applications

Considering constructional point of view application of these fabrics are using mostly for the following areas.

- Separation
- Reinforcement
- Drainage
- Erosion Control
- Forms
- Impermeable Fabrics.

Among all listed above, our concern is to use geotextile as reinforcement as discussed in the next section. The principal types of reinforcing materials that have been used for slopes and embankments are geotextile fabrics, geogrids, steel strips, steel grids, and high strength steel tendons.

2.1.6.5 Geotextile as reinforcement

Problems involving slope and subgrade reinforcement appear to be particularly well suited for fabric utilization. Currently, most fabrics appear to be used in this type of application. The concept is theoretically sound since the fabric decreases the levels of stress in the soil due to horizontal shear stresses mobilized by the vertical loads. This in turn places the fabric in tension (similar in action to a prestressing tendon in reinforced concrete), which spreads the load over a large area and thereby decreases its intensity. That is, the unit vertical stress is decreased. A decrease in stress means less likelihood of failure and /or less settlement. Among others, typical examples are as follows:

- Increase in the stability of embankments and dams.
- Construction of fabric walls and reinforcement material.
- Reduction of the need for removing existing soil (of relatively poor characteristics) in marginal situations.

2.1.6.6 Reinforcement Forces

The long-term capacity of reinforcement, denoted here as T_{lim}, depends on the following factors (Duncan, et al., 2005):

- ***Tensile strength:*** For steel, the tensile strength is the yield strength. For geosynthetics, the tensile strength is measured using short-term wide-width tensile tests.

- ***Creep characteristics:*** Steel does not creep appreciably, but geosynthetic materials do. The tensile loads used for design of geotextile- and geogrid reinforced walls must be reduced to values lower than those measured in short-term tensile tests, to stresses that are low enough so that little or no creep deformation will occur over the design life of the structure.

- ***Installation damage:***. Geotextiles and geogrids are subject to damage during installation that result in holes and tears in the material. Epoxy-coated and PVC coatings on steel are subject to damage during installation, and galvanization is therefore preferred for corrosion protection.

- ***Durability:*** The mechanical properties of geosynthetics are subject to deterioration during service as a result of attack by chemical and biological agents. Steel is subject to corrosion.

- ***Pullout resistance:*** Near the ends of the reinforcement, capacity is limited by the resistance to pullout, or slip between the reinforcement and the soil within which it is embedded.

- ***Reinforcement stiffness and tolerable strain within the slope:*** To be useful for slope reinforcement, the reinforcing material must have stiffness as well as strength. A very strong but easily extensible rubber band would not provide effective reinforcement, because it would have to stretch so much to mobilize its tensile capacity that it would not be able to limit the deformation of the slope.

Values of T_{lim}, the long-term capacity of reinforcing materials, must satisfy the following three criteria:

- T_{lim} - capacity determined by short-term tensile strength, creep, installation damage, and deterioration of properties over time.
- T_{lim} - capacity determined by pullout resistance.

- T_{lim} - capacity determined by stiffness and tolerable strain. Methods of applying these requirements to geosynthetics and steel reinforcing are described in the following sections.

Criterion 1: Creep, Installation Damage, and Deterioration in Properties over Time

Geotextiles and geogrids. The effects of creep, installation damage, and long-term deterioration on geosynthetic materials can be evaluated using the expression

$$T_{lim} = \frac{T_{ult}}{(RF_{CR})(RF_{ID})(RF_D)} \tag{2.5}$$

Where

T_{lim} - the long-term limit load (F/L);

T_{ult} - the short-term ultimate strength, measured in a wide-strip tension test (F/L);

RF_{CR} - the strength reduction factor to allow for creep under long-term load;

RF_{ID} - the strength reduction factor to allow for installation damage;

RF_D - the strength reduction factor to allow for deterioration in service.

Values of RF_{CR}, RF_{ID}, and RF_D recommended by the FHWA are given in Table 2.1.The units of T_{lim} and T_{ult} are force per unit length of reinforced slope.

Table 2.1: Reduction factors for tensile strengths of geotextiles and geogrids for use in Eq.2.5

Reduction for:	Factor	Polymer	Range of values [a]
Creep	RF_{CR}	Polyester	1.6 – 2.5
		Polypropylene	4.0 – 5.0
		Polyethylene	2.6 – 5.0
Installation damage	RF_{ID}	Any polymer	1.1 – 3.0
Deterioration in service	RF_D	Any polymer	1.1 – 2.0

[a] These values (from FHWA, 2000) are applicable to reinforcement in granular soils with maximum particle sizes up to 19 mm, values of pH from 4.5 to 9.0, and inservice temperatures below 30^{o}C. Geotextiles weighing less than 270 g/m2 are subject to greater damage during installation and should not be used for reinforcement.

Criterion 2: Pullout Resistance

To develop tensile capacity, reinforcement must be restrained sufficiently by friction in the soil. The maximum possible resistance (*T*po) is proportional to the effective overburden pressure. *T*po begins from zero at the end of the reinforcement, where the embedded length is zero and increases with distance from the end, as shown in Figure 2.4. The slope of the curve representing the variation of *T*po with distance can be expressed as

$$\frac{dT_{po}}{dL} = 2\gamma z\alpha F^* \quad (2.6)$$

Where

*T*po - is the pullout resistance (F/L);
L - the length of embedment, or distance from the end of the reinforcement (L);
γ - the unit weight of fill above the reinforcement (F/L3);
z - the depth of fill above the reinforcement (L);
α - the adjustment factor for extensible reinforcement (dimensionless); and
*F** - the pullout resistance factor (dimensionless).
Values of α and *F** recommended by the FHWA (2000) are listed in Table 2.2. These values are conservative estimates. Larger values may be applicable and can be used if they are supported by tests performed on the specific soil and reinforcing material. Equation (2.6) gives the slope of the pullout resistance curve at any location. If the thickness of fill above the reinforcement is constant, the slope of the pullout curve is constant, and the pullout resistance can be expressed as

$$Tpo = 2\gamma\alpha F^* Le \quad (2.7)$$

Where *Le* is the distance from the end of the reinforcement or length of embedment (L).

Table 2.2: Pullout Resistance Factors α and F* for use in Eq. 2.7

Pullout resistance [a]	**Types of reinforcement**	**Resistance factor value**
$\boldsymbol{\alpha}$	Geotextiles	0.6
	Geogrids	0.8
	Steel strips and steel grids	1.0
F*	Geotextiles	0.67tanØ
	Geogrids	0.8tanØ
	Steel strips and steel grids	1.0tanØ

[a] Larger values of both α and *F** may be applicable and can be used if they are supported by tests performed on the specific soil and reinforcing material. *Source:* FHWA (2000).

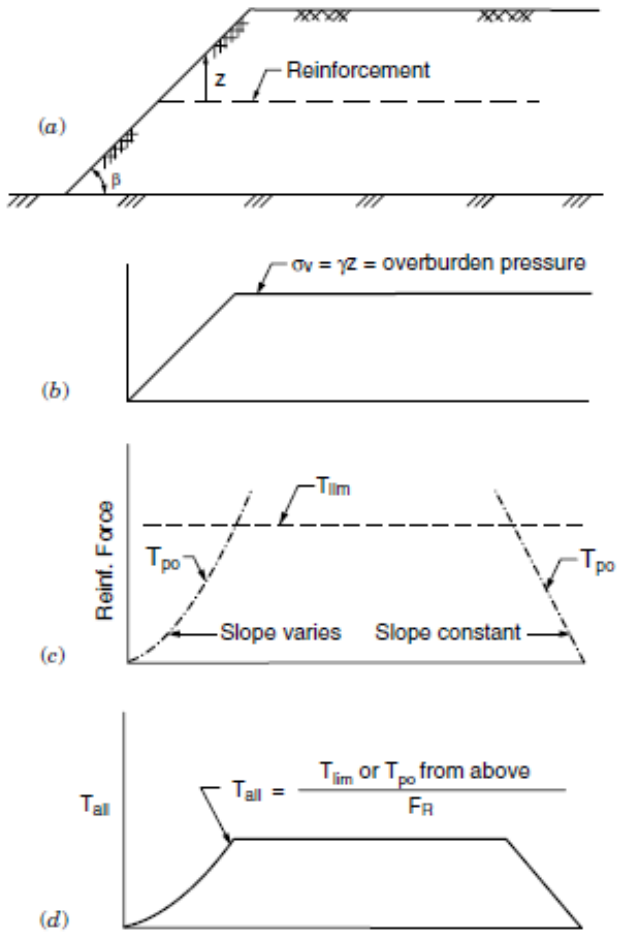

Fig. 2.4: Variation of Tlim and Tall with distance along reinforcement (Duncan, et al., 2005)

Criterion 3: Reinforcement Stiffness

Reinforcing materials must be stiff enough so that reinforcement forces can be mobilized without excessive strain. The value of T_{lim} should not exceed the product of the long-term secant modulus of the reinforcement multiplied by the tolerable strain for the slope:

$$T_{lim} \leq E_{secant} \epsilon_{tolerable} \quad (2.8)$$

Where

E_{secant} is the secant modulus of reinforcing at axial strain $\varepsilon_{tolerable}$ (F/L) and

$\varepsilon_{tolerable}$ is the strain within the slope at the location of the reinforcing that can be tolerated without excessive slope deformation or failure (dimensionless).

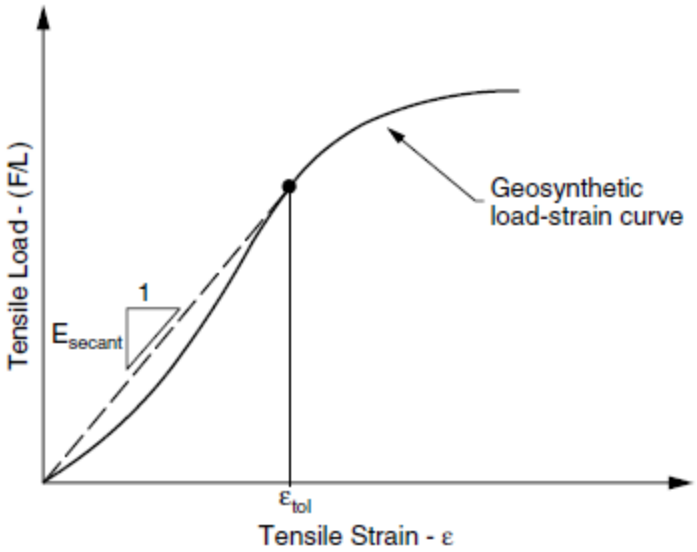

Fig. 2.5: Definition of E_{secant} for geosynthetic reinforcement (Koerner, 2005)

The stiffness of geosynthetic materials may be low enough so that criterion 3 governs the value of T_{lim} for applications where the tolerable strain is small. As shown in Figure 2.5, *E*secant is the slope of a line extending from the origin to the point on the *T*–ε curve where the strain is equal to $\varepsilon_{tolerable}$. Note that the units of E_{secant}, like the units of T_{lim}, are force per unit length.

Tolerable strain values are based on the results of finite element analyses (Rowe and Soderman, 1985); and on experience (Fowler, 1982; Christopher and Holtz, 1985; Haliburton et al., 1982; Bonaparte et al., 1987) and a summary of published recommendations is given in Table 2.3 (Duncan, 2005).

Table 2.3: Tolerable Strains for Reinforced Slopes and Embankments

Application	$\varepsilon_{tolerable}$ **(%)**
Reinforced soil walls	10
Reinforced slopes of embankments on firm foundations	10
Reinforced embankments on non-sensitive clay, moderate crest deformations tolerable	10
Reinforced embankments on non-sensitive clay, moderate crest deformations not tolerable	5-6
Reinforced embankments on highly sensitive clay	2-3

Source: Compiled from (Fowler, 1982), (Christopher, et al., 1985), (Haliburton , et al., 1982), (Rowe, et al., 1985) and (Bonaparte, et al., 1987).

2.1.6.7 Allowable Reinforcement Forces and Factors of Safety

The preceding section is concerned with the long-term capacity of reinforcement (T_{lim}). These values of *T*lim reflect consideration of long-term loading, installation damage, deterioration in properties over time, pullout resistance, and tolerable strains, but they do not include a factor of safety. The allowable load assigned to reinforcing materials should include a factor of safety, as indicated by

$$T_{all} = \frac{T_{lim}}{F_R} \tag{2.9}$$

Where:

T_{all} is the allowable long-term reinforcement force (F/L) and
F_R is the factor of safety for reinforcement force.

The value of *FR* should reflect

- the degree of uncertainty involved in estimating the value of *T*lim,
- the degree of uncertainty involved in estimating the load that the reinforcement must carry, and
- the consequences of failure.

Recommended values of *FR* are given in Table 8.5.

2.1.6.8 Reinforcement Forces Orientation

Orientation of reinforcement forces is important in slope stability analysis of reinforced slopes and embankments. Various orientations have been suggested (Leshchinsky, et al., 1989) (Schmertmann, et al., 1987); (FHWA, 2000), (Koerner, 2005);. The extremes are

- reinforcement forces that are aligned with the original orientation of the reinforcement, and
- Reinforcement forces that are parallel to the slip surface

The latter assumption, which results in larger factors of safety, has been justified by the concept that the reinforcement will be realigned where the slip surface crosses the reinforcement. This is more likely if the reinforcement is very flexible. The assumption that the orientation of the reinforcement force is the same as the orientation of the reinforcement is more conservative, is supported by the findings of (Zornberg, et al., 1989a), and is the more logical, reliable choice and this approach is recommended by (Duncan, et al., 2005).

2.2 Static Slope Stability Analysis

2.2.1 General

Stability analysis of earth structures is the oldest type of numerical analysis in geotechnical engineering. The idea of discretizing a potential sliding mass into slices was introduced early in the 20th Century. In 1916, (Petterson, 1955) presented the stability analysis of the Stigberg Quay in Gothenberg, Sweden where the slip surface was taken to be circular and the sliding mass was divided into slices. During the next few decades, (Fellenius, 1936) introduced the Ordinary or Swedish method of slices. In the mid-1950s (Janbu, 1954) and (Bishop 1955) developed advances in the method. The advent of electronic computers in the 1960's made it possible to more readily handle the iterative procedures inherent in the method which led to mathematically more rigorous formulations such as those developed by (Morgenstern, et al., 1965) and by (Spencer, 1967). One of the reasons the limit equilibrium method was adopted so readily, is that solutions could be obtained by hand-calculations. Simplifying assumption had to be adopted to obtain solutions, but the concept of numerically dividing a larger body into smaller pieces for analysis purposes was rather novel at the time.

Presently, stability analyses are by far the most common type of numerical analysis in geotechnical engineering. This is in part because stability is obviously a key issue in any project – will the structure remain stable or collapse? This, however, is not the only reason. Concepts associated with the method of slices are not difficult to grasp and the techniques are rather easy to implement in computer software – the simpler methods can even be done on a spreadsheet.
Modern limit equilibrium software is making it possible to handle ever-increasing complexity within an analysis. It is now possible to deal with complex stratigraphy, highly irregular pore-water pressure conditions, various linear and nonlinear shear strength models, almost any kind of slip surface shape, concentrated loads, and structural reinforcement. Limit equilibrium formulations based on the method of slices are also being applied more and more to the stability analysis of structures such as tie-back walls, nail or fabric reinforced slopes, and even the sliding stability of structures subjected to high horizontal loading arising, for example, from ice flows.

The analysis of the stability of dams and other slopes is usually carried out using Limit Equilibrium Analysis (LEA). In most situations more detailed analysis using numerical methods, e.g. finite element analysis, is not necessary. However if it is necessary to model the deformations of the dam or the effects of strain weakening, as in progressive failure, numerical methods must be used. Comprehensive reviews of slope stability analysis have been written by (Fredlund, et al., 1977), (Duncan, 1992), (Duncan, 1996a) and (Morgenstern, 1992).

2.2.2 Conditions of Slope Stability Analysis

2.2.2.1 General

Variations of the loads acting on slopes, and variations of shear strengths with time, result in changes in the factors of safety of slopes. As a consequence, it is often necessary to perform stability analyses corresponding to several different conditions, reflecting different stages in the life of a slope.

When an embankment is constructed on a clay foundation, the embankment load causes the pore pressures in the foundation clay to increase. Over a period of time the excess pore pressures will dissipate, and eventually, the pore pressures will return to values governed by the groundwater conditions. As the excess pore pressures dissipate, the effective stresses in the foundation clay increase, the strength of the clay will increase, and the factor of safety of the embankment will also increase. Fig. 2.6 illustrates these relationships. If, as shown, the embankment height stays constant and there is no external loading, the most critical condition occurs at the end of construction. In this case, therefore, it is only necessary to analyze the end-of construction condition.

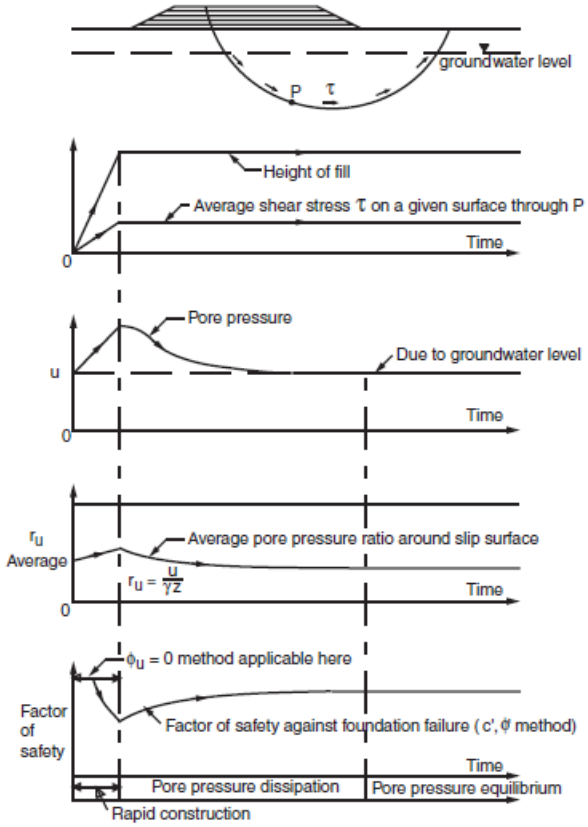

Fig. 2.6: Variations with time of shear stress, pore pressure, and factor of safety for an embankment on saturated clay. (After Bishop and Bjerrum, 1960.)

In the case of an embankment dam, several different factors affect stability. Positive pore pressures may develop during construction of clay embankments, particularly if the material is compacted on the wet side of optimum. The same is true of clay cores in zoned embankments. Over time, when water is impounded and seepage develops through the embankment, the pore pressures may increase or decrease as they come to equilibrium with steady seepage conditions. Reservoir levels may vary with time during operation of the dam. A rapid drop in reservoir level may create a critical loading condition on the upstream slope. A rise from normal pool level to maximum pool level may result in a new state of seepage through the embankment and a more severe loading condition on the downstream slope. Earthquakes subject slopes to cyclic variations in load over a period of seconds or minutes that can cause instability or permanent deformations of the slope, depending on the severity of the shaking and its effect on the strength of the soil.

2.2.2.2 Drained and Undrained Conditions

The concepts of drained and undrained conditions are of fundamental importance in the mechanical behavior of soils, and it is worthwhile to review these concepts at the beginning of this examination of soil mechanics principles. Drained is the condition under which water is able

to flow into or out of a mass of soil in the length of time that the soil is subjected to some change in load. Under drained conditions, changes in the loads on the soil do not cause changes in the water pressure in the voids in the soil, because the water can move in or out of the soil freely when the volume of voids increases or decreases in response to the changing loads. Undrained is the condition under which there is no flow of water into or out of a mass of soil in the length of time that the soil is subjected to some change in load. Changes in the loads on the soil cause changes in the water pressure in the voids, because the water cannot move in or out in response to the tendency for the volume of voids to change (Duncan, et al., 2005)

2.2.2.3 End-Of-Construction Stability

Slope stability during and at the end of construction is analyzed using either drained or undrained strengths, depending on the permeability of the soil. Many fine grained soils are sufficiently impermeable that little drainage occurs during construction. This is particularly true for clays. For these fine-grained soils, undrained shear strengths are used, and the shear strength is characterized using total stresses. For soils that drain freely, drained strengths are used; shear strengths are expressed in terms of effective stresses, and pore water pressures are defined based on either water table information or an appropriate seepage analysis. Undrained strengths for some soils and drained strengths for others can be used in the same analysis

2.2.2.4 Steady state long-term stability

Over time after construction the soil in slopes may either swell (with increase in water content) or consolidate (with decrease in water content). Long-term stability analyses are performed to reflect the conditions after these changes have occurred. Shear strengths are expressed in terms of effective stresses and the pore water pressures are estimated from the most adverse groundwater and seepage conditions anticipated during the life of the slope. Seepage analyses can be performed using either graphical techniques (flow nets) or numerical analyses (finite element, finite difference), depending on the complexity of the cross section.

2.2.3 Rapid (Sudden) Drawdown

When the reservoir level behind an embankment dam is lowered, the stabilizing influence of the water pressure on the upstream slope is lost. If the water level is dropped sufficiently quickly that the pore pressures in the slope do not have time to reach equilibrium with the new reservoir water level, the slope is less stable.

Stability at the end of rapid drawdown has been analyzed in two basically different ways:

- using effective stress methods, and
- using total stress methods.

Both methods treat free-draining materials in the same way. The strengths of free-draining materials are expressed in terms of effective stresses, and the pore water pressures are estimated assuming either steady seepage or hydrostatic conditions depending on the particular slope.

2.2.4 Earthquake

Earthquakes affect the stability of slopes in two ways: (1) The acceleration produced by the seismic ground motion during an earthquake subjects the soil to cyclically varying forces, and (2) the cyclic strains induced by the earthquake loads may cause reduction in the shear strength of the soil. If the strength of the soil is reduced less than 15% by cyclic loading, pseudostatic analyses of the earthquake loading can be used. In pseudostatic analyses, the effect of the earthquake is represented crudely by applying a static horizontal force to the potential sliding mass. This type of analysis provides a semi-empirical means of determining whether deformations due to an earthquake will be acceptably small. If the strength of the soil is reduced more than 15% as a result of cyclic loading, dynamic analysis is needed to estimate the deformations that would result from earthquakes. Some engineers perform this type of analysis for all slopes, even if the strength reduction due to earthquake loading is less than 15%. In addition to analyses to estimating the potential for earthquake-induced deformation, analyses are also needed to evaluate post-earthquake stability.

2.3 Dynamic Stability Analysis

2.3.1 General

Earth dams, like most of engineering structures, may fail due to faulty design, improper construction and poor maintenance practices, etc. The various causes of failure may be hydraulic failure, seepage failure, piping through dam body, structural failure and due to earthquake. An earthquake is a vibration of the earth produced by a rapid release of energy (Tarbuck, et al., 1996). The main features include the focus, the location within the earth where the earthquake rupture starts, and the epicenter, the point on the earth's surface directly above the focus.

Stability and deformation are two major issues that need to be considered in assessing the seismic performance of earth fill dams under earthquakes (Siddappa, 2012) . The Augusta dam is the first dam which is failed due to an earthquake. According to the (USCOLD, 2000) reports, less than 30 dams have failed during an earthquake. These were primarily tailings or hydraulic fill dams, or relatively small embankments of questionable design. Few large embankment dams have been severely damaged. In 1925, an earthquake (M 6.3) caused catastrophic slope sliding failure of the 25-feet high Sheffield Dam in Santa Barbara, CA. This was the first recognition that shaking of embankments with low relative density materials may cause liquefaction failures.
Experience has shown that well-compacted, impervious rolled-fill dams are resistant to earthquake forces, provided they are constructed on rock or overburden foundations resistant to liquefaction. There are two major issues that need to be resolved in assessing the seismic performance of earth dams under earthquakes:

- Stability: Is dam stable during and after earthquake?
- Deformation: How much deformation will occur in the dam?

Strain-dependent equivalent dynamic shear moduli and damping ratios as first introduced by (Seed, et al., 1970a) are essential to EQL analyses. EQL response is sometimes obtained for representative soil columns within the dam section using SHAKE91 (Idriss and Sun, 1992).

The response and behavior of earth structures subjected to earthquake shaking is highly complex and multifaceted (Kramer, 1996). Generally, there are the issues of:

- the motion, movement and inertial forces that occur during the shaking,
- the generation of excess pore-water pressures, the potential reduction of the soil shear strength,
- the effect on stability created by the inertial forces, excess pore-water pressures and possible shear strength loses, and
- the redistribution of excess pore-water pressures and possible strain softening of the soil after the shaking has stopped.

2.3.2 Liquefaction Analysis

Liquefaction is one of the most important, interesting, complex, and controversial topics in geotechnical earthquake engineering. Its devastating effects sprang to the attention of geotechnical engineers in a three-month period in 1964 when the Good Friday earthquake *(Mw* = 9.2) in Alaska was followed by the Niigata earthquake *(Ms* = 7.5) in Japan. Both earthquakes produced spectacular examples of liquefaction-induced damage, including slope failures, bridge and building foundation failures (Fig. 2.7), and flotation of buried structures. In the 30 years since these earthquakes, liquefaction has been studied extensively by hundreds of researchers around the world. Much has been learned, but the road has not been smooth. Different terminologies, procedures, and methods of analysis have been proposed, and a prevailing approach has been slow to emerge.

Fig. 2.7: Liquefaction induced bearing capacity failures of kawagishi- echo apartment buildings following the 1964 Nigata earthquake (courtesy of USGS)

Similarly, in Southern California, the San Fernando earthquake occurred on February 9, 1971 at 6:00 a.m. local time and had a 6.6 Richter magnitude. The earthquake created a liquefaction failure at a water storage facility known as the Lower San Fernando Dam and Reservoir in the San Fernando community on the northern edge of the greater metropolitan Los Angeles area (Fig. 2.8).

Liquefaction is defined as the transformation of a granular material from a solid to a liquefied state as a consequence of increased pore pressure and reduced effective stress (Marcuson , 1978). Increased pore water pressure is induced by the tendency of granular materials to compact when subjected to cyclic shear deformation. The change of state occurs most readily in loose to moderately dense granular soils with poor drainage, such as silty sands and gravel capped by or containing seams of impermeable sediment.

Fig. 2.8: Lower San Fernando Dam following failure of upstream slope in the 1971 San Fernando earthquake (Courtesy of EERC, University of California).

Liquefaction is most commonly observed in shallow, loose, saturated deposits of cohesion-less soils subjected to strong ground motions in large magnitudes earthquakes. Unsaturated soils are not subjected to liquefaction because volume compression dose not generate excess pore pressure. Generally, liquefaction is associated with loose fine sands. For a sand to be in a loose state in the field it likely was deposited in a calm fluvial or sedimentation environment and has not been subject to past loading and unloading. In a sense, it is like the material is normally consolidated.

When cohensionless soils are saturated, however, rapid loading occurs under undrained conditions, so the tendency for densification causes excess pore pressures to increase and effective stresses to decrease. Liquefaction phenomena that result from this process can be divided into two main groups (Kramer, 1996):

- Flow liquefaction and
- Cyclic mobility.

Flow liquefaction produces the most dramatic effects of all the liquefaction-related phenomena and results in tremendous instabilities known as flow failures. Flow liquefaction can occur when the shear stress required for static equilibrium of a soil mass (the static shear stress) is greater than the shear strength of the soil in its liquefied state. Once triggered, the large deformations produced by flow liquefaction are actually driven by static shear stresses. The cyclic stresses may simply bring the soil to an unstable state at which its strength drops sufficiently to allow the static stresses to produce the flow failure.

Cyclic mobility is another phenomenon that can also produce unacceptably large permanent deformations during earthquake shaking. In contrast to flow liquefaction, cyclic mobility occurs

when the static shear stress is less than the shear strength of the liquefied soil. The deformations produced by cyclic mobility failure~ develop incrementally during earthquake shaking. In contrast to flow liquefaction, the deformations produced by cyclic mobility are driven by both cyclic and static shear stresses.

As liquefaction occurs, the soil stratum softens, allowing large cyclic deformations to occur. In loose materials, the softening is also accompanied by a loss of shear strength that may lead to large shear deformations or even flow failure under moderate to high shear stresses, such as beneath a foundation or sloping ground. In moderately dense to dense materials, liquefaction leads to transient softening and increased cyclic shear strains, but a tendency to dilate during shear inhibits major strength loss and large ground deformations. A condition of cyclic mobility or cyclic liquefaction may develop following liquefaction of moderately dense granular materials. Beneath gently sloping to flat ground, liquefaction may lead to ground oscillation or lateral spread as a consequence of either flow deformation or cyclic mobility. Loose soils also compact during liquefaction and reconsolidation, leading to ground settlement. Sand boils may also erupt as excess pore water pressures dissipate (Youd, et al., 2001).

2.3.3 Seismic slope stability analysis

Procedures for static slope stability analysis have been used for many years and calibrated against many actual slope failures. The database against which seismic slope stability analyses can be calibrated is much smaller (Kramer, 1996). Analysis of the seismic stability of slopes is further complicated by the need to consider the effects of the following two cases.

- Dynamic stresses induced by earthquake shaking, and
- The effects of those stresses on the strength and stress-strain behavior of the slope materials.

Seismic slope instabilities may be grouped into two categories on the basis of which of these effects is predominant in a given slope.

- **Inertial Instabilities**, the shear strength of the soil remains relatively constant, but slope deformations are produced by temporary exceedances of the strength by dynamic earthquake stresses.

- **Weakening Instabilities** are those in which the earthquake serves to weaken the soil sufficiently that it cannot remain stable under earthquake-induced stresses. Flow liquefaction and cyclic mobility are the most common causes of weakening instability.

A number of analytical techniques, based on both limit equilibrium and stress-deformation analyses, are available for both categories of seismic instability.

2.3.3.1 Analysis of Inertial Instability

Earthquake motions can induce significant horizontal and vertical dynamic stresses in slopes. These stresses produce dynamic normal and shear stresses along potential failure surfaces within a slope. When superimposed upon previously existing static shear stresses, the dynamic shear stresses may exceed the available shear strength of the soil and produce inertial instability of the slope. A number of techniques for the analysis of inertial instability have been proposed. These techniques differ primarily in the accuracy with which the earthquake motion and the dynamic response of the slope are represented.

2.3.3.1.1 Pseudostatic Analysis

Pseudostatic analysis produces a factor of safety against seismic slope failure in much the same way that static limit equilibrium analyses produce factors of safety against static slope failure. The analysis is treated as a static problem and the horizontal force is expressed as the product of a seismic coefficient K, and the weight W, of the potential sliding mass. Sometimes is assumed that the embankment dam behaves as a rigid body and so the accelerations will be uniform throughout the section and equal at all times to the ground accelerations.

Even though this method of analysis is relatively simple and straightforward, it has a limitation of representing the complex, transient, dynamic effects of earthquake shaking by a single constant unidirectional pseudostatic acceleration which is obviously quite crude. Terzaghi (Terzaghi, 1950) stated that "the concept it conveys of earthquake effects on slopes is very inaccurate, to say the least," and that a slope could be unstable even if the computed pseudostatic factor of safety was greater than 1. Besides, the main limitations of this approach are (Seed, 1979):

- it is evident from field tests that all earth dams do not behave as rigid bodies;
- the maximum acceleration will be developed in an embankment dam for only a short period of time, so that the deformation resulting from it may be small.

Table 2.4: Results of Pseudostatic analysis of earth dams that failed during earthquakes (Source Seed 1979)

Dam	k_h	FS	Effect of Earthquake
Sheffield Dam	0.10	1.2	Complete failure
Lower San Fernando Dam	0.15	1.3	Upstream slope failure
Upper San Fernando Dam	0.15	~2–2.5	Downstream shell, including crest slipped about 6 ft downstream
Tailings dam (Japan)	0.20	~1.3	Failure of dam with release of tailings

In their most common form, Pseudostatic analyses represent the effects of earthquake shaking by Pseudostatic accelerations that produce inertial forces, F_h and F_v; which act through the centroid of the failure mass (Fig. 2.9). The magnitudes of the Pseudostatic forces are

$$F_h = \frac{a_h W}{g} = K_h W \quad (2.10a)$$

$$F_h = \frac{a_v W}{g} = K_v W \quad (2.10b)$$

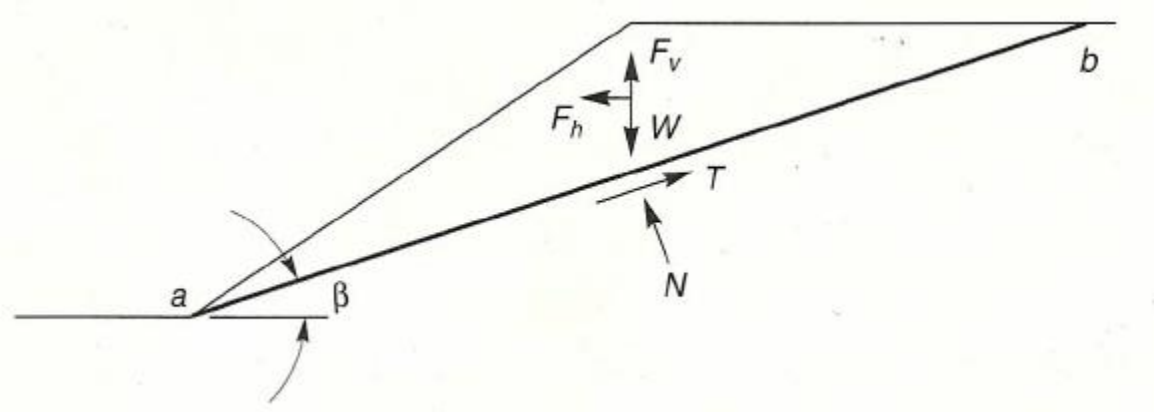

Fig. 2.9: Forces acting on triangular wedge of soil above planar failure surface in Pseudostatic slope stability analysis (Kramer, 1996)

$$FS = \frac{\text{resisting force}}{\text{driving force}} = \frac{cl_{ab} + [(W - F_v)\cos\beta - F_h \sin\beta]\tan\phi}{(W - F_v)\sin\beta + F_h \cos\beta} \quad (2.11)$$

All the other approaches attempt to evaluate permanent slope displacements produced by earthquake shaking.

2.3.3.1.2 Newmark Sliding Block Analysis

Newmark (Newmark, 1965)succeeded in computing displacements induced by an earthquake in embankments by assuming that movements occur when forces on a rigid block of soils above a fixed potential failure surface exceed its sliding resistance. He assumed that the slope deformed only during those portions of the earthquake when the out-of-slope earthquake forces cause the pseudo static factor of safety to drop below 1.0.

He has suggested an approach suitable for rigid-plastic material involving the determination of a yield acceleration, k_{yg}, at which sliding will begin to occur and the computation of the displacements which develop when this acceleration is exceeded. The procedure is illustrated in Fig. 2.10. If the acceleration pattern acting on a potential sliding mass is similar to that shown in

the figure, then no displacement will occur until time t_1 , when the induced acceleration reaches the yield acceleration for the first cycle k_{y1} . If the yield acceleration is assumed to remain constant throughout the first cycle, it may be marked off as shown on Fig. 2.10, and the variation in velocity of the sliding mass may be computed by integration over the shaded area. The velocity will continue to increase until time t_2 when the acceleration again drops below the yield value, and the velocity is finally reduced to zero at time t_3, as the direction of the sliding mass may then be computed by integration of the velocity versus time relationship. The result looks like as shown in Fig. 2.11.

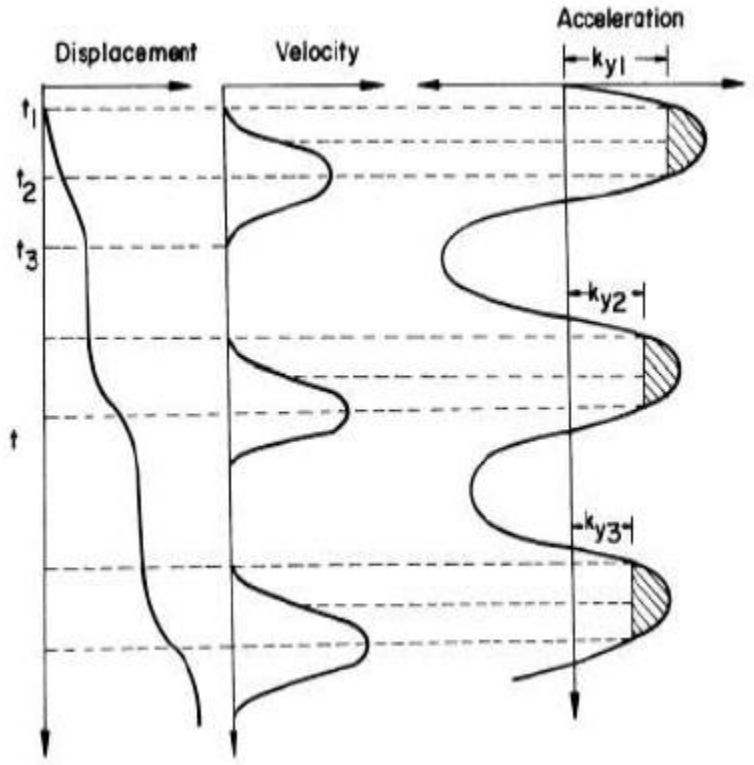

Fig. 2.10: Integration of accelerograms to determine downslope displacements

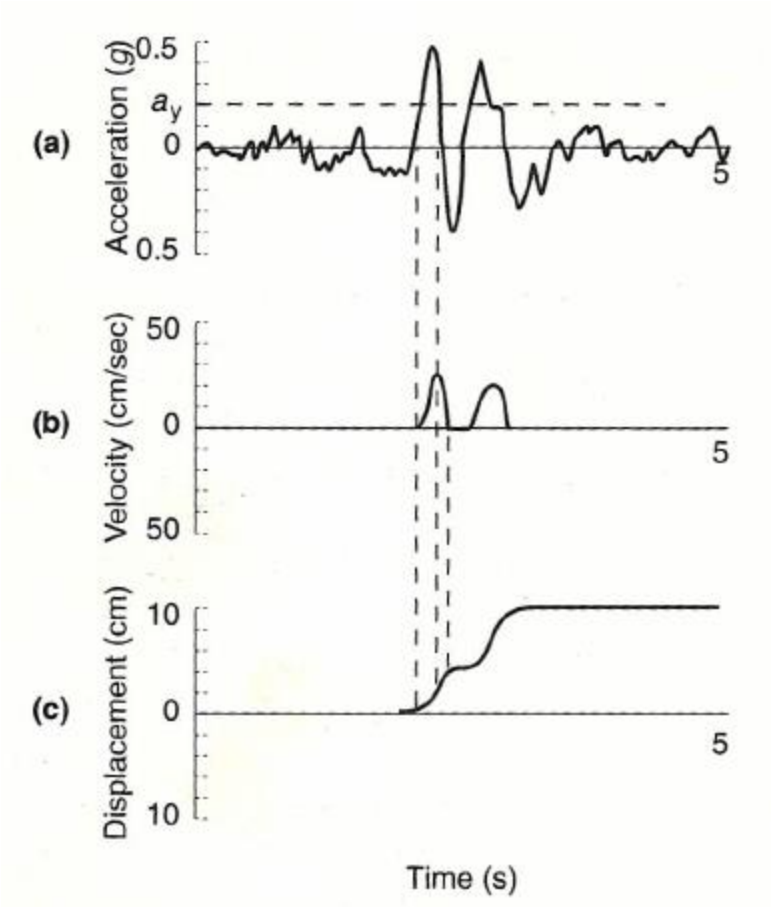

Fig. 2.11: Development of permanent slope displacements for actual earthquake ground motion. (After Wilson and Keefer, 1985)

Yield Acceleration effect on Slope Displacements

Newmark sliding block model will predict zero permanent slope displacement if earthquake induced accelerations never exceed the yield acceleration *(a_y/a_{max}* = 1.0) as illustrated in Fig. 2.12 a. Since the permanent displacement is obtained by double integration of the excess acceleration, the computed displacements for a slope with a relatively low yield acceleration (small *a_y/a_{max})* will be greater than that of a slope with a higher yield acceleration (Fig.2.12 b, c). He found that a reasonable upper bound to the permanent displacements produced by earthquake motions was given by the following equation (Eq.2.12).

$$d_{max} = \frac{V_{max}^{\,2}}{2a_y}\frac{a_{max}}{a_y} \qquad (2.12)$$

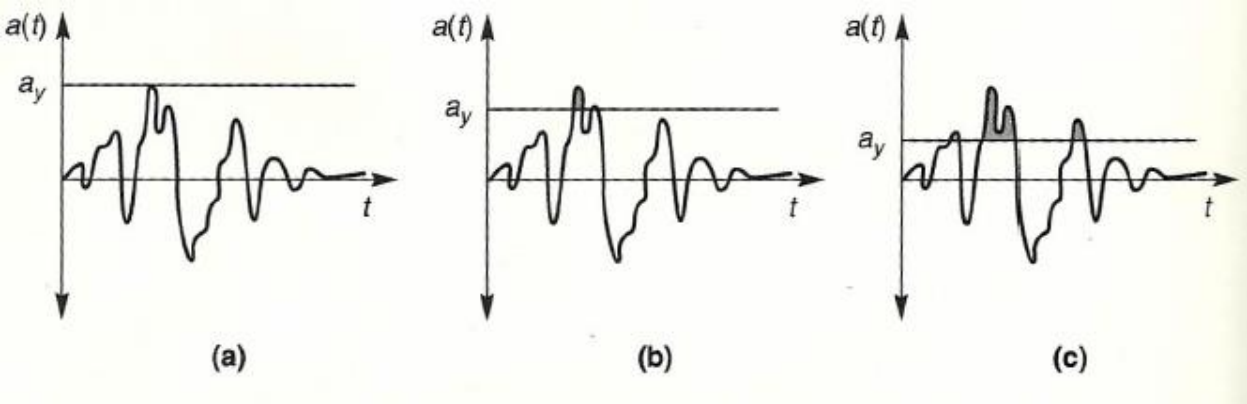

Fig. 2.12: Permanent slope displacements depend on the relationship between the yield acceleration and the maximum acceleration. (a) If the yield acceleration of a slope is greater than the maximum acceleration of a particular ground motion, no displacement will occur. As yield accelerations decrease, as in (b) and (c), slope displacements increase quickly.

2.3.3.2 Analysis of weakening Instability

Through a process of pore pressure generation and/or structural disturbance, earthquake induced stresses and strains can reduce the shear strength of a soil. Weakening instabilities can occur when the reduced strength drops below the static and dynamic shear stresses induced in the slope. Weakening instabilities are usually associated with liquefaction phenomena and can be divided into two main *categories, flow failures* and *deformation failures*).

Flow failures occur when the available shear strength becomes smaller than the static shear stress required to maintain equilibrium of a slope. Flow failures, therefore, are actually driven by static stresses. They can produce very large deformations that occur quickly and without warning.

Deformation failures occur when the shear strength of a soil is reduced to the point where it is temporarily exceeded by earthquake-induced shear stresses. Much like inertial failures, deformation failures occur as a series of "pulses" of permanent displacement that cease at the end of earthquake shaking. Different procedures are available for the analysis of flow failures and deformation failures.

2.3.3.2.1 Flow Failure Analysis

Because they usually involve significant reduction in soil strength, flow failures usually produce large deformations and severe damage. The first step in their analysis is generally to determine whether or not one will occur. To estimate the extent of the damage produced by flow failures, procedures for estimation of flow failure deformations have also been developed.

Analysis of Stability

Potential flow slide instability is most commonly evaluated by conventional static slope stability analyses using soil strengths based on end-of earthquake conditions (Marcuson et al., 1990).

Analysis of Deformations

If stability analyses indicate that flow failure is likely, the extent of the zone influenced by the failure can be determined from an analysis of flow failure deformations. By neglecting the small deformations that precede the triggering of flow sliding, rough estimates of flow sliding deformations can be obtained from procedures based on limit equilibrium, fluid mechanics, and stress-deformation analyses.

2.3.3.2.2 Deformation Failure Analysis

Although deformation failures generally involve smaller deformations than flow failures, they are capable of causing considerable damage. Lateral spreading is the most common type of deformation failure. In recent years a number of investigators have developed methods to estimate permanent displacements produced by deformation failures. Because the mechanisms that produce deformation failures are so complicated, procedures for prediction of the resulting displacements are largely empirical in nature.

Hamada et al (Hamada, et al., 1986) considered the effects of geotechnical and topographic conditions on permanent ground displacements observed in uniform sands of medium grain size in the 1964 Niigata *(M* = 7.5), 1971 San Fernando *(M* = 7.1), and 1983 Nihonkai-Chubu *(M* = 7.7) earthquakes. Permanent displacements were found to be most strongly influenced- by the thickness of the liquefied layer and the slopes of the ground surface and lower boundary of the liquefied zone.

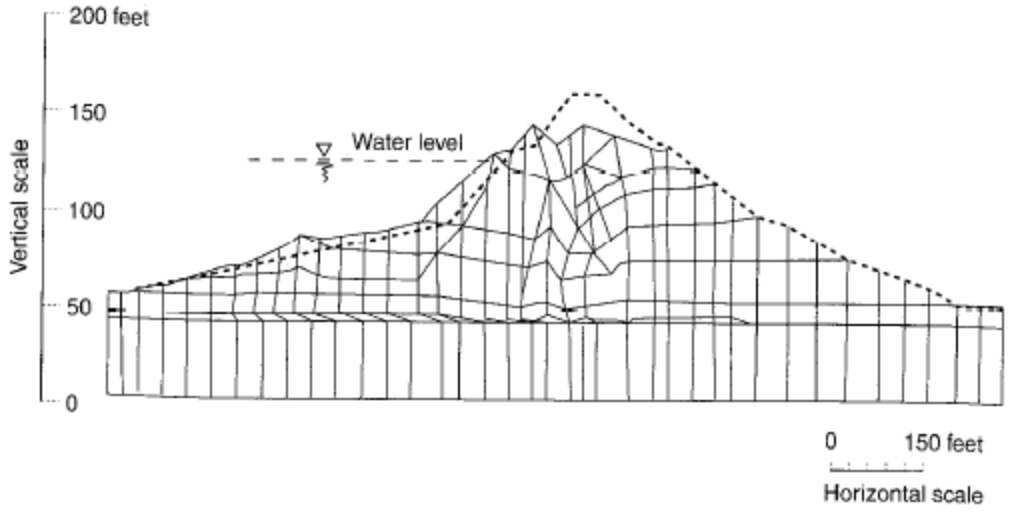

Fig. 2.13: Initial (dashed) and postliquefaction (solid) configurations of Sardis Dam in Mississippi from TARA-3FL analyses. Note the large strains due to liquefaction in core and thin seam below the upstream shell.

Byrne (1991) used work-energy principles with an elastic perfectly plastic model of liquefied soil to develop expressions for estimation of permanent slope displacements. He extended this approach (Byrne, et al., 1992) to determine factors by which the initial stiffness of a soil should be reduced for finite-element analysis of deformation failures. Deformations predicted by this approach were in good agreement with those observed in the 1971 failure of Upper San Fernando Dam (Fig. 2.14).

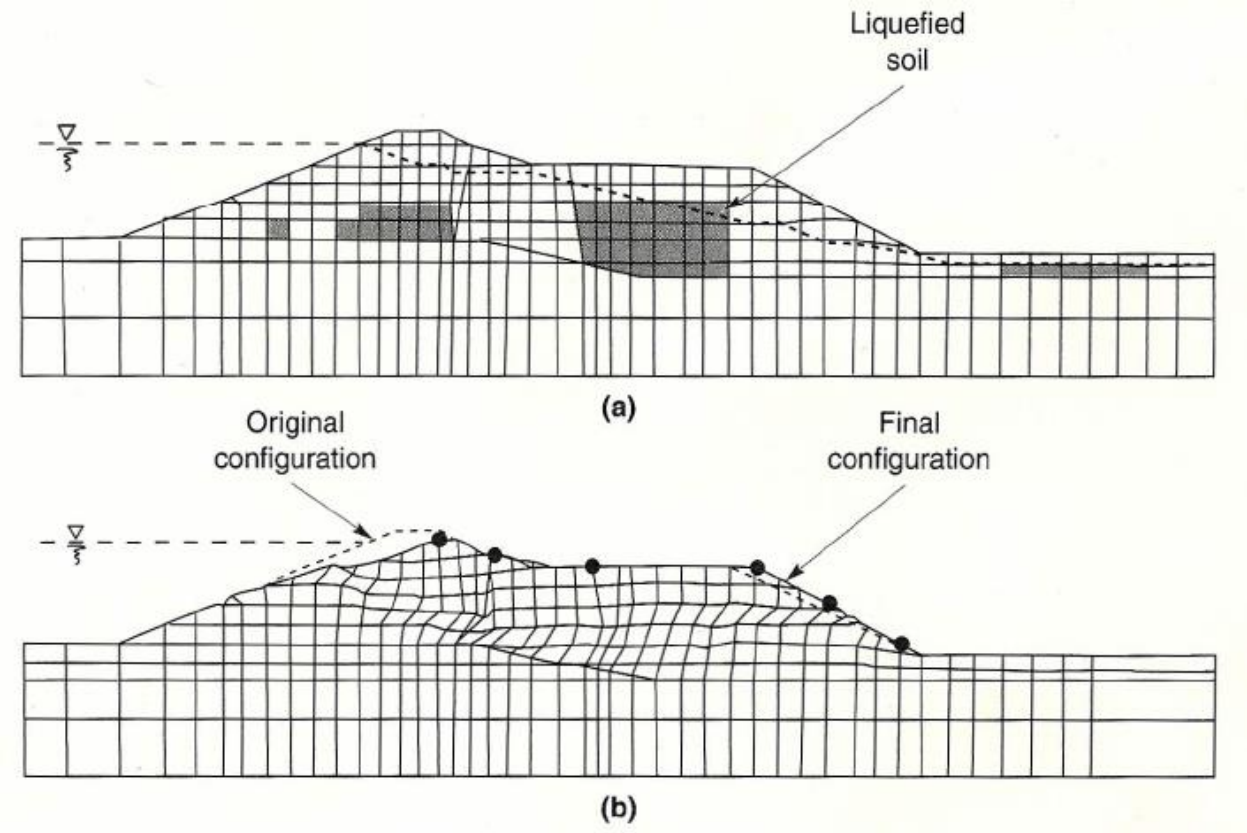

Fig. 2.14: (a) Finite-element mesh for analysis of Upper San Fernando Dam with elements determined to have liquefied by Serffet et al. (1976) shaded; (b) positions of original and final meshes (displacements exaggerated by factor of 2) by procedure of Byrne et al. (1992). Note large shear strains in liquefied zones.

3 Project characterization

3.1 General

3.1.1 Location of the Gidabo Earth Fill Dam

The project area is located in the Abaya-Chamo sub basin of the Rift Valley.This Lake Basin is found in the Southern part of the country within Oromiya and SNNPR States. The dam site is approachable from Addis Ababa via Dilla town. Addis Ababa to Dilla is 360 Km by asphalt road and from Dilla town to Gidabo dam site is 17 km by fair weather road.

The river is one of the main flow contributors to Lake Abaya. The project area lies approximately between 696000 and 726200N and 386000 and 422000E, a short distance east of Lake Abaya and just south of Gidabo river flood plain, at an average elevation of 1190m a.s.l. Gidabo irrigation project is found in Abaya district, Borena zone of Oromia region and Dale district, Sidama zone of SNNPRS near Dilla town to east of Lake Abaya. The location of the project area is shown in Fig. 3.1.

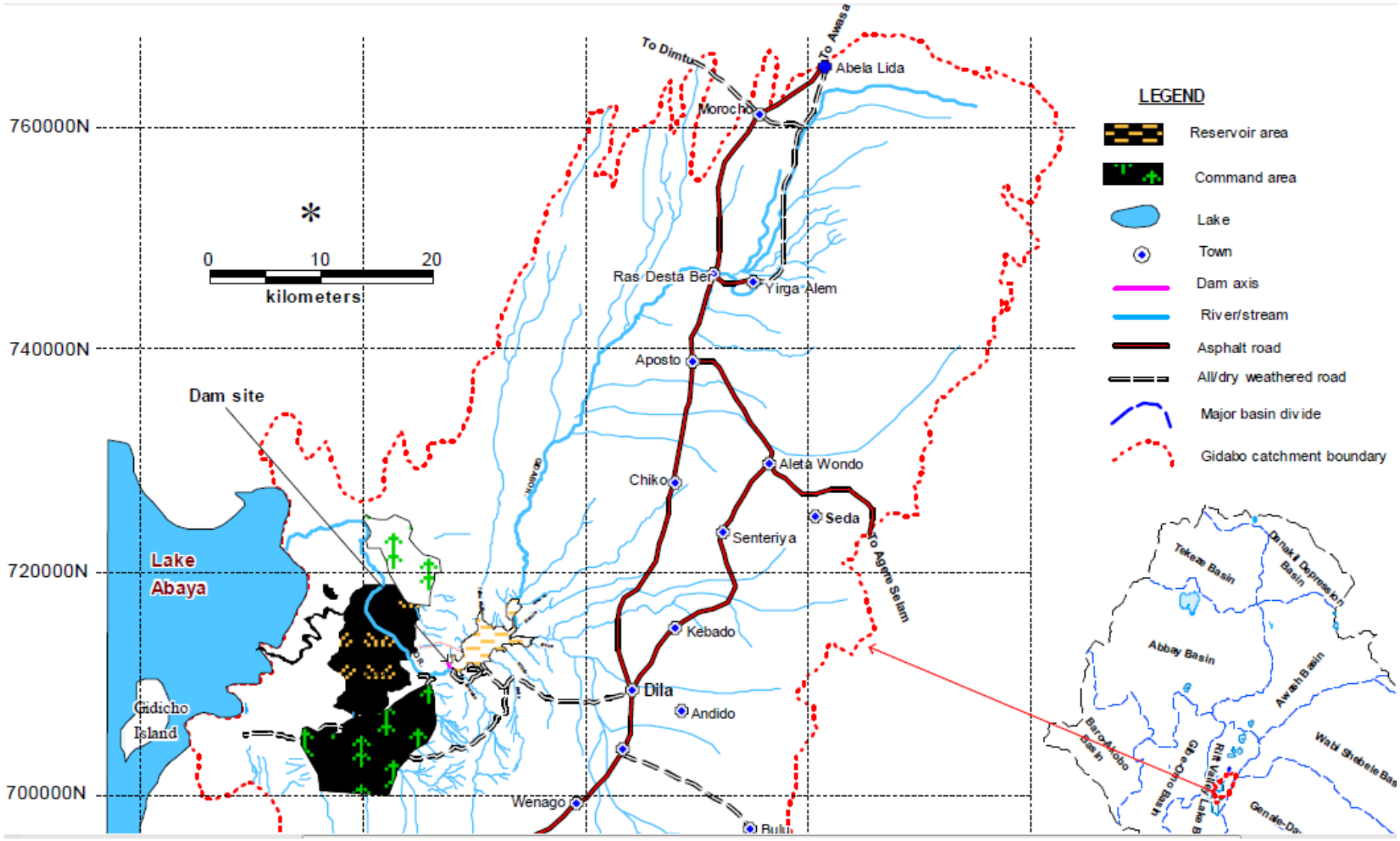

Fig. 3.1: Location map of Gidabo Irrigation Project

3.1.2 General description of the project

Gidabo Irrigation project includes a construction of about 22.5m high Earth-fill dam on Gidabo river. The project also includes spillway, two outlets for taking water from the reservoir and canal networks and irrigation structures. The project is planned to develop a total irrigable land of 7374 ha through its canal distribution network.

The command area is situated in the northern part of Lake Abaya, southern part of Ethiopia. The northern Lake Abaya area, which is located in the southern part of the Main Ethiopian Rift (MER), encloses irrigable lands at different places. It indicates the existence of economically exploitable agricultural land use. The general arrangement of the dam and appurtenant structures are shown in Fig. 3.2.

3.1.3 Topography

The overall topography and drainage network development within the Gidabo River basin is the result of geologic history of pyroclastic volcanic rocks, NNE-SSW and E-W striking faults with east, westerly high angle downthrows, characterized by moderately dissected to undulated local relief. The topographic elevation of the Gidabo basin is mostly an expression of landforms with hills. Gidabo Dam site falls within two narrow steep hills downstream of the confluence with its tributary (Ameleki river). The physiographic around Gidabo Dam site is the result of volcano-tectonic, sedimentary and erosion processes (WWDSE, 2009).

3.1.4 Climate

The mean monthly temperature at Gidabo is in the range of 15^0 to 30^0 C. The catchment area at Gidabo dam site is estimated at around 2532 km2, with mean annual discharge of 110.8 m^3/sec. The annual mean rain fall at the north tip of Abaya is 818 mm and 745.1 mm at Mirab Abaya (WWDSE, 2009).

3.1.5 Vegetation

The dam site and reservoir area of Gidabo irrigation project is covered by dense vegetation (natural bushes and trees). There is no settlement within the proposed dam and reservoir area. Moderate to scarce vegetation and partly plain barren lands characterize the command area of Gidabo irrigation project, this area has been commonly used for grazing (WWDSE, 2009).

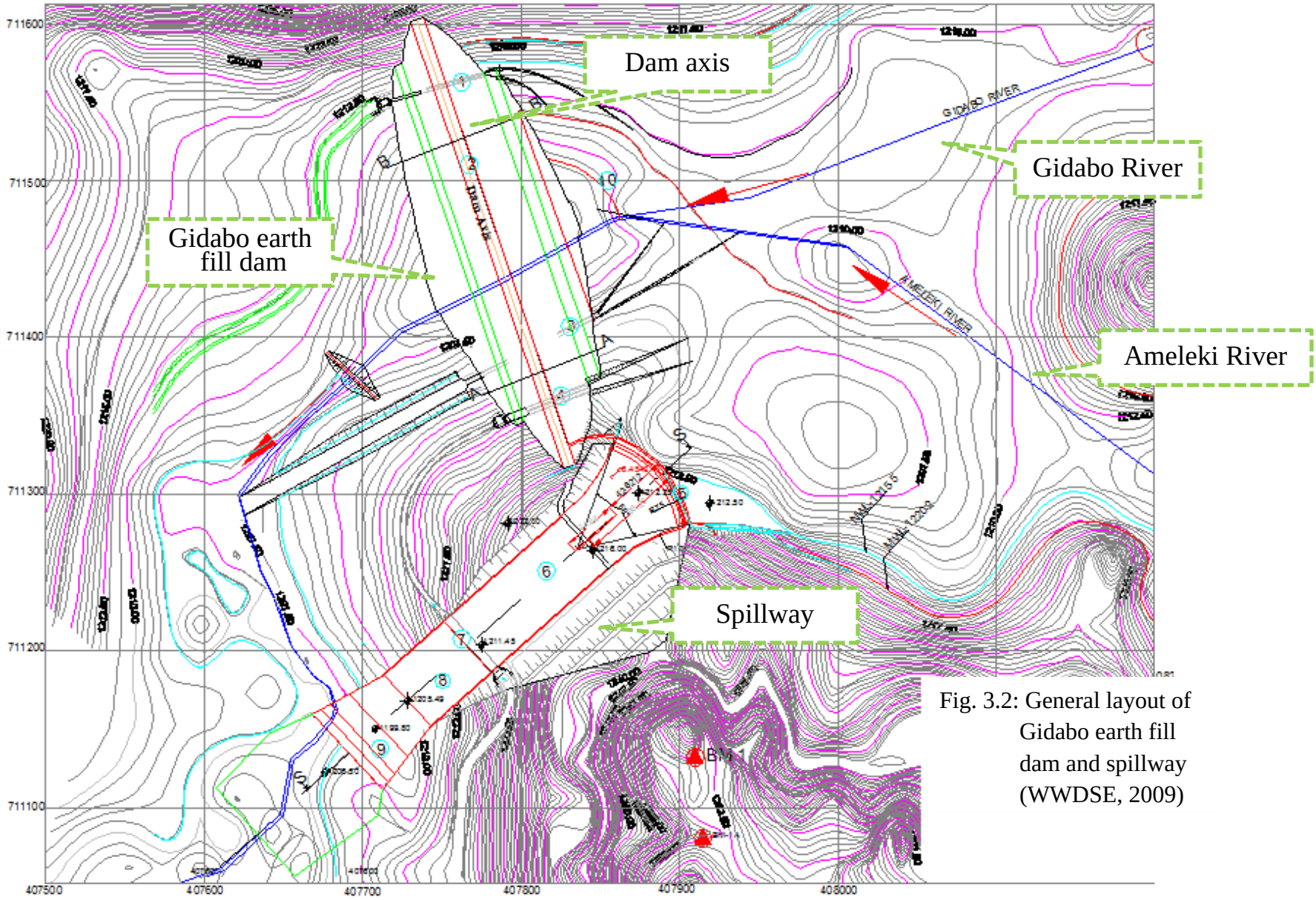

Fig. 3.2: General layout of Gidabo earth fill dam and spillway (WWDSE, 2009)

3.2

3.1.6 Geology of the area

The dam site surface physiography shows that the area is mainly covered by pyroclastic fall (agglomerated tuff) deposits and the highest average hill slopes gradients are commonly covered by thin residual soil layers. Exceptionally, the steep slope forming and top of Gidabo right abutment hill are covered by rhyolitic rocks. Surfacially recognized geomorphological break up due to lineaments (normal fault) was observed on the hills around the dam site. River channel and plain land around the dam axis is covered by flood plain and river channel deposits (mainly silt and sand with minor gravel and clay) (WWDSE, 2009).

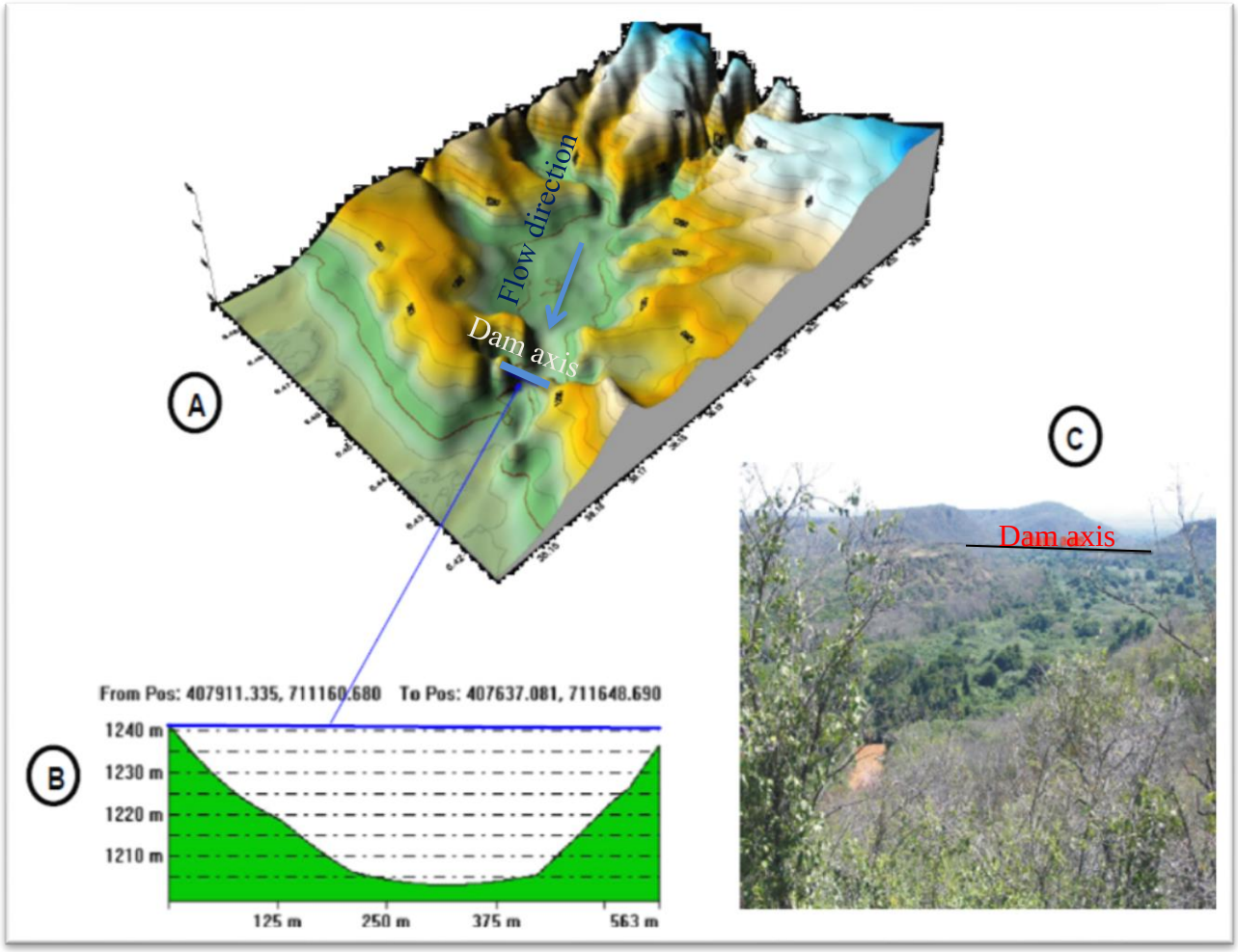

Fig. 3.3: (a) Geomorphological map of Gidabo dam and reservoir area, (b) Geomorphological cross-section along Gidabo dam site (not limited to the dam crest) - extracted from DEM, and(c) photo showing vegetation cover upstream and downstream of Gidabo dam axis (WWDSE, 2009).

3.1.7 Regional Geology

3.1.7.1 Structural Set-up

The Gidabo valley lies in the Ethiopian rift system, which forms a part of the complex tectonic feature of down faulted troughs extending for approximately 5000 km from Mozambique in the south, then northwards through East Africa, through the Red sea and into Israel, Jordan and Syria. Ethiopia forms part of the Arabo-Ethiopian swell which was uplifted during upper Eocene times. As a result of this uplift, fissures formed, up which basaltic lavas were extruded. These lavas are known as the "Trap Series". The upper part of these basalts is inter-bedded with more silicic lavas, pyroclastic and lacustrine sediments. It is thought that the outcropping of lavas gave rise to the crustal collapse that formed the rift valley (Raunet 1978), which followed after extrusion of the trap series. The cause of the up swell is not known but it is almost certain that the longitudinal arching caused a weakness to develop, which results faulting. A subdued expression of this tectonic and volcanic activity is currently apparent as local thermal springs and occasional low to moderate intensity earthquakes.

The East African Rift System in the region around Gidabo can be subdivided in to three main areas: - Lake Turkana Rift, Lake Chew Bahir Rift, Main Ethiopian Rift (shown in fig.3.4)

After the development of the Main Ethiopian Rift, the Quaternary episodes of tectonics were formed, and active spreading axis, along the center of the rift that is known as Wonji Fault Belt (WFB) is developed. The WFB is an intense zone of normal faulting and volcanism, which forms rift-in-rift structures and consists of several segments disposed in echelon fashion along the center of MER. It is the presence of active axis extensional in the MER (Abebe et. al., 2002). In general, two main fault systems have been distinguished in the MER: N30°E-N40E° and N20°E trending fault systems, which mainly characterizes the rift margins and WFB (rift floor), respectively (WWDSE, 2008).

Gidabo River is the major river in the southern Main Ethiopian Rift region that flows from the western rift escarpment towards the rift floor and draining into Lake Abaya. A series of intense normal faulting and quaternary volcanism observed in Gidabo river basin is believed to represent the southern sector of the WFB (WWDSE, 2008).

3.1.7.2 Stratigraphy

From the primary observation of the geology of the catchments and around dam site, the following rocks are observed: Ignimbrite, rhyolite, ignimbrite tuff, lithic & crystal tuff, agglomerate and basalt. The fault zone is frequently marked by central volcanoes, which erupt significant amount of felsic product. The surface geology of Gidabo dam site and surrounding area is probably belonging to such volcanic product (Wonji Group of Mohr, 1967a).

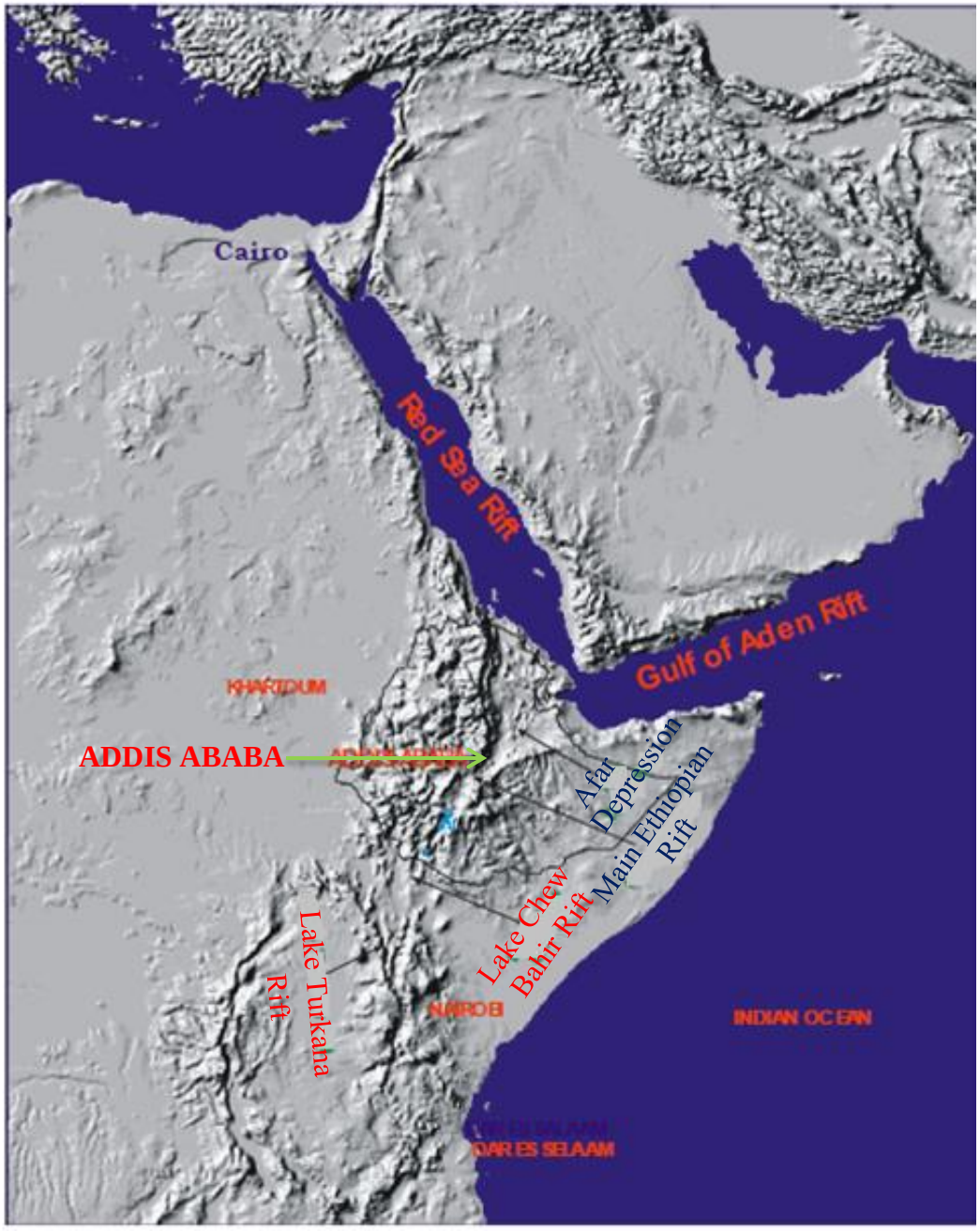

Fig. 3.4: Relationship of the Ethiopian rift system of the Main East African Rift system

3.1.8 Surface Geological studies

The Gidabo dam, reservoir and spillway areas lay within the Southern Main Ethiopian Rift (SMER) characterized by active extensional tectonics that produced series of horst and graben structures. The area around Gidabo Dam site is covered by recent volcanic-tectonic events and fluvial deposits, in which the former (volcano-tectonic events with some water action) are an essential part of the area.

3.2 Seismicity of the Project area

3.2.1 Regional Seismicity study of Gidabo Irrigation Project

The embankment and critical appurtenant structures should be evaluated for seismic stability. Information on the historical seismicity of Gidabo Irrigation project area has been obtained from different sources. These are: country seismicity map and from the study of Sir Alexander GIBB and partners in association with W.S. Atkins International (WWDSE, 2008).

One of the methods of analysis is a function of the seismic zone. The Gidabo Irrigation project area is located on southern part of the main Ethiopian Rift, which constitutes the northern part of the African Rift Valley. Based on the regional studies (Intensity and Zoning map of Ethiopia) as shown in Fig.3.5, this area is found within the area having 20% ground acceleration and VIII intensity with 100 years return period and probably of 0.01 per annum of being exceeded and the site falls under zone 4 with a corresponding major damage (WWDSE, 2008).

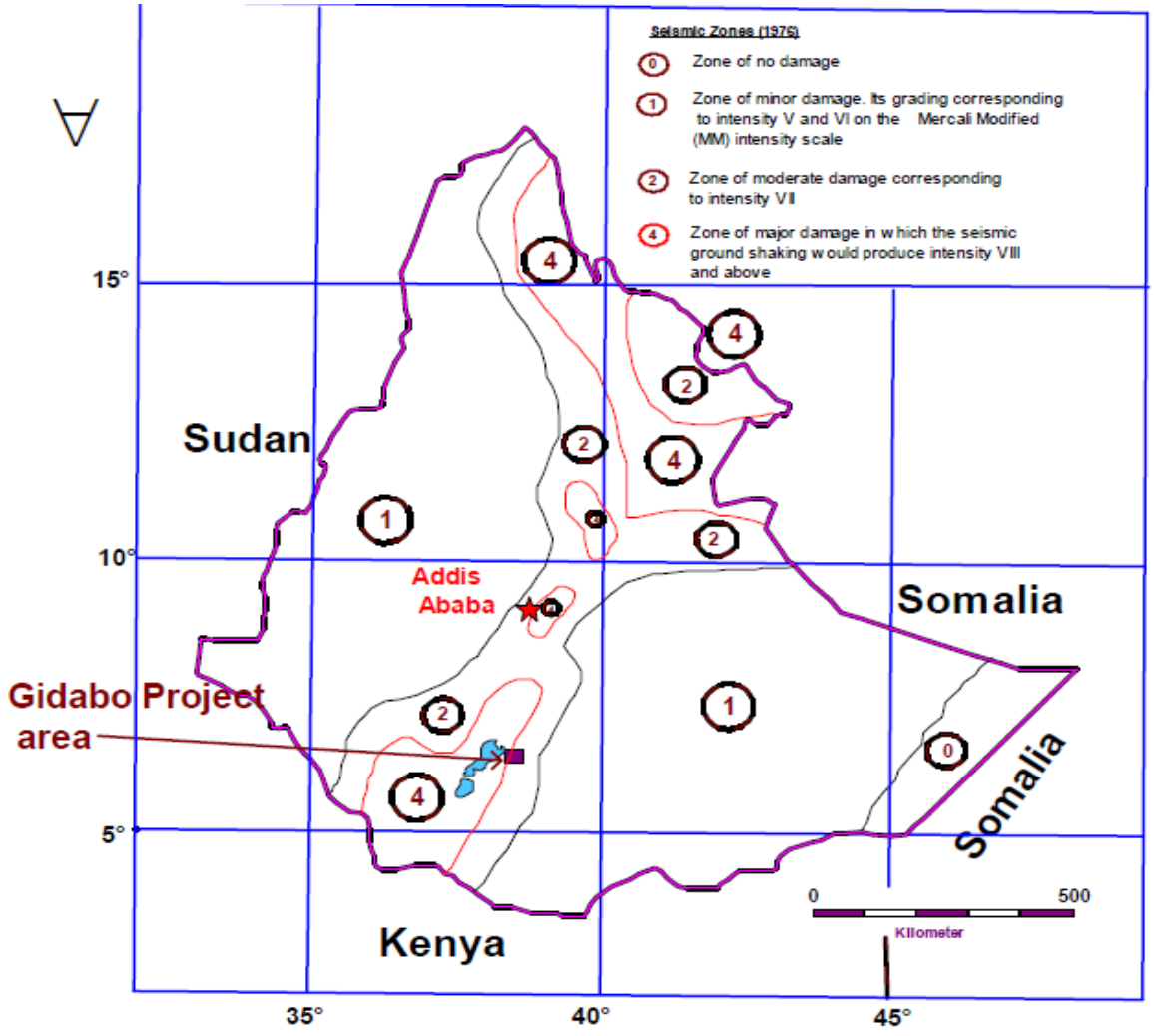

Fig. 3.5: Seismic zoning map of Ethiopia (WWDSE, 2008)

3.2.2 Ground acceleration estimation of the area

Following the guidelines recommended by the international Commission on Large Dams (ICOLD, 1983) two different earthquakes: the maximum credible earthquake (MCE) and the design base earthquake (DBE) have been used for the dynamic analysis of the gidabo earth fill dam. The MCE is the largest reasonably conceivable earthquake that appears possible along a recognized fault or within a geographically defined tectonic province, under the presently known or presumed tectonic framework. The DBE is the earthquake which is expected to occur at least once during the expected life period of the dam.

ICOLD indicates that under the DBE condition, the structure of the dam should not be significantly impaired and should remain operational, even though some deformation is acceptable. ICOLD also indicates that the embankment dams, the MCE should not cause the dam (Fell, et al., 2005)

- to lose its free board
- to fail due to liquefaction of material in the dam or its foundations
- to collapse due to movement at a slip surface in the slope or through the foundation

The peak ground acceleration for the project area corresponding to maximum credible earthquake (MCE) and design base earthquake (DBE) is estimated by Addis Ababa University, Institute of geophysics, space science and astronomy (IGSSA).

Peak ground acceleration data corresponding to MCE and DBE estimated for the project area by Addis Ababa University, Institute of geophysics, space science and astronomy (IGSSA) and values from Gidabo dam design report has been adopted for the analysis. Table 3.1 below summarizes the design horizontal and vertical PGA used in the analysis. Based on international standards, the vertical PGA has been taken as ½ of the horizontal component.

Table 3.1: Design peak ground acceleration

Description	Horizontal	Vertical
Maximum Credible Earthquake (MCE)	0.33g**	0.165g**
Design Base Earthquake (DBE)	0.15g*/0.136g**	0.075g*/0.068g**

*Gidabo dam design report ** IGSSA calculation

3.3 Embankment type and geometry

3.3.1 Embankment type

The dam site is located in a relatively narrow stream valley and the foundation has thick depth of low strength soil overlying bedrock. Hence, the foundation conditions suggest adopting an embankment dam section over a concrete dam. The dam lies between 696000 and 726200 N and 386000 and 422000 E.

Construction material suitable for the impervious core is available in sufficient amount for both earth fill and rock fill type dam alternatives. According to the geotechnical investigations, the foundation at the dam site consists of considerably thick, "sandy gravel" layer. In such foundation conditions, an earth fill dam is a better alternative.

The earth fill material site is predominantly gravel size of fragmented aphanites basalt (over 80% gravel) with different degree of weathering and strength (fresh to completely weathered and strong to weak). Therefore, based on the foundation conditions and the construction material availability an earth fill dam with central core has been selected as a suitable dam type.

3.3.2 Embankment Geometry/ Cross section/ Zoning

The proposed dam is an earth fill (gravel fill) dam with an impervious central core composed of clayey material from borrow areas; in the reservoir and downstream nearby areas. A central core has the advantage of providing higher pressure at the contact between the core and the foundation, thus, reducing the possibility of leakage and piping. The top level of the core has been fixed at the maximum flood level for the 1 in 10,000 years flood, which is 1223.8 m.

A core top width of 3m has been provided as the minimum for construction purposes. Consequently, the width of the base of the core, at river bottom level (EL 1204.55 m), will be approximately 22.2 m. At the deepest excavation elevation at the lowest point (EL 1996 m.), the core width will be about 30.6m.

Vertical transition and filter zones of suitable gradations will border the core on both sides and horizontal drain composed of fine and coarse filter layers is provided to safely discharge the seepage water from the vertical chimney filter/drain and to protect erosion of fines from the downstream excavated foundation.

The impervious core of Gidabo Dam is proposed to be flanked by a 1V:2.5H and 1V:3H in upstream slope and 1V:3.0H downstream slope free draining earth fill.

3.4 Material parameters used in different analysis

3.4.1 General

Engineering properties of soils are vital components of any geotechnical analysis. Thus, these geotechnical soil parameters used in the analysis of the present study are extracted from the geological and geotechnical investigation report and final design report of Gidabo earth fill dam [(WWDSE, 2008) and (WWDSE, 2009)] and summarized in the upcoming sections.

3.4.2 Hydraulic parameters of embankment and foundation materials

Permeability of the embankment and foundation materials has been adopted from final design report for Gidabo earth fill dam studied by water works design and supervision enterprise (WWDSE, 2009) and tabulated in Table 3.2 below. In addition to this, saturated volumetric water content has been adopted from sample functions estimated for different soils by J. Krhan (Krhan, 2007) and are shown in Table 3.3.

Table 3.2: Average permeability coefficients used in the analysis (adopted from final design report, (WWDSE, 2009)

No.	Description	K(cm/s)(Sat)	Remarks
1	Impervious Clay Core	3×10-6	Average values
2	Filter layer	1×10-2	Average values
3	Gravel Shell	2×10-3	Average values
4	Foundation	1.5×10-4	Average values
5	Compacted Alluvium	1.5×10-3	Average values
6	Rock Toe	1×10-1	Average values

Table 3.3: Saturated volumetric water content (SVWC) values used in the analysis (taken from Seep/W modeling Engineering book, (Krhan, 2007))

No.	Description	SVWC(Porosity)	Remarks
1	Impervious Clay Core	0.48	Typical Values
2	Transition/Filter layer	0.35	Typical Values
3	Gravel Shell	0.28	Typical Values
4	Foundation	0.38	Typical Values
5	Compacted Alluvium	0.39	Typical Values
6	Rock Toe	0.25	Typical Values

3.4.3 Shear strength parameters and unit weight

Material properties have been adopted from Gidabo earth fill dam final design report and summarized in Table 3.4 below. According to the report, the shear strength parameters for clay core are obtained from CU tri axial test. The parameters for gravel shell filter and rock toe materials are based on reasonable assumptions derived from similar projects. In the case of the foundation material, the parameters have been determined based on correlation with SPT, N values obtained in the bore holes (WWDSE, 2009). As we can see from the table, the friction angle for gravel shell is somewhat less than that of filter; this is due to some weathering effect on gravel shell.

Table 3.4: Shear strength parameters and unit weight to be used in the analysis (adapted from, (WWDSE, 2009)).

No.	Description	$\Upsilon(kN/m^3)$	ϕ' (^{0})	c' (kPa)
1	Impervious clay core	16	20	10
2	Gravel shell	19	32	0
3	Fine filter	18	34	0
4	Coarse filter	18	35	0
5	Foundation	17	28	0
6	Compacted alluvium	17	26	0
7	Rock toe	22	40	0

3.4.4 Geotextile reinforcement parameters

When a geotextile is used as a reinforcement material, the critical properties required are the tensile strength and pullout resistance due to friction or adhesion. The ultimate tensile strength of the geotextile reinforcement to be provided for reinforcing the slopes of the dam is shown in the Table 3.5. Even though we can not estimate the elongation of the reinforcement in limit equilibrium analysis(which is the drawback of limit equilibrium method), the allowable strain values have also been included as shown in the parenthesis.

Table 3.5: Ultimate tensile strength and long term design strength adopted from geosynthetics magazine (IFAI, 2012)

Name of fabric	**Mass per unit area ASTM D5261 (g/m2)**	**Reinforcement Applications**					
		Wide Width Tensile/Elongation ASTM D 4595 (kN/m)/ (%)				**Creep Limited Strength-MD ASTM D5262 kN/m**	**LTDS MD kN/m**
		Strength @5% strain		**Ultimate Strength % (T_{ult})**			
		Machine Direction	**Cross Machine Direction**	**Machine Direction**	**Cross Machine Direction**		
Comtrac175(W/PET)	**410**	**90**	**NA**	**200(10)**		**122**	**95**
Comtrac400 (W/PET)	**700**	**180**	**NA**	**400(10)**	**50**	**245**	**203**

Table 3.6: Frictional properties and stiffness of geotextile (Koerner, 2005)

Geotextile name	**Thickness (mm)**	**Friction (^{o})**	**Stiffness(E) (kPa)**
Comtrac175(W/PET)	4.0	0.86Φ	1 000 000
Comtrac400 (W/PET)	6.0	0.86Φ	1,250,000

3.4.5 Dynamic material properties

Material properties required for the dynamic response analysis using the equivalent linear approach are: total unit weights, Poisson's ratio, dynamic shear modulus at low strain (Gmax) and the relationships of the modulus reduction factors, G/Gmax, and damping ratio with shear strain. However, the dynamic characteristics of the dam materials have not been investigated by means of dynamic triaxial tests. Therefore, the material properties required for the dynamic analysis have been estimated with the help of the geotechnical literatures as will be explained in the next sections.

3.4.5.1 Stifness as a Function of Depth

The soil stiffness is generally a function of the stress state. As the confining stress increases, the soil stiffness increases. QUAKE/W uses the following relationship(Eq.3.1) to describe the soil stiffness as a function of depth (QUAKE/W, 2010).

$$G = K_G(\sigma'_m)^n \tag{3.1}$$

where G is the shear modulus, K_G is a soil modulus, σ'_m is the mean effective stress, and n is a power exponent (generally n is taken as 0.5). To determine Gmax and the corresponding soil modulus K_G, the following widely used empirical equation, which was developed by Seed and Idriss (Seed, et al., 1970a), has been utilized.

$$G_{max} = 220 \, . \, K_{2max} ((\sigma'_m)^{0.5} \tag{3.2}$$

From Eq. 3.1 and 3.2

$$K_G = 220 \, . \, K_{2max} \tag{3.3}$$

According to Seed et al. (Seed, et al., 1986), the magnitude of K_{2max} for gravels ranges between 80 to 180. The K_{2max} values for Gidabo dam materials are determined based on the curves published by Seed and Idriss (Seed, et al., 1970a) and shown in fig. 3.6 . The Gidabo shell materials are composed of sandy gravel soils, thus a K_{2max} value of 90 is used. Table 3.7 summarize the K_{2max} values and the corresponding K_G values used in the analyses. Assumed Poisson's ratios (ν) for each material are also shown in these tables. The K_{2max} value for the clay core has been taken from tendaho earthfill dam dynamic analysis (Hadush, et al., 2010) which is inturn determined based on the publication by Malla et al (Malla, et al., 2005).

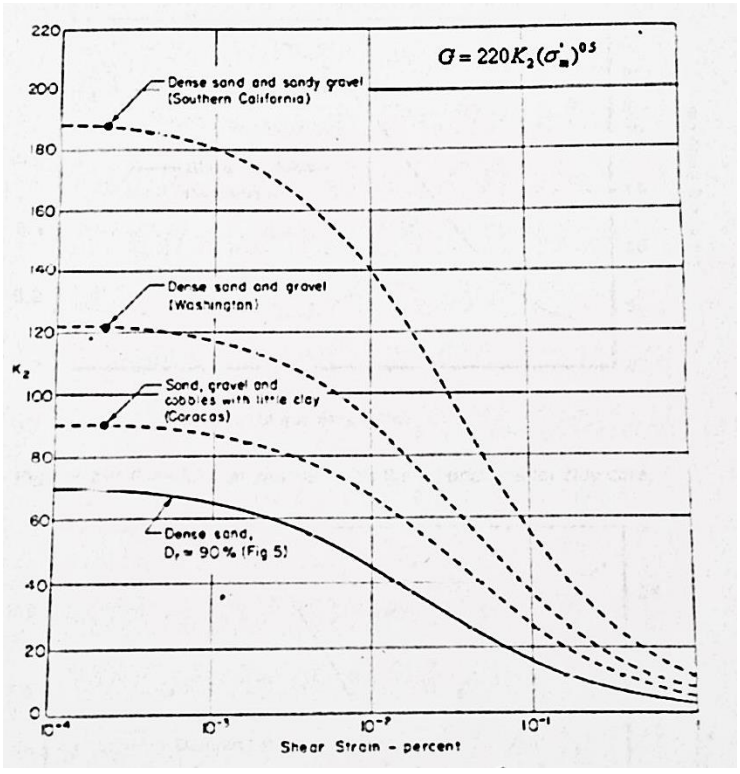

Fig. 3.6: Values of K_2 moduli for different soils ((Seed, et al., 1970a)

Table 3.7: K_{2max} and K_G values based on Eq.3.3

Material	K_{2max}	K_G	ν
Clay Core	50	11000	0.4
Sandy Gravel Shell	90	19800	0.3
Transition/Filter	70	15400	0.3
Compacted Alluvium	85	18700	0.3
Foundation	90	19800	0.3

3.4.5.2 Shear modulus reduction and damping ratio functions

As the dynamic shear strain increases, the effective dynamic shear modulus becomes smaller than the maximum value G_{max}. At the same time, the nonlinear response at higher dynamic strains leads to a higher rate of energy dissipation, which is represented by a damping ratio that increases at higher strain levels. The strain-dependent dynamic shear modulus and damping ratio values for different soils and rock published by Sun et al (Sun, et al., 1988) and (Idriss, 1990) have been used for Gidabo dam dynamic analysis. These functions are summerized in Fig. 3.7 to 3.13.

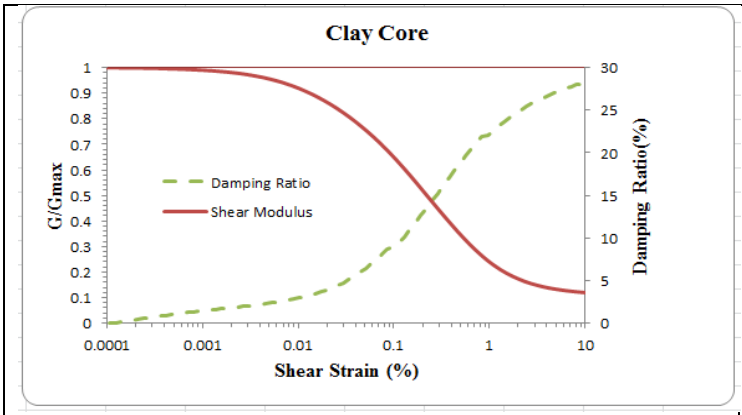

Fig. 3.7: G-Reduction and Dumping ratio Functions for Clay Core

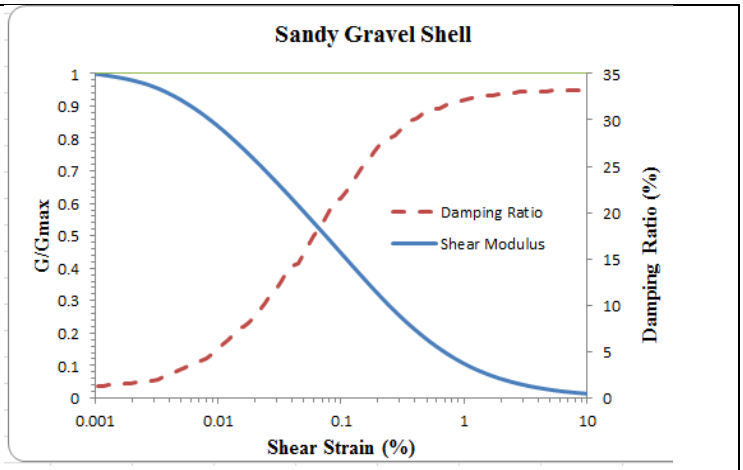

Fig. 3.8: G-Reduction and Damping Ratio Functions for Sandy Gravel Shell

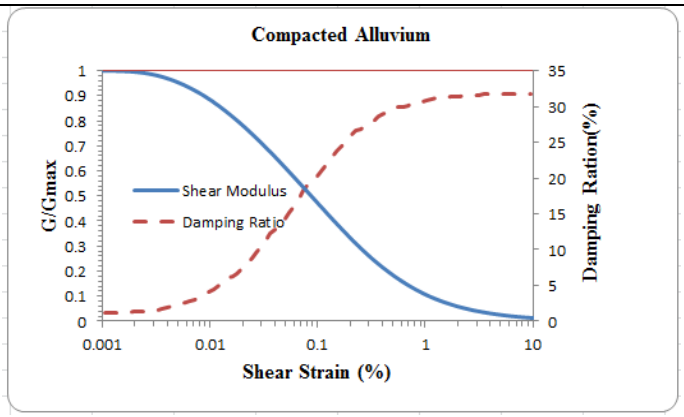

Fig. 3.9: G-Reduction and Damping Ratio Functions for Compacted Alluvium

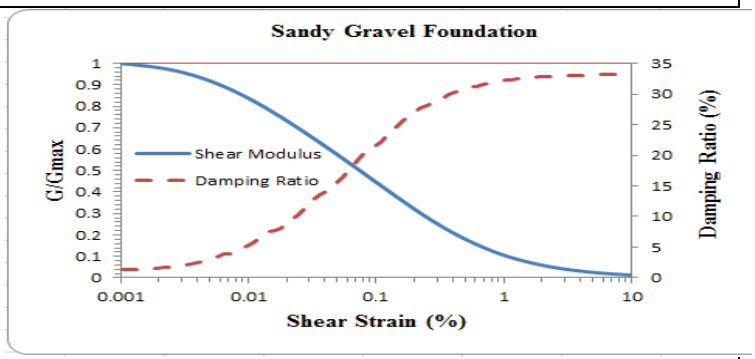

Fig. 3.10: G-Reduction and Damping Ratio Functions for Sandy Gravel Foundation

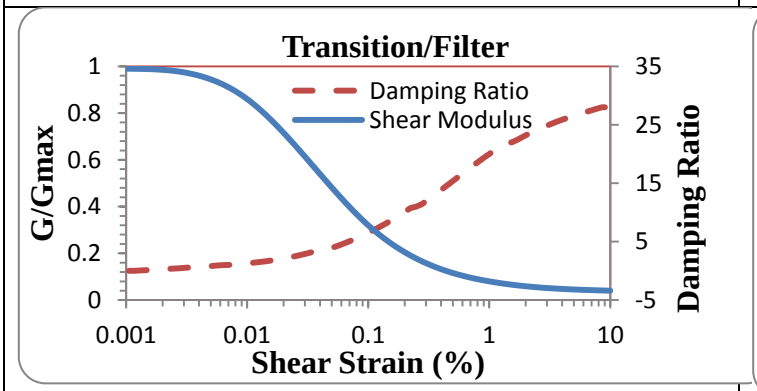

Fig. 3.11: G-Reduction and Damping Ratio Functions for Transition/filter

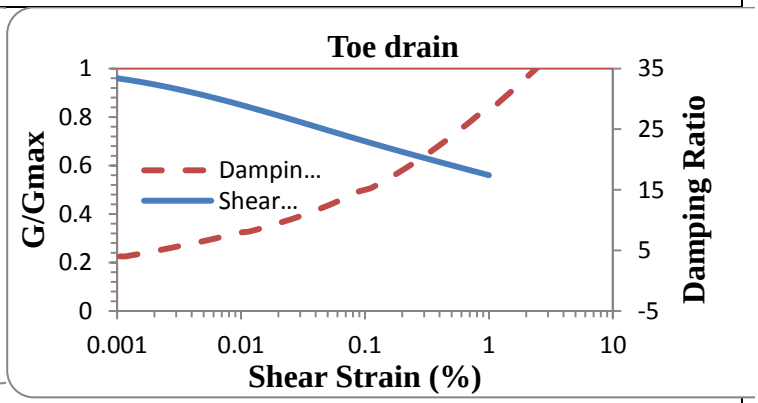

Fig. 3.12: G-reduction and damping ratio functions for toe drain

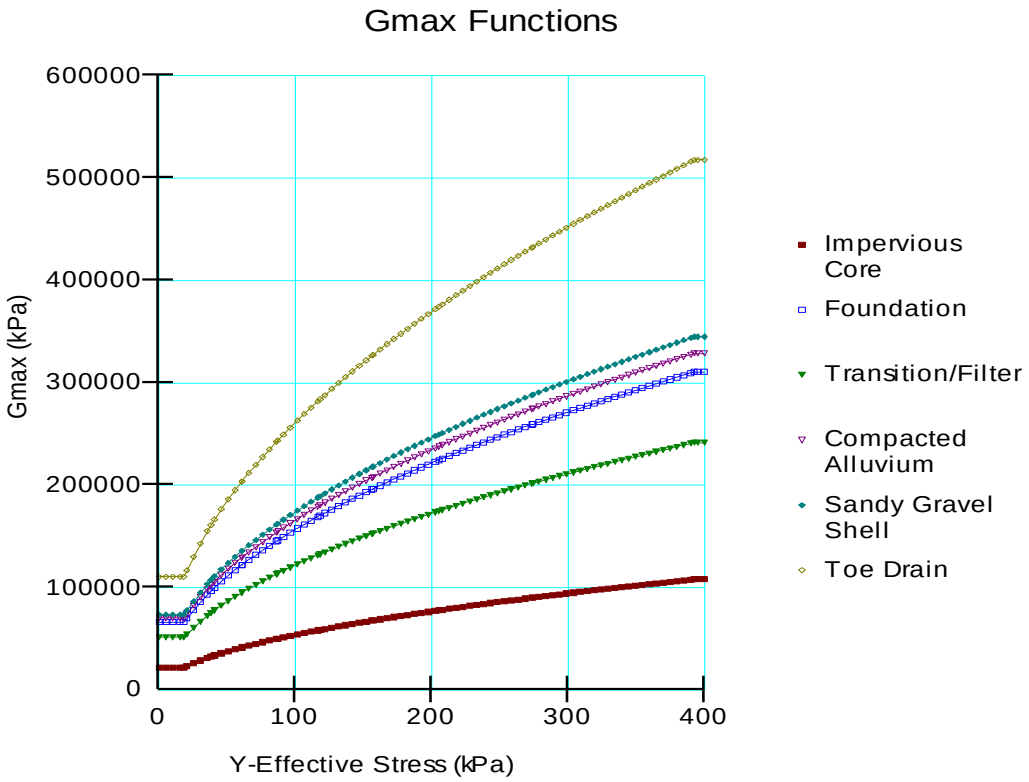

Fig. 3.13: Gmax functions for various embankment and foundation materials

3.4.5.3 Pore pressure function

The pore pressures developed during earthquake shaking are a function of the equivalent number of uniform cycles N for a particular earthquake and the number of cycles N_L, which will cause liquefaction for a particular soil under a particular set of stress conditions. According to Seed et al. (Seed, et al., 1975) , N = 10 for earthquake magnitude M = 7.0 (corresponding to MCE), and N = 6 for M = 6.5 (corresponding to DBE). The ratio of N/N_L is then related to a pore pressure parameter r_u [(QUAKE/W, 2010), (Kramer, 1996)]. Lee and Albaisa (Lee , et al., 1974) and DeAlba et al. (DeAlba, et al., 1975) found that the pore pressure function can be described by the following equation:

$$r_u = \frac{1}{2} + \frac{1}{\pi}\sin^{-1}\left[2\left(\frac{N}{N_L}\right)^{1/\alpha} - 1\right] \qquad \text{(Eq.3.4)}$$

The above equation is used to estimate the pore pressure function in QUAKE/W. For saturated sand α= 0.7 (Das, 1993). Therefore, the pore pressure function shown in Fig. 3.14 (obtained using Eq. 3.4, for α = 0.7) has been used for the sandy gravel foundation and sandy gravel shell of Gidabo dam if liquefaction analysis is required.

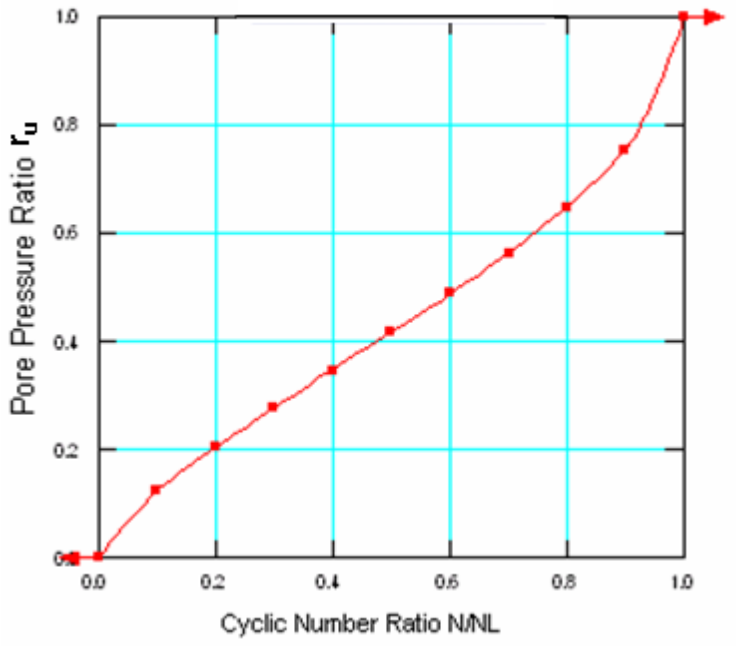

Fig. 3.14: Pore pressure function used for liquefiable material

Case I: Pore Pressure Ratio Function for potentially liquefiable soil

Incase of liquefaction potential assesment of a given material during an earthquake shaking, pore pressure ratio which is a function of the equivalent number of uniform cycles N for a particular earthquake and the number of cycles N_L, which will cause liquefaction for a particular soil under a particular set of stress conditions has been deployed for analysis. However, as will be discussed in section 5.2.3, there is no soil which is susceptible to liquefaction, hence; pore pressure function is not required for our QUAKE/W analysis.

Besides, in tendaho earth fill dam dynamic analysis by Messele and Hadush (Messele, et al., 2006), analysis is carried out by assuming sandy gravel shell as potentially liquefiable soil and the result shows all the materials have been liquefied. However, they didn't accept the result by explaining as the pore pressure function shown in Fig 3.14 is mainly developed for potentially liquefiable sands and cannot represent the behavior of these materials. Hence, liquefaction analysis by assuming sandy gravel material and foundation as potentially liquefiable material for Gidabo earth fill dam will lead to the same conclusion.

Case II: Pore Pressure ratio considering potential pore pressure build up

As stated in section 5.2.3.3, assessment of the liquefaction susceptibility on the basis of grain size distribution and other criteria for Gidabo Sandy gravel shell and compacted alluvium show that 60 to 90% of these materials lie outside the boundaries for potentially liquefiable soils. Moreover, the selected materials for the dam construction are in most cases well graded and suitable for achieving good compaction (or densification) which minimizes liquefaction

susceptibility. Therefore, these materials are considered to be non-liquefiable soils but with a potential for some pore water pressure build up during earthquake shaking. To account for the pore water pressure build up, a constant r_u value of 0.3 has been used. This value has been determined based on the publication by Malla et al. (Malla, et al., 2005), which deals with the dynamic analysis of a 75 m earth-fill dam in India. For the clay core r_u = 0.35 has been used based on Gidabo dam design report (WWDSE, 2009).

3.4.5.4 Cyclic number function

A Cyclic Number Function must be attached to the Pore Pressure Function so that N_L is defined. For high shear stress ratios (defined as the ratio of cyclic deviatoric stress to initial static effective vertical stress), only a few cycles may be required to cause liquefaction, while for low ratios, a larger number of cycles are required. The cyclic number function specifies this relationship. Fig. 3.15 shows cyclic number function curves obtained from shaking table tests on sand (DeAlba, et al., 1976) and (USNRC, 1985). Based on these publications, the Cyclic Number Function shown in Fig. 3.16 (corresponding to D_r = 70%, which was considered in the dam design report) has been used for the compacted alluvium, sandy gravel foundation and sandy gravel shell of the Gidabo dam.

The number of cycles required to cause liquefaction (N_L) can be corrected for overburden and initial static shear stresses by attaching K_a and K_σ correction functions to the cyclic number function which are discussed below.

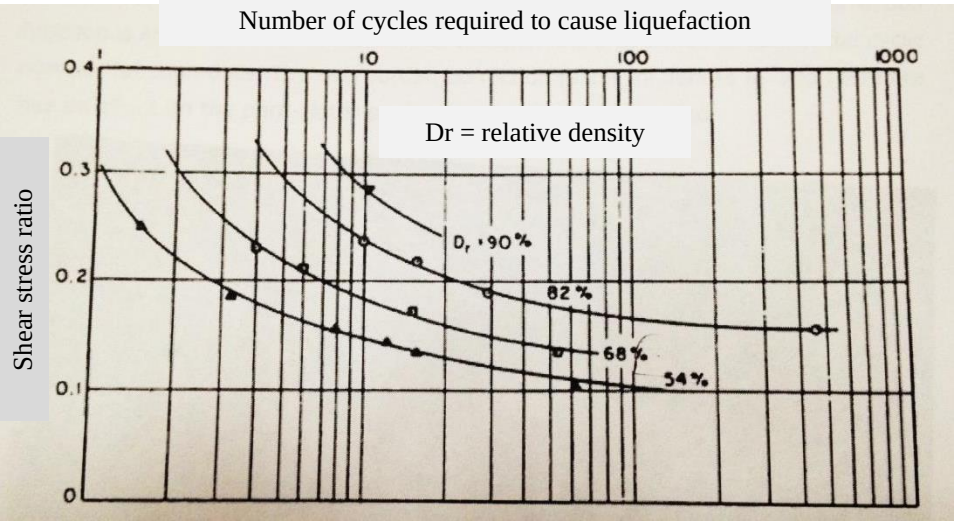

Fig. 3.15: Cyclic number function used for analysis (DeAlba, et al., 1976)

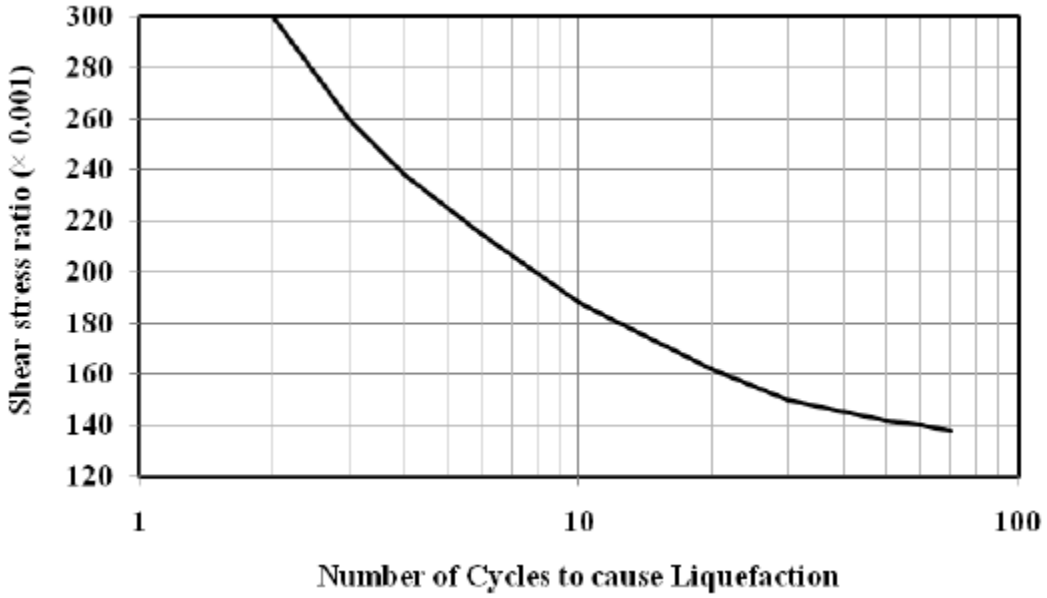

Fig. 3.16: Cyclic number function used in the analysis (DeAlba, et al., 1976) (USNRC, 1985)

Overburden Pressure Correction Function, $K\sigma$

The cyclic shear stress required to trigger liquefaction increases as the confining stress increases (Kramer, 1996). In QUAKE/W a K_σ function is specified to account for this. Marcuson et al. (Marcuson, et al., 1990) reported variation of correction factor K_σ with effective overburden pressure for different soils. The K_σ correction function is attached to the cyclic number function and is specified as part of the cyclic number function data. The overburden correction factor influences N_L and therefore has an effect on the pore-water pressure value that is computed.

Based on the work of Marcuson et al. (Marcuson, et al., 1990), the K_σ function shown in Fig. 3.17 (corresponding to the estimated average curve for sand) has been used for the compacted alluvium, sandy gravel foundation and sandy gravel shell of the Gidabo dam.

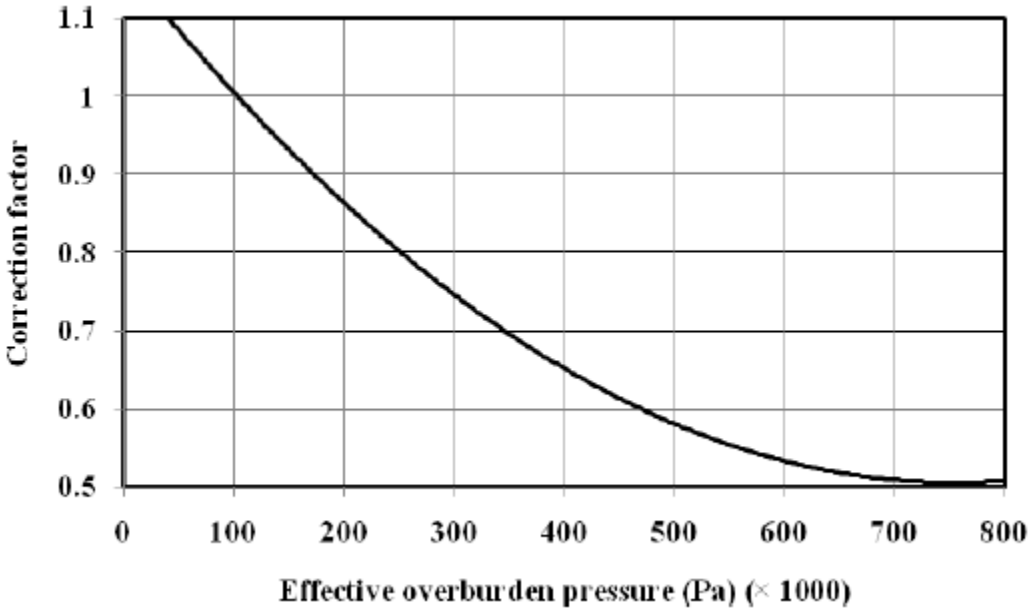

Fig. 3.17: Kσ correction function used for the analysis

Shear Stress Correction Function, Ka

The initial in-situ static shear stresses also influence the cyclic stress required to trigger liquefaction (Kramer, 1996). This function is dependent on density of the soil. Seed and Harder (Seed, et al., 1990) reported the shear stress correction function for different relative densities as shown in fig 3.18.

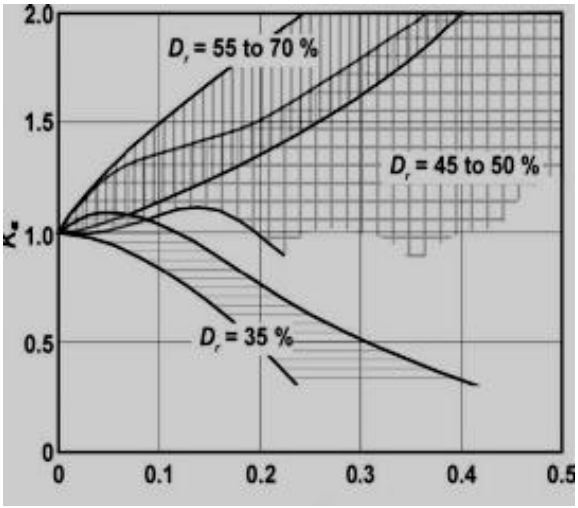

Fig. 3.18: Ka Correction factor (Seed, et al., 1990)

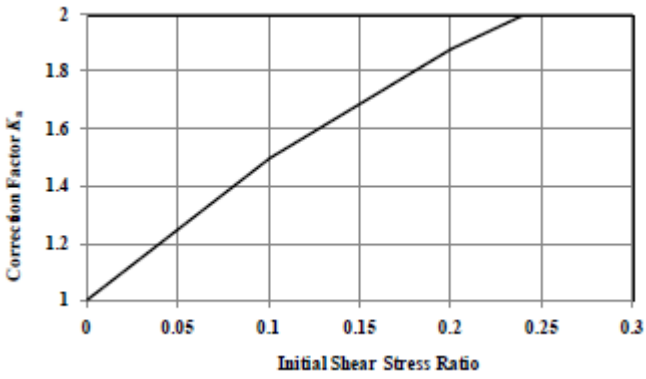

Fig. 3.19:Ka correction function used for analysis

Based on Fig. 3.18, the Ka function shown in Fig. 3.19 (corresponding to Dr = 70%) has been used for the shell, compacted alluvium and sandy gravel foundation of Gidabo dam.

4 Material models, material properties and methodology

4.1 General

4.1.1 Limit equilibrium method

These methods all employ the same definition of the factor of safety, F:

$$F = \frac{Shear\ Strength\ of\ the\ soil}{Shear\ stress\ required\ for\ equilibrium} \quad (4.1)$$

The analyses assume the factor of safety is uniform along the whole of the failure surface and cannot directly allow for localized strain weakening or progressive failure effects. The number of equations of equilibrium available is smaller than the number of unknowns in limit equilibrium analysis, so assumptions are made to make the problem determinate. Fig. 4.1 shows the slice discretization and slice forces in a sliding mass for limit equilibrium analysis.

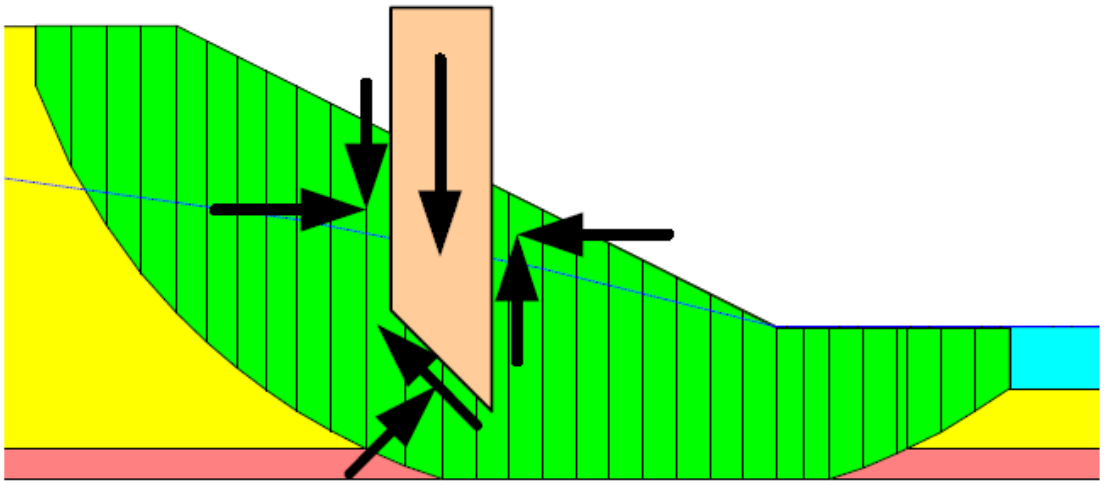

Fig. 4.1: Slice discretization and slice forces in a sliding

4.1.2 Finite element method

The role and significance of analysis and numerical modeling in geotechnical engineering has been vividly illustrated by Professor John Burland, Imperial College, London (UK). He advocated that geotechnical engineering consists of three fundamental components: the ground profile, the soil behavior and modeling. He represented these components as the apexes of a triangle, as shown in Fig. 4.2. This has come to be known as the Burland triangle ((Burland, 1987); (Burland, 1996)).

In National Research Council Report (National Research Council, 1990),*"A mathematical model is a replica of some real-world object or system. It is an attempt to take our understanding of the process (conceptual model) and translate it into mathematical terms."*

The Burland triangle idea has been widely discussed and referred to by others since it was first presented. An article on this topic was presented in an issue of Ground Engineering (Anonymous., 1999).

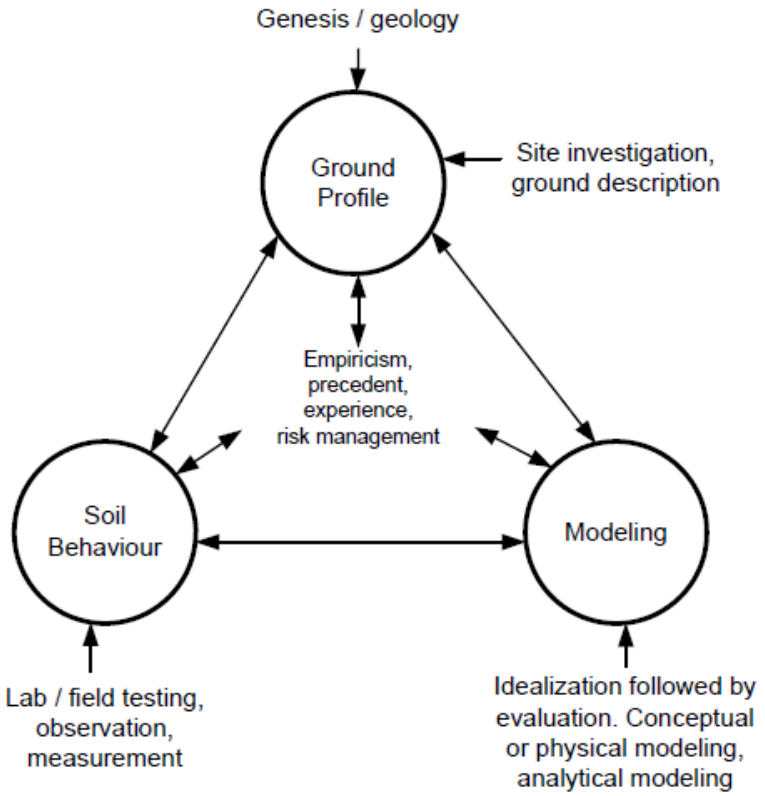

Fig. 4.2: The enhanced Burland triangle (after Anon., 1999)

Considering the importance of modeling that the Burland triangle suggests for geotechnical engineering, it is prudent that we do the modeling carefully and with a complete understanding of the modeling processes. This is particularly true with numerical modeling.

4.2 Seepage analysis using SEEP/W

4.2.1 Introduction

The flow of water through soil is one of the fundamental issues in geotechnical and geo-environmental engineering. In fact, if water were not present in the soil, there would not be a need for geotechnical engineering.

A numerical model is a mathematical simulation of a real physical process. SEEP/W is a numerical model that can mathematically simulate the real physical process of water flowing through a particulate medium. Numerical modeling is purely mathematical and in this sense is very different than scaled physical modeling in the laboratory or full-scaled field modeling.

4.2.2 Material models and properties

There are four different material models to choose from when using SEEP/W. A summary of these models and the required soil properties are given below and a discussion of the individual parameters and functions are provided in the next section (Seep/W, 2008).

Material models in SEEP/W

1) None (used to removed part of a model in an analysis)
2) Saturated / Unsaturated model
   - Hydraulic conductivity function, ratio and direction
   - Water content function
3) Saturated only model
   - Hydraulic saturated conductivity (Ksat), ratio and direction
   - Saturated water content
4) Interface model
   - Hydraulic normal and tangent conductivity

The Saturated only soil model is very useful for quickly defining a soil region that will always remain below the phreatic surface, but it should not be used for soils that will at some point during the analysis become partially saturated. If this happens, the model will continue to solve but you will be saying, in effect, that the unsaturated zone can transmit the water at the same rate as for the saturated soil. This will result in an over estimate of flow quantity and can result in an unrealistic water table.

Based on the above stated clues, material models which have been attached to different zones of embankment material have been shown in Table 4.1.

Table 4.1: Material models and properties used in seepage analysis using Seep/W

Material zone	Model	Material properties
Clay Core	Saturated/Unsaturated	Hydraulic Conductivity function Water content function
Sandy Gravel Shell	Saturated/Unsaturated	Hydraulic Conductivity function Water content function
Transition/Filter	Saturated/Unsaturated	Hydraulic Conductivity function Water content function
Compacted Alluvium	Saturated only	Hydraulic saturated conductivity (Ksat) Saturated water content
Foundation	Saturated only	Hydraulic saturated conductivity (Ksat) Saturated water content
Interface element	Both models	Hydraulic Conductivity function Water content function

4.2.3 Boundary Conditions

4.2.3.1 Fundamentals

SEEP/W uses finite element approach in seepage analysis. For a seepage analysis, the finite element equation is (Seep/W, 2008):

$$[K]\{H\} = \{Q\} \quad (4.2)$$

Where:

{H} = a vector of the total heads at the nodes, and

{Q} = a vector of the flow quantities at the node

In a finite element analysis, the prime objective is to solve for the primary unknowns, which in a seepage analysis is the total hydraulic head at each node. The unknowns will be computed relative to the H values specified at some nodes and/or the specified Q values at some other nodes. Without specifying either H or Q at some nodes, a solution cannot be obtained for the finite element equation. In a steady-state analysis, at least one node in the entire mesh must have a specified H condition. The specified H or Q values are the boundary conditions. A very important point to note is that boundary conditions can only be one of two options. We can only specify either the H or the Q at a node (Seep/W, 2008).

When specifying seepage boundary conditions, you only have one of two fundamental options – you can specify H or Q. These are the only options available, but they can be applied in various ways.

Head boundary conditions

In SEEP/W the primary unknown or field variable is the total hydraulic head, which is made up of pressure head and elevation. The elevation represents the gravitational component. In equation form the total head is defined as:

$$H = \frac{u}{\gamma_w} + y \tag{4.3}$$

Where:

H = the total head (meters)

u = the pore- pressure (kpa)

γ_w = the unit weight of water (KN/m3)

y = the elevation (meters)

The term u/γ_w is referred to as the pressure head – represented in units of length

4.2.3.2 Boundary functions

SEEP/W is formulated to accommodate a very wide range of boundary conditions. In a steady state analysis, all of the boundary conditions are either fixed heads (or pressure) or fixed flux values. In a transient analysis however, the boundary conditions can also be functions of time or in response to flow amounts exiting or entering the flow regime. Among different boundary functions integrated in SEEP/W, head versus time boundary function is a very useful boundary condition used in the present analysis.

Head versus time

A very useful boundary function is user-specified Head versus Time. The advantage of using a Head versus Time function on the reservoir side of the dam is that it avoids a "shock" unloading of the water pressure on the dam if the water level in the reservoir were instantly drawn down to some elevation.

4.2.4 Analysis Types

There are two fundamental types of finite element seepage analyses, steady-state and transient. Numerous additional constraints and conditions can be applied within each fundamental type. In steady state analysis; the pore pressure condition is estimated for long term steady state situation. Hence, the condition of the analysis is constant. Transient seepage analysis, on the other hand, is carried out in a changing condition of pore water pressure. It is changing because it considers how long the soil takes to respond to the user specified boundary conditions. Both analyses have been used in the present study.

4.3 Slope stability analysis using SLOPE/W

4.3.1 Introduction

SLOPE/W is a limit equilibrium method software package and has different methods available for slope stability analysis. Table 4.2 lists the methods available in SLOPE/W and indicates what equations of statics are satisfied for each of the methods. Table 4.3 gives a summary of the interslice forces included and the assumed relationships between the interslice shear and normal forces.

Among the listed methods, Morgenstern-Price and Spencer methods include all interslice forces and satisfy all equations of statics. Hence, Morgenstern – Price method has been used in the present study.

Table 4.2: Equations that satisfy static equilibrium

Method	Moment Equilibrium	Force Equilibrium
Ordinary or Fellenius	Yes	No
Bishop's Simplified	Yes	No
Janbu's Simplified	No	Yes
Spencer	Yes	Yes
Moregenstern – Price	Yes	Yes
Corps of Engineers – 1	No	Yes
Corps of Engineers – 2	No	Yes
Lowe – Karafiath	No	Yes
Janbu Generalized	Yes(by Slice)	Yes
Sarma-vertical slices	Yes	Yes

Table 4.3: Interslice force characteristics and relationships

Method	Interslice Normal(E)	Interslice Shear(X)	Inclination of X/E Resultant and X-E Relationship
Ordinary or Fellenius	Yes	No	No interslice forces
Bishop's Simplified	Yes	No	Horizontal
Janbu's Simplified	No	No	Horizontal
Spencer	Yes	Yes	Constant
Moregenstern – Price	Yes	Yes	Variable; user function
Corps of Engineers – 1	No	Yes	Inclination a line from crest to
Corps of Engineers – 2	No	Yes	Inclination of a ground surface at a top of slice
Lowe – Karafiath	No	Yes	Average of ground surface and slice base inclination
Janbu Generalized	Yes(by Slice)	Yes	Applied line of thrust and moment equilibrium
Sarma-vertical slices	Yes	Yes	$X = C + E\tan\Phi$

Fig. 4.3 illustrates a typical sliding mass discretized into slices and the possible forces on the slice. Normal and shear forces act on the slice base and on the slice sides.

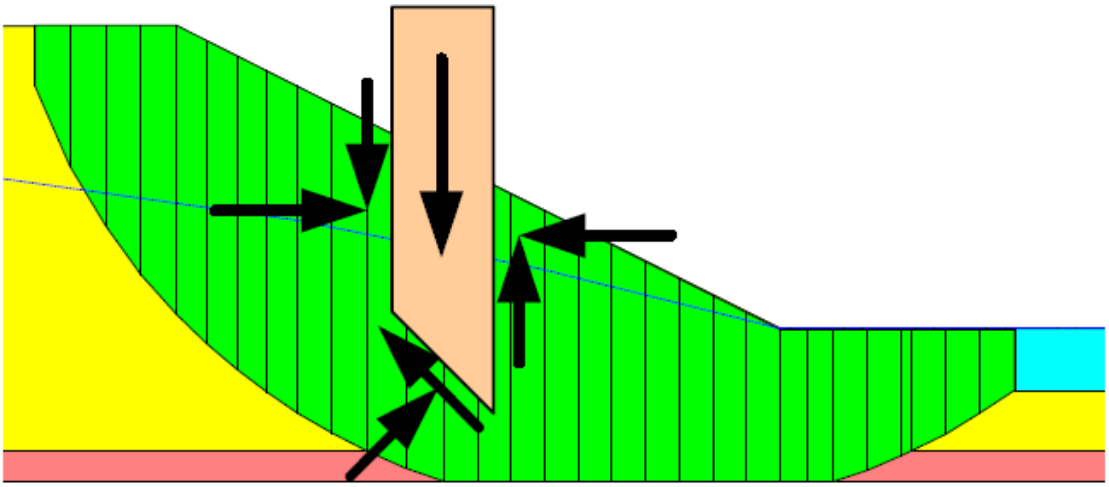

Fig. 4.3: Slice discretization and slice forces in a sliding mass

4.3.2 Material Strength and model

There are many different ways of describing the strength of the materials (soil or rock) in a stability analysis. Among various soil models built in SLOPE/W, Mohr-Coulomb has been used for material strength characteristics. The most common way of describing the shear strength of geotechnical materials is by Coulomb's equation which is expressed as in equation form:

$$\tau = c + \sigma_n \tan\varphi \qquad (4.4)$$

Where:

τ = shear strength (i.e. shear at failure)
c = cohesion
σ_n = normal stress on shear plane, and
φ = angle of internal friction

Unsaturated shear strength

Soil suction or negative water pressures have the effect of adding strength to a soil. In the same way that positive pore-water pressures decrease the effective stress and thereby decrease the strength, negative pore-water pressures increase the effective stress and in turn increase the strength. The shear strength of unsaturated soil is:

$$s = c' + \sigma_n \tan\phi' + (u_a - u_w)\tan\phi^b \quad (4.5)$$

Where:

u_a = the pore – air pressure

u_w = the pore – water pressure

φ^b = the angle defining the increase in strength due to the negative pore – water pressure

The term (ua – uw) is called suction when presented as a positive number. The angle φ*b* is a material property. For practical purposes, φ*b* can be taken to be about ½ φ*'* (Slope/W, 2008).

Considerable research has been done to better quantify the unsaturated shear strength of a soil using the soil-water characteristic curve and the effective shear strength parameters (c' and φ'). As a better alternative to the use of φ*b* to model the increase of shear strength due to soil suction, the following estimation equation proposed by Vanapalli et. al. ((Vanapalli, et al., 1996) is implemented in SLOPE/W:

$$s = c' + (\sigma_n - u_a)\tan\phi' + (u_a - u_w)\left[\left(\frac{\theta_w - \theta_r}{\theta_s - \theta_r}\right)\tan\phi'\right] \quad (4.6)$$

In the above equation, θw is the volumetric water content, θs is the saturated volumetric water content and θr is the residual volumetric water content. The residual volumetric water content is assumed to be equal to 10% of the saturated volumetric water content in SLOPE/W. Note that φ*b* is not used in the above equation. It is this option which has been used in the analysis of this study.

Soil unit weight

The sliding mass weight or gravitational force is applied by assigning the soil a unit weight. The slice cross sectional area times the specified unit weight determines the weight of the slice. SLOPE/W is formulated on the basis of total forces. The unit weight consequently needs to be specified as the **total** unit weight. SLOPE/W allows for a separate unit weight above the water table, but use of this parameter is seldom necessary (Slope/W, 2008).

Pore-water

The most realistic position of the critical slip surface is obtained when effective strength parameters are used in the analysis. Effective strength parameters, however, are only meaningful when they are used in conjunction with pore-water pressures. Accordingly, the pore-water pressure in this study has been taken from SEEP/W steady-state seepage analysis and transient analysis at any particular time step.

4.3.3 Mobilization of reinforcement forces

The SLOPE/W equilibrium equations are based on the shear mobilized at the base of each slice, and the mobilized shear is the shear strength divided by the factor of safety. In equation form, the mobilized shear *Sm* is:

$$S_m = \frac{S_{soil}}{F\ of\ S} \tag{4.7}$$

If the reinforcement is to be included to increase the shear resistance, then the reinforcement forces must also be divided by the factor of safety. *Sm* then is:

$$S_m = \frac{S_{soil}}{F\ of\ S} + \frac{S_{\text{reinforcement}}}{F\ of\ S} \tag{4.8}$$

A point of significance is that the soil strength and the shear resistance arising from the reinforcement are both divided by the same overall global factor of safety. The implication is that the soil shear resistance and reinforcement shear resistance are developed and mobilized at the same rate.

If the reinforcement is considered as contributing to reducing the destabilizing force, then it is assumed that the reinforcement is fully mobilized immediately and the reinforcement forces consequently are not divided by the overall global factor of safety. Thus, as geofabrics are used as a reinforcing material, an option which considers reinforcement as addition for shearing resistance of the soil is followed in the present analysis

Geo-fabric reinforcement

The specified parameters for fabrics are shown in Table 4.4 below.

Table 4.4: Fabric (geotextile) parameters used in the analysis

Item nr	Parameters	Values used in the analysis	Remarks
1	Bond skin friction per unit area(F/L2)	Function of overburden pressure	Coefficient taken as percentage of φ'
2	Bond safety factor	Unity	function of overburden stress
3	Fabric ultimate capacity	Long term design strength	Corrected
4	Fabric safety factor	Unity	Since LTDS used
5	Load orientation	Along the reinforcement	
6	Interface factor	2	Double face

Bond resistance a function of overburden stress

The Skin Friction can be a function of the overburden stress, friction parameters, *c'* and φ', and an interface factor. With this option, SLOPE/W computes the effective overburden stress from the slice that includes the reinforcement force; that is, the slice base that intersects the fabric. Note that both the overburden stress and porewater pressure are computed at the slice base center. The Bond Resistance for each fabric then is:

Bond Resistance = (c + effective overburden stress x $tan\ \phi$) x interface factor

It is this approach which has been used in the present study.

4.4 Stress-deformation modeling with SIGMA/W

4.4.1 Applications

SIGMA/W can be used to compute stress-deformation with or without the changes in pore-water pressures that arise from stress state changes. In addition, it is possible to model soil structure interaction using beam or bar elements (SIGMA/W, 2010).

4.4.2 Material models and properties

Linear-elastic model

The simplest SIGMA/W soil model is the linear elastic model (Fig.4.4) for which stresses are directly proportional to the strains. The proportionality constants are Young's Modulus, *E*, and Poisson's ratio, ν. Other relevant parameters have been presented in Table 4.5.

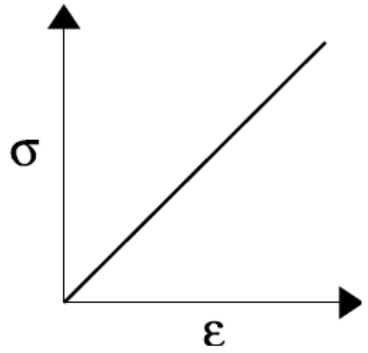

Fig. 4.4: Linear elastic model

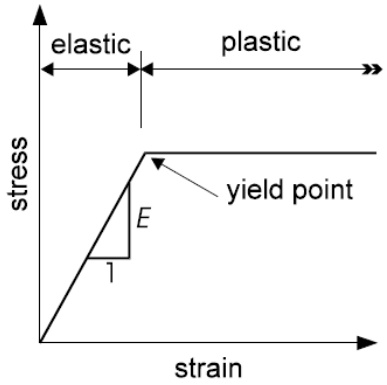

Fig. 4.5: Elastic-perfectly plastic constitutive relationship

Table 4.5 **:** Linear-elastic properties

Edit Box Label	Property
E Modulus	Young's Modulus
Poisson's Ratio	constant value
Cohesion	constant value
Friction angle	degrees

Elastic-plastic model

The Elastic-Plastic model in SIGMA/W describes an elastic, perfectly-plastic relationship. A typical stress-strain curve for this model is shown in Fig.4.5. Stresses are directly proportional to strains until the yield point is reached. Beyond the yield point, the stress-strain curve is perfectly horizontal. Important parameters required for this model are presented in Table 4.6.

Table 4.6: Elastic – plastic material properties

Edit Box Text	Property
E modulus	Initial linear – elastic stiffness of the soil
Poisson's ratio	Constant value
cohesion	Cohesive strength of the soil
phi	Soil internal friction angle in degrees

E-modulus functions

The soil stiffness modulus *E* can be specified as a constant or as a function of the effective overburden stress.

4.4.3 Boundary conditions

Different boundary condition types are implemented to support virtually all load deformation modeling scenarios. In SIGMA/W, displacement, force or spring boundary conditions may be applied to points or nodes along lines, and stress and fluid pressure boundary conditions may be applied to element edges on lines (SIGMA/W, 2010).

4.4.4 Analysis Types

In SIGMA/W, different analyses are incorporated. Among this, insitu analysis and stress – deformation analysis have been adopted in the present study. Insitu analysis has been carried out to simulate the initial stress condition and stress – deformation analysis has been carried out to find forces in the reinforcement.

4.5 Dynamic modeling with QUAKE/W

4.5.1 Introduction

QUAKE/W is a geotechnical finite element software product used for the dynamic analysis of earth structures subjected to earthquake shaking and other sudden impact loading such as, for example, dynamiting or pile driving (QUAKE/W, 2010).

4.5.2 Material models and properties

The shear modulus G is the most common soil property in a dynamic analysis. There are a couple of ways in QUAKE/W to specify G and how G is affected by cyclic stresses. Closely related to the soil stiffness is the soil's ability to dissipate energy associated with seismic waves. This property is called damping.

4.5.2.1 Soil behavior models

In Quake/W software package, there are four different material models to choose from (QUAKE/W, 2010). These are none model, linear elastic model, equivalent linear model and non-linear model. Among this equivalent linear model has been selected and used in the present study. Summary of equivalent linear model and the required soil properties are presented in the following section.

Equivalent linear model

In equivalent linear model, the soil stiffness *G* is modified in response to computed strains. With the equivalent linear model, QUAKE/W starts a dynamic analysis with the specified soil stiffness. QUAKE/W steps through the entire earthquake record and identifies the peak shear strains at each Gauss numerical integration point in each element. The shear modulus is then modified according a specified *G* reduction function and the process is repeated. This iterative procedure continues until the required *G* modifications are within a specified tolerance. The important behavior to comprehend here is that *G* is a constant while stepping through the earthquake record. *G* may be modified for each pass through the record, but remains constant during one pass. Fig. 4.6 illustrates this graphically. The straight lines indicate that *G* is a constant during one iterative pass through the earthquake record. The change in slope reflects the reduction in *G* between iterations. It this model which has been used in this study. Material properties used in this model are summaerized as follows.

- Unit weight, Poisson's ratio, c′ and Ø′
- Damping ratio constant or function
- Ka and Ks functions
- Pore-water pressure function

- G reduction function
- Gmax constant or function
- Steady state strength and collapse surface angle (for liquefied zones)

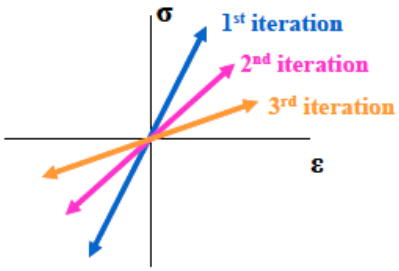

Fig. 4.6: Change in G with each iteration through the earthquake

In the Equivalent Linear method, the excess pore-pressures are calculated based on peak dynamic shear stresses. The peak values however are not known until the end of the dynamic analysis and so the effective stresses cannot be changed during the shaking. Excess pore-pressures can only be calculated after the dynamic part of the analysis has been completed.

4.5.2.2 Material properties

Shear modulus, G

The shear modulus *G* can be specified as a constant for all three constitutive soil models discussed above. The shear modulus is referred to as Gmax. It is considered to be a small-strain shear modulus and therefore the maximum value for a particular soil and consequently the designation Gmax. It is much more common and realistic to define Gmax as a function of the stress state in the soil. Generally, the soil stiffness increases with increases in confining or overburden stress. To capture this behavior, Gmax values in QUAKE/W can be specified as functions (QUAKE/W, 2010).

QUAKE/W has some sample functions which can be useful for research purposes and preliminary analyses. The sample functions included with QUAKE/W are provided to assist designers for analysis that shall be used in case of shortage of specific project material properties.

G-reduction function

A soil subjected to dynamic stresses tends to ‘soften’ in response to cyclic shear strain. In the Equivalent Linear soil model, this softening is described as a ratio relative to Gmax as illustrated in Fig. 4.7. This is called a G-reduction function. The cyclic shear strain comes from the finite element analysis. The computed shear strain together with the function and the specified Gmax are used to compute new *G* values for each of the iterations.

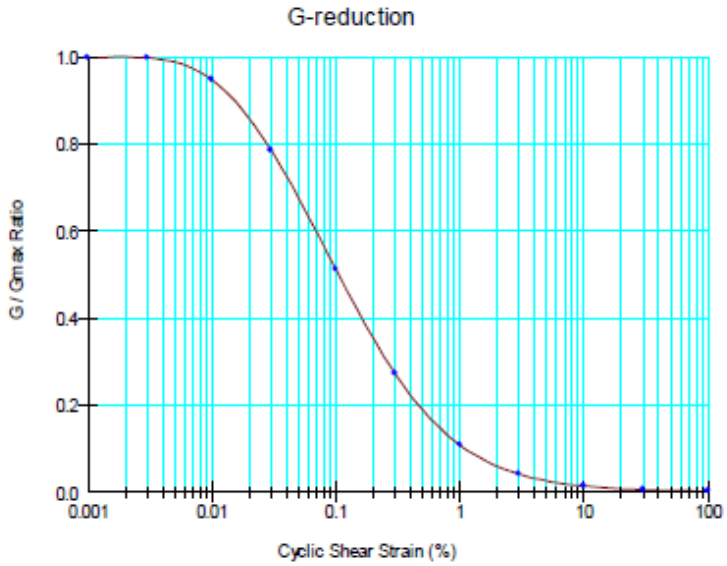

Fig. 4.7: Typical G reduction function

Damping ratio

As with Gmax, the damping ratio in QUAKE/W can be specified as a constant or as a function. The damping ratio is a function of the cyclic shear strain, the same as the G-reduction function. A typical damping ratio function is presented in Fig. 4.8.

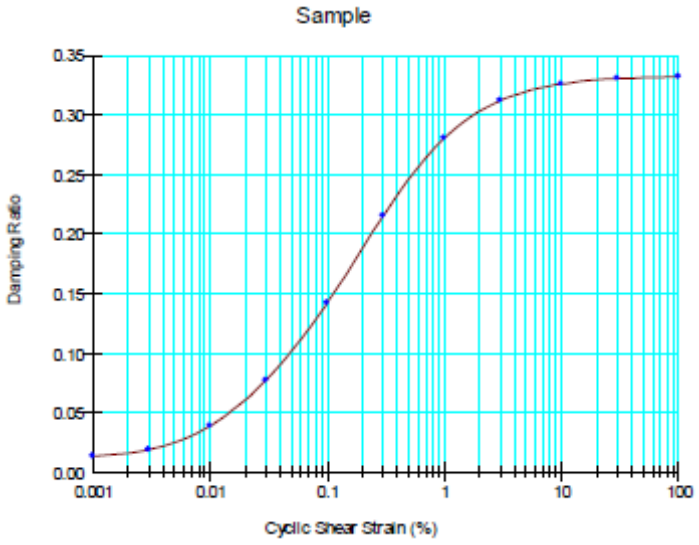

Fig. 4.8: A damping ratio function

The above Damping Ratio formula was developed for confining pressures expressed in units of kPa. The Damping ratio, however, is not very sensitive to the confining pressure, so the exact units are not too important. It is important though to realize the expression for G/Gmax was developed for pressure in kPa units.

4.5.2.3 Boundary Conditions

Boundary condition locations

In Quake/W, all boundary conditions must be applied directly on geometry items such as region faces, region lines, free lines or free points. There is no way to apply a BC directly on an element edge or node. The advantage of connecting the BC with the geometry is that it becomes independent of the mesh and the mesh can be changed if necessary without losing the boundary condition specification (QUAKE/W, 2010).

Nodal displacement boundary conditions

Nodal displacements are most often specified to give the analysis a frame of reference – usually the displacement is zero. Take for example, the case in Figure 4.9. Along the base of the problem, the displacement is specified as zero. This means the computed motion will be relative to the base being fixed on both the *x* and *y* directions.

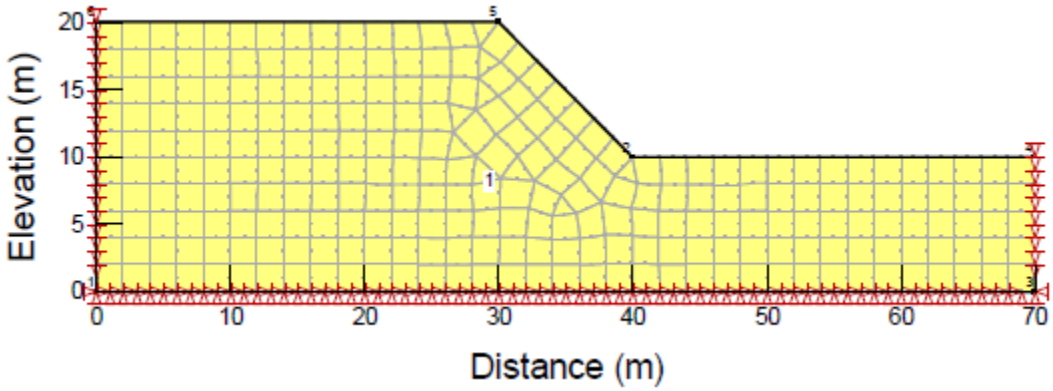

Fig. 4.9: Illustrations of fixed boundary conditions

In Fig.4.9, it is deemed appropriate to allow horizontal motion at the ends of the problem, but not vertical motion. The reasoning is that the horizontal motion beyond the ends of the problem will be the same as at the ends of the mesh.

Shear in the soil will, however, prevent, or keep to a minimum, the vertical displacement at the ends of the problem. Consequently, only the vertical displacements are specified at the ends of the problem.

Specifying a vertical displacement of zero at the ends is not strictly correct, but the boundary is sufficiently far away from the slope so that a zero-displacement boundary does not significantly affect the dynamic shear stresses in the slope, which is the main objective of this analysis. Accordingly, more than three times of the dam height away from the bottom of the slope of the dam has been used to fix the vertical boundary condition.

4.5.2.4 Analysis types

4.5.2.4.1 Introduction

There are basically four types of analyses available in QUAKE/W. They are:

- Initial Static
- Equivalent Linear Dynamic
- Equivalent Linear PWP Only
- Nonlinear Dynamic

4.5.2.4.2 Initial in-situ stresses

A QUAKE/W dynamic analysis cannot be solved without first establishing the initial stresses. Material properties like the Shear Modulus (G), for example, are usually a function of the effective stresses in the ground. Other variables like the Cyclic Stress Ratio are based on the initial effective stresses. Consequently, it is essential to know the initial state of stress in the ground before starting the dynamic analysis.

QUAKE/W has a special type of analysis called 'Initial Static' that is formulated specifically for establishing the initial stresses. Alternatively, the initial stresses can be obtained from a SIGMA/W analysis. The Initial Static method is identical to the SIGMA/W Insitu method. In the present study SIGMA/W in situ stress method has been used in initial insitu stress analysis.

4.5.2.4.3 Dynamic analysis

Performing a dynamic analysis is the main essence of using QUAKE/W. It is that part of the analysis that models the response of an earth structure to some kind of osculating or sudden impulse force – forces such as those that arise from earthquake shaking or blasting. Broadly speaking, the main aspects of a dynamic analysis are the:

- Dynamic driving forces: are the seismic forces associated with earthquake shaking. Acceleration time history records are commonly given as dynamic driving forces
- Boundary conditions: it is required to solve the problem from some user defined boundary condition such that the motion of the structure or domain is relative to some kind of specified displacement.
- Material properties: whether the materials behave in a linear or non-linear manner during a dynamic analysis is controlled by the type of Material Model selected.
- Temporal integration; that is, time stepping through the time history record of the dynamic input forces

5 Analysis results and discussions of Gidabo earth fill dam

5.1 Static Stability Analysis

5.1.1 Embankment type and geometry

As it is discussed in project characterization section (chapter 3), Gidabo dam is a zoned earth fill type of dam as shown in Fig 5.1. The as built geometric data has been presented as shown in Table 5.1.

Table 5.1: As Constructed Geometry data for Gidabo earth fill dam

Upstream Slope					Downstream Slope				
RL	Berm Width(m)	Remarks	Slope (H:V)	Elevation	RL	Berm Width (m)	Remarks	Slope (H:V)	Elevation
1204.55		GL	3.0:1.0	1204.55 ~ 1212.10	1204.55		GL	3.0:1	1204.55 ~ 1214.50
1212.10	8	Coffer dam Crest	3.0:1.0	1212.10 ~ 1220.792	1214.50	5	Berm	3.0:1	1214.50 ~ 1220.79
1226.78	8	Dam Crest	2.46~1.0	1220.792 ~ 1126.785	1226.78	8	Dam Crest	2.46~1	1220.79 ~ 1126.78

5.1.2 Loading condition and minimum factor of safety

The stability of an embankment depends on the characteristics of the foundation and fill materials, on the geometry of the embankment section, and additional factors such as presence of water, loading conditions etc. Loading condition, shear strength parameters used in the analysis, pore pressure characteristics and minimum factor of safety required in the analysis are presented in Table 5.2.

The stability of the proposed Gidabo Dam has been analyzed using state of the art software – Slope/W from Geo-Slope International Ltd of Canada. The stability analyses had been conducted in order to determine the factor of safety for various slip surfaces of:

- Downstream slopes under steady state seepage condition without earthquake.
- Upstream slope under sudden drawdown condition.

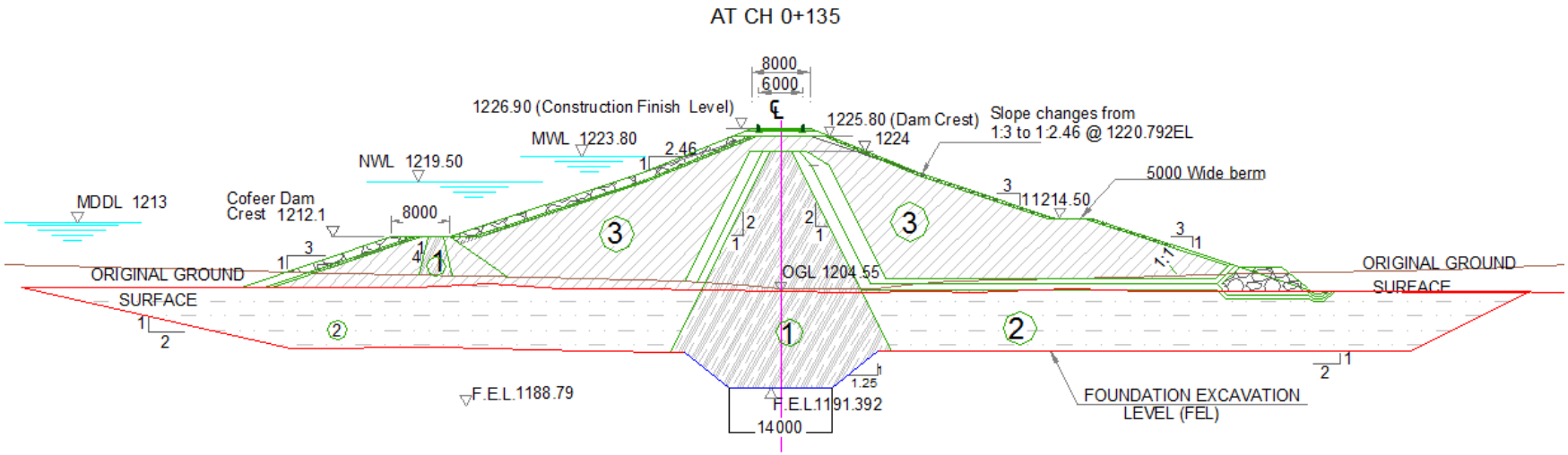

Legend: 1 Impervious Core material

2 Compacted alluvium (DR>=70 %)

3 Compacted granular material (DR>=70%)

Fig. 5.1: Typical Section Gidabo Earth Fill Dam

Table 5.2: Minimum factors of Safety (adapted from USBR Design standards Nr 13: embankment dams, static stability analysis)

Loading Condition	Shear strength parameters	Pore pressure characteristics	Minimum factor of safety
Steady-state seepage	effective	Steady – state seepage under active conservation pool	1.5
Operational condition	Effective or undrained	Rapid drawdown from normal water surface to inactive water surface	1.3

5.1.3 Model of the Gidabo earth fill dam

The dam has been modeled uisng SLOPE/W and shown in Fig.5.2

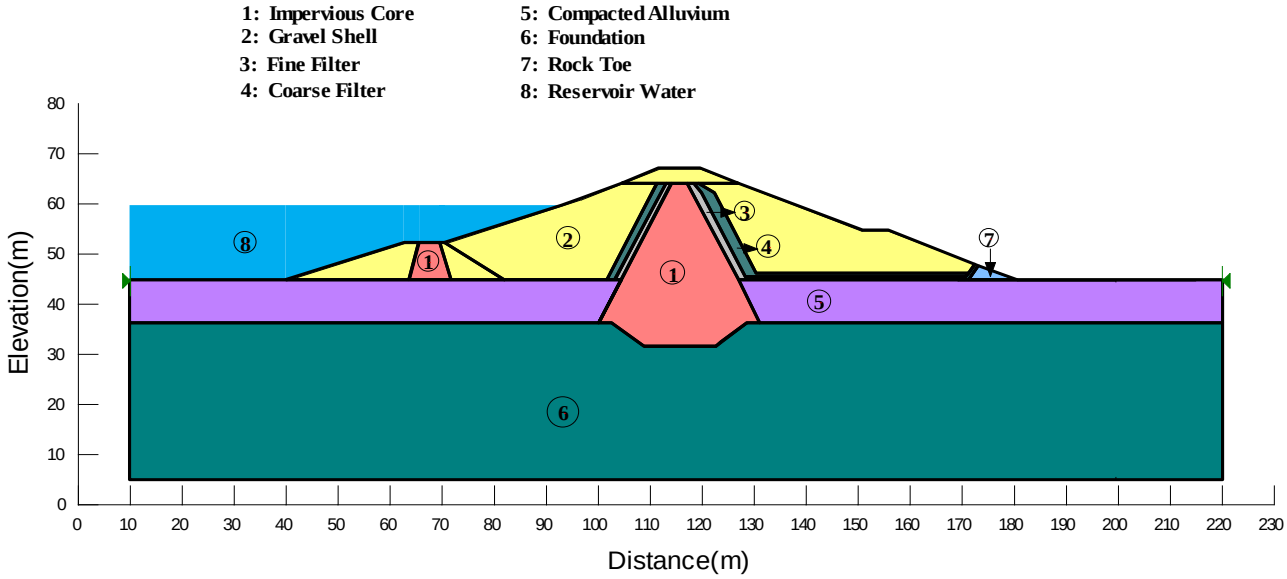

Fig. 5.2: Model of Gidabo Earth Fill Dam from Slope/W

5.1.4 Downstream slope stability analysis of dam for steady state seepage condition

Gidabo earth fill dam designed by water works design and supervison enterprise has been used for the study. Modeling of the dam has been carried out and come up with the figure as shown in Fig. 5.2. In this study, different packages of Geoslope has been used for analysis and the sequence followed in the study is shown in fig. 5.3. Hence, before stability analysis, pore pressure condition has to be determined. This can be done by seepage analysis using SEEP/W as presented in the following section.

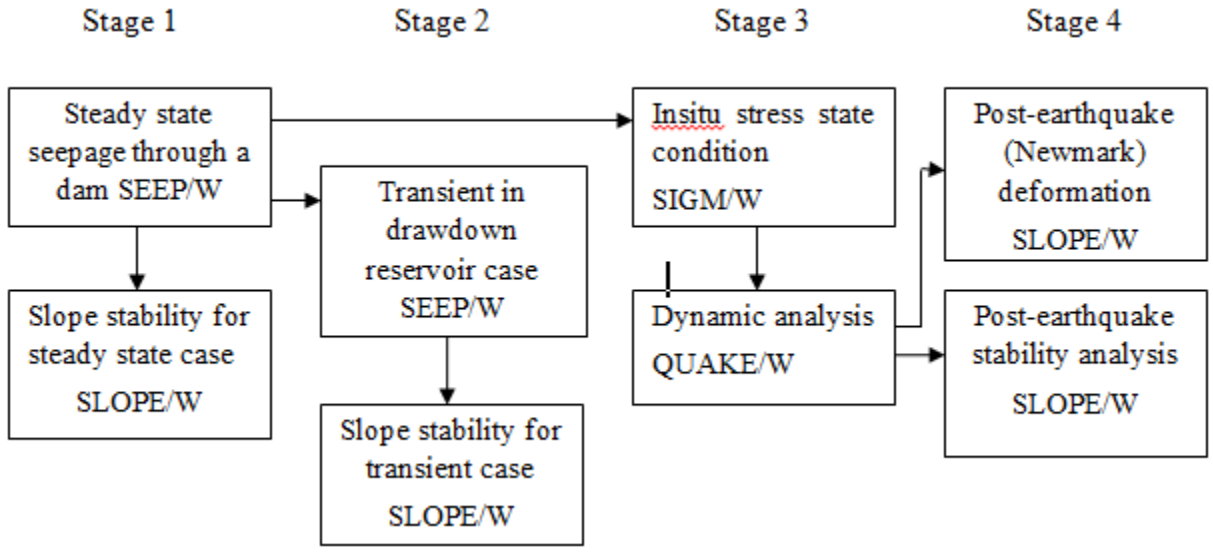

Fig. 5.3: Diagram showing the sequence of analysis followed in this research.

5.1.4.1 Seepage analysis results from SEEP/W

The dam in this study is modeled by SEEP/W ,which could be used to analyze any seepage problems. Seep/W uses the finite element method for two dimesional darcy's flow in both saturated and unsaturated soils. The major differences between water flow in saturated and unsaturated soil are:

- The coefficient of permeability is not a constant but it is a function of degree of saturation or matric suction in unsaturated soils
- The volumetric water content of unsaturated soil can vary with time.

Having modeled the dam using seep/W and attaching the necessary hydraulic parameters, the results of the analysis have been shown in Fig. 5.4 to 5.6. Fig.5.4 shows the finite element model with head boundary condition for upstream and downstream side of the dam. Fig. 5.5 shows total head contour for the given boundary condition. The pore water pressure to be used as an input for stability analysis has been presented as shown in Fig.5.6. Thus, SEEP/W generated pore pressure is taken to SLOPE/W for stability analysis.

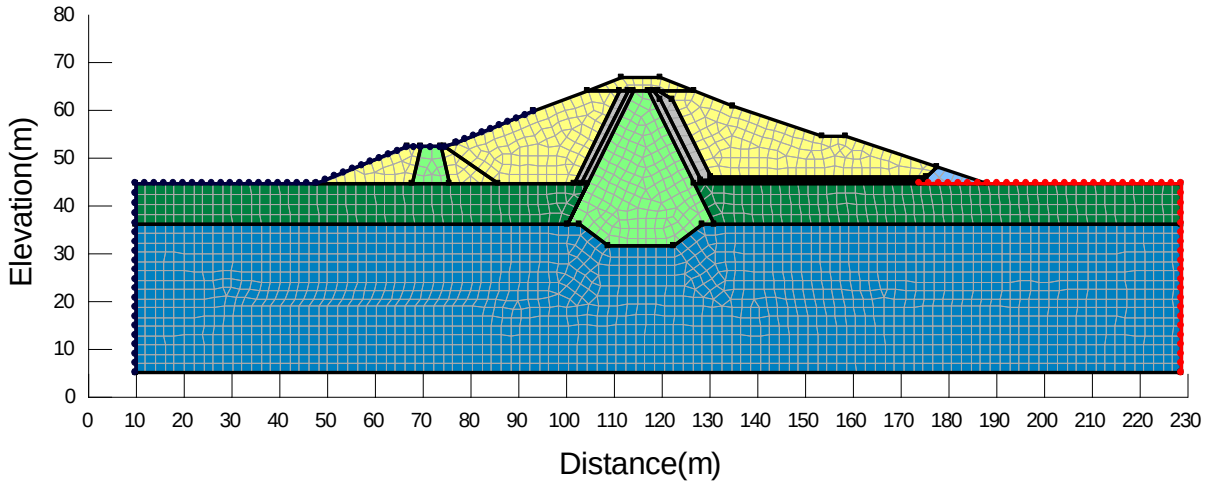

Fig. 5.4: Finite element model for seepage analysis (taken from Seep/W)

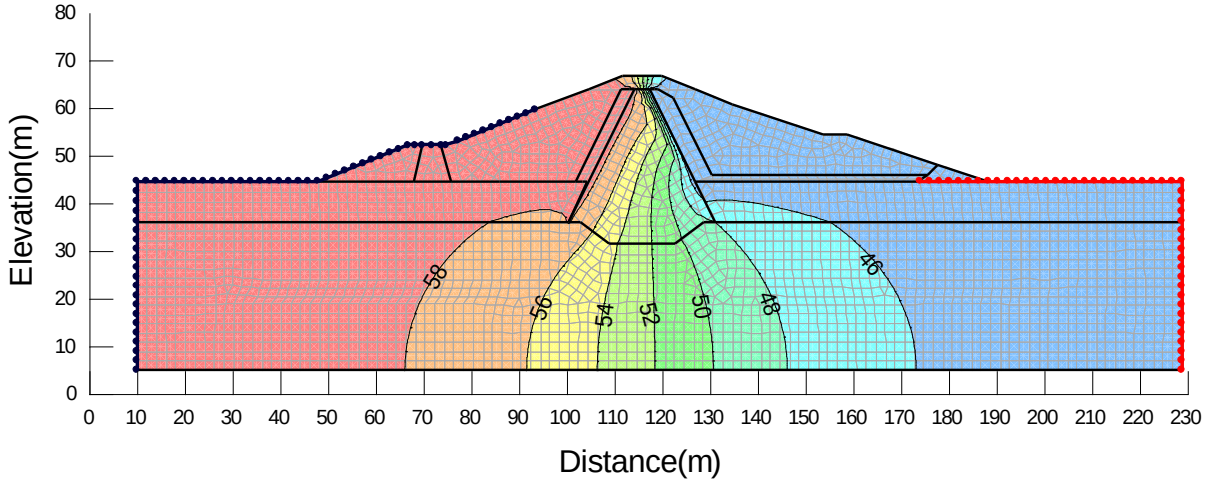

Fig. 5.5: Isopotential lines (total head) contour

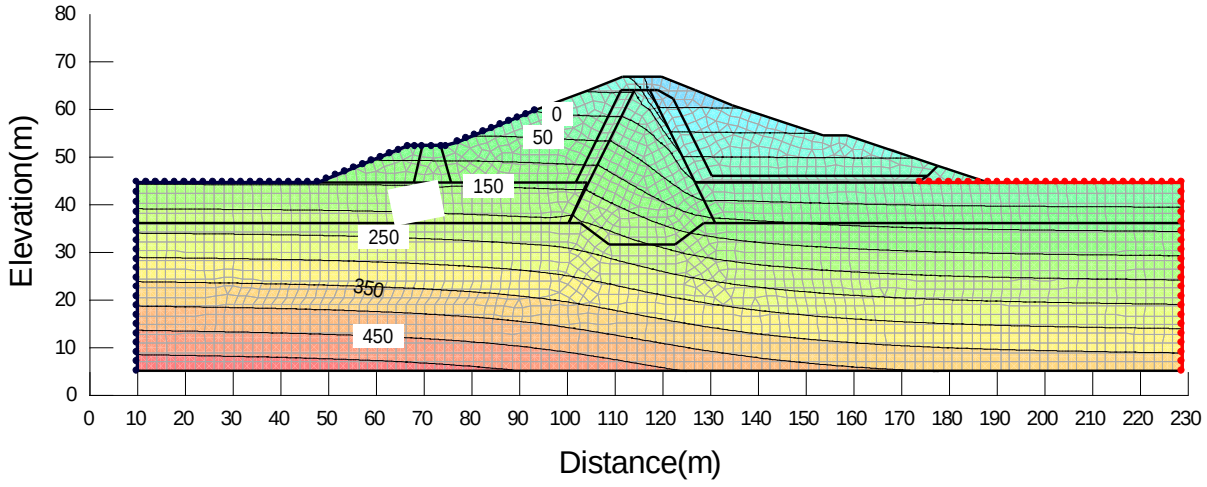

Fig. 5.6: Pore Water Pressure Contour (kPa)

The stability analysis of downstream slope under steady state condition has been checked by considering Normal water level (NWL) for normal loading condition. The phreatic surface computed with the help of Seep/W (see Fig. 5.6) was used to set up the pore water pressure line in the stability analysis. The result of the analysis has been presented in the next sub section with the corresponding reinforced analysis results.

5.1.4.2 Stability analysis of reinforced downstream slope for steady state seepage condition(using SEEP/W generated pore pressure)

The downstream slope of Gidabo earth fill dam is then considered to be reinforced with horizontal layers of geotextile. As provision of reinforcing layers of geotextile would result in increase in factor of safety,steeper slopes may be provided to the downstream side of the dam. The downstream slope of the dam is therefore changed in decreament by 0.25H:1V. The spacing between reinforcing layers was varied from 0.4 to 3.2m for each case. Analysis is then carried out for each case separately. During analysis of each case the length of reinforcing layer and the offset from the downstream face of the dam was varied in such a way that the reinforcing layers remains activated i.e. intersect the the potential slip surface and govering criteria of failure for reinforcing layer remains as tensile. This insures the maximum utilization of reinofrcing layers and results in economy. Analysis results for each case is presented as in the following section.

Analaysis has been made for each slope before reinforcement and horizontal layers of geotextile have been inroduced to the slope and analysis is made by varying spacing of reinforcement from 0.4m to 3.2m. Accordingly, to save paper space we will going to present factor of safety figure of one reinforcement spacing case for each slope, but it will be summarized using graph for all spacing cases of a given slope.

2.5H:1V Slope case

Stability analysis of a downstream slope for long term steady state seepage condition before reinforcement is carried out and the result is shown in Fig. 5.7. Then, horizontal layers of reinforcement has been introduced to the slope and analysis is done. During analysis, keeping the spacing constant, the length of reinforcement and offset from the downstream slope have been varied until the improvement gets its maximum value. For example as shown in Fig 5.8, the analysis has been carried out for a spacing of 0.4m by varying length and offset from the downstream slope until it gets a maximum value of improvement. Hence, due to reinforcement, the factor of safety is improved from 1.594 to 2.058. This analysis procedure continues for another spacing and the summary of results for all reinforcement spacing corresponding to this slope has been presented as shown in Fig 5.10. From this summary figure, we can see that the factor of safety has been improved by from 21% to 29%.

Similar procedures have been followed for other slope cases and analysis results have been presented in the subsequent sections (Fig.5.10 to 5.28).

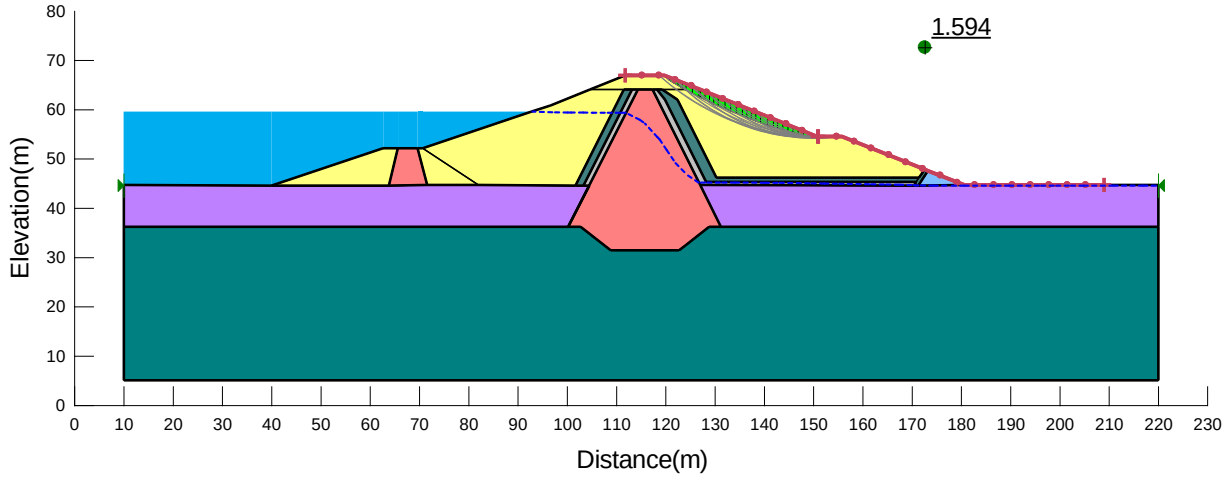

Fig. 5.7: Stability analysis of downstream slope under steady state condition (unreinforced: 2.5H: 1V)

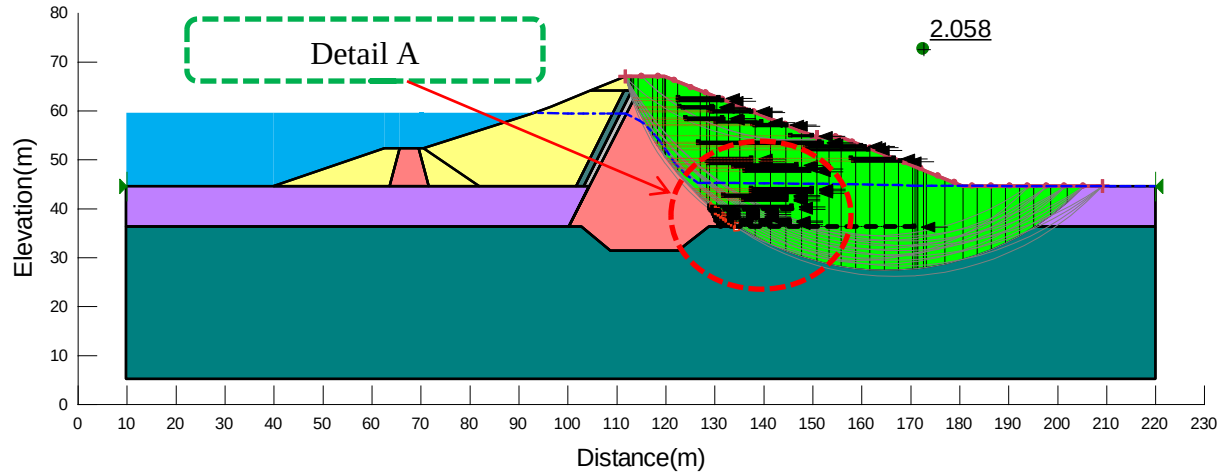

Fig. 5.8: Analysis of reinforced downstream slope under steady state condition (2.5H: 1V)

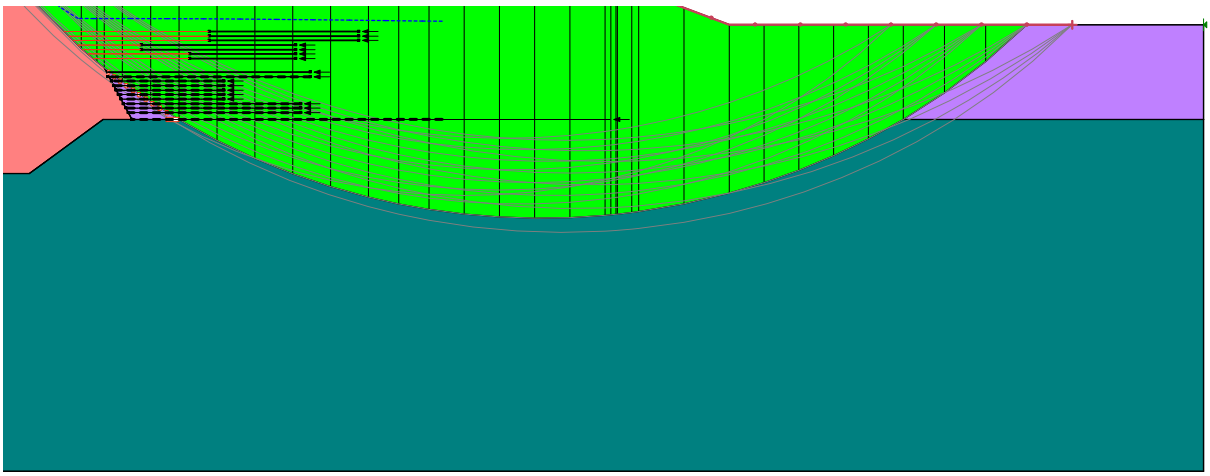

Fig.5.9: Detail A which shows how failure surface is intersected by reinforcement (2.5H: 1V)

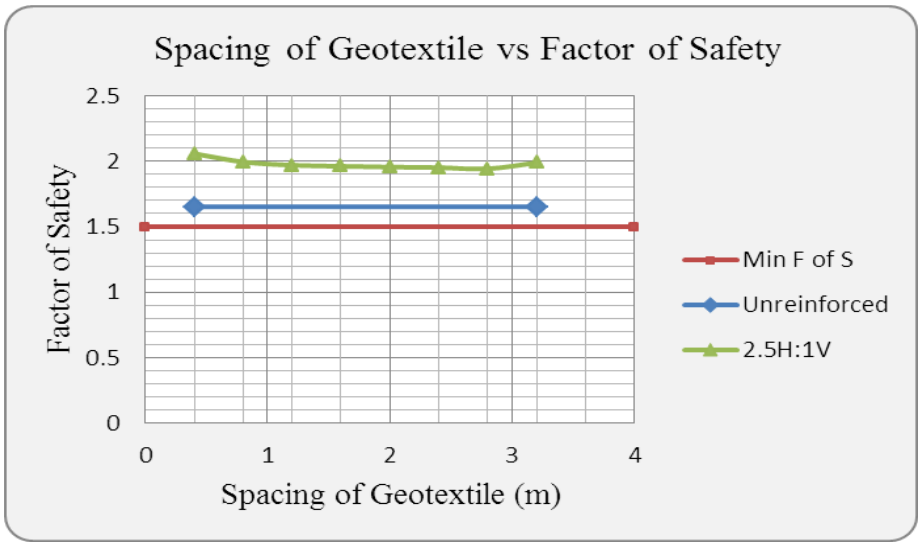

Fig. 5.9: Variation of factor of safety with respect to spacing between geotextile layers for steady state condition

2.25H:1V slope case

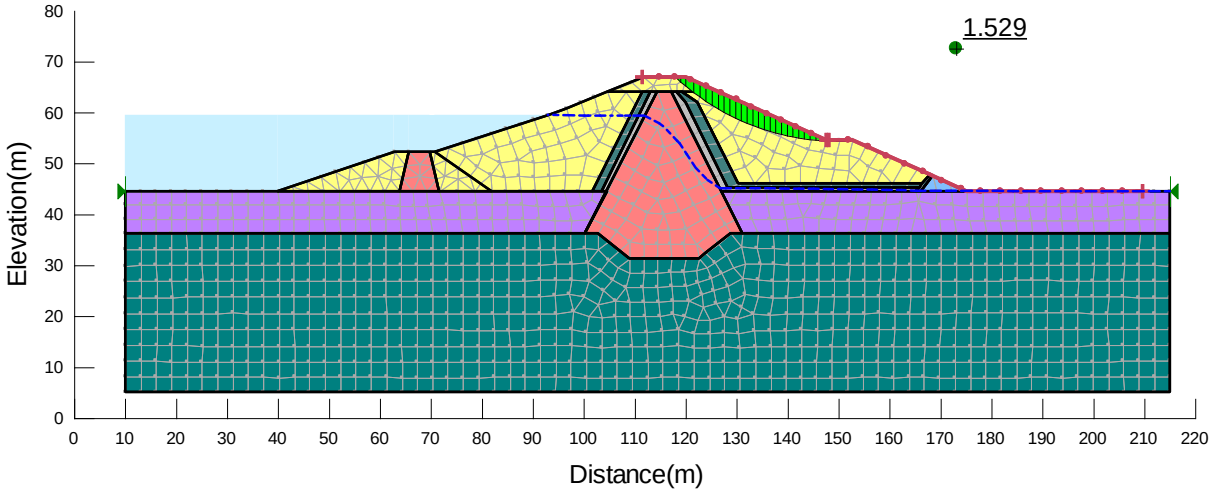

Fig. 5.10: Stability analysis downstream slope under steady state condition (unreinforced: 2.25H: 1V)

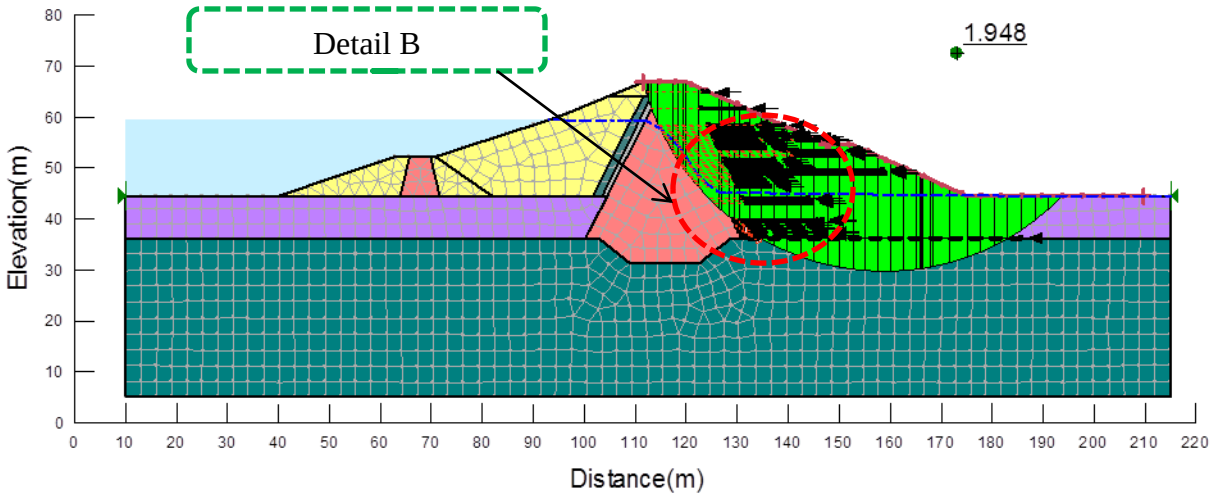

Fig. 5.11: Stability analysis of reinforced downstream slope under steady state condition (2.25H: 1V)

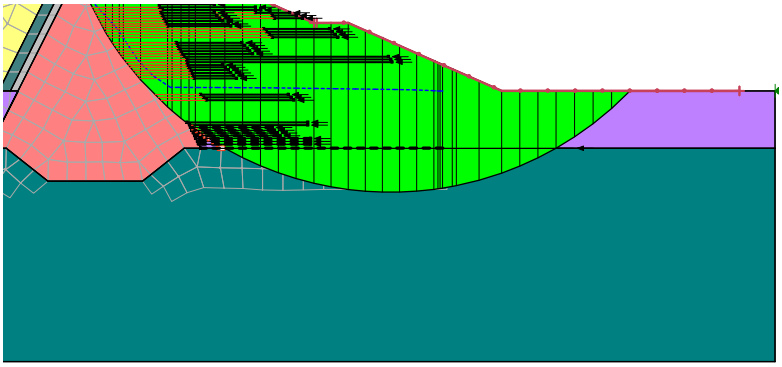

Fig.5.12: Detail B which shows how failure surface is intersected by reinforcement (2.25H: 1V)

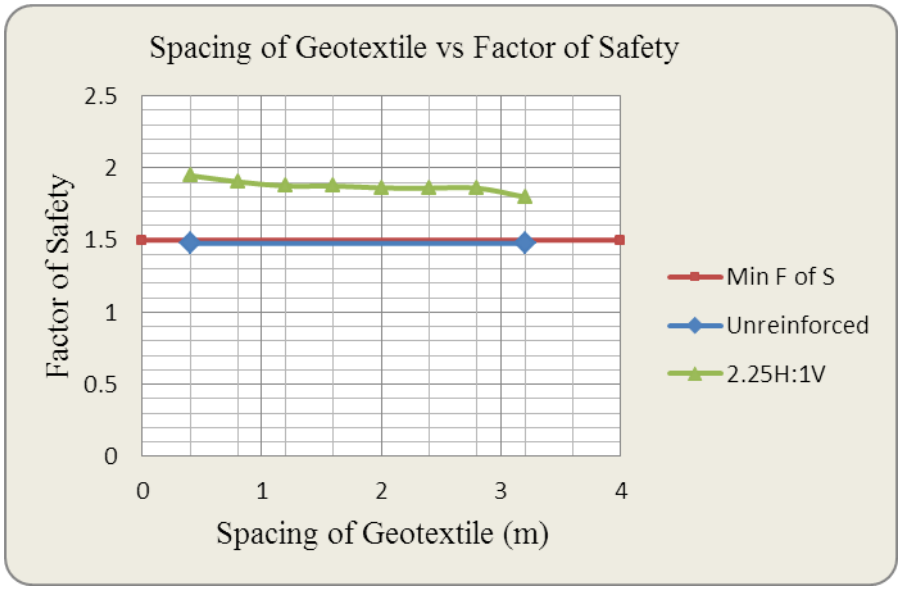

Fig. 5.12: Variation of factor of safety with respect to spacing between geotextile layers for steady state condition

2.0H:1V slope case

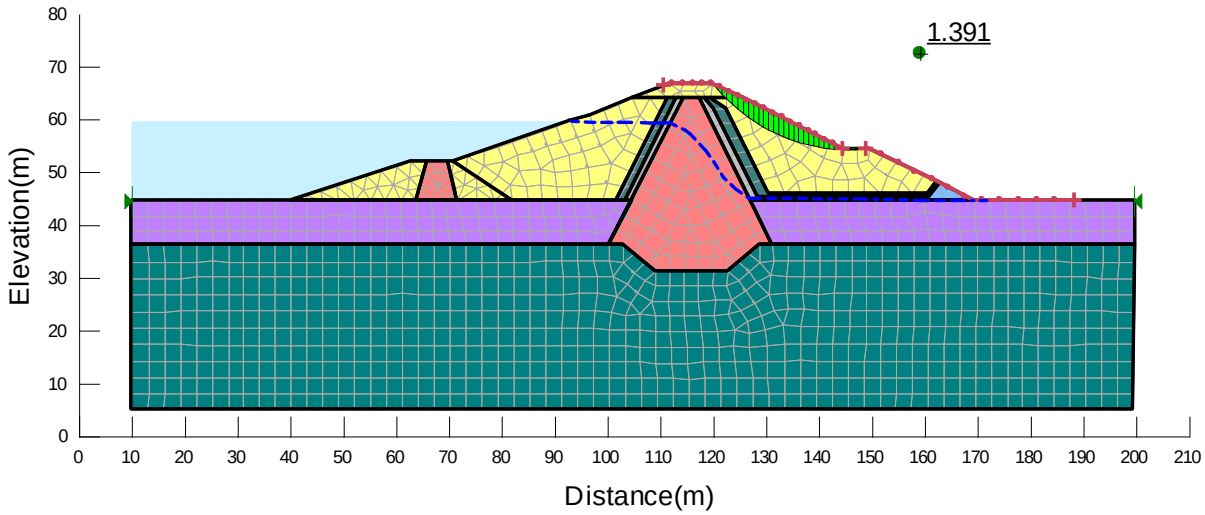

Fig. 5.13: Stability analysis downstream slope under steady state condition (unreinforced; 2.0H:1V)

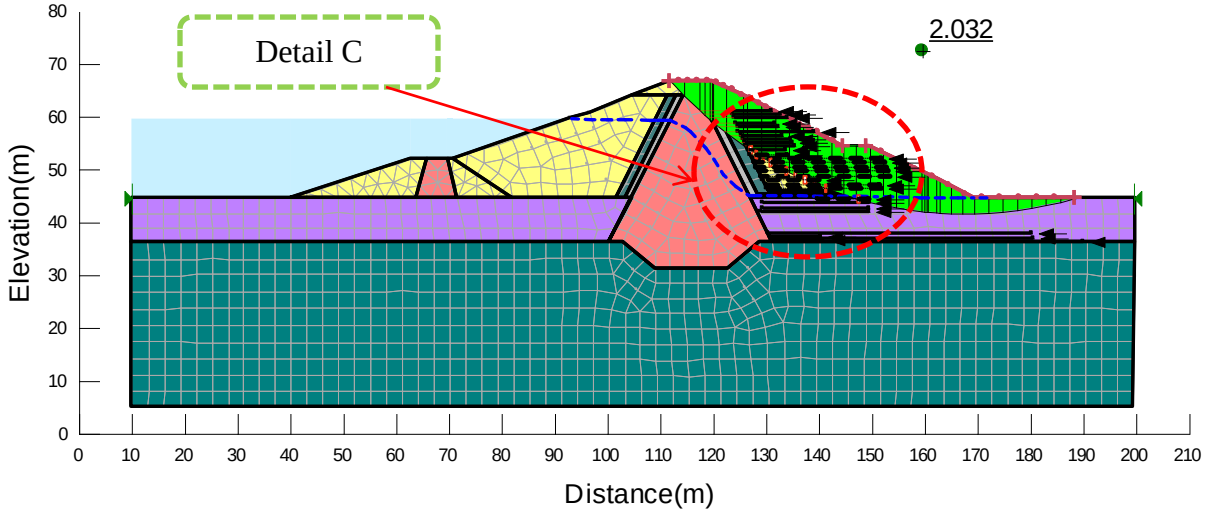

Fig. 5.14 : Analysis of reinforced downstream slope under steady state condition (2.0H: 1V)

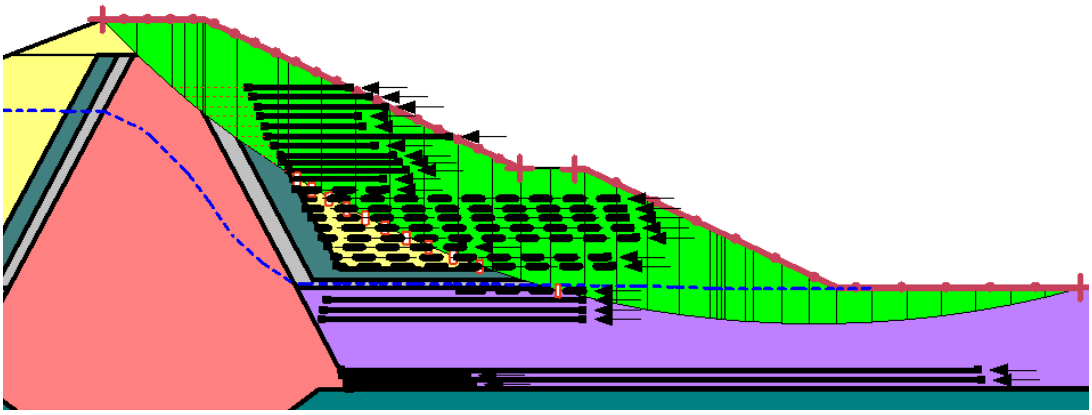

Fig. 5.15: Detail C: shows how critical failure surface is intersected by reinforcement (2.0H: 1V)

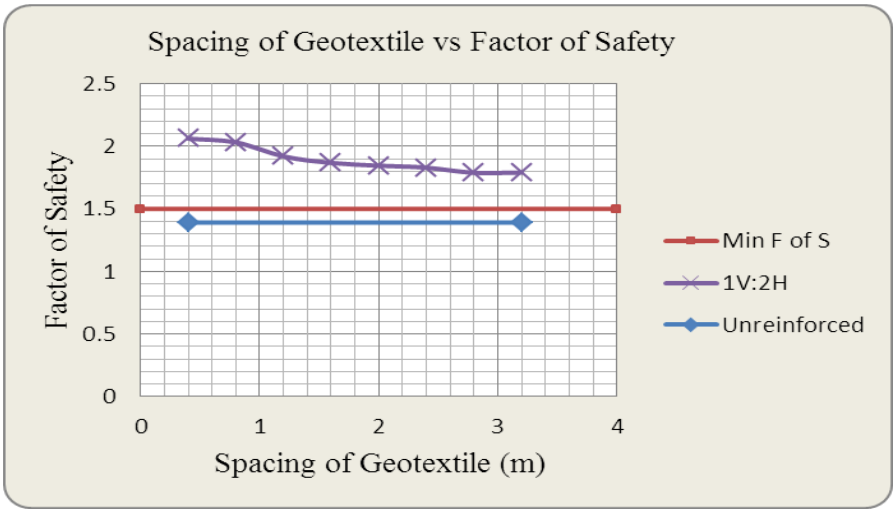

Fig. 5.16: Variation of factor of safety with respect to geotextile layers spacing for steady state

1.75H:1V slope case

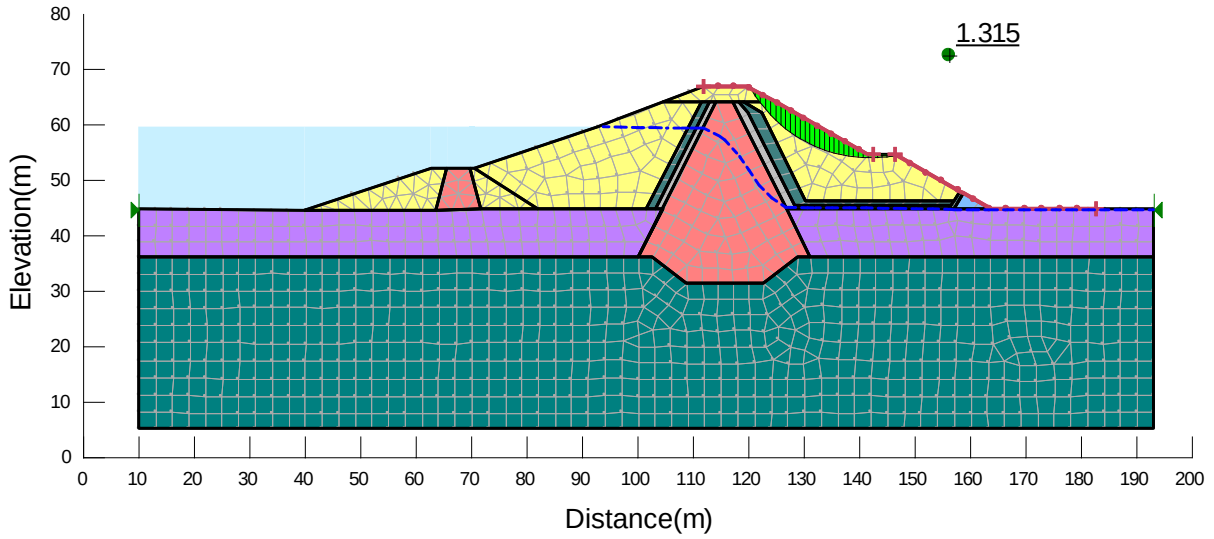

Fig. 5.17: Stability Analysis downstream slope under steady state condition (unreinforced; 1.75H: 1V)

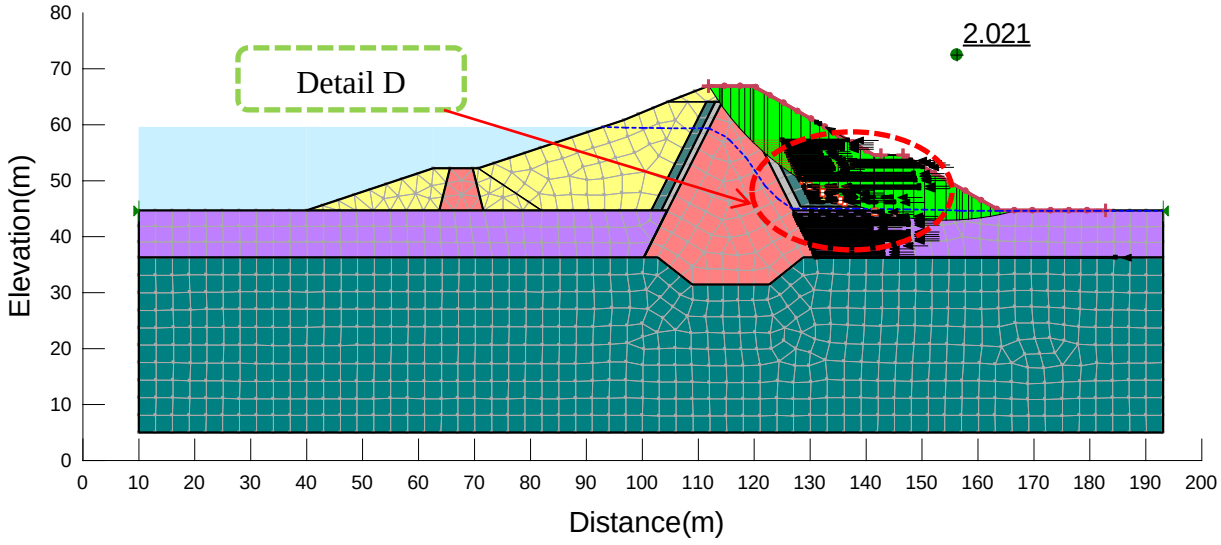

Fig. 5.18: Stability analysis of reinforced downstream slope under steady state condition (1.75H:1V)

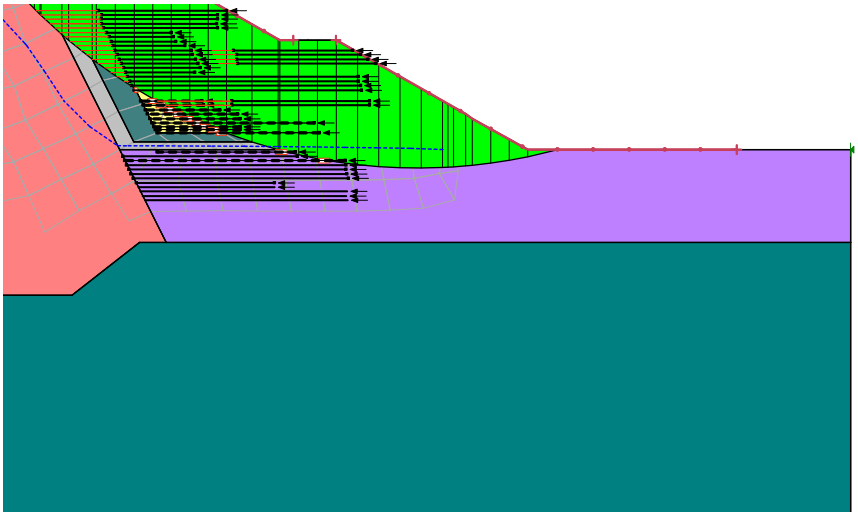

Fig. 5.19: Detail D: shows intersection of critical failure surface and reinforcement (1.75H: 1V)

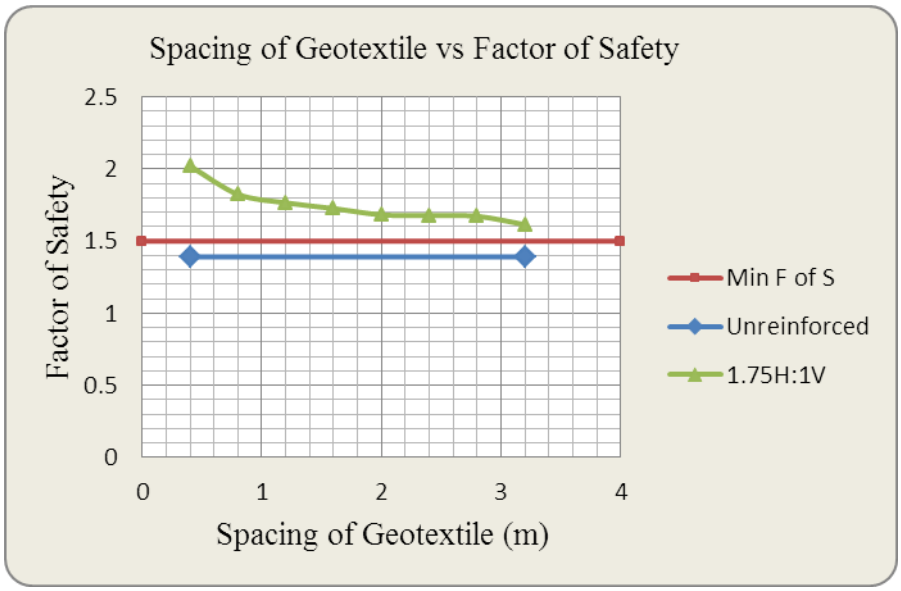

Fig. 5.20: Variation of factor of safety with respect to spacing between geotextile layers for steady state condition

1.5H:1V slope case

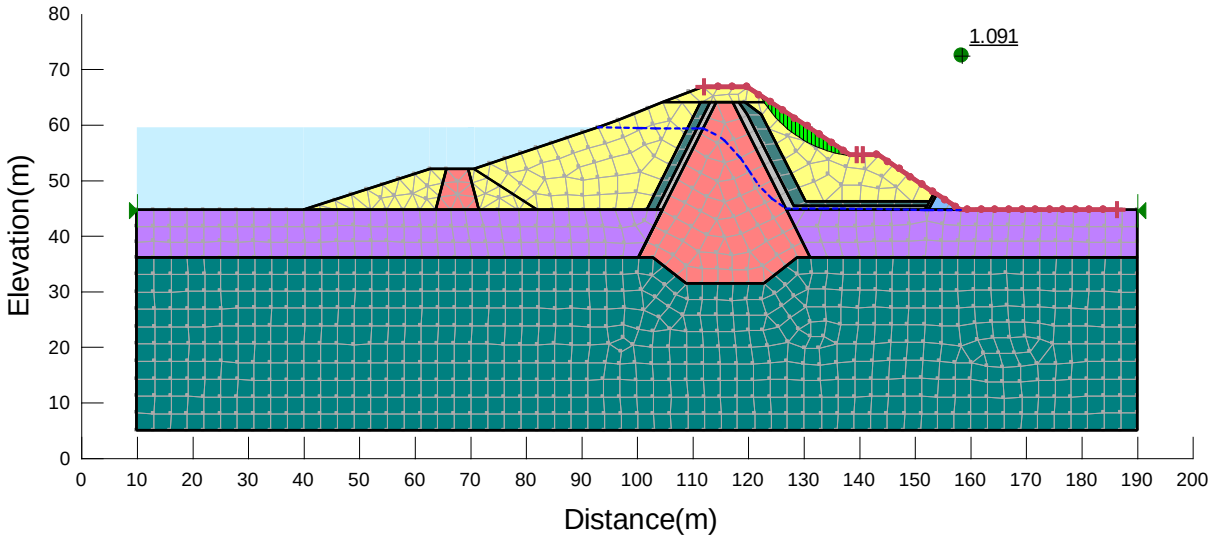

Fig. 5.21: Stability Analysis downstream slope under steady state condition(unreinforced; 1.5H:1V)

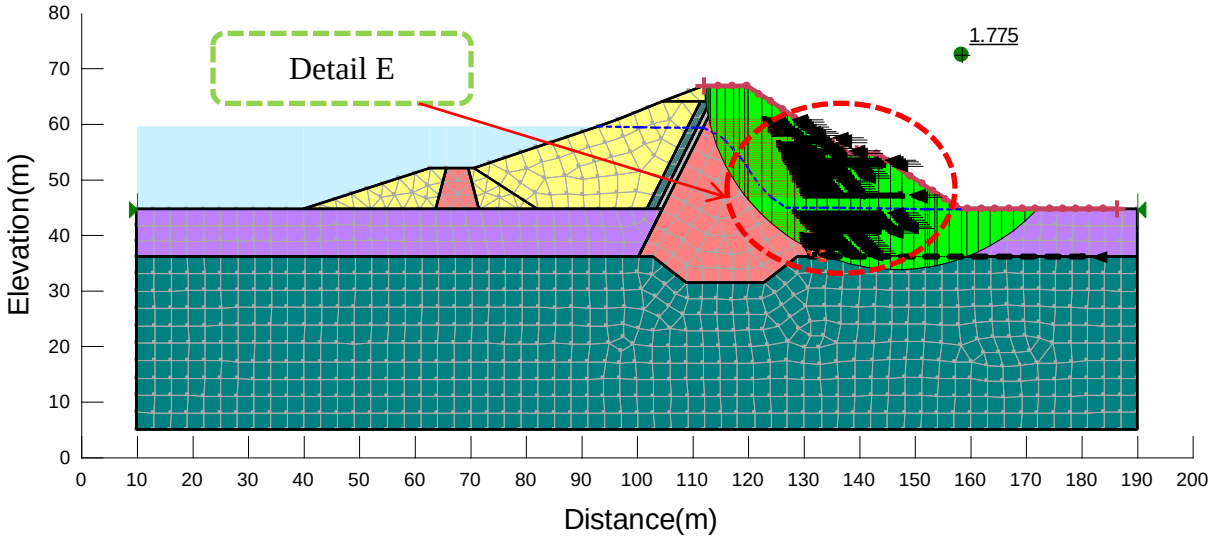

Fig. 5.22: Stability analysis of reinforced downstream slope under steady state condition

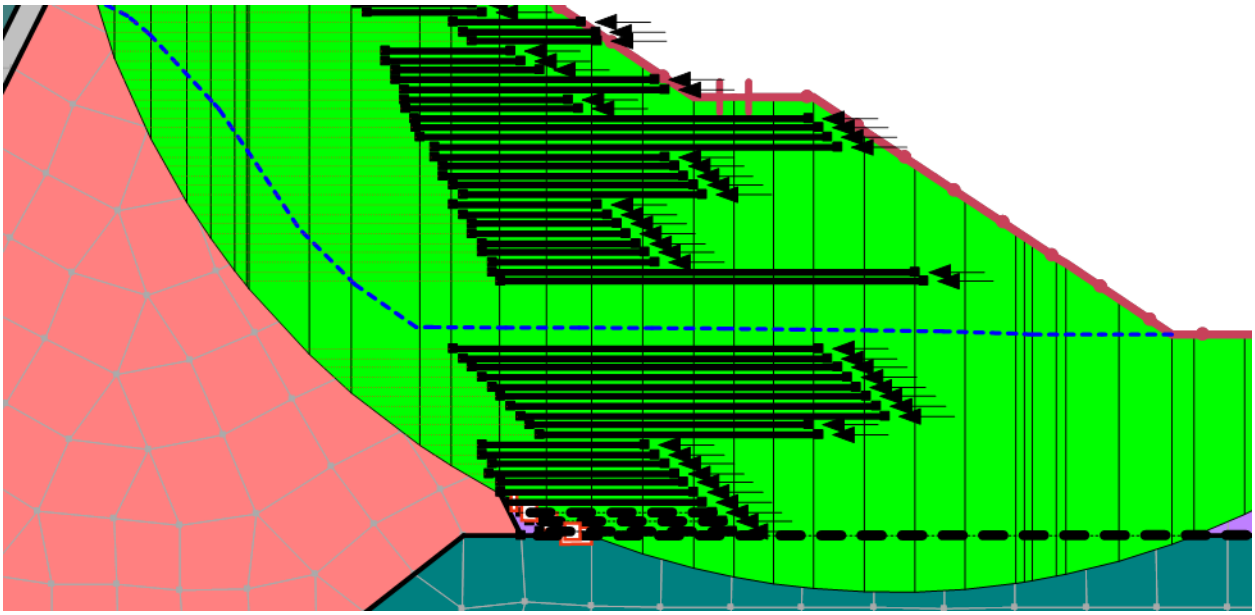

Fig. 5.23: Detail E; shows the intersection between critical failure surface and reinforcement (1.5H: 1V)

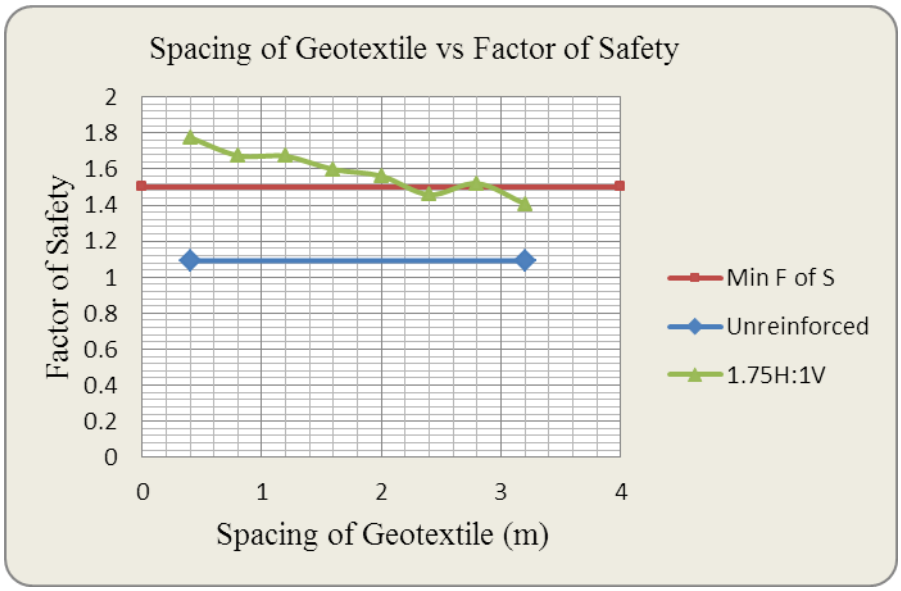

Fig. 5.24: Variation of factor of safety with respect to spacing between geotextile layers for steady state condition

1.25H:1V slope case

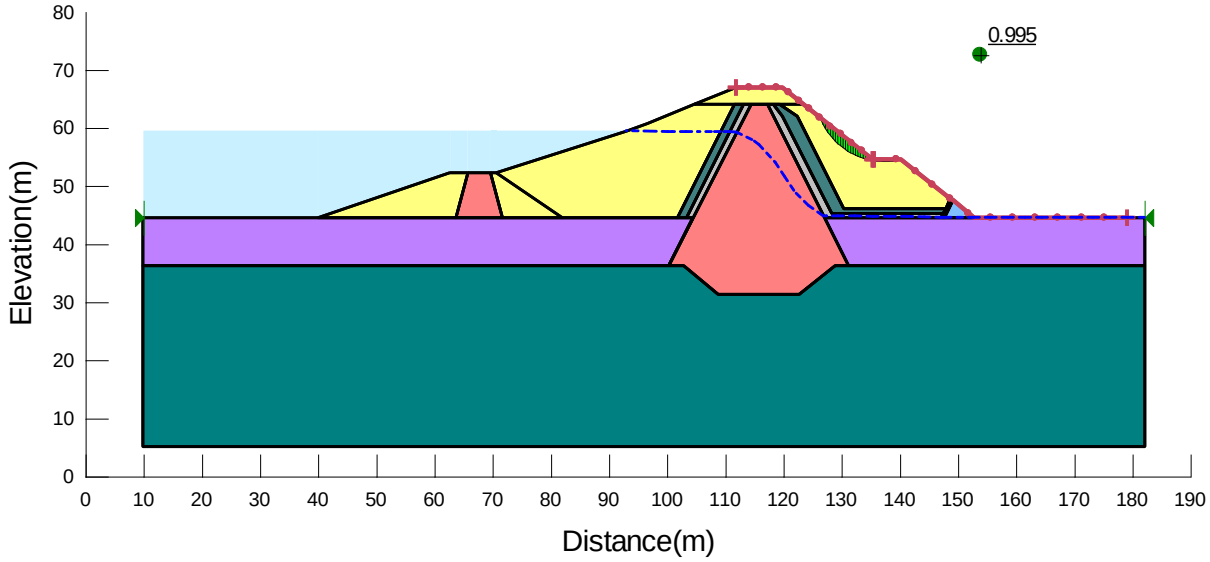

Fig. 5.25: Stability analysis downstream slope under steady state condition (unreinforced 1.25H:1V)

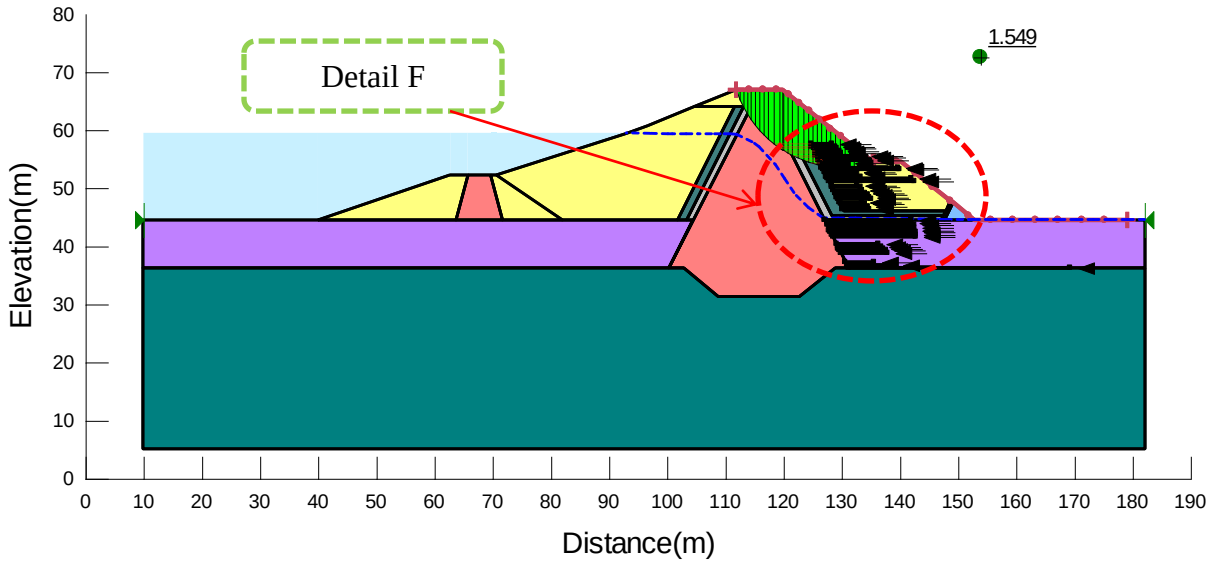

Fig. 5.26: Stability analysis of reinforced downstream slope under steady state condition (1.25H: 1V)

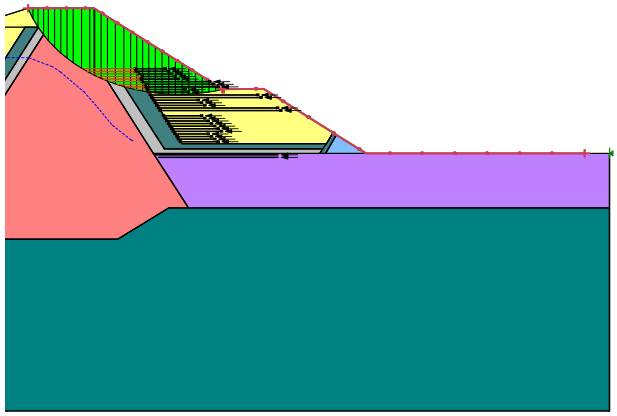

Fig. 5.27: Detail F, shows the intersection between critical failure surface and reinforcement (1.25H: 1V)

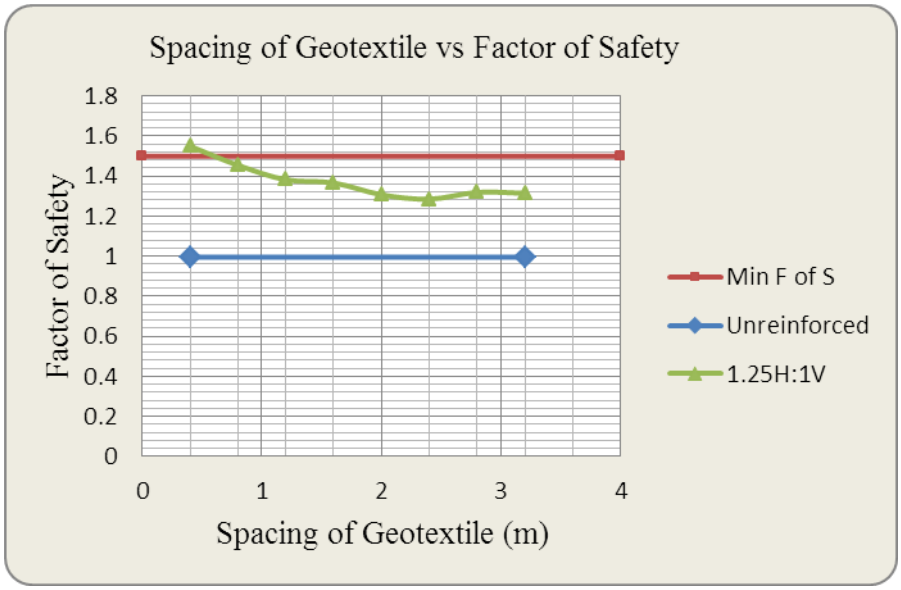

Fig. 5.28: Variation of factor of safety with respect to spacing between geotextile layers for steady state condition

Summary of results and discussions for downstream reinforced sope analysis

The results of the downstream reinforced analysis under steady state seepage condition have been summarized and tabulated as shown in Table 5.3 and Fig.5.29.

Table 5.3: Summary of factor of safety against reinforcement spacing for downstream slope under steady state condition

Factor of safety against reinforcement Spacing (Downstream Slope under Steady State Condition)						
Spacing(m)	Factor of Safety					
	2.5H:1V	2.25H:1V	2.0H:1V	1.75H:1V	1.5H:1V	1.25H:1V
0.4	2.058	1.948	2.062	2.021	1.775	1.549
0.8	1.995	1.905	2.032	1.825	1.675	1.454
1.2	1.97	1.876	1.92	1.766	1.671	1.382
1.6	1.962	1.876	1.868	1.727	1.598	1.366
2	1.956	1.862	1.846	1.683	1.561	1.307
2.4	1.952	1.861	1.83	1.677	1.458	1.285
2.8	1.943	1.861	1.789	1.673	1.52	1.319
3.2	1.989	1.799	1.791	1.615	1.407	1.314

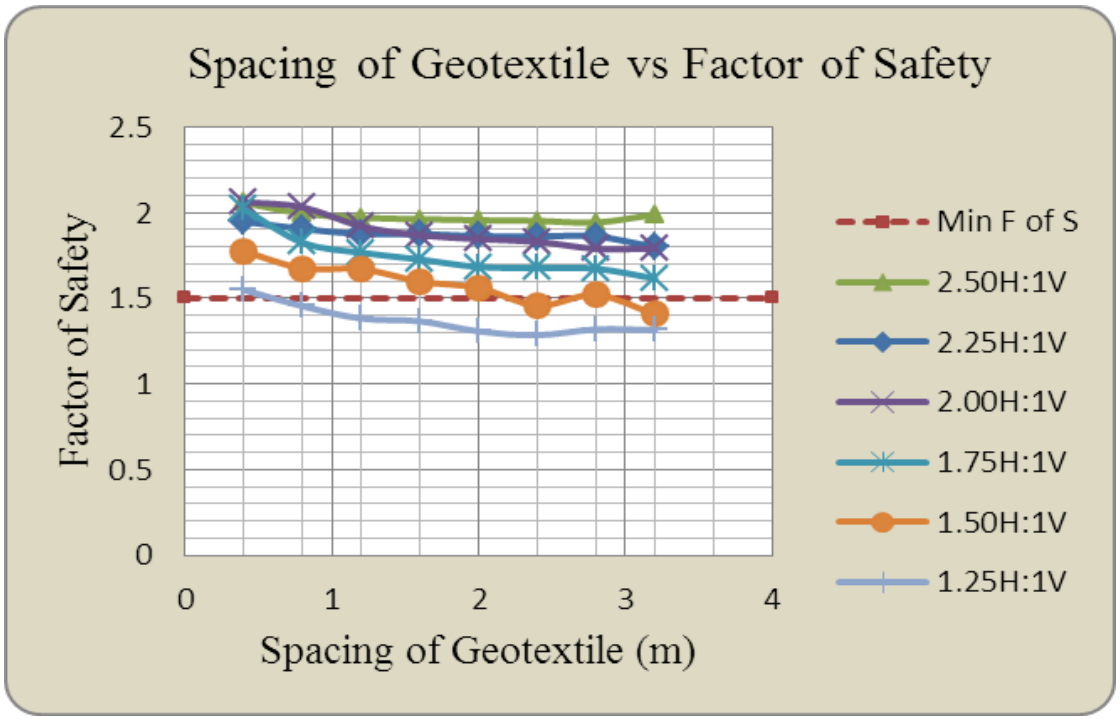

Fig. 5.29: Variation of factor of safety with respect to spacing between geotextile layers for steady state condition

From the above results,it is concluded that

- By providing the geotextile layers at spacing of 3.2m,the downstream slope of a dam can be made steeper up to 1.75H:1V. Fore more steeper slope,the veritcal spacing between geotextile layers is required to be reduced up to 2m.
- The length of the geotextile layers required for reinforceing the downstream slope is found to be in the range of 6m to 30m.
- Offset from downstream slope are found to be in the range of 0m to 42m depending upon the location of geotextile layers.

5.1.4.3 Sudden Drawdown Analysis for Upstream Slope

5.1.4.3.1 Transient analysis using Seep/W

When the pore water pressure and exposure condition in the system varies with time, a time dependent seepage analysis is required. This type of analysis is called *transient analysis.* It means one that is always changing. It is changing because it considers how long the soil takes to respond to the user defined boundary conditions. An example of this is when a reservoir upstream of a dam is drawn down suddenly (Seep/W, 2008).

5.1.4.3.1.1 Initial condition

For a transient analysis, it is essential to define the initial (starting) total head at all nodes. Initial condition has been specified from steady state seepage analysis carried out in previous analysis. For quick reference purpose, the result has been shown again as in Fig.5.38 and 5.39 below.

In transient analysis, in addition to components required for steady state analysis, one additional important component, a boundary condition with function of time is required. In other words, in steady state analysis the boundary condition is not changing with time. But, in transient analysis, the boundary conditions are function of time.

Four water evacuation times (8, 16, 21 and 30 days) (as shown in Table 5.4) have been selected for the analysis and the critical condition has been selected for further analysis. For comparison purpose, instantaneous drawdown has also been included in the analysis. Duration of the analysis has been taken to be 30 days with 10 time steps.

Table 5.4: Water evacuation time during transient rapid drawdown at 8, 16, 21 and 30 days

Step #	Initial	1	2	3	4	5	6	7	8	9	10	Water evacution time (days)
Time (days)	0	2	4	6	9	12	15	18	22	26	30	30
	0	2	4	6	9	12	15	18	22	26	30	21
	0	2	4	6	9	12	15	18	22	26	30	16
	0	2	4	6	9	12	15	18	22	26	30	8

Functions used in seepage analysis

The Saturated Only soil model is very useful for quickly defining a soil region that will always remain below the phreatic surface, but it should not be used for soils that will at some point during the analysis become partially saturated. If this happens, the model will continue to solve but we will be saying, in effect, that the unsaturated zone can transmit the water at the same rate as for the saturated soil (Seep/W, 2008). This will result in an over estimate of flow quantity and can result in an unrealistic water table. Hence, to consider such effect, hydraulic property functions shall be used in the analysis.

Two important hydraulic property functions are hydraulic conductivity functions and volumetric water content functions. These functions are prepared using matric suction developed in the system. Accordingly, hydraulic conductivity functions used for different materials in the analysis have been presented as shown in the following figures (Fig.5.30 to 5.34). Two techniques, namely, estimation from grain size distribution and estimation from sample function have been followed in this study based on availability of grain size distribution data. Similar procedure has been followed in estimating volumetric water content function and the results are presented as shown in figures from Fig.5.35 to 5.37.

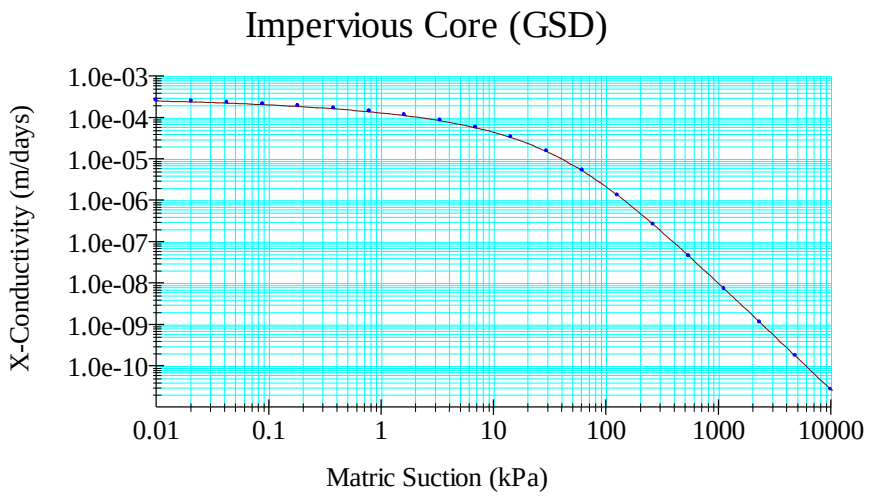

Fig. 5.30: Hydraulic conductivity function for impervious core

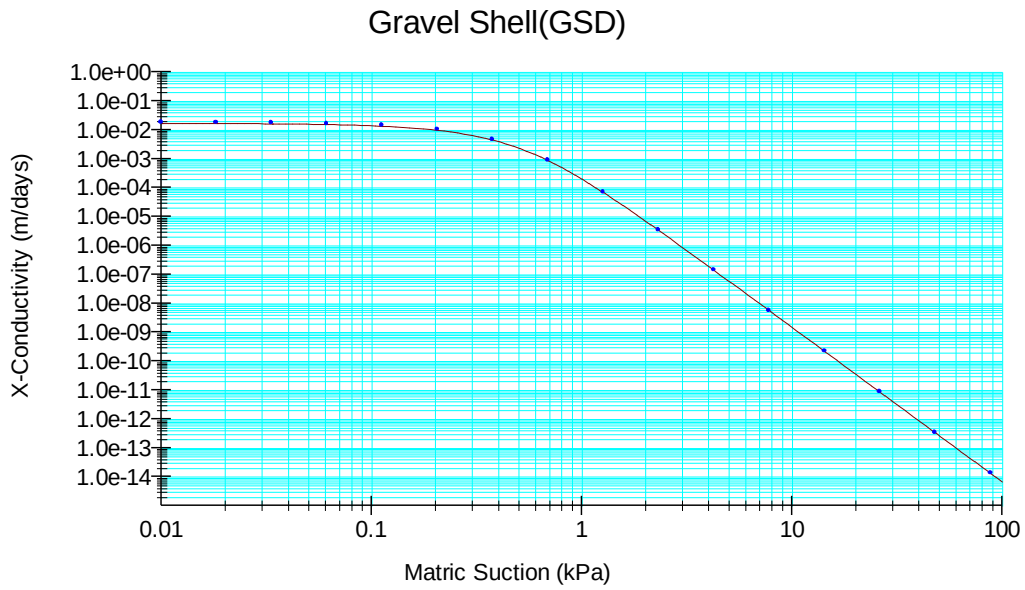

Fig. 5.31: Hydraulic conductivity function for gravel shell

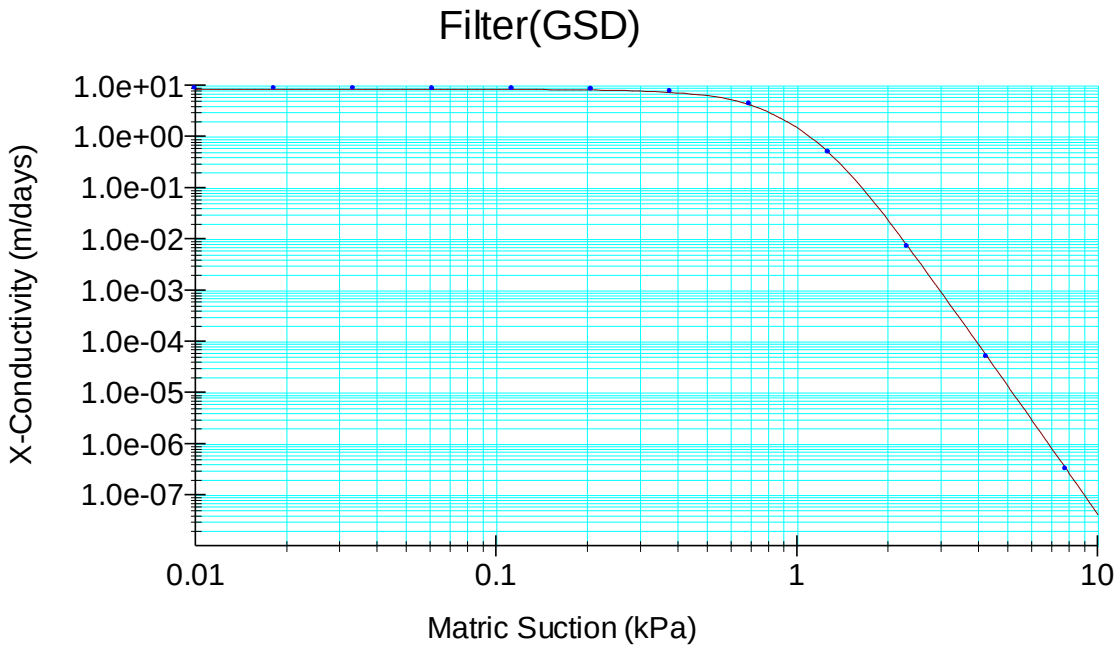

Fig. 5.32: Hydraulic conductivity function for filter

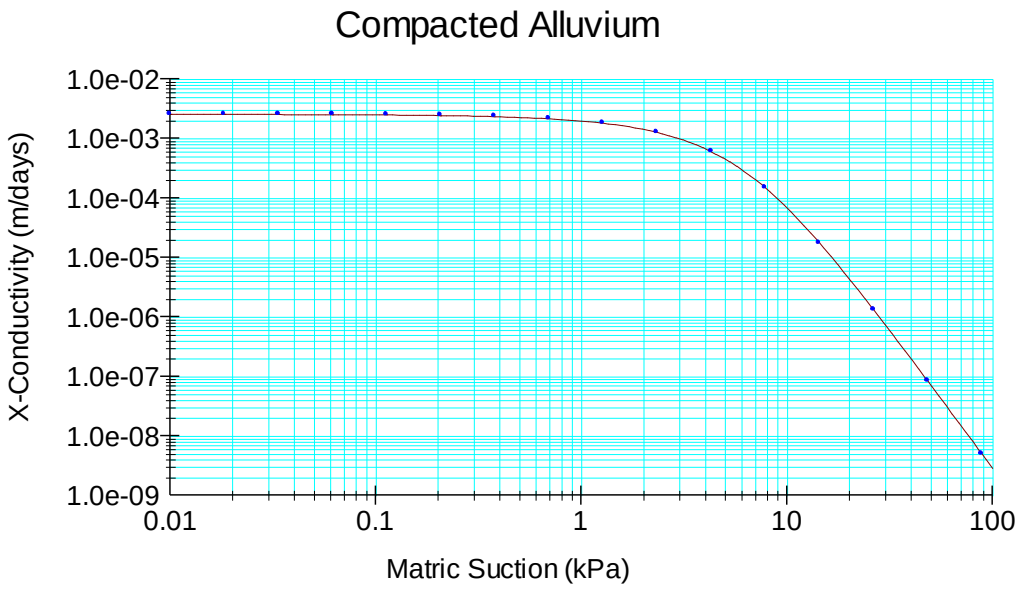

Fig. 5.33: Hydraulic conductivity function for compacted alluvium

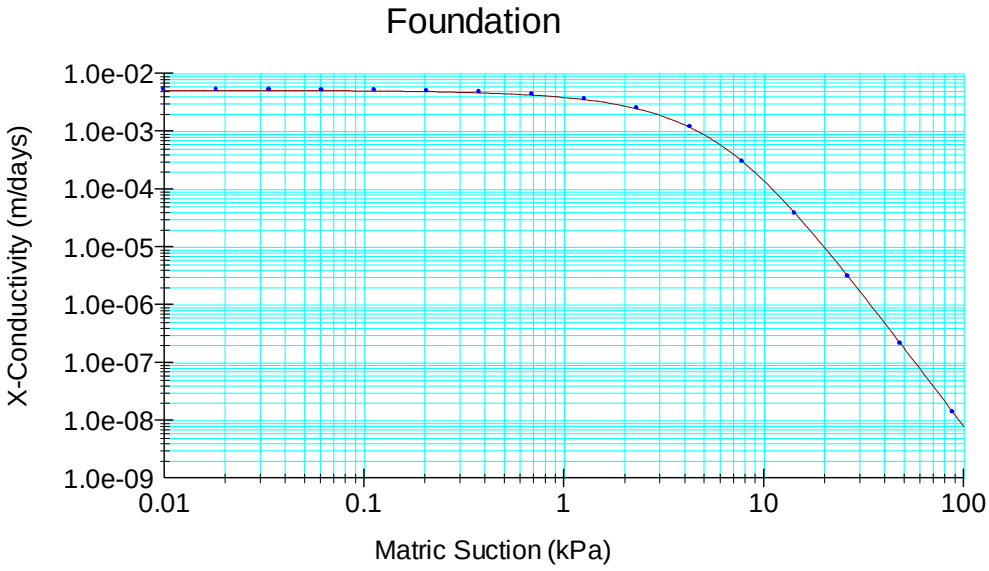

Fig. 5.34: Hydraulic conductivity function for foundation

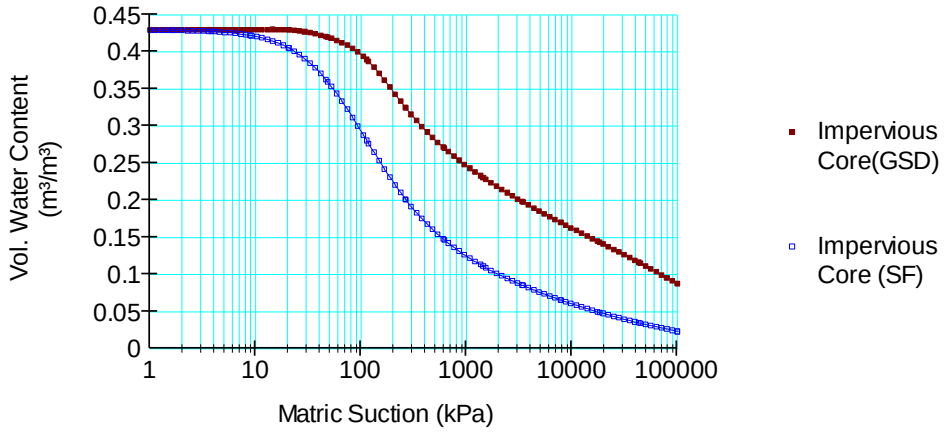

Fig. 5.35: Volumetric water content function for impervious core

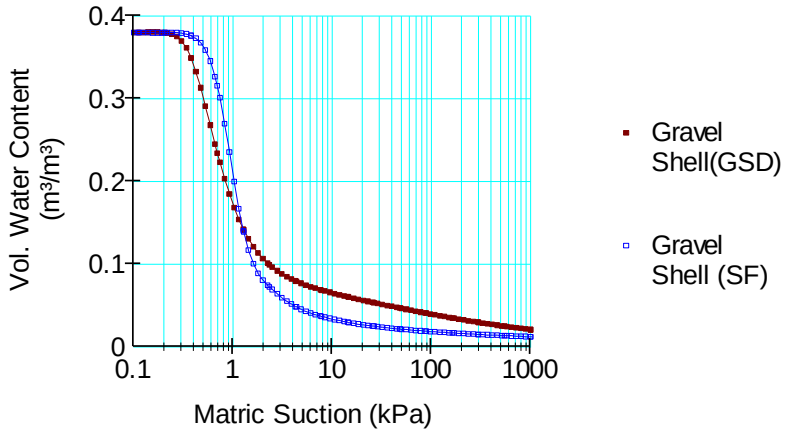

Fig. 5.36: Volumetric water content function gravel shell

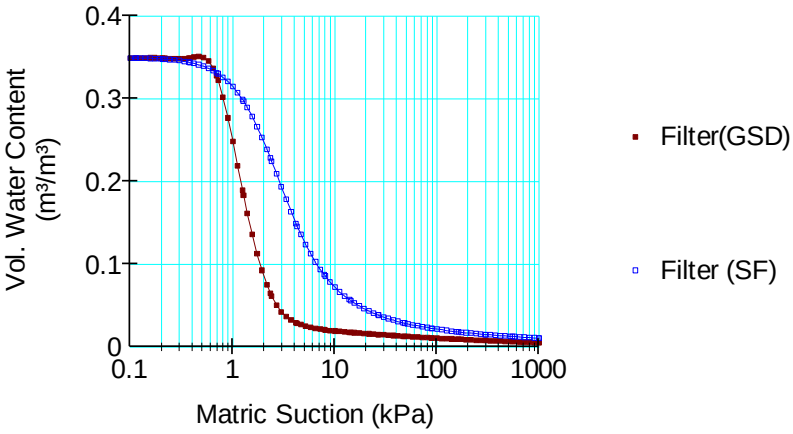

Fig. 5.37: Volumetric water content function for filter

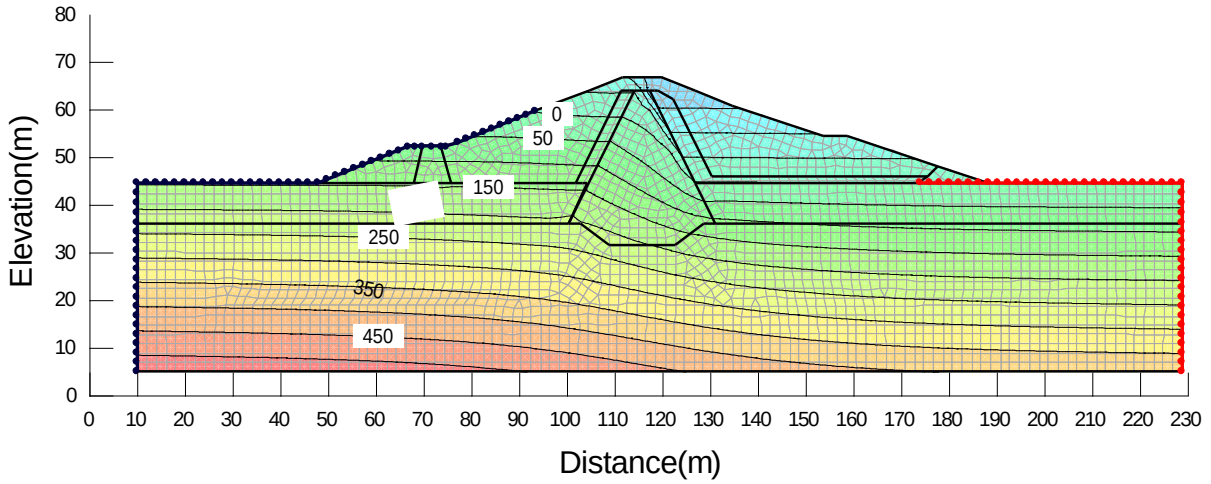

Fig. 5.38: Pore water pressure contour used as initial steady state seepage for transient analysis

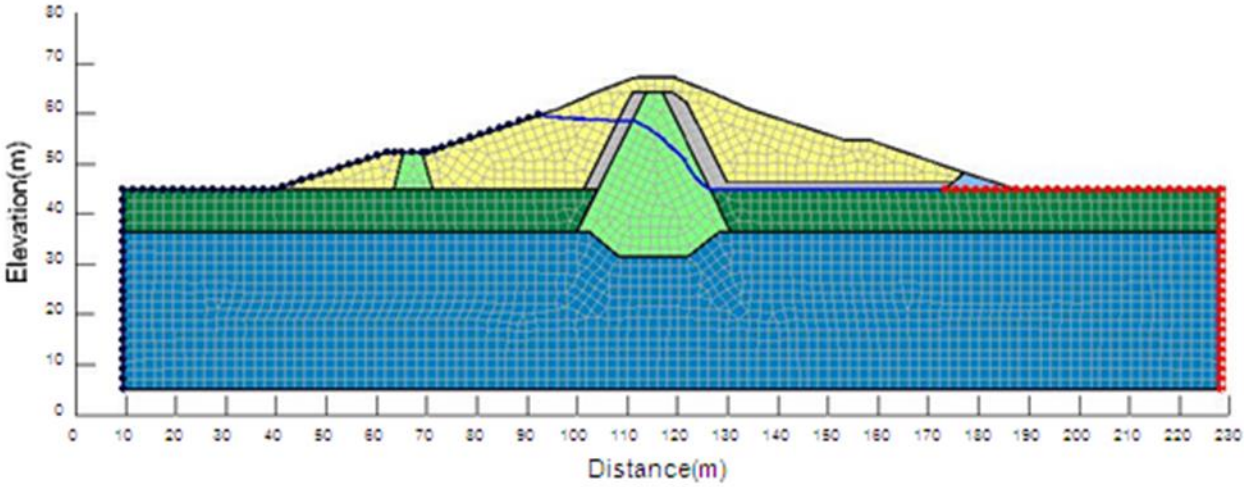

Fig. 5.39: Zero pressure line in steady state analysis

Transient Analysis

As stated above, the aforementioned steady state analysis will be used as initial condition for transient analysis. The transient analysis has been carried out for Five conditions of drawdown; namely; Instantaneous (Fast drawdown), 8, 16, 21 and 30 days of drawdown and among these; critical condition has been selected for further stability analysis.

Drawdown boundary condition for different evacuation times will be given to the solver in the form of function (drawdown level versus time). Thus, these functions have been prepared and summarized in one figure as shown in Fig. 5.40. As it can be seen from the figure, taking 8 days evacuation curve for example, 8 days are required to draw down the reservoir level by 6.5m. Seepage analysis has been carried out for all slope conditions and for both reinforced and unreinforced slopes.

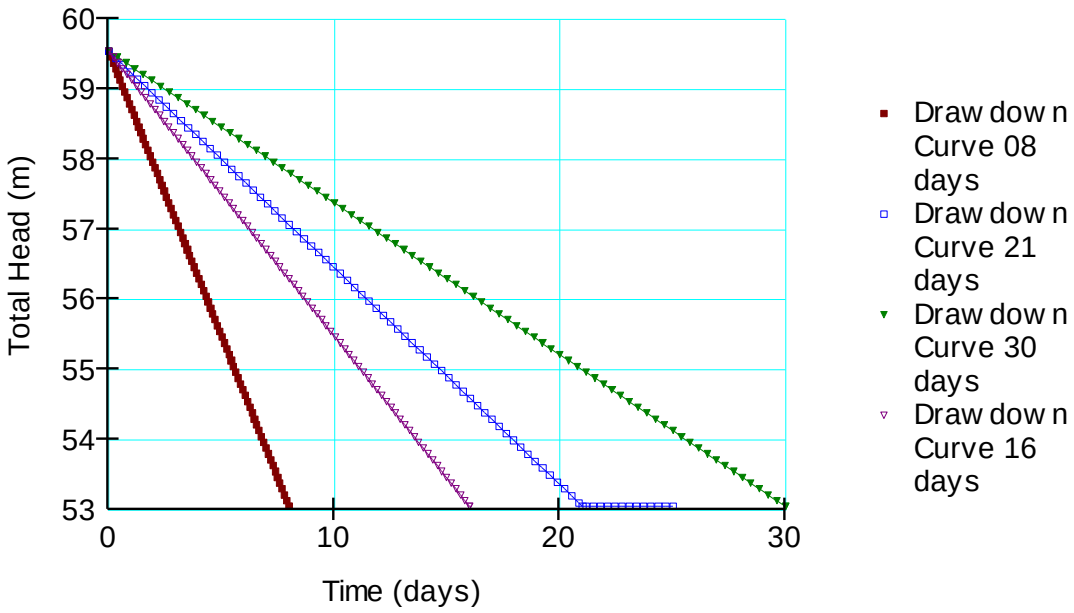

Fig. 5.40: Drawdown boundary functions used in transient analysis for various evacuation times

Finally, giving all the above information to the solver, transient analysis has been carried out and come up with pore water pressure condition for various draw down times. To save paper space, only the result for 08 days draw down period has been shown as in Fig. 5.41 and 5.42. The analysis has been carried out for 30 days duration in 10 different ime steps as shown in table 5.4.

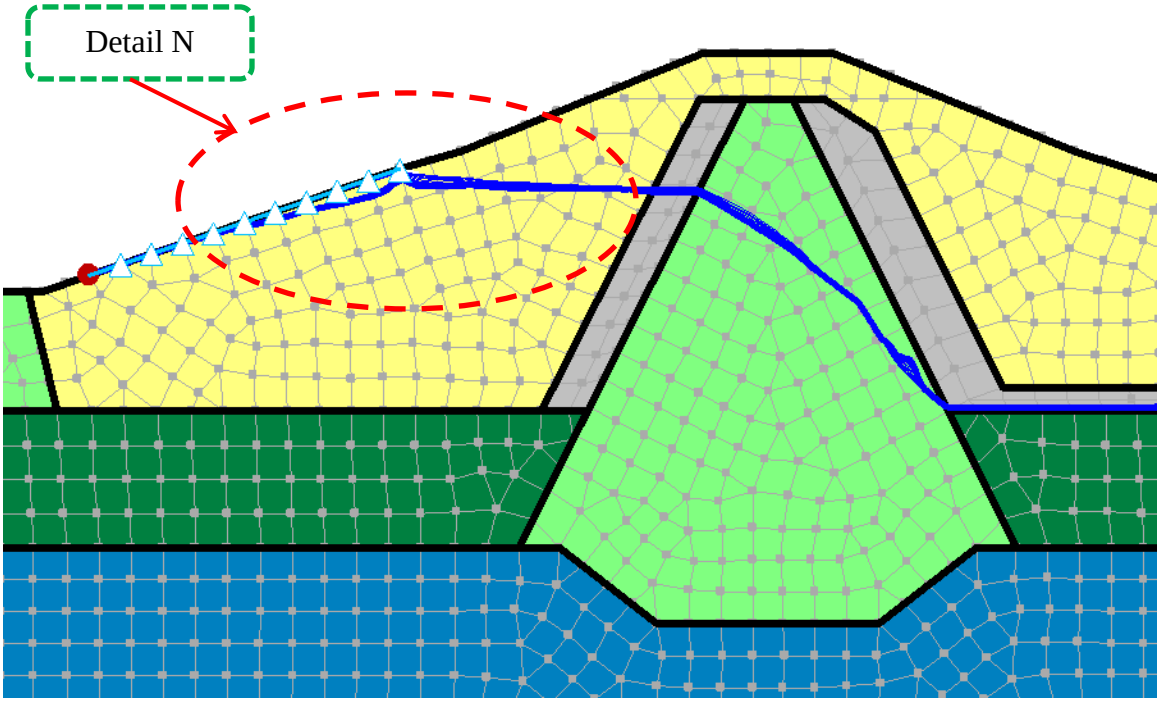

Fig. 5.41: Isolines (zero pressure line) for 08 days draw down and 30 days analysis duration

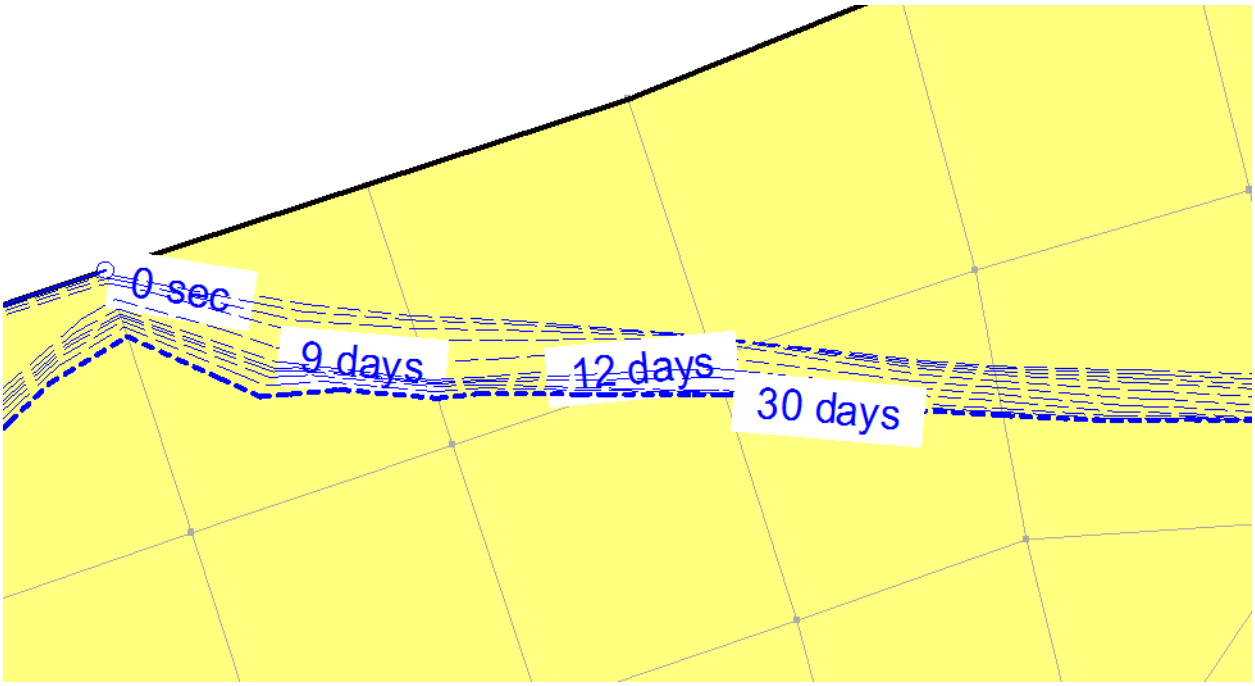

Fig. 5.42: Detail N: Isolines (zero pressure lines) for different analysis days

In Fig. 5.42, it can be seen that the phreatic level drops as the analysis duration increases. It means that as the analysis duration increases, the pore pressure gets time to dissipate. It this pore water pressure condition is given to the solver in slope stability analysis as presented in the following section.

5.1.4.4 Stability analysis of reinforced upstream slope for sudden drawdown condition

The upstream slope of the gidabo earth fill dam is then considered to be reinforced with horizontal layers of geotextile. As the provision of reinforcing layer of geotextile would result in increasing in factor of safety,the steeper slopes may be provided on the upstream of the dam. The upstream slope is reduced by 0.25H:1V in increments. The spacing beween layers is varied from 0.4m to 3.2m for each case. Analysis is then carried out for each case separately. During analysis of each case the length of reinforcing layer and their offset from the upstream face of dam was varied in such a way that the reinofrcing layers remains activated i.e intersect the potential failure surface and govering criteria of failure for the reinforcement as tensile.This ensures the maximum utilization of reinforcing layers and resluts in economy. The analysis results are presented in the following sections.

Transient analysis has been carried out for all slope cases and the critical case has been selected for further (reinforced slope) analysis. Accordingly, for the 2.5H:1V slope case, the result from transient analysis is shown in Fig. 5.43 and from this figure we can see that, the minimum factor of safety is found on the 9^{th} day of 8 days drawdown analysis. Hence, the critical case is the 8 days drawdown case and reinforced slope stability analysis shall be carried out for this condition.

2.5H: 1V (Upstream slope_ sudden drawdown)

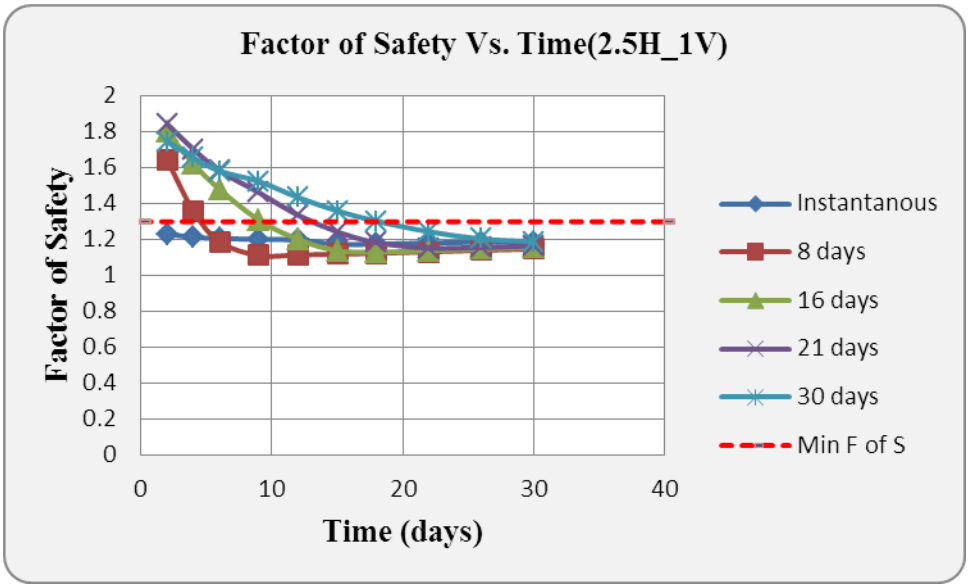

Fig. 5.43: Factor of Safety vs. time for sudden drawdown analysis (upstream slope 2.5H: 1V)

Stability analysis of a upstream slope for sudden draw down condition before reinforcement is carried out and the result is shown in Fig. 5.44. Then, horizontal layers of reinforcement has been introduced to the slope and analysis is done. During analysis, keeping the spacing constant, the length of reinforcement and offset from the upstream slope have been varied until the improvement gets its maximum value. For example as shown in Fig 5.45, the analysis has been carried out for a spacing of 1.6m by varying length and offset from the upstream slope until it gets a maximum value of improvement. Hence, due to reinforcement, the factor of safety is improved from 1.103 to 1.74. This analysis procedure continues for another spacing (0.4m to 3.2m) and the summary of results for all reinforcement spacing corresponding to this slope has been presented as shown in Fig 5.47. From this summary figure, we can see that the factor of safety has been improved by from 40% to 72%.

Similar procedures have been followed for other slope cases and analysis results have been presented in the subsequent sections starting from Fig.5.48 to 5.73.

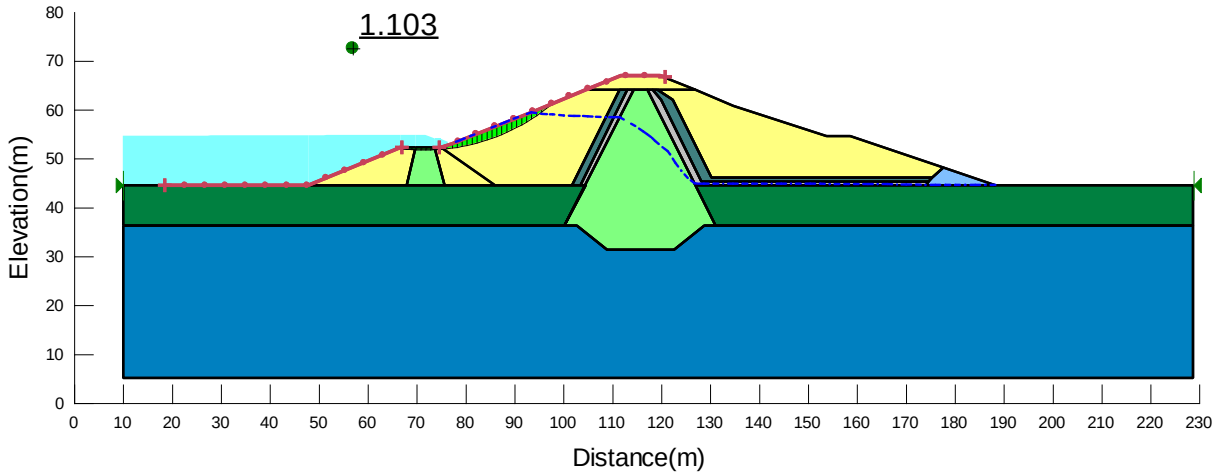

Fig. 5.44: Stability analysis for 8 days sudden drawdown (9th day) (upstream slope/unreinforced) (2.5H:1V)

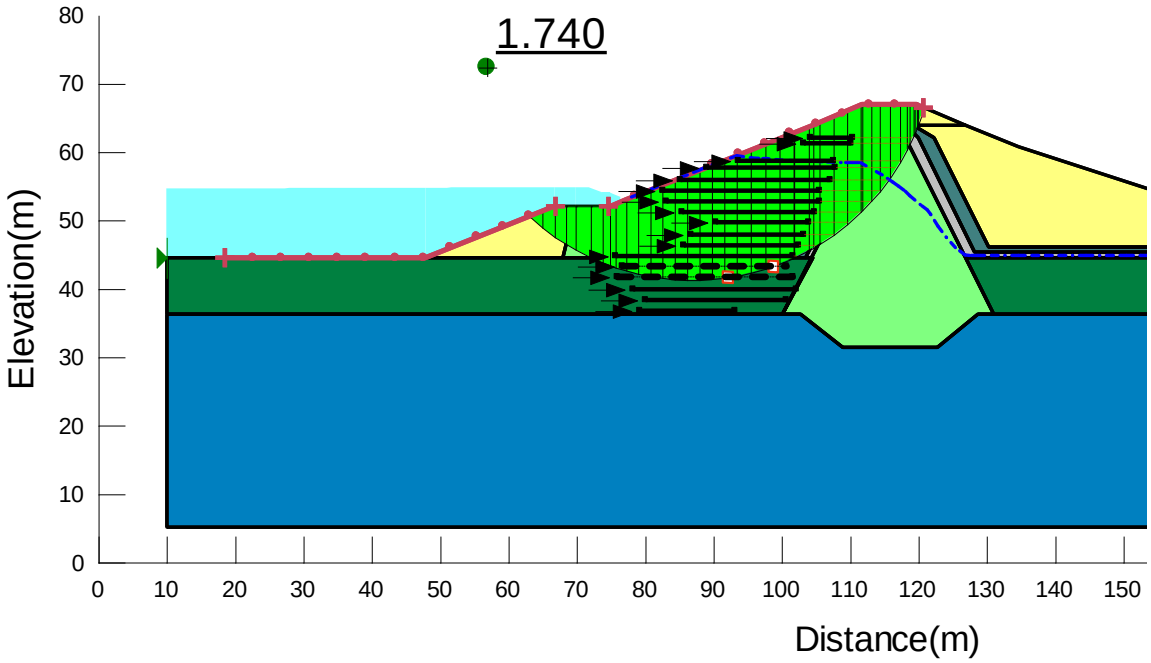

Fig. 5.45: Stability analysis (on 9th day) (upstream slope/reinforced with 1.6m Spacing) (2.5H: 1V)

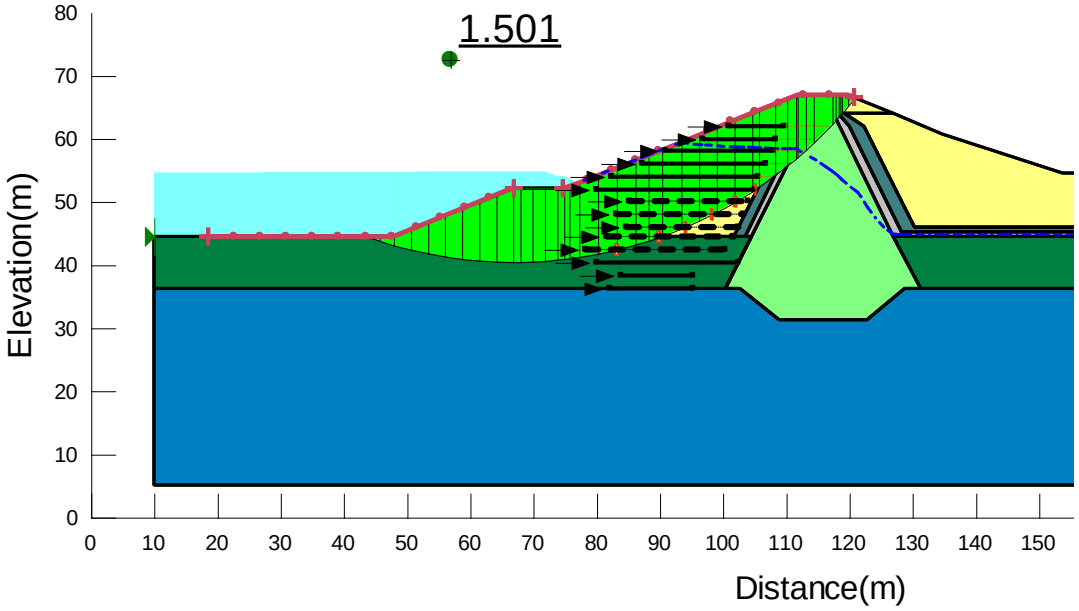

Fig. 5.46: Stability analysis (on 9th day) (upstream slope/reinforced with 2.0m Geotextile spacing) (2.5H: 1V)

The summary for variation of factor of safety with spacing of geotextile reinforcement has been given in the following figure.

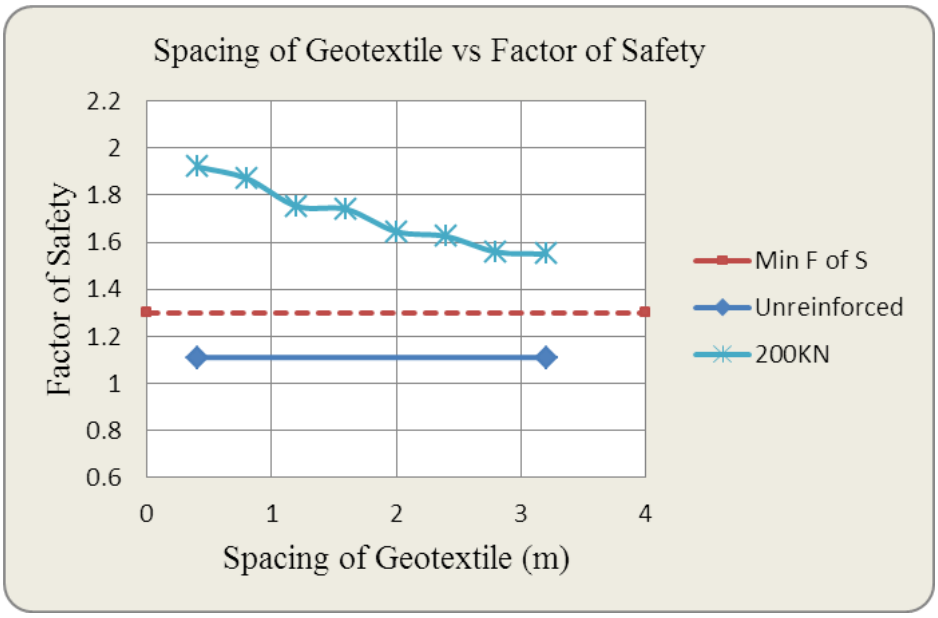

Fig. 5.47: Variation of Factor of Safety with spacing of Geotextile (upstream slope, sudden draw down condition_2.5H:1V)

2.25H: 1V (upstream Slope/Sudden drawdown condition)

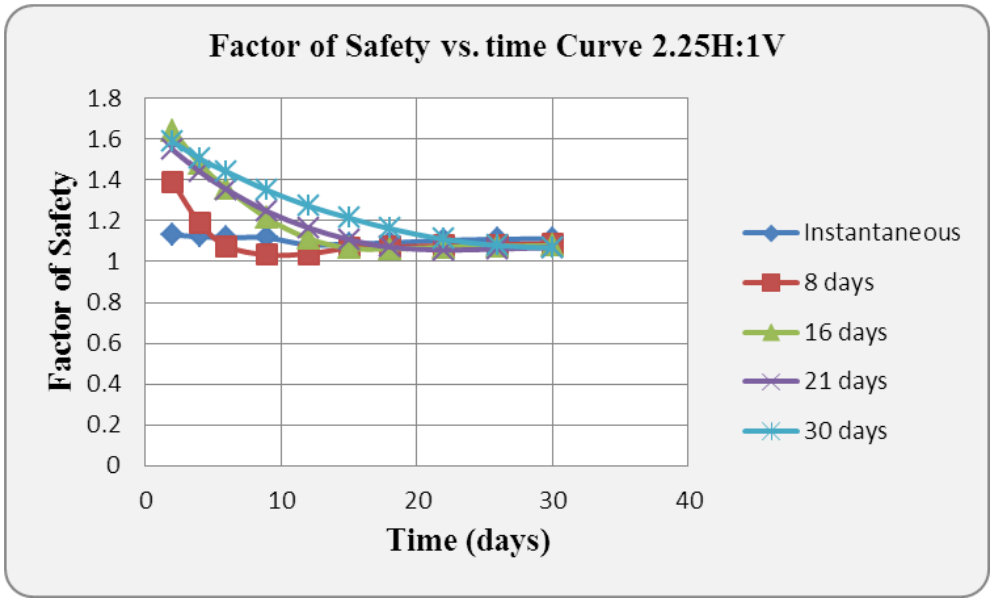

Fig. 5.48: Factor of Safety vs. time for sudden drawdown analysis (upstream slope 2.25H: 1V)

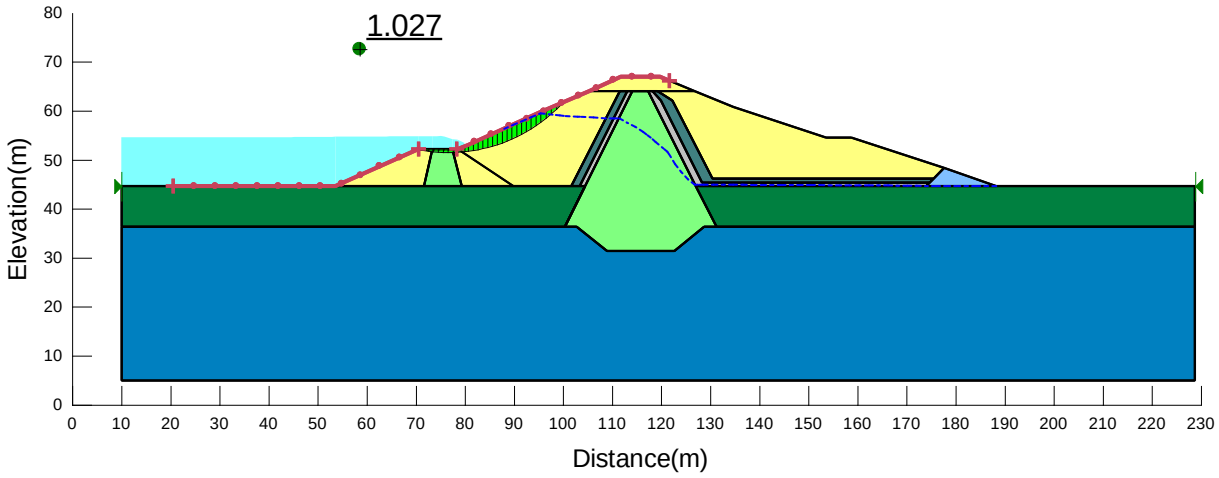

Fig. 5.49: Stability analysis for 8 days sudden drawdown (9th day) (upstream slope/unreinforced; 2.25H: 1V)

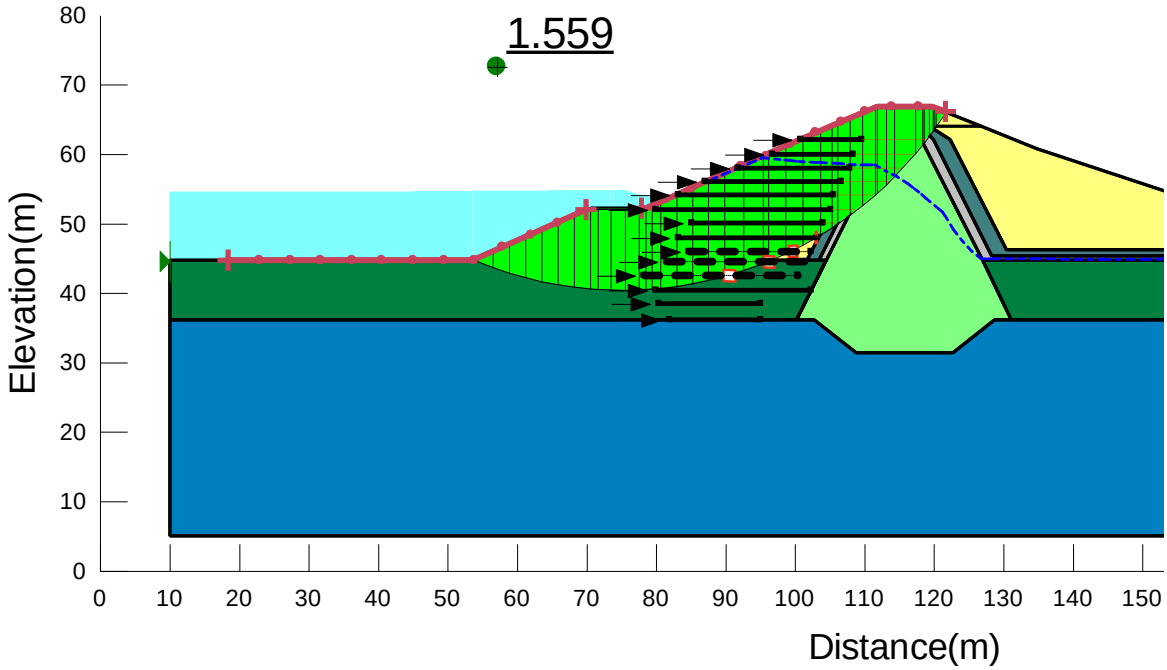

Fig. 5.50: Stability analysis (on 9th day) (upstream slope/reinforced with 2.0m Geotextile spacing) (2.25H: 1V)

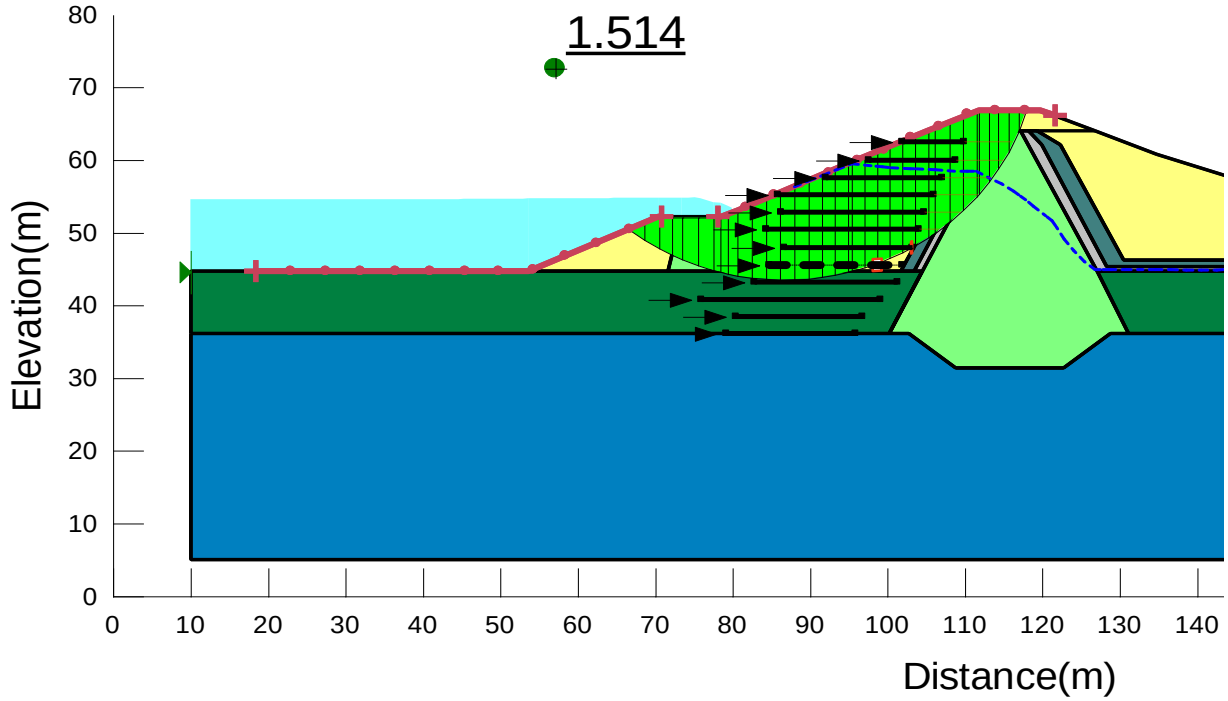

Fig. 5.51: Stability analysis (on 9th day) (upstream slope/reinforced with 2.4m Geotextile spacing) (2.25H: 1V)

The summary for variation of factor of safety with spacing of geotextile reinforcement has been given in the following figure.

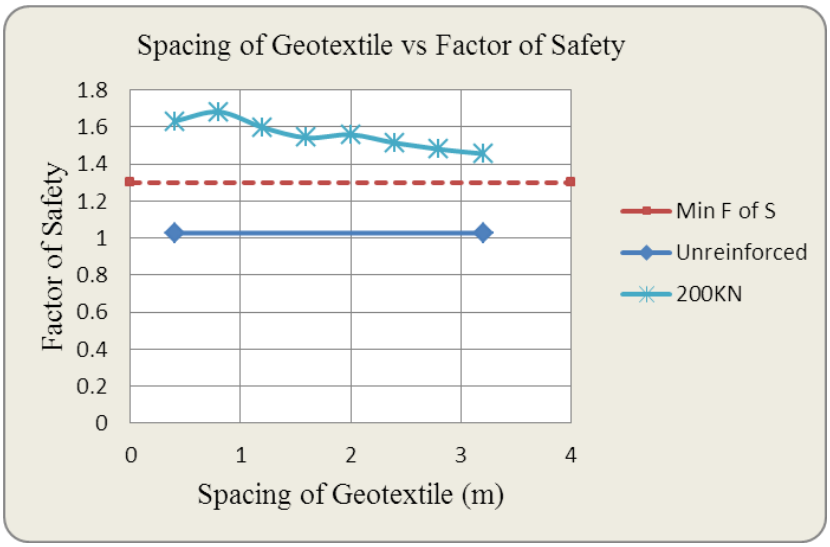

Fig. 5.52: Variation of Factor of Safety with spacing of Geotextile (upstream Slope_sudden draw down condition_2.25H:1V)

2.0H: 1V (Upstream Slope_Sudden drawdown condition)

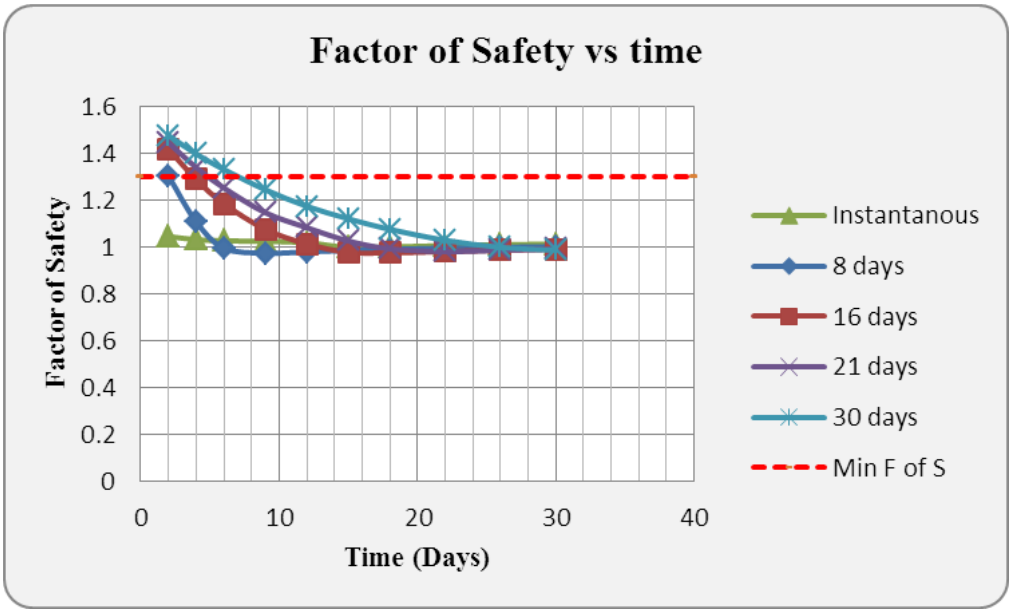

Fig. 5.53: Factor of Safety vs. time for sudden drawdown analysis (upstream slope 2.0H: 1V)

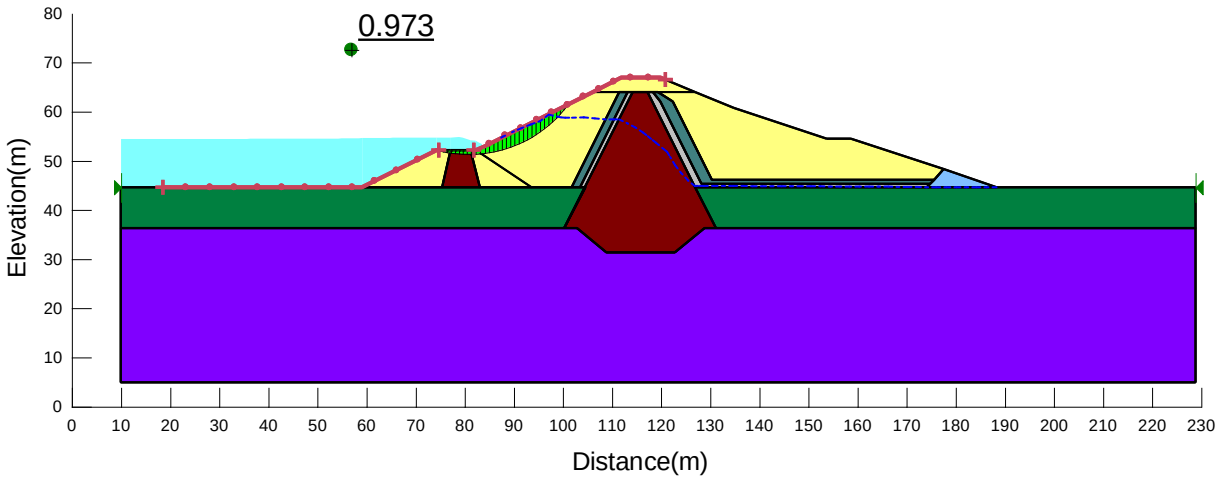

Fig. 5.54: Stability analysis for 8 days sudden drawdown (9th day) (upstream slope/unreinforced) (2.0H: 1V)

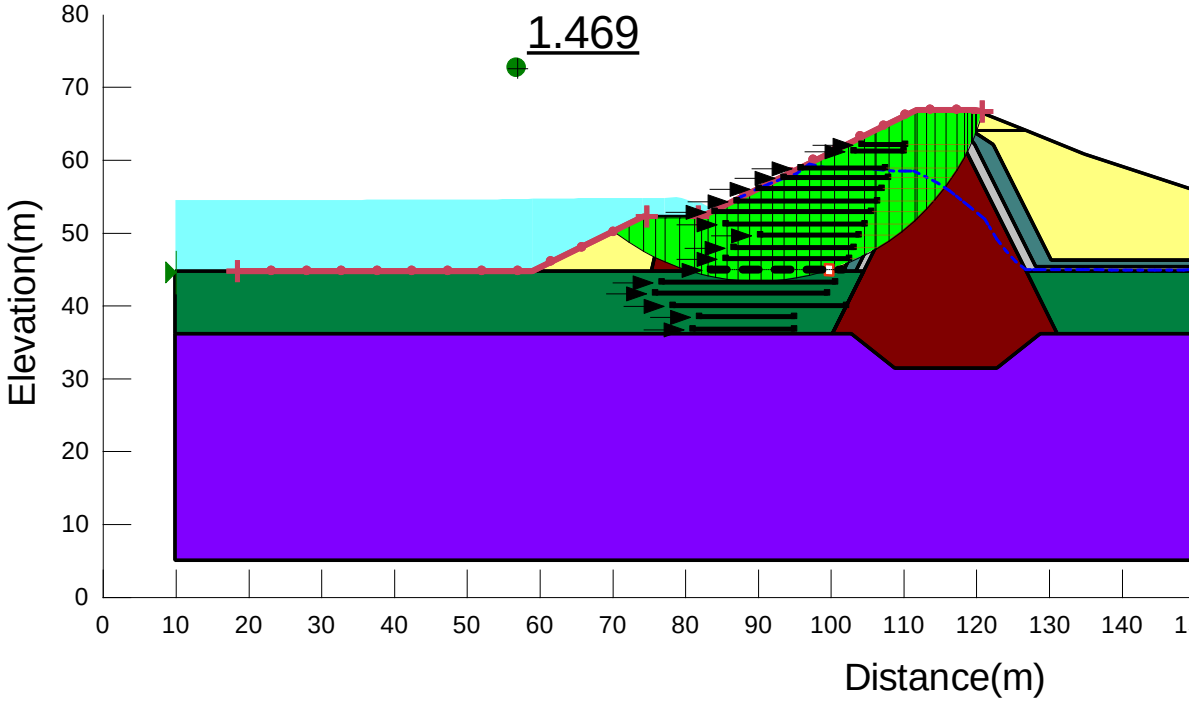

Fig. 5.55: Stability analysis (on 9th day) (upstream slope/reinforced with 1.6m Geotextile spacing) (2.0H: 1V)

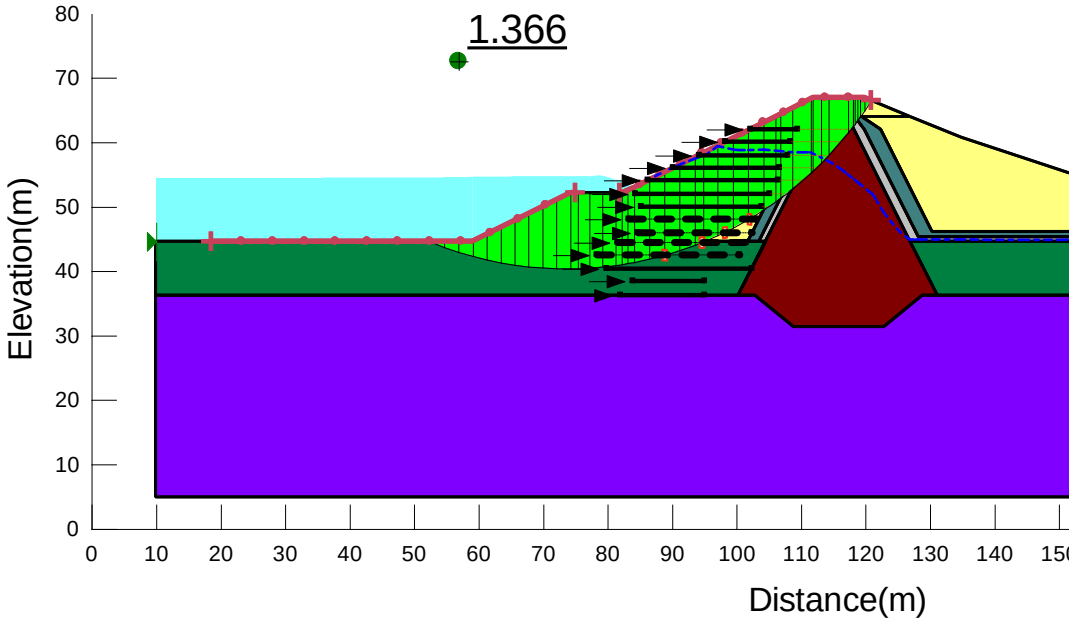

Fig. 5.56: Stability analysis (on 9th day) (upstream slope/reinforced with 2.0m Geotextile spacing) (2.0H: 1V)

The summary for variation of factor of safety with spacing of geotextile reinforcement has been given in the following figure.

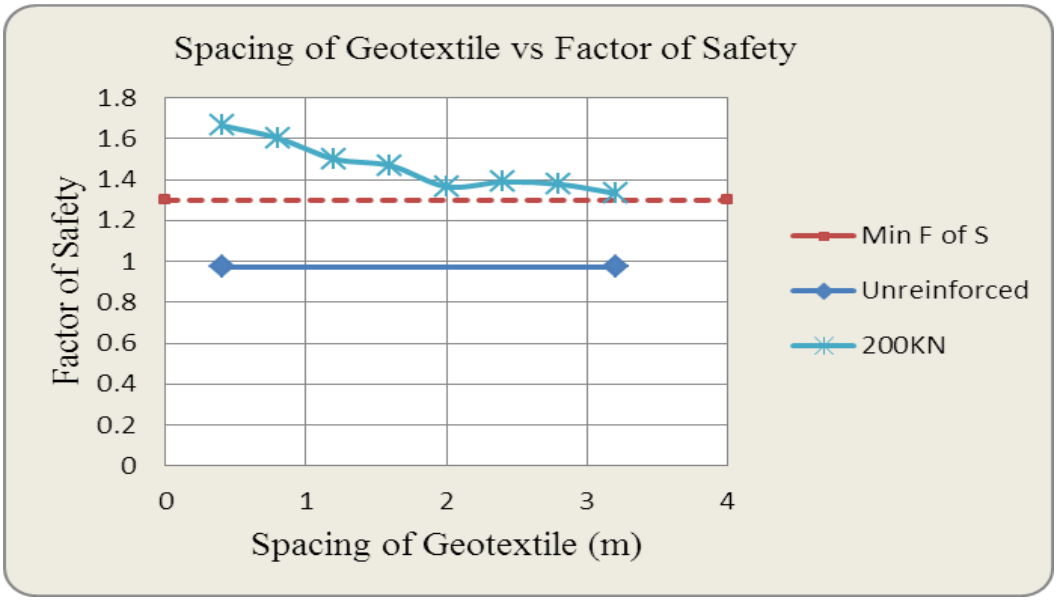

Fig. 5.57: Variation of Factor of Safety with spacing of Geotextile (upstream slope_sudden draw down condition_2.0H:1V)

1.75H: 1V (Upstream Slope_Sudden drawdown condition)

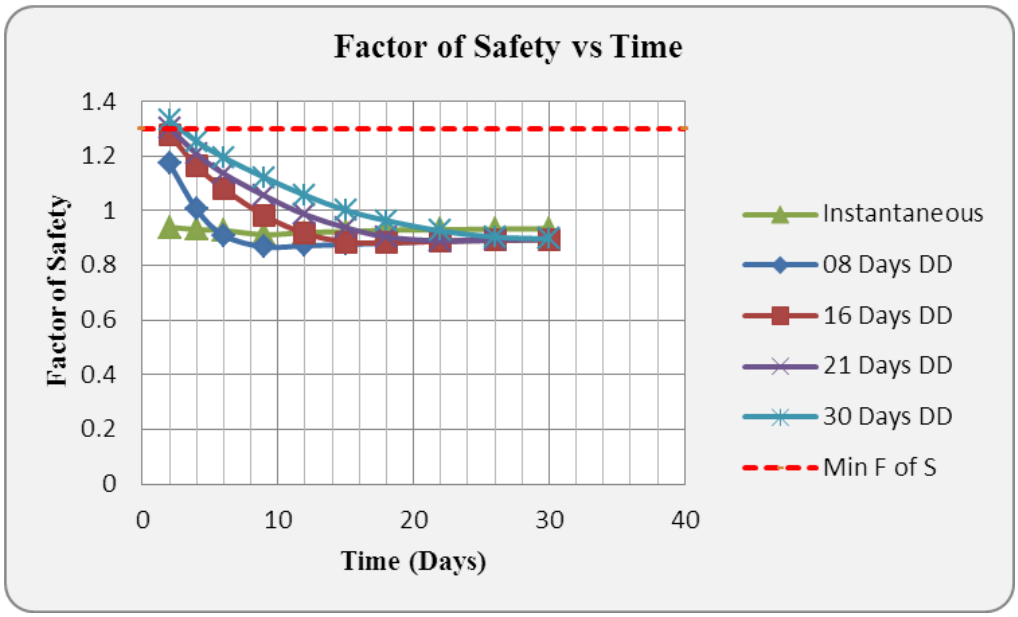

Fig. 5.58: Factor of Safety vs. time for sudden drawdown analysis (Upstream slope 1.75H: 1V)

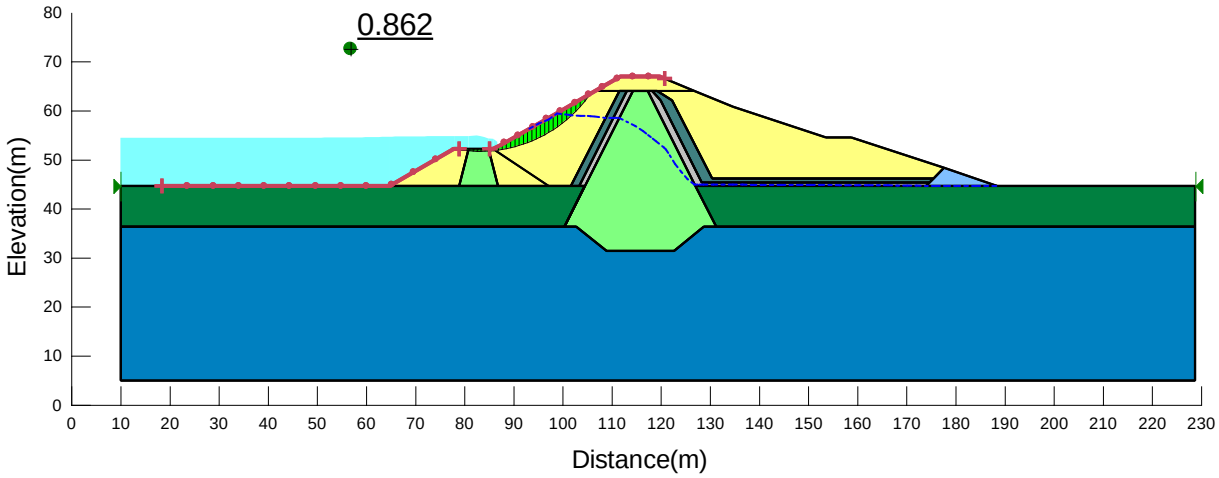

Fig. 5.59: Stability analysis for 8 days sudden drawdown (9th day) (upstream slope/unreinforced) (1.75H:1V).

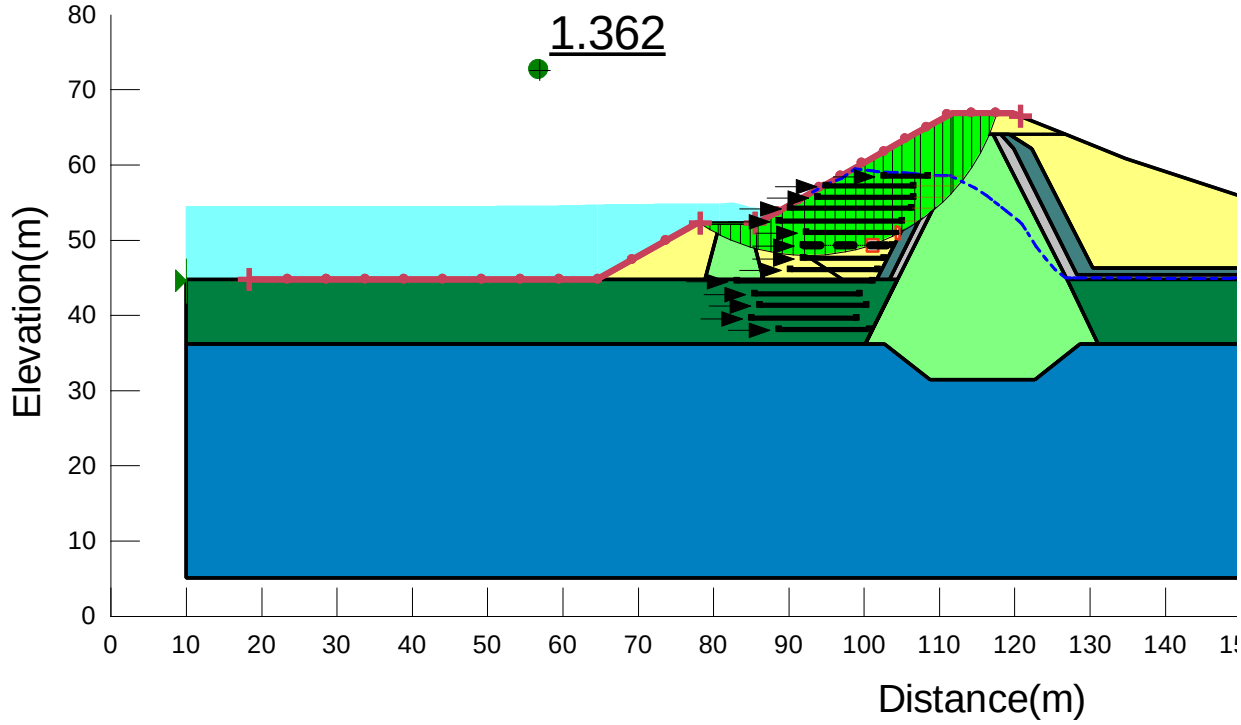

Fig. 5.60: Stability analysis (on 9th day) (upstream slope/reinforced with 1.6m Geotextile spacing) (1

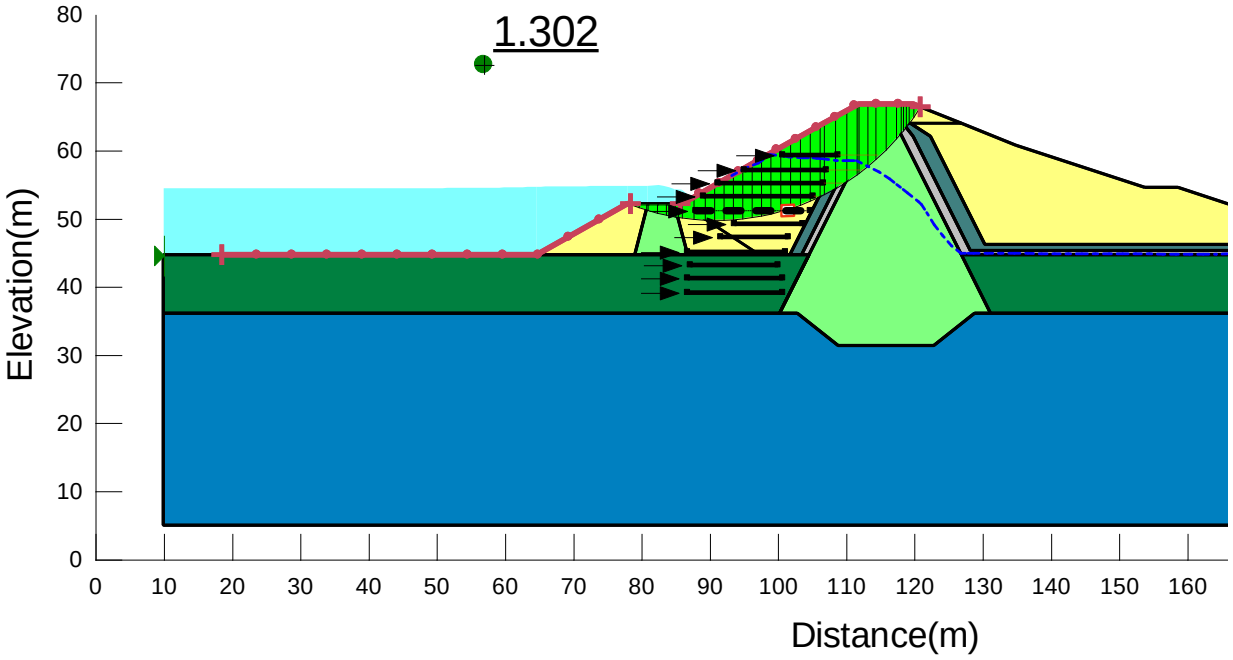

Fig. 5.61: Stability analysis (on 9th day) (upstream slope/reinforced with 2.0m Geotextile Spacing)

The summary for variation of factor of safety with spacing of geotextile reinforcement has been presented in the figure below.

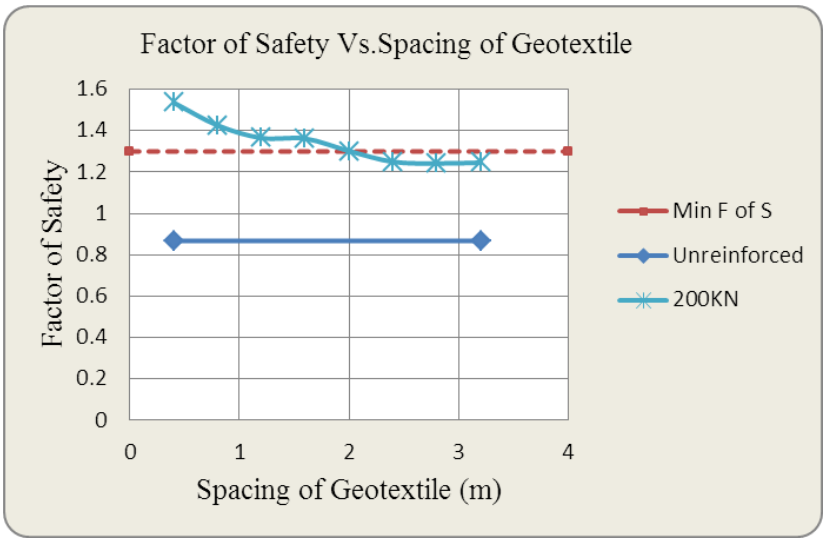

Fig. 5.62: Variation of Factor of Safety with spacing of Geotextile (upstream Slope_SDDC_1.75H:1V)

1.50H: 1V (Upstream Slope_Sudden drawdown condition)

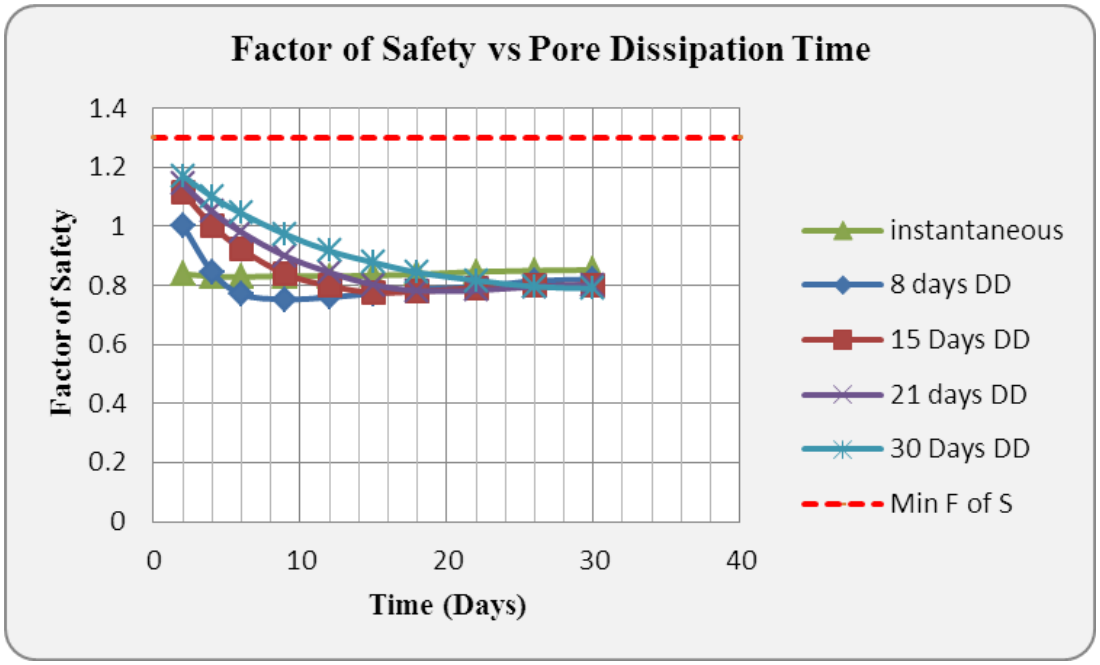

Fig. 5.63: Factor of Safety vs. time for sudden drawdown analysis (Upstream slope 1.5H: 1V)

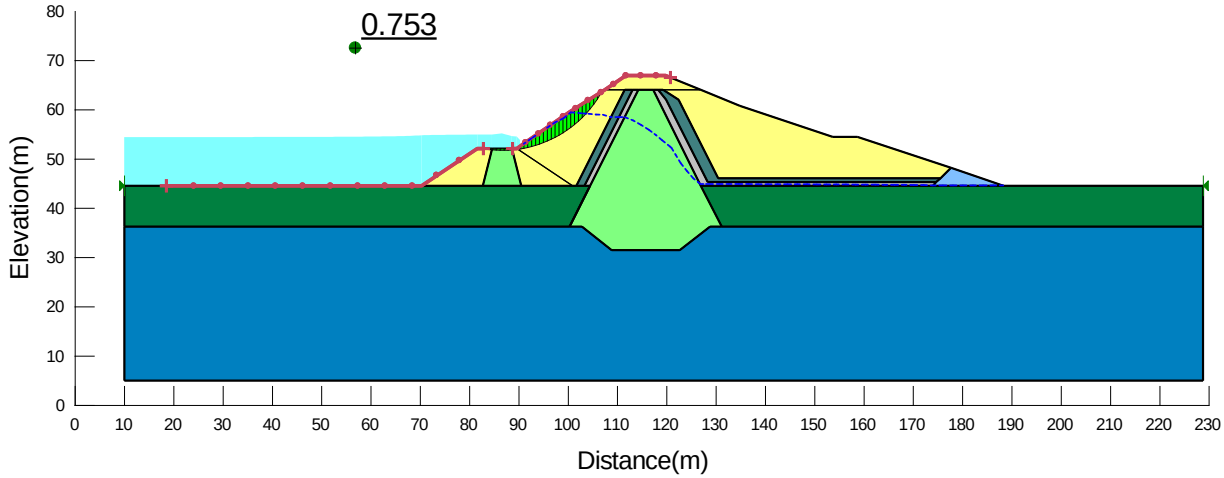

Fig. 5.64: Stability analysis for 8 days sudden drawdown (9th day) (upstream slope/unreinforced) (1.5H: 1V)

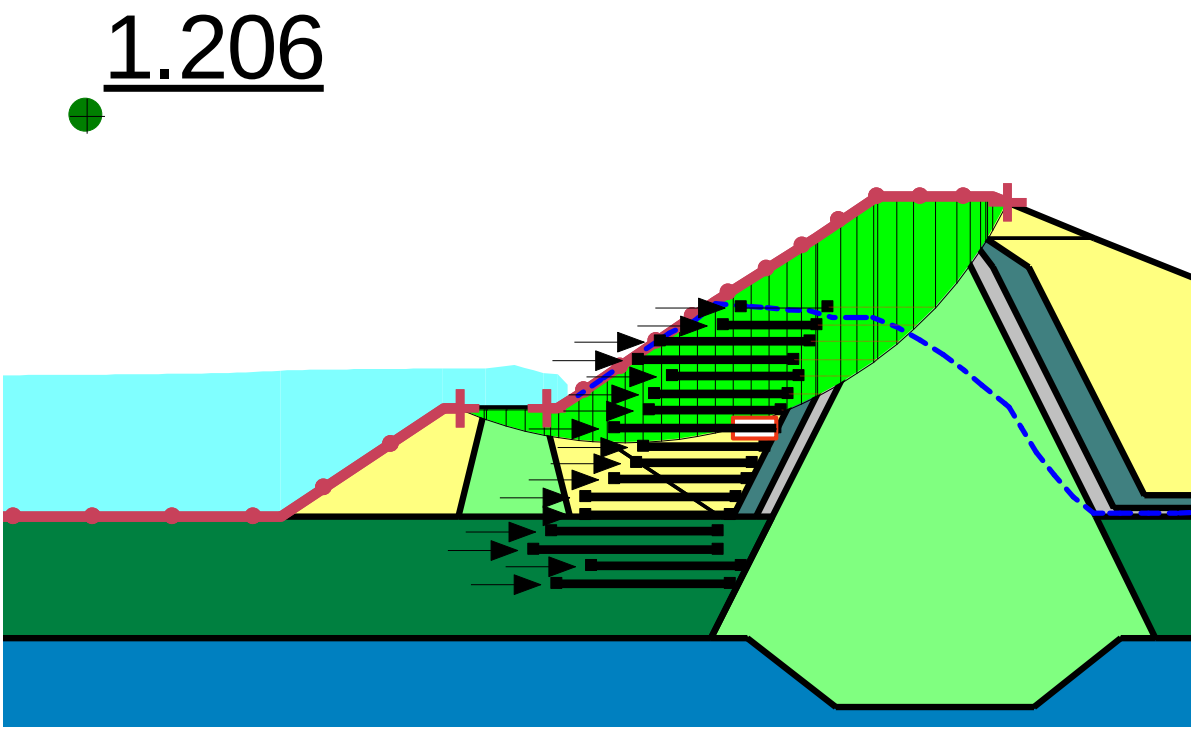

Fig. 5.65: Stability analysis (on 9th day) (upstream slope/reinforced with 1.6m Geotextile Spacing) (1.5H: 1V)

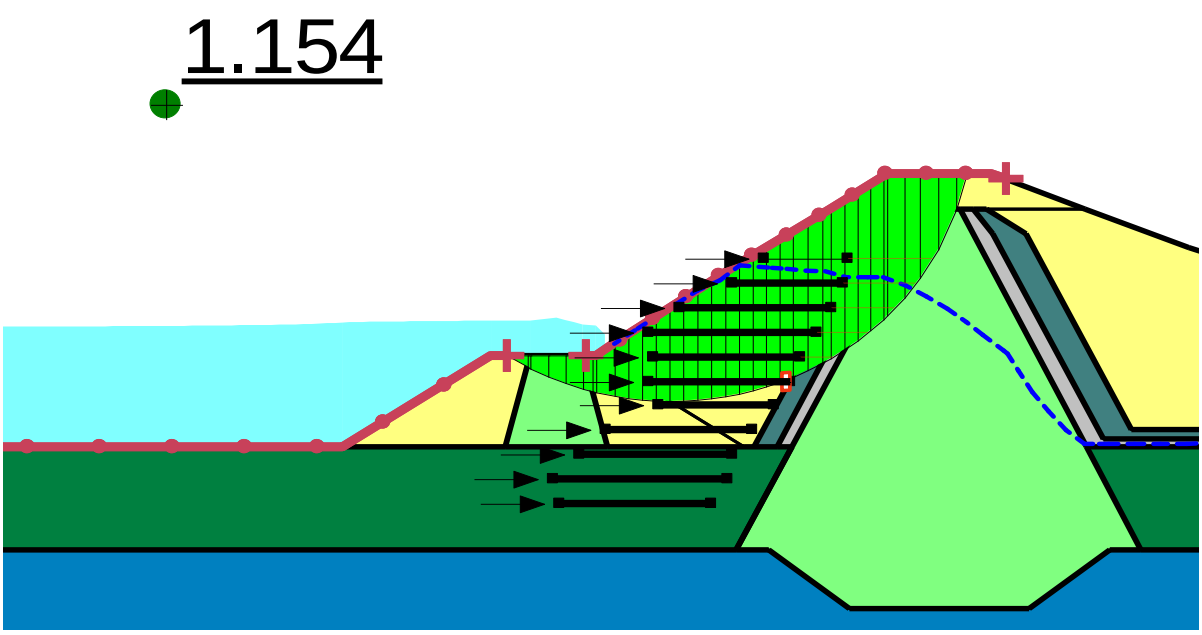

Fig. 5.66: Stability analysis (on 9th day) (upstream slope/reinforced with 2.0m Geotextile Spacing) (1.5H: 1V)

The summary for variation of factor of safety with spacing of geotextile reinforcement has been presented in the figure below.

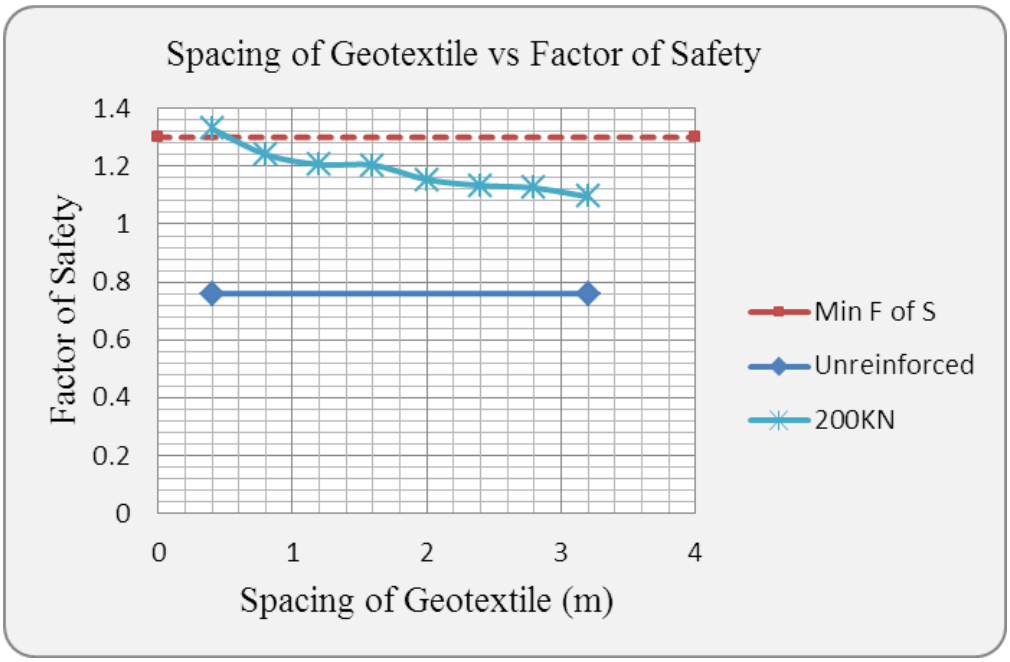

Fig. 5.67: Variation of Factor of Safety with spacing of Geotextile (upstream slope_sudden draw down condition_1.5H:1V)

1.25H: 1V (Upstream Slope_Sudden drawdown condition)

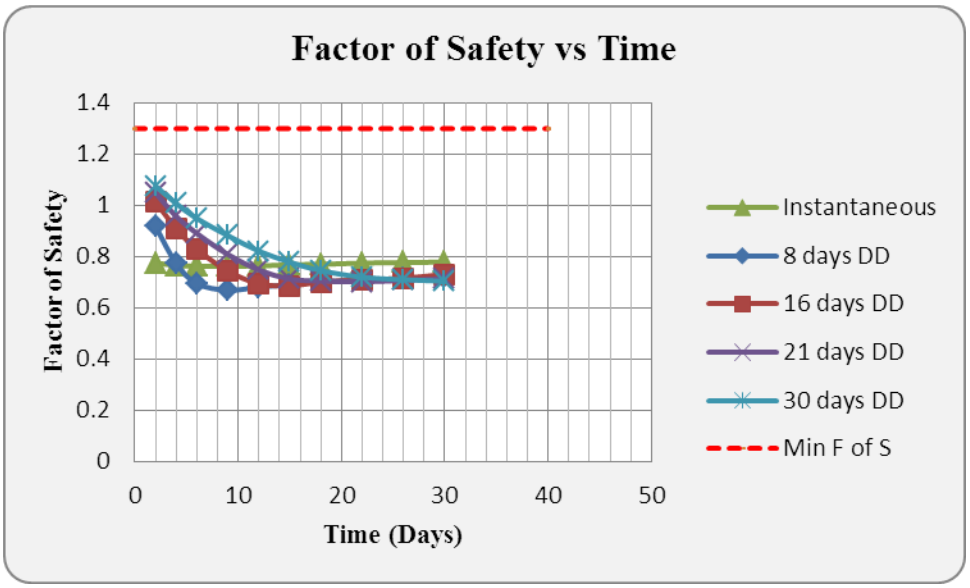

Fig. 5.68: Factor of Safety vs. time for sudden drawdown analysis (Upstream slope 1.25H: 1V)

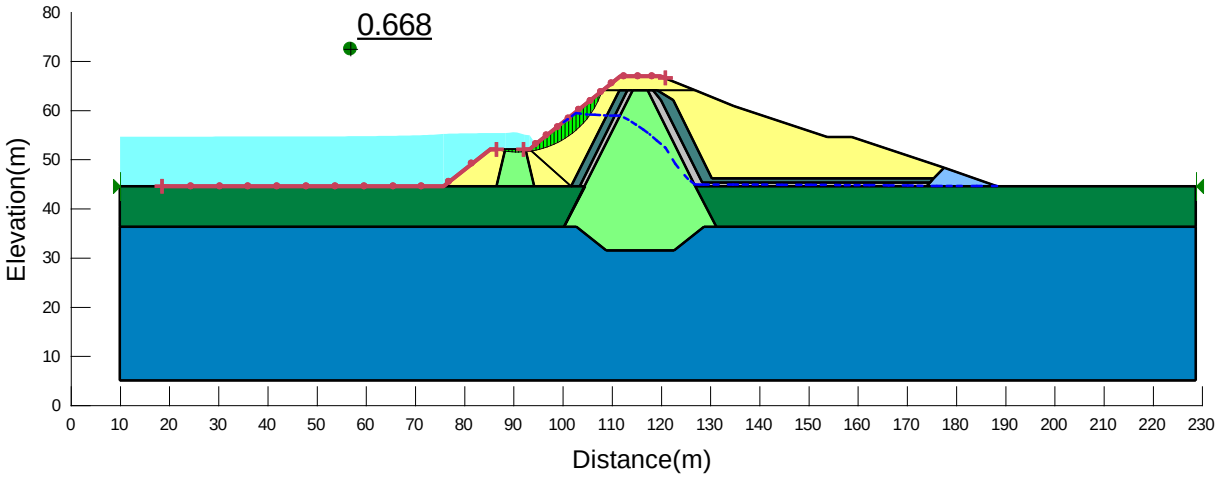

Fig. 5.69: Stability analysis for 8 days sudden drawdown (9th day) (upstream slope/unreinforced) (1.25H:1V)

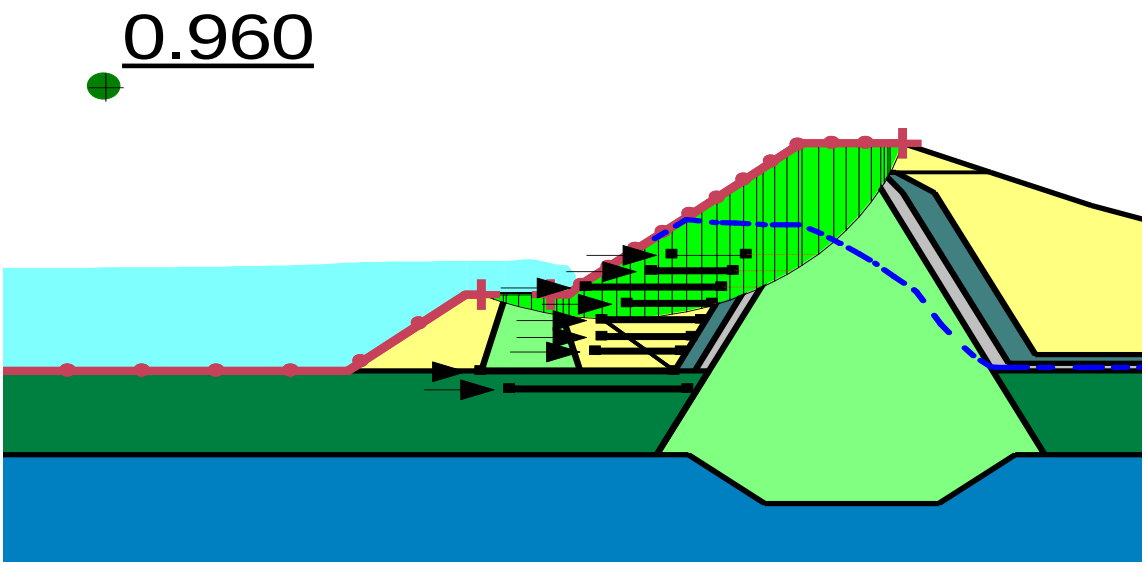

Fig. 5.70: Stability analysis (on 9th day) (upstream slope/reinforced with 1.6m Geotextile Spacing) (1.25H: 1V)

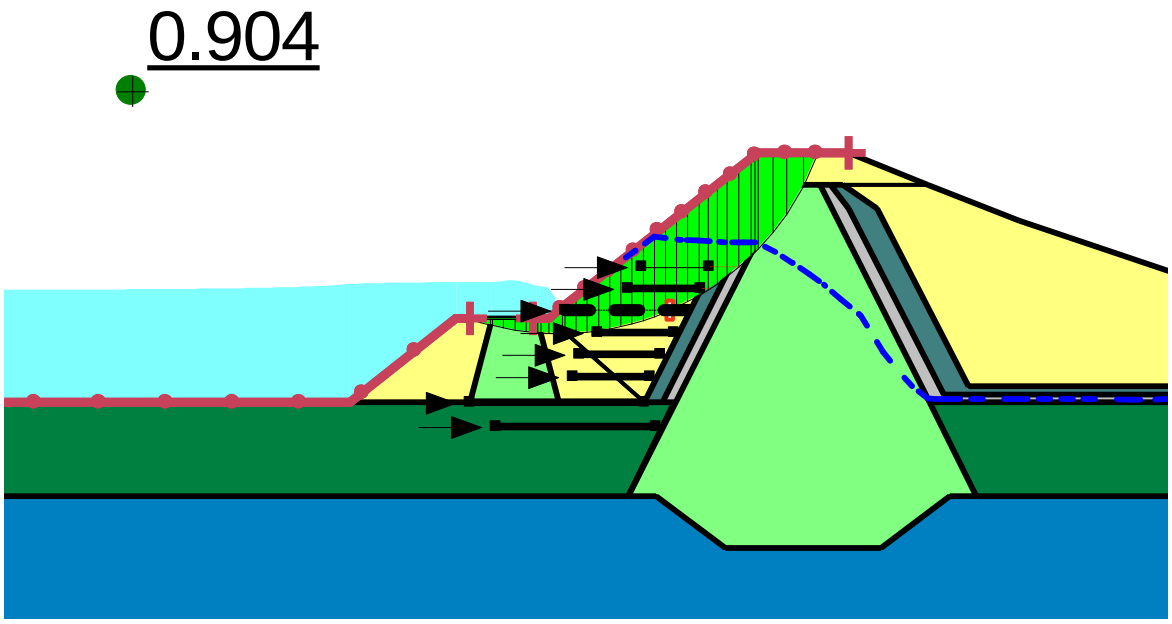

Fig. 5.71: Stability analysis (on 9th day) (upstream slope/reinforced with 2.0m Geotextile Spacing) (1.25H: 1V)

The summary for variation of factor of safety with spacing of geotextile reinforcement has been presented in the figure 5.72 below.

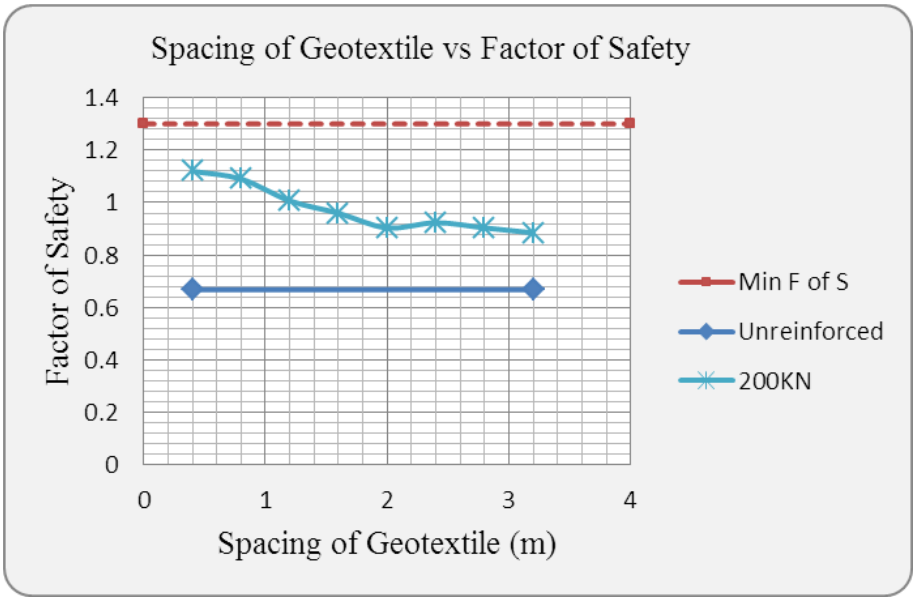

Fig. 5.72: Variation of Factor of Safety with spacing of Geotextile (upstream Slope_sudden draw down condition_1.25H:1V)

Summary of results and discussions for upstream reinforced sope analysis

The results of the downstream reinforced analysis under steady state seepage condition have been summarized and tabulated as shown in table 5.6 and Fig.5.73.

Table 5.5: Summary of analysis results for sudden drawdown condition for the upstream slope

Factor of safety against Geotextile reinforcement Spacing(Upstream Slope_under Sudden Drawdown Condition)						
Spacing(m)	Factor of Safety					
	2.5H:1V	2.25H:1V	2.0H:1V	1.75H:1V	1.5H:1V	1.25H:1V
0.4	1.921	1.631	1.665	1.536	1.33	1.12
0.8	1.871	1.682	1.603	1.426	1.241	1.09
1.2	1.753	1.598	1.501	1.365	1.206	1.007
1.6	1.74	1.542	1.469	1.362	1.204	0.96
2	1.645	1.559	1.366	1.302	1.154	0.904
2.4	1.625	1.514	1.389	1.25	1.134	0.924
2.8	1.559	1.48	1.378	1.242	1.125	0.904
3.2	1.55	1.456	1.333	1.216	1.095	0.885

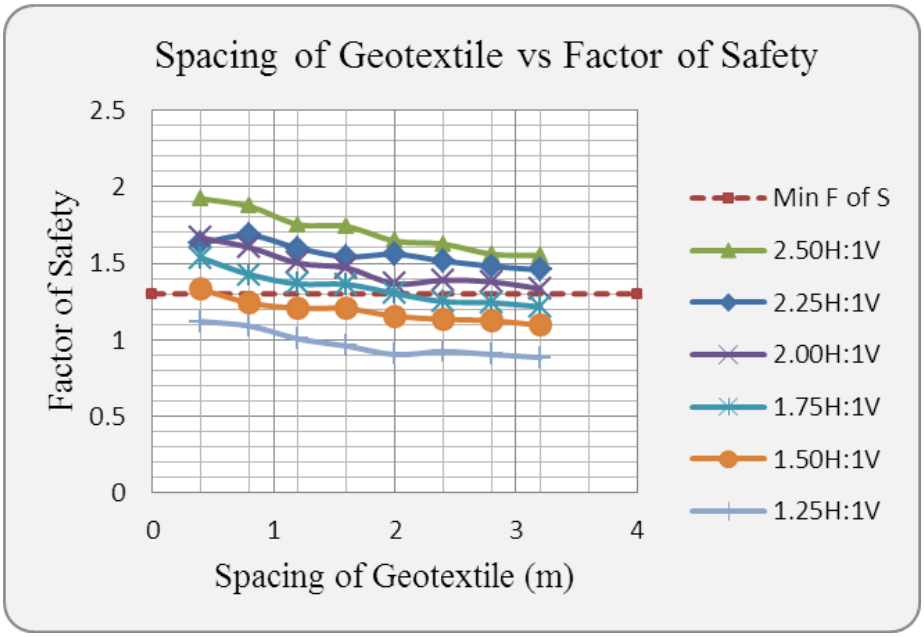

Fig. 5.73: variation of factor of safety with respect to spacing of geotextile layers (summary)

From the above figure we can deduce that

- Factor of safety is decreasing with increase in spacing between geotextile layers.
- By providing the geotextile layers at spacing of 2.0m, the upstream slopes of a dam can be made steeper up to 1.75H: 1V. The spacing can be up to 3.2m for gentler slopes
- The length of the geotextile layers required for reinforcing the upstream slope is found to be in the range of 8m to 16m.
- Offset from upstream slope are found to be in the range of 0m to 20m depending upon the location of geotextile layers.

5.1.4.5 Economic analysis

The economic analysis of the optimized reinforced section is carried out and compared with the unreinforced dam section. From the analysis it is observed that the reinforced dam section is 70% more economical.

Table 5.6: Earth fill material and foundation excavation saved due to reinforcement and its amount in Ethiopian birr

Description	Quantity (m3)	Unit rate (ETB)	Amount (ETB)
Downstream zone			
Earth fill	50,776.60	131.2	6,661,889.92
Foundation Excavation	50,035.85	109.5	5,478,925.58
Foundation backfill	50,035.85	131.2	6,564,703.52
Upstream zone			
Earth fill	50,229.10	131.2	6,590,057.92
Foundation Excavation	45,182.50	109.5	4,947,483.75
Foundation backfill	45,182.50	131.2	5,927,944.00
Total			36,171,004.69

Description	Area (m2)	Unit rate(ETB)	Amount (ETB)
Downstream zone			
Geotextile reinforcement	53384	80	4,270,720.00
Upstream zone			
Geotextile reinforcement	64726	100	6,472,600.00
Total amount			10,743,320.00
Difference amount			25,427,684.69
Amount saved (%)			70.30

5.2 Dynamic Stability Analysis

5.2.1 General

The QUAKE/W was used to compute the seismic embankment response. The program is two-dimensional, dynamic finite element software that uses equivalent linear strain-dependent modulus and damping properties. It is a time-step analysis that uses Rayleigh damping and allows variable damping for different elements. The program uses an iterative process to estimate nonlinear strain-dependent properties. Initially, shear modulus and damping ratios are estimated for each element in the finite element model, and the system is analyzed using these initial properties. After each cycle, values of the effective shear strain are computed for each element, and the corresponding modulus and damping properties, at the computed strain level, are compared with the estimated from the previous iteration. The analysis repeated until convergence is achieved.

5.2.2 Design Earthquake

5.2.2.1 Acceleration Time History (ATH)

The dynamic analysis of the Gidabo earth fill dam has been carried out by the Finite Element Method based state of the art computer program QUAKE/W (Geo slope, 2007). Horizontal and vertical acceleration time histories are key input parameters for QUAKE/W analysis. Therefore, site specific horizontal and vertical ATH for Gidbo earth fill dam should be produced using the peak accelerations and records of actual earthquakes. However, because there are no ATH records near the dam site, actual accelerographs recorded elsewhere have been used. The following three ATH data have been considered for the analysis (Messele, et al., 2006).

A. The 1940 Elcentro Record, USA (M=6.7, H=11 km, R=11.5 km).
B. ii) The 1995 Kobe JMA record, Japan (M=7.2, H=14.3 km, R=19 km).
C. iii) The 1968 Hachinohe record, Japan (M=7.9, H=0 km, R=200 km).

Since the 1940 Elcentro earthquake has been recorded on alluvium deposit, this appears to have the closest resemblance with the earthquake records that could happen in gidabo dam site area. However, in order to represent other possible earthquakes with different magnitude, time duration and frequency content, the 1995 Kobe JMA record (with shorter duration, big pulse) and the Hachinohe record (with longer duration) have also been considered.

5.2.2.2 Deconvolved ATH

In order to remove site and path effects, deconvolved ATH data have been used in the analyses for all the three cases (Messele, 1996). Also, the three ATH data have all been scaled to PGA values of 0.33g horizontal and 0.165g vertical corresponding to site specific MCE, and 0.13g horizontal and 0.075g vertical corresponding to site specific DBE (rifer Table 3.1). Fig. 5.74 to 5.75 below show the deconvolved ATH used for the analysis.

The 1940 El Centro Record (USA)

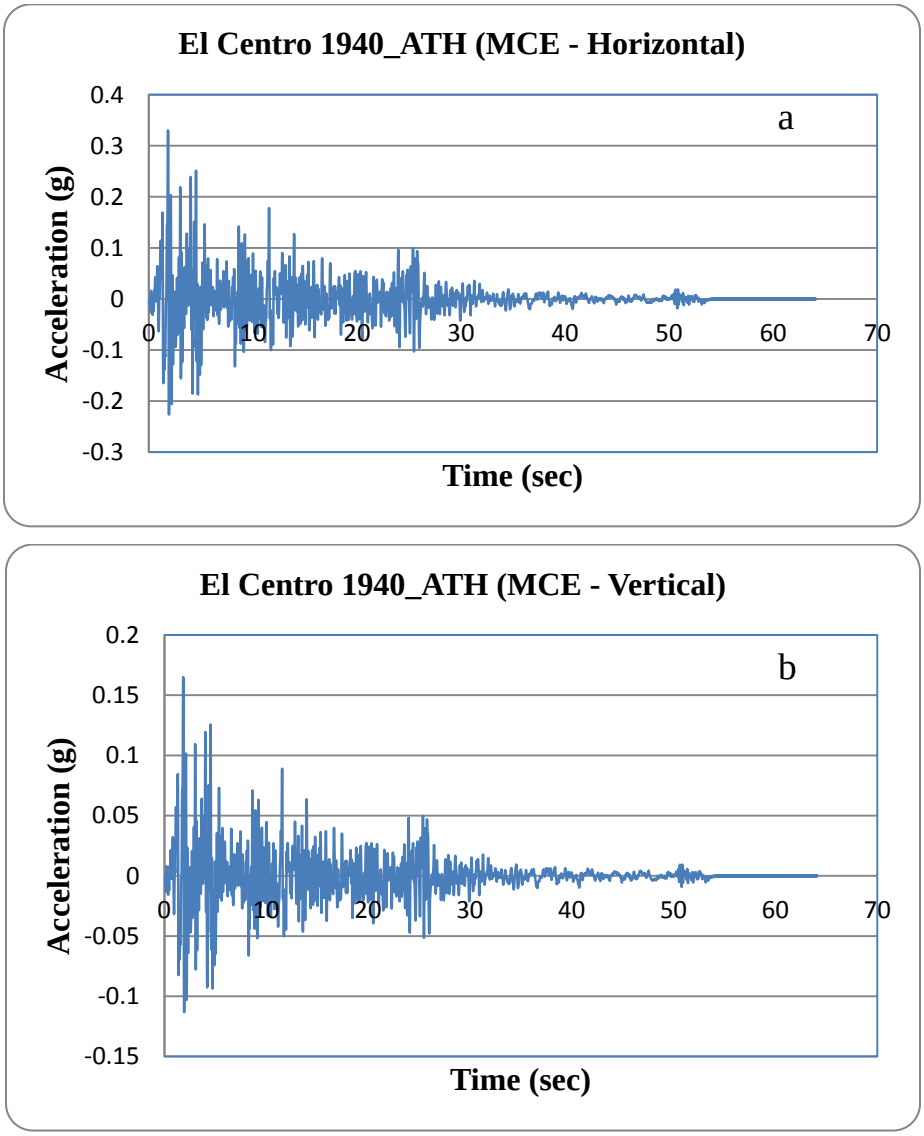

Fig. 5.74: El Centro 1940 a) MCE -Horizontal b) MCE –Vertical

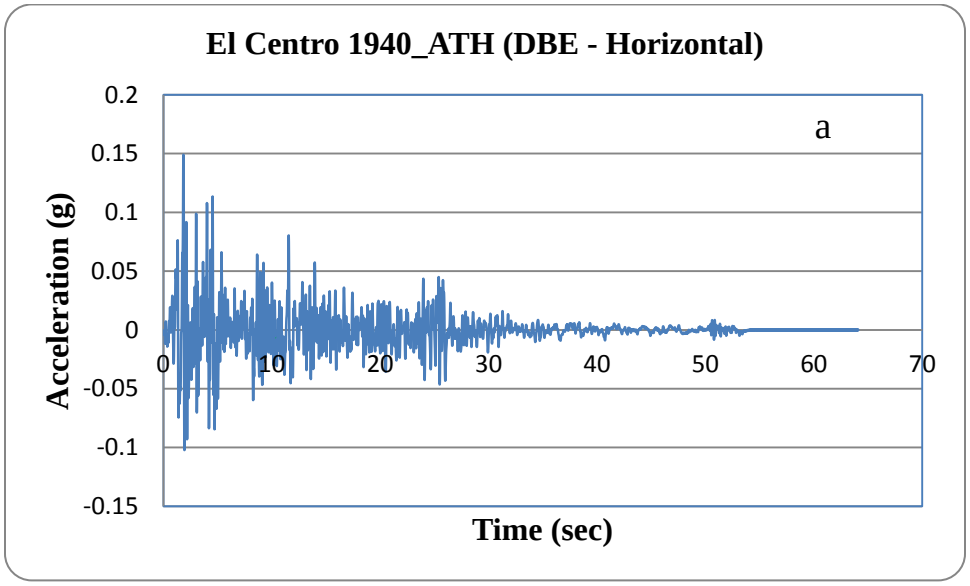

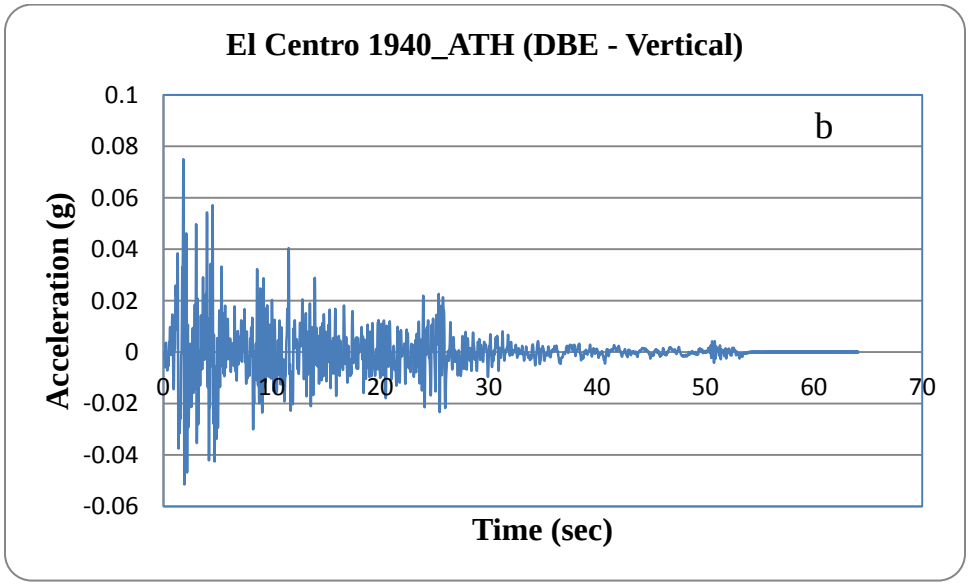

Fig. 5.75: El Centro 1940 a) DBE -Horizontal b) DBE –Vertical

5.2.3 Liquefaction Susceptibility Assessment of Gidabo Dam Materials

5.2.3.1 Based on Historic Criteria

Post-earthquake field investigations have shown that liquefaction effects have historically been confined to a zone within a particular distance of the seismic source. Ambraseys (1988) compiled worldwide data from shallow earthquakes to estimate a limiting epicentral distance beyond which liquefaction has not been observed in earthquakes of different magnitudes (Fig.5.76**).** The distance to which liquefaction can be expected increases dramatically with increasing magnitude.

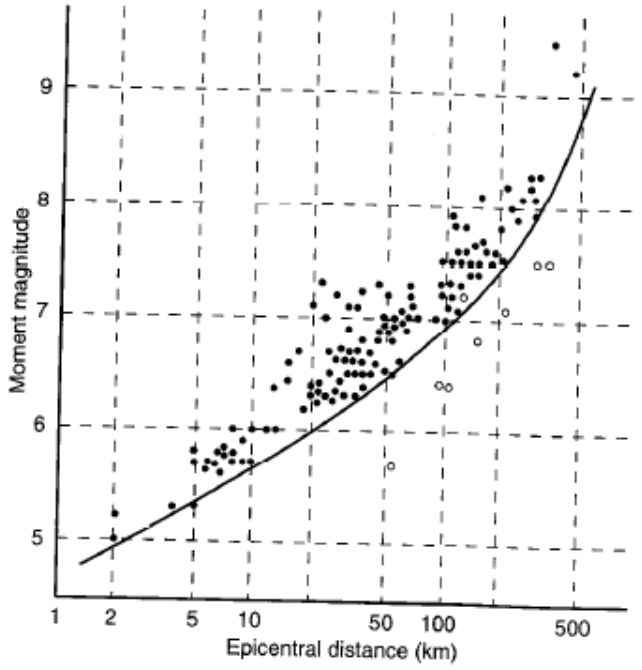

Fig.5.76: Relationship between limiting epicentral distance of sites at which liquefaction has been observed and moment magnitude for shallow earthquakes. Deep earthquakes (focal depth > 50 km) have produced liquefaction at greater distances. After (Ambraseys, 1988)

There is substantial evidence of movements along the faults of the Wonji Fault belt having occurred during the last 10,000 years. These faults are active but are located some away of the Gidabo site and From the interpretation of the data between 1400 and 1985 and the extreme value distribution of events with the magnitude and recurrence relationship, it is predicted a maximum magnitude (M max) of approximately 7.5 this value is adopted for the studies of Gidabo Project. Hence, taking this information to Figure 5.78, the gidabo dam site lies in non-liquefaction zone

5.2.3.2 Based on Geologic Criteria

Soil deposits that are susceptible to liquefaction are formed within a relatively narrow range of geological environments (Youd, 1991). The depositional environment, hydrological environment, and age of a soil deposit all contribute to its liquefaction susceptibility (Youd, et al., 1977).Geologic process that sort soil into uniform grain size distributions and deposit them in loose states produce soil deposits with high liquefaction susceptibility. Consequently, fluvial deposits and colluvial and oeolian deposits when saturated are likely to be susceptible to liquefaction. The Susceptibility of older soil deposits to liquefaction is generally lower than that of the newer deposits.

The geological profile along the gidabo dam axis (Fig. 5.76) shows that the top 8 to 10m is a recent loose and compressible deposit and it has been removed with a fear of foundation settlement and liquefaction susceptibility. The remaining (10 to 39m) depth of the foundation is a sandy gravel material. Besides, the dark brown color material located in the middle of the foundation has been removed and treated locally with competent foundation material. The embankment (shoulder) and compacted alluvium (which is used to replace the removed part of the foundation) comprised of sandy gravel material. Hence, gidabo dam site materials don't satisfy the liquefaction susceptibility based on geologic criteria.

5.2.3.3 Based on Compositional Criteria

The liquefaction, which requires the development of excess pore pressure, susceptibility is influenced by the compositional characteristics that influence volume change behavior. Compositional characteristics associated with high volume change potential tend to be associated with high liquefaction susceptibility. These characteristics include particle size, shape and gradation.

Fine-grained soils were considered incapable of generating the high pore pressures commonly associated with liquefaction, and coarser-grained soils were considered too permeable to sustain any generated pore pressure long enough for liquefaction (Kramer, 1996).

Liquefaction of nonplastic silts has been observed (Ishihara, 1984) and (Ishihara , 1985)in the laboratory and the field ,indicating that plasticity charactersitics rather than grain size alone influence the liquefaction susceptiblity of fine grained soils. Clays remain nonsusceptible to liquefaction. Fine grained soils that satisfy each of the following four chinese criteria (Wang, 1979) may be considered susceptible to significant strength loss:

- Fraction finer than 0.005 mm≤15%
- Liquid limit LL≤35%
- Natural water content ≥ 0.9LL
- Liquidity index ≤0.75

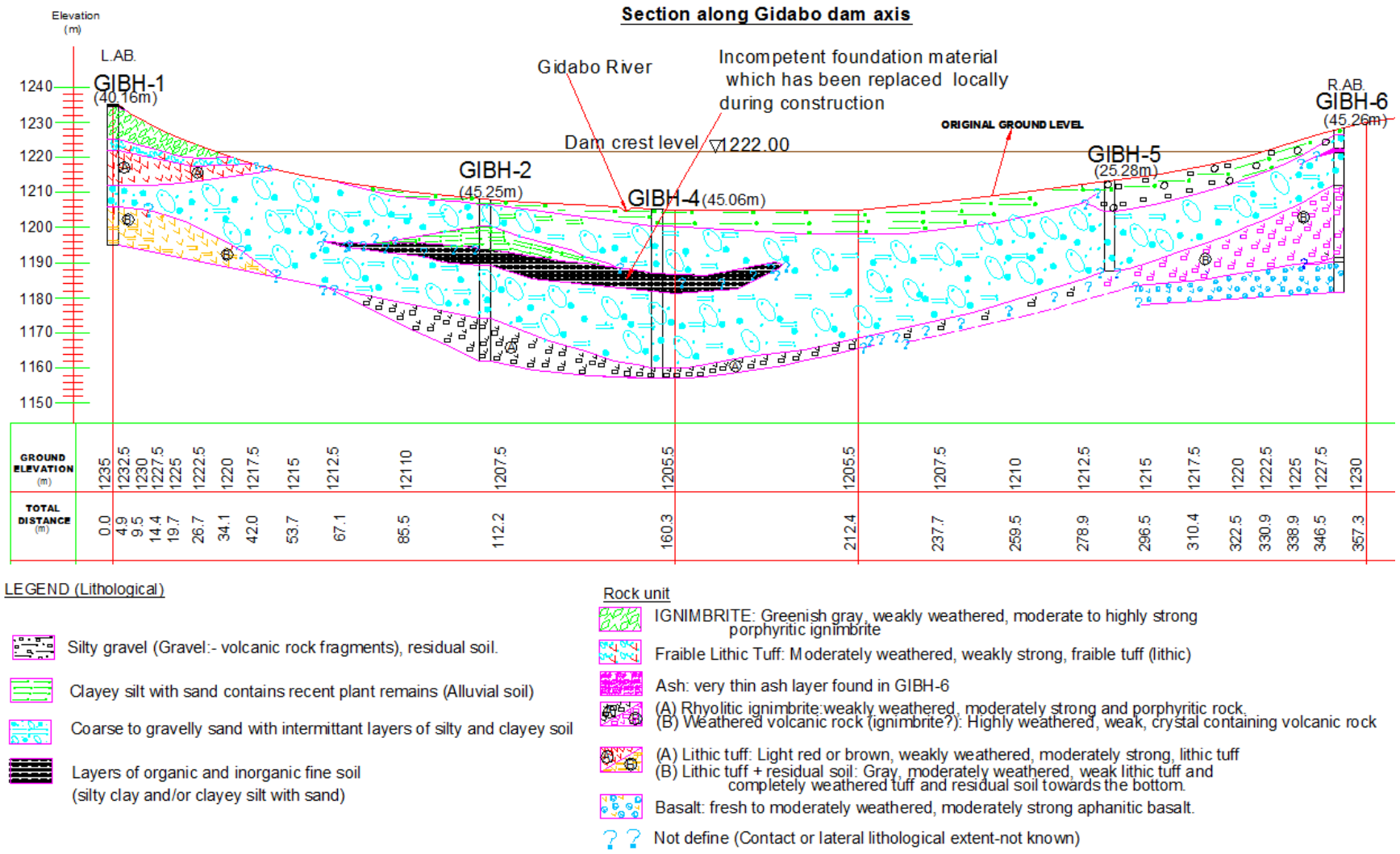

Fig. 5.76: Geological profile along the dam axis

At the other end of the grain size spectrum, liquefaction of gravels has been observed in the field (Wong, 1984), (Youd,T.L et al) When pore pressure dissipation is impeded by the presence of impermeable layers so that truly undrained conditions exist, gravelly soils can also be susceptible to liquefaction.

Liquefaction susceptibility is influenced by gradation. Well-graded soils are generally less susceptible to liquefaction than poorly graded soils; the filling of voids between larger particles by smaller particles in a well graded soil results in lower volume change potential under drained conditions and, consequently, lower excess pore pressures under undrained conditions. Field evidence indicates that most liquefaction failures have involved uniformly graded soils (Kramer, 1996).

USNRC 1985 proposed grain size distribution boundaries separating liquefiable and non-liquefiable soils as shown in Fig. 5.77 and is widely used by geotechnical engineers worldwide.

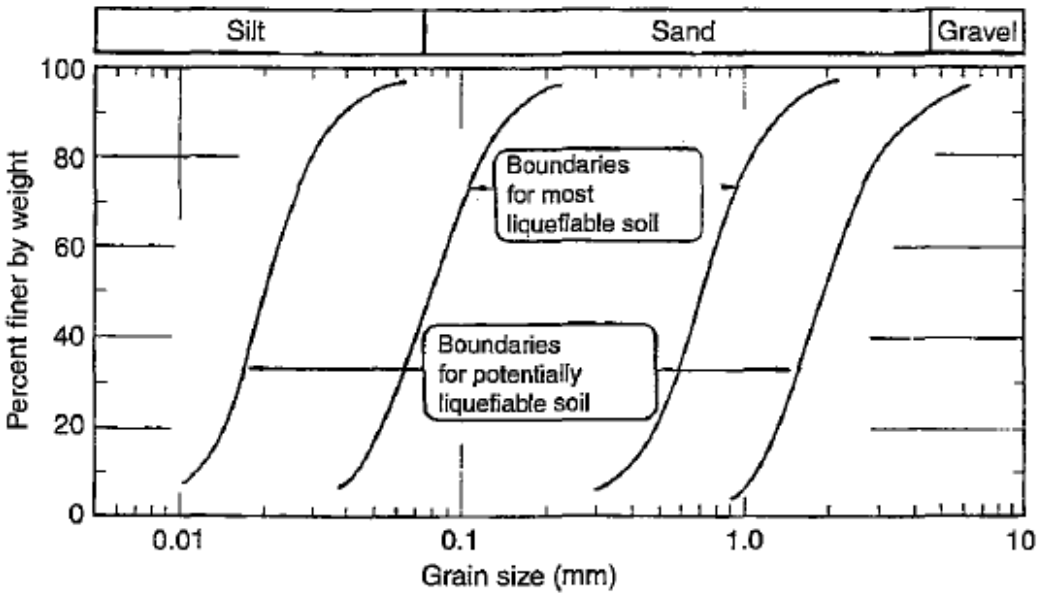

Fig. 5.77: Limits in the particle size gradation curves separating liquefiable and nonliquefiable soils as suggested in 1985 by USNRC (USNRC, 1985).

As shown in Fig. 5.78, this criterion is used for assessment of liquefaction susceptibility of gidabo dam shell and compacted alluvium materials. The liquefaction susceptibility on the basis of grain size distributions shows that the shell and alluvium materials are well graded and 60 to 90% of these materials lie outside the boundaries for potentially liquefiable soils.

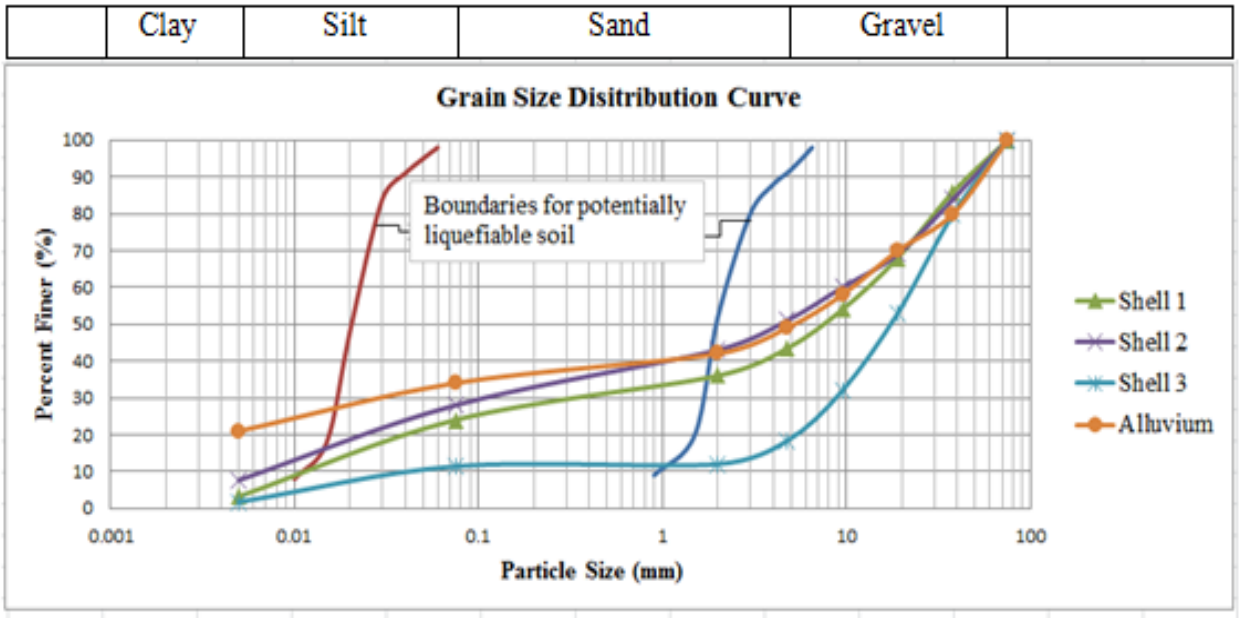

Fig. 5.78: Gradation curves for borrow areas (shell 1, Shell 2, shell 3 and compacted alluvium)

Since the loose and compressible fine layer has been removed up 8 to 10 meter from the foundation layer, the remaining layer of the foundation is mainly comprised of sandy gravel material which has SPT value between 17 to 34. Thus, based on the above listed criteria, the foundation is not categorized in to liquefaction susceptible material.

5.2.4 Finite Element Model

Figure 5.79 shows the finite element model used for the dynamic analysis of Gidabo earth fill dam. The model is prepared using the QUAKE/W program for the maximum cross-section of the dam. Both structured and unstructured meshes are used. The bottom boundary of the model has been taken at the surface of the ignibrite bed-rock underlying a 10 m replaced compacted alluvium and a 30 m sandy gravel layer as shown in Fig 5.76. In order to minimize the disturbance due to the boundary wave reflection in the dynamic analyses, the side boundaries were extended by 100 m (about 3 to 4 times the dam height) on both left and right directions. To account for damping of the soils on left and right boundaries, both horizontal and vertical dumping boundary conditions have been applied on left and right ends of the models. Some details have also been given in Fig. 5.80.

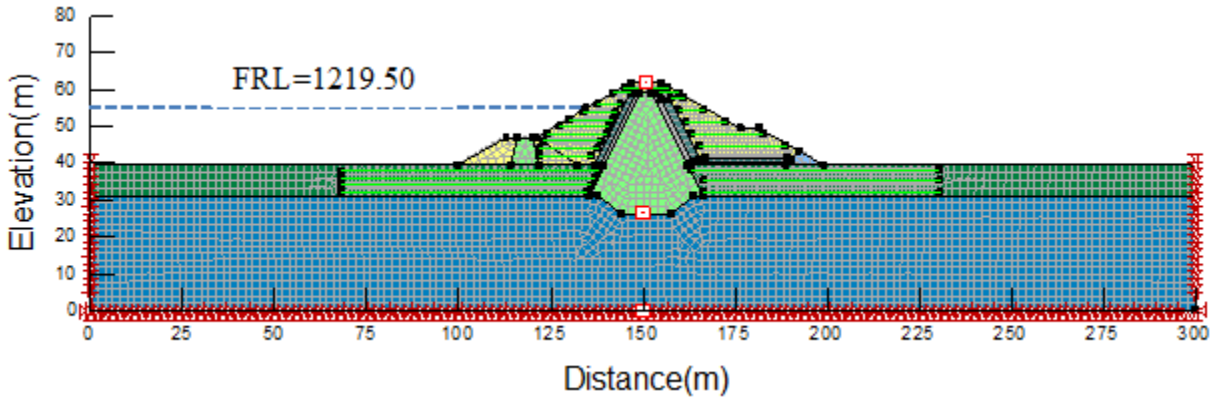

Fig. 5.79: Finite element model for dynamic analysis

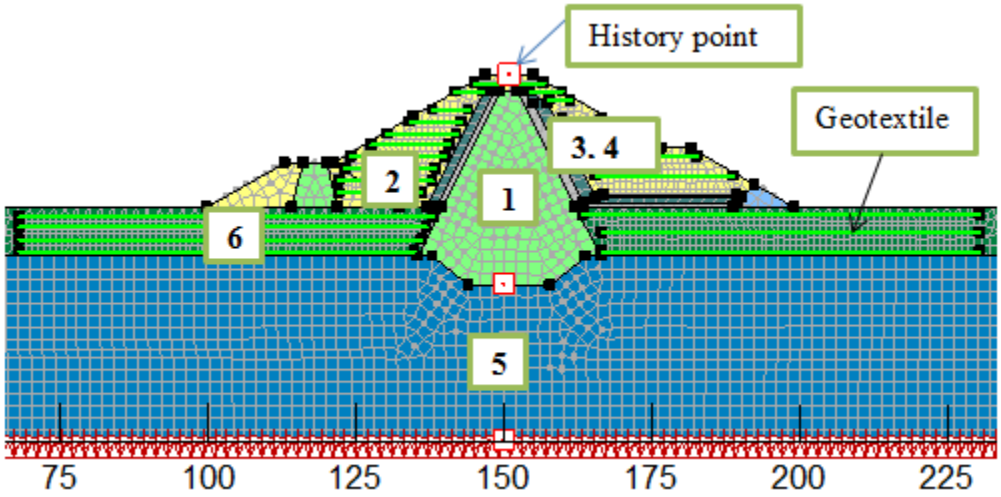

1: Clay Core 2: Sandy Gravel Shell 3: Fine Filter 4: Coarse Filter 5: Foundation 6: Compacted Alluvium

Fig. 5.80: Finite Element Model for dynamic Analysis (Impervious Boundary and History Points)

5.2.5 Dynamic analysis results

5.2.5.1 General

Material properties required for the dynamic response analyses using the equivalent linear approach are: total unit weights, Poisson's ratio, dynamic shear modulus at low strain (Gmax) and the relationships of the modulus reduction factors, G/Gmax, and damping ratio with shear strain. However, the dynamic characteristics of the dam materials have not been investigated by means of dynamic triaxial tests. Therefore, the material properties required for the dynamic analysis have been estimated with the help of the geotechnical literatures as explained in chapter 3.

5.2.5.2 Pore pressure ratio function for potentially liquefiable soil

Incase of liquefaction potential assesment of a given material during an earthquake shaking, pore pressure ratio which is a function of the equivalent number of uniform cycles N for a particular earthquake and the number of cycles N_L, which will cause liquefaction for a particular soil under a particular set of stress conditions has been deployed for analysis. However, as we discussed in section 5.2.3.2 and 5.2.3.3 of this chapter, there is no soil which is susceptible to liquefaction, hence, pore pressure function is not required for our QUAKE/W analysis.

Besides, in Tendaho earth fill dam dynamic analysis by Messele H. and Hadush S. (Messele, et al., 2006), analysis is carried out by assuming sandy gravel shell as potentially liquefiable soil and the result shows all the materials have been liquefied. However, they didn't accept the result by explaining as the pore pressure function shown in Fig 3.14 is mainly developed for potentially liquefiable sands and cannot represent the behavior of these materials. Hence, liquefaction analysis by assuming sandy gravel material and foundation as potentially liquefiable material for Gidabo earth fill dam will lead to the same conclusion.

5.2.5.3 Pore Pressure ratio considering potential pore pressure build up

As stated earlier, assessment of the liquefaction susceptibility on the basis of grain size distribution and other criteria for Gidabo Sandy gravel shell and compacted alluvium show that 60 to 90% of these materials lie outside the boundaries for potentially liquefiable soils. Moreover, the selected materials for the dam construction are in most cases well graded and suitable for achieving good compaction (or densification) which minimizes liquefaction susceptibility. Therefore, these materials are considered to be non-liquefiable soils but with a potential for some pore water pressure build up during earthquake shaking. To account for the pore water pressure build up, a constant r_u value of 0.3 has been used. This value has been determined based on the publication by (Malla, et al., 2005) , which deals with the dynamic analysis of a 75 m earth-fill dam in India. For the clay core r_u = 0.35 has been used based on Gidabo dam design report (WWDSE, 2009).

5.2.6 Initial In-Situ Stress Analysis

A QUAKE/W dynamic analysis can not be solved without first establishing the initial stresses. Hence before the dynamic analysis, the initial insitu stresses of Gidabo dam has been established by SIGMA/W " Initial Static" method.

Pore Water Pressure

Initial pore water pressure has been used from finite element computed pore water pressure using SEEP/W analysis.

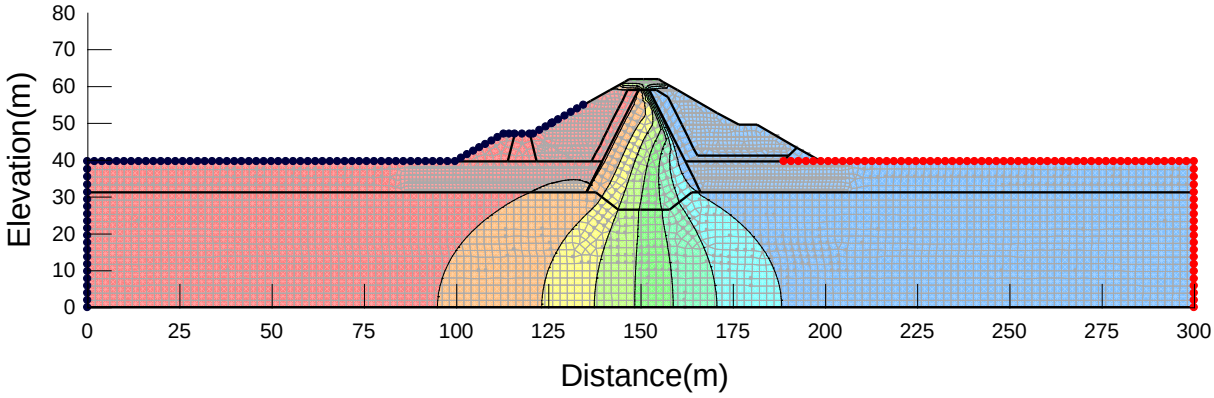

Fig. 5.81: Total Head Contour from SEEP/W Steady state analysis

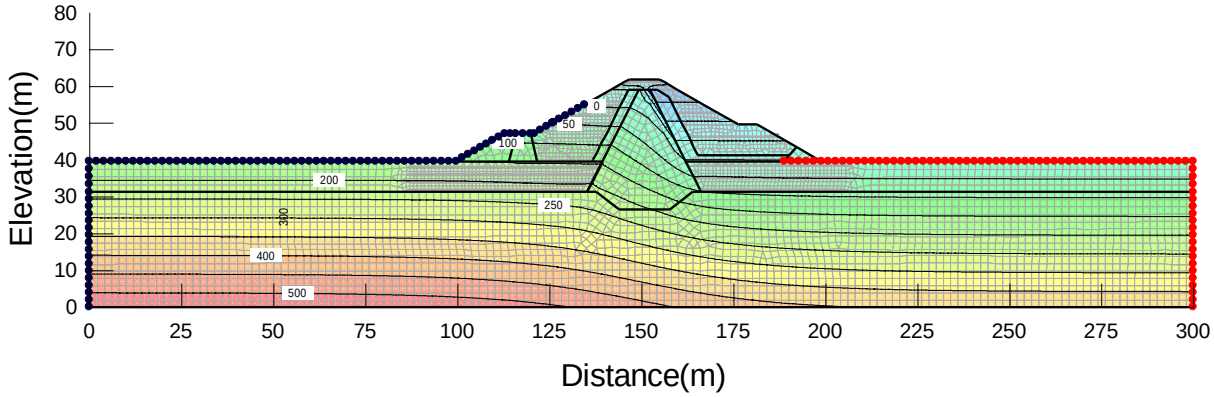

Fig. 5.82: Pore Water Pressure Contour taken from SEEP/W

The computed initial static stress results were counter checked using manual calculations and the results were in very good agreement. Then, the computed results of the initial static stress were then imported to the dynamic analysis part of the QUAKE/W program.

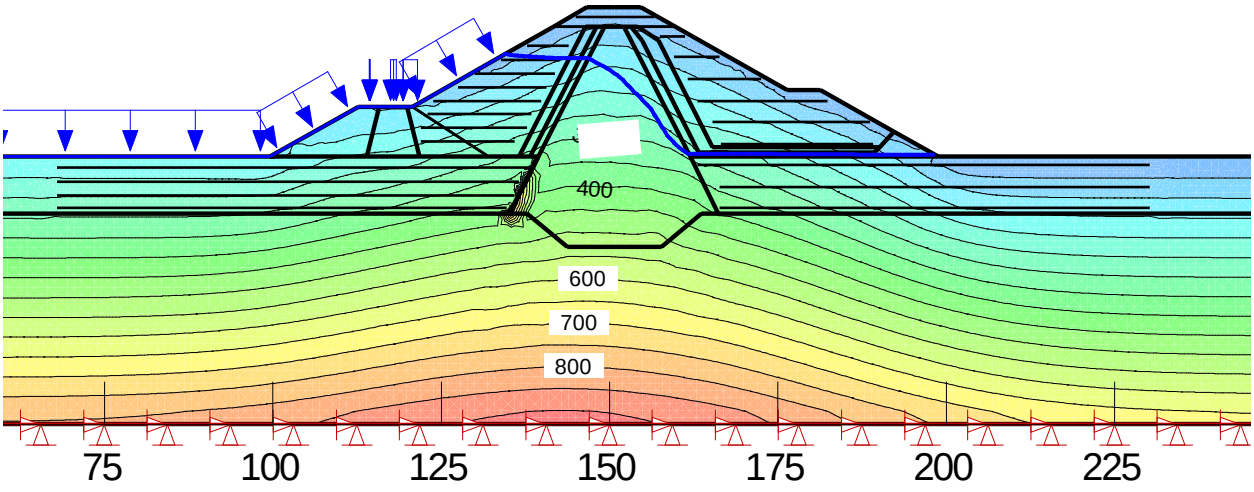

Fig. 5.83: Total Vertical Stress at in situ condition

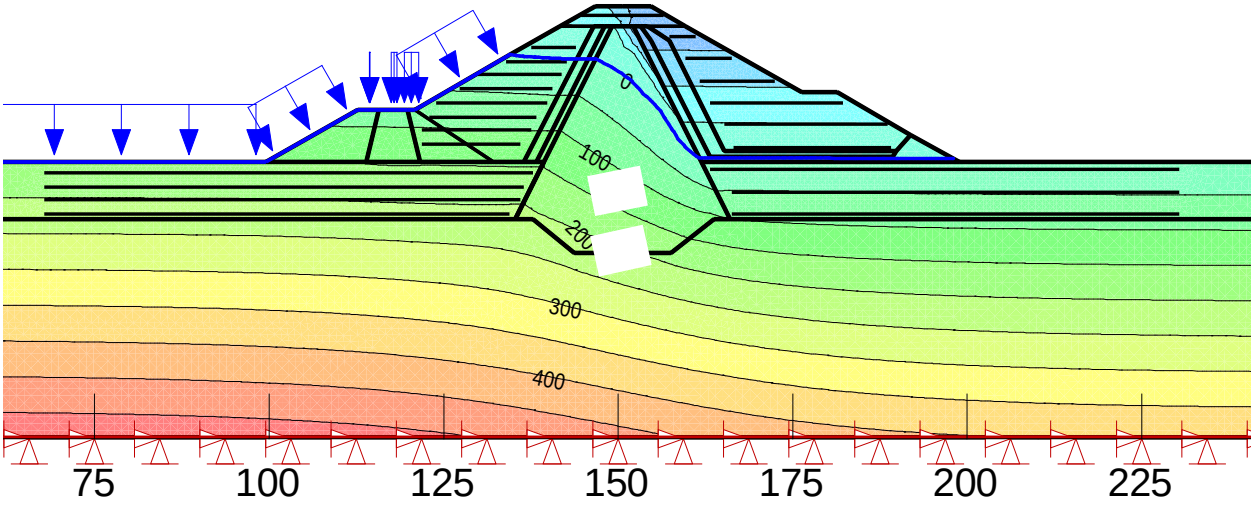

Fig. 5.84: Pore Water Pressure Contour for insitu state condition

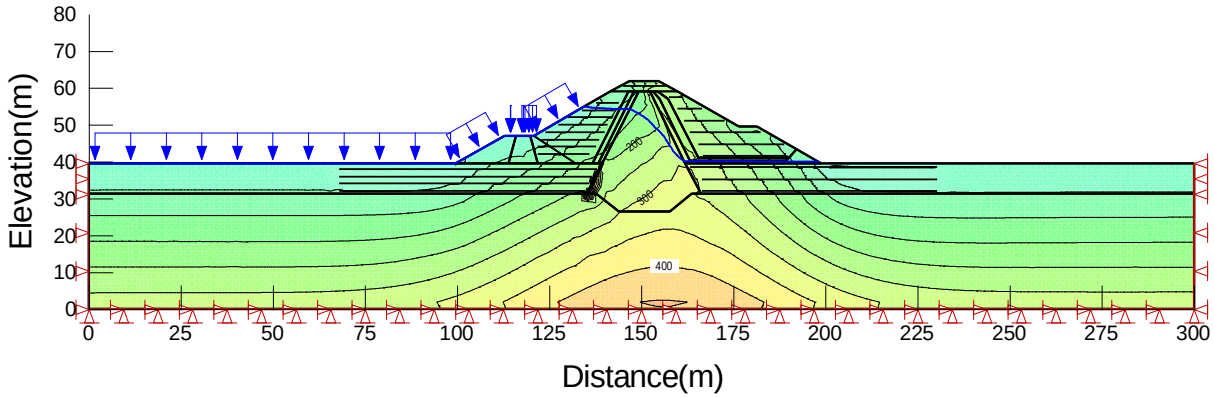

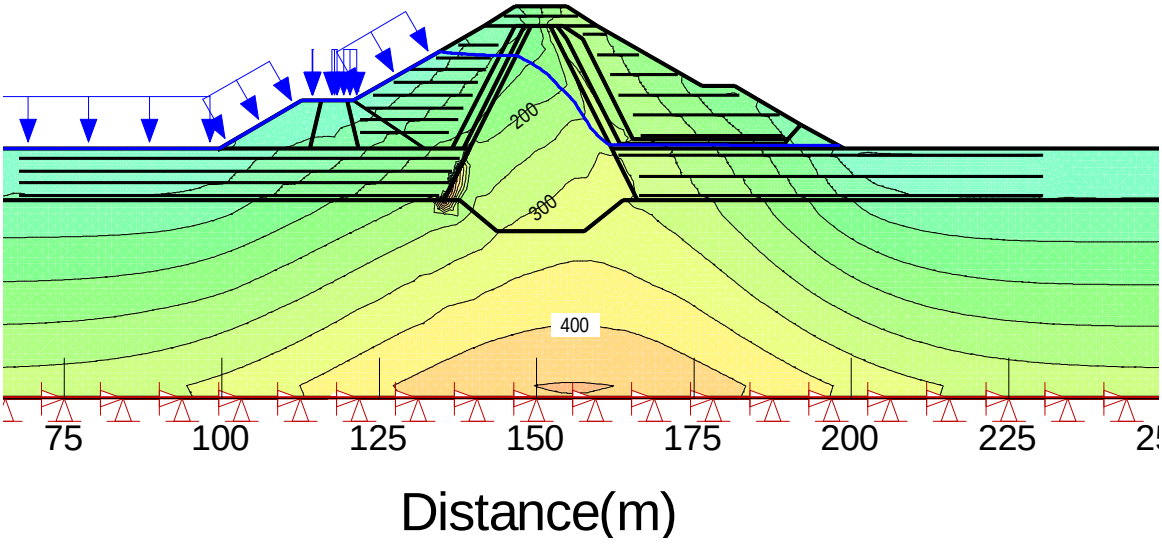

Fig. 5.85: Vertical Effective Stress Contour at in situ condition

5.2.7 Dynamic analysis results and discussions

5.2.7.1 Acceleration response at the dam crest

Figure 5.86 and 5.88 show the acceleration response at the dam crest corresponding to the site specific MCE horizontal and vertical PGA, respectively for Elcentro earthquake. As shown in figure a, the predicted ground accelerations at the dam crest are 0.85g and 0.403g ,for the horizontal and vertical MCE accelerations, respectively,as compared to base input accelerations of 0.33g horizontal and 0.165g vertical. This amplification of acceleration is at the crest is expected. Similarly, as shown in Fig. 5.87 and 5.89,the predicted peak ground accelerations at the dam crest are 0.47g and 0.26g ,for horizontal and vertical DBE accelerations,respectively,as compared to base input acceleration of 0.15g horizontal and 0.075g vertical. Results for other earthquakes are given in Appendix C and D.

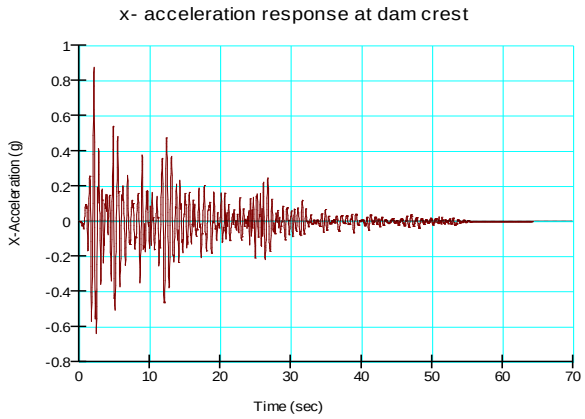

Fig. 5.86: x- acceleration response at dam crest for El Centro (MCE)

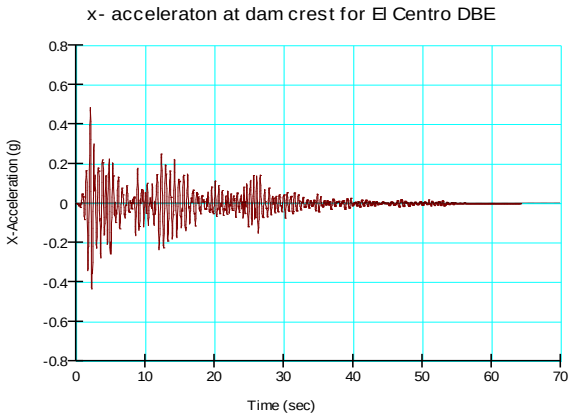

Fig. 5.87: x- acceleration response at dam crest for El Centro (DBE)

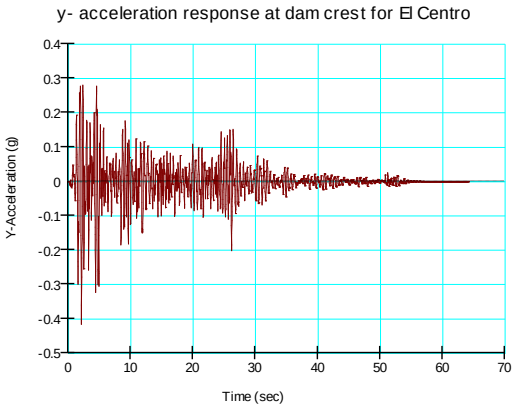

Fig. 5.88: y- acceleration response at dam crest for El Centro (MCE)

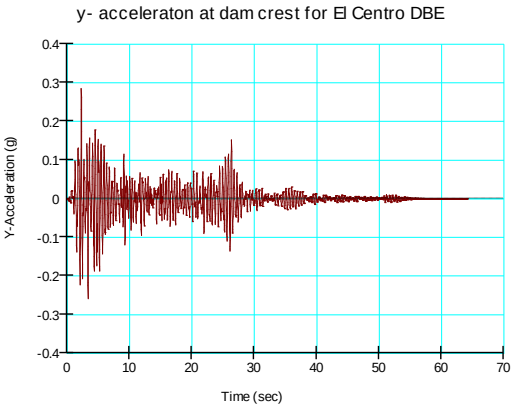

Fig. 5.89: y- acceleration response at dam crest for El Centro (DBE)

5.2.7.2 Spectral response at dam crest

As it can be seen from Fig. 5.90 and 5.91, the maximum spectral response for the dam corresponding to maximum credible earthquake (MCE) is found on a period of 0.55sec (frequency of 1.82 cycles per second) which is nearly the same for both horizontal and vertical components and it is found to be in the range of natural frequency of embankment dams (0.5 Hz to 10Hz). Similarly, for the case of design base earthquake (DBE), as shown in Fig.5.92 and 5.93, the maximum spectral response is found on 0.56sec (1.79 cycles per second) corresponding to horizontal component and 0.42sec (2.38 cycles per second) corresponding to vertical component and it is also within the range of natural period or frequency for embankment dams.

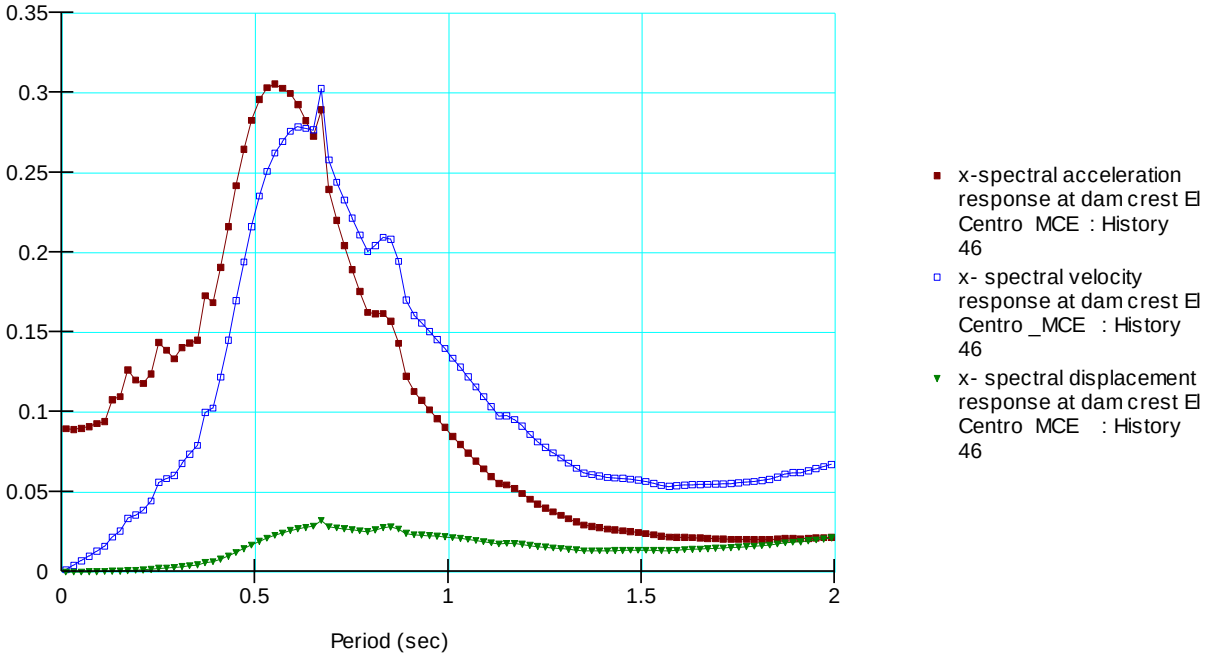

Fig. 5.90: Horizontal spectral response at dam crest corresponding to MCE (El Centro)

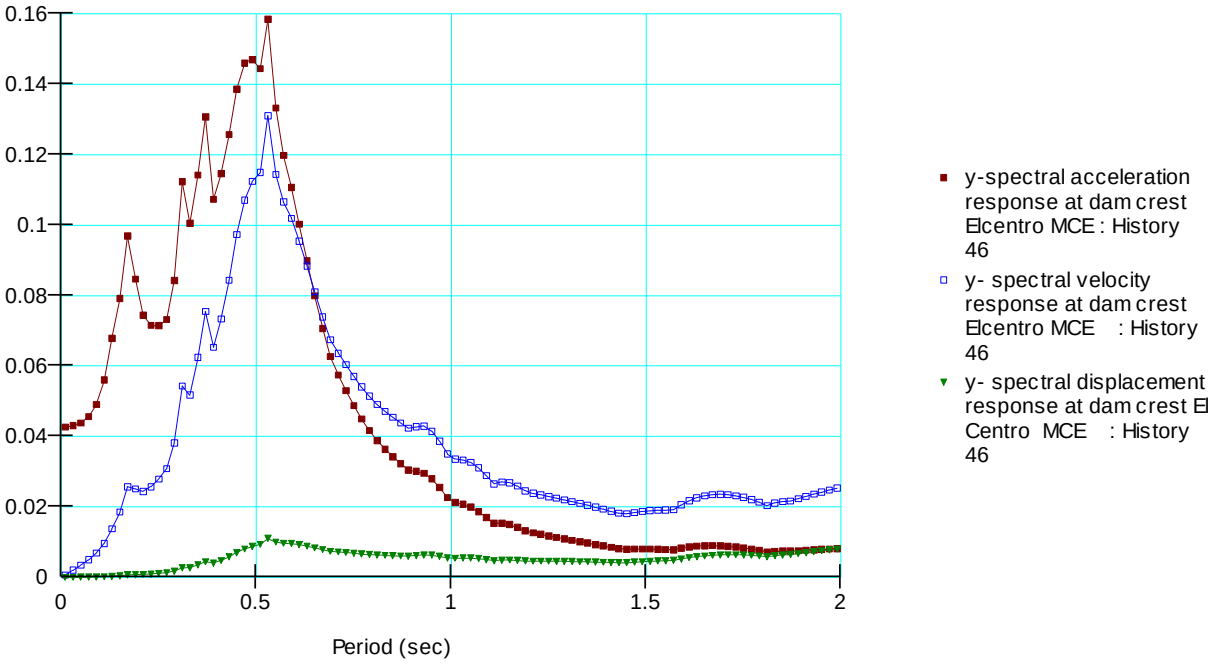

Fig. 5.91: Vertical spectral response at dam crest corresponding to MCE (El Centro)

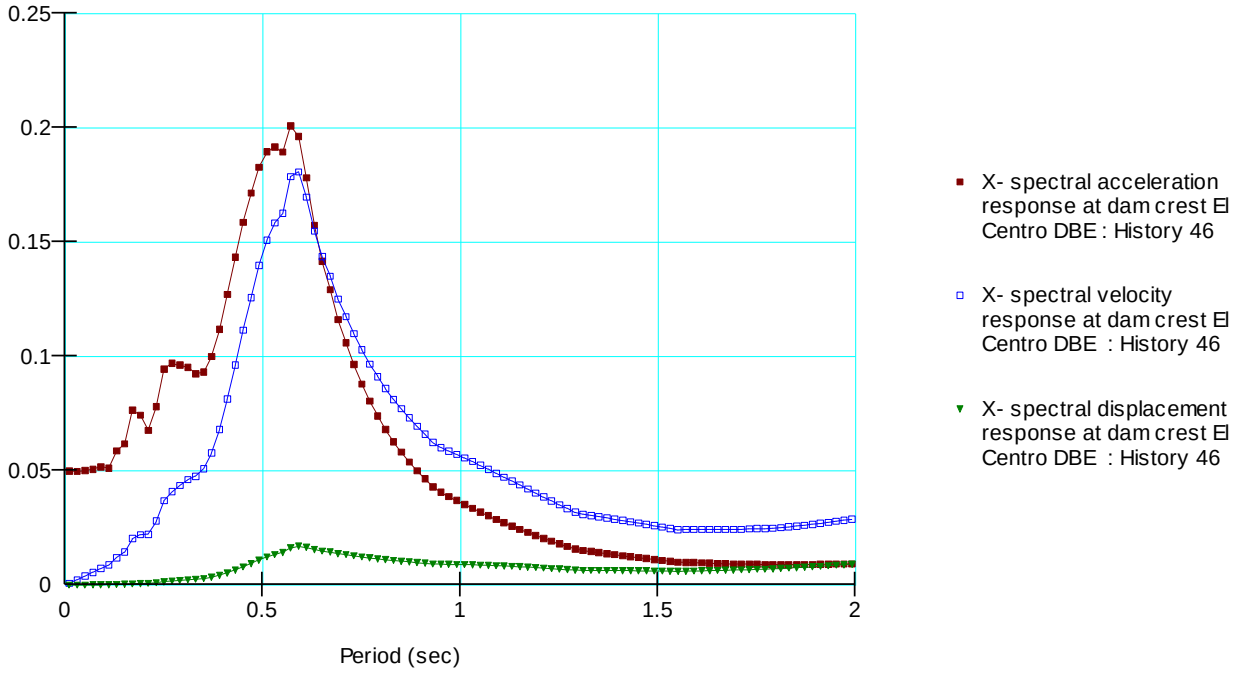

Fig. 5.92: Horizontal spectral response at dam crest corresponding to DBE (El Centro)

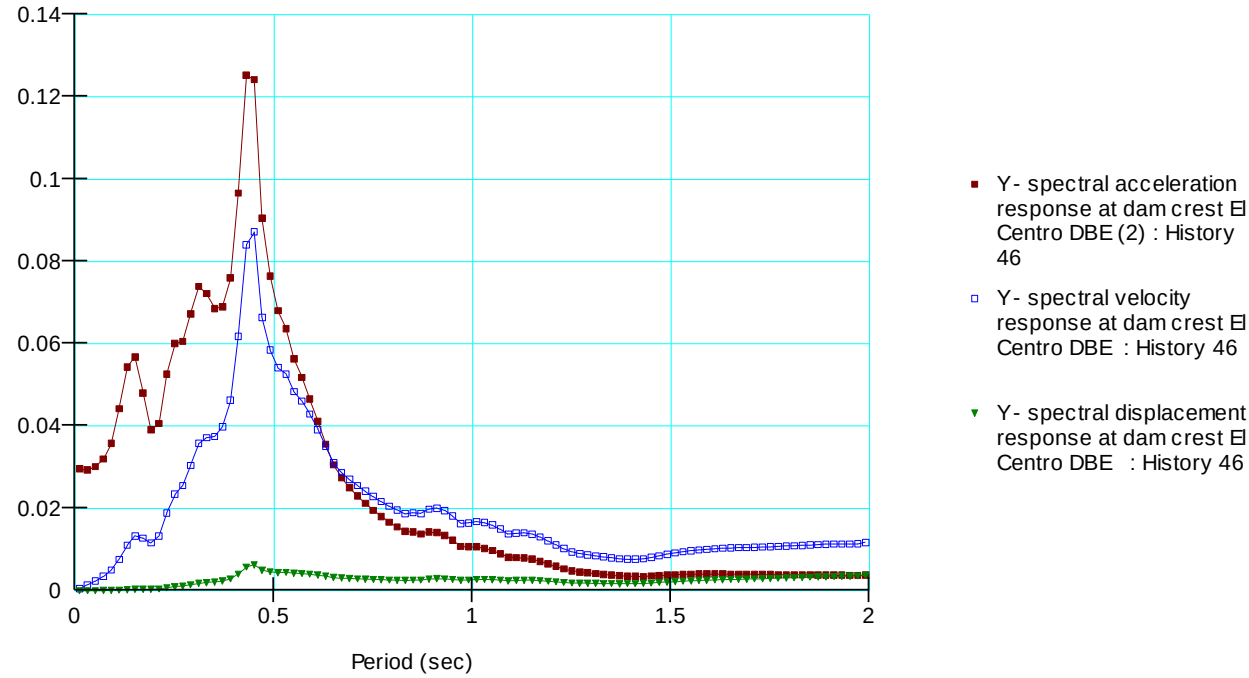

Fig. 5.93: Vertical spectral response at dam crest corresponding to DBE (El Centro)

5.2.7.3 Post Earthquake Stabiltiy

Post earthquake Stability analysis has been carried out to assess the stabiltiy of the dam after the earhquake shaking. The analysis has been done using SLOPE/W by taking post earthquake pore pressure from QUAKE/W dynamic analsysis. As shown in Fig 5.94 and 5.95 and Table 5.7, the factor of safety results greater than unity.

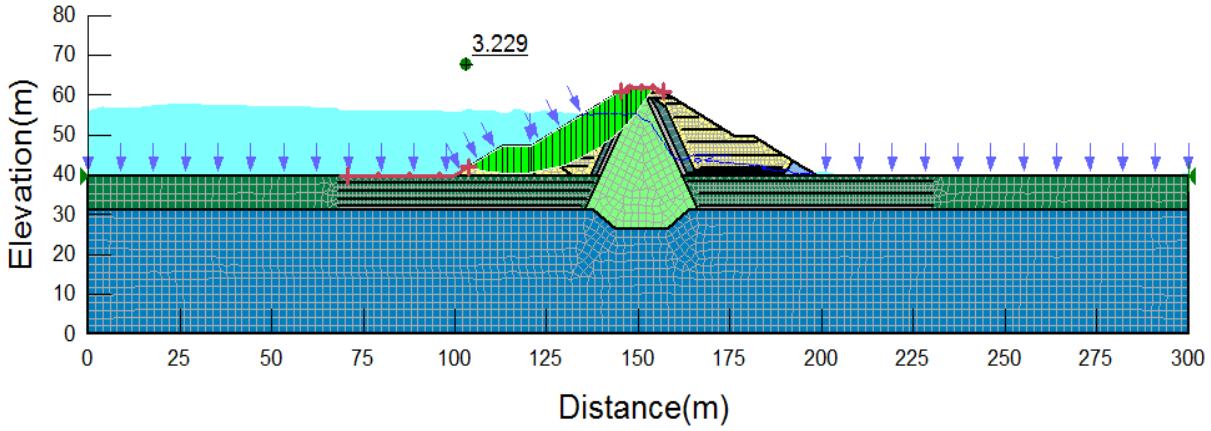

Fig. 5.94: Post earthquake stability (upstream slope)

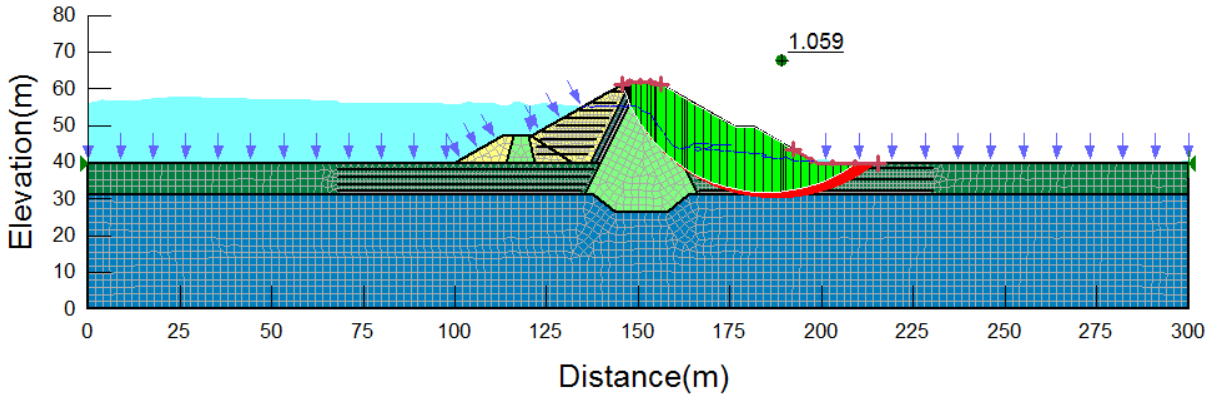

Fig. 5.95: Post earthquake stability (downstream slope)

5.2.7.4 Post Earthquake Deformation

One of the important things in dynamic analysis is to carry out deformation analysis after an earhquake shaking has stopped. The ability to link SIGMA/W with output results from a QUAKE/W dynamic analysis.

After QUAKE/W dynamic analysis, the output results will include the new soil total stresses and pore-water pressures at each saved time step. SIGMA/W can read in the output from QUAKE/W at each time step, subtract it from the time before, and create an incremental force at each node. The force will then result in a deformation.The maximum displacement has been found 1.32 m (Table 5.8) and this value is less than the free board section of the dam. Hence, the result is within acceptable limit. Fig. 5.96 shows the deformed shape of the dam after the earthquake.

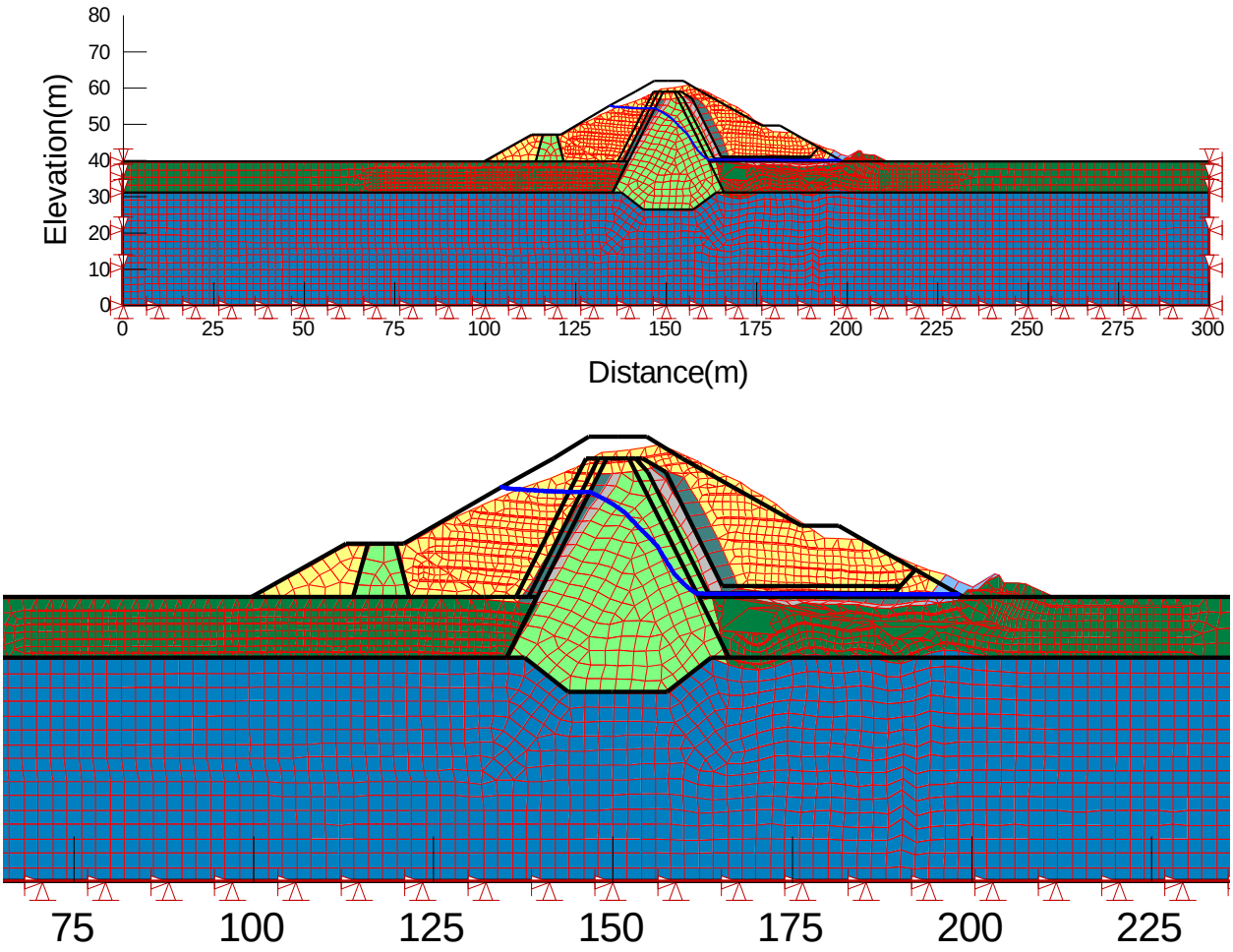

Fig. 5.96 : Post Earthquake deformation

5.2.7.5 Permanent deformation

Earthquake shaking creates inertial forces. These inertial forces cause the stresses in the ground to vary with time. Along a potential slip surface, the mobilized shear strength increases and decreases in response to the inertial forces. There may be times during the shaking that the mobilized shear strength exceeds the available shear resistance, which causes a temporary loss of stability. At times when the factor of safety is less than unity, the ground may experience some displacement. An accumulation of these displacements gives rise to permanent deformation

(QUAKE/W, 2010). Examining the permanent deformations resulting from the dynamic inertial forces is an important forces is an important aspect of dynamic analysis of dams. In the Geostudio software, SLOPE/W uses the QUAKE/W computed results together with the Newmark sliding block concept to perform the earthquake induced permanent deformations in dams. The Newmark method is based on the assumption that a potential sliding mass behaves like a rigid body, which would move down a slope as soon as the total (static and dynamic) driving force would exceed the available resisting force. The critical value of the resulting acceleration that will cause the sliding mass to move is known as the yield acceleration. It corresponds to the resultant acceleration for which the factor of safety against sliding is equal to 1.0

5.2.7.5.1 Reduction in freeboard due to vertical permanent displacements

From the earthquake safety of the dam point of view, sliding displacements in the crest region need important consideration as they would lead to the reduction of the available freeboard. The result of the analysis for El Centro earthquake corresponding to maximum credible earthquake has been presented in the following table. The permanent displacement result that is obtained from SLOPE/W analysis represents the resultant displacement of the sliding block. However, in order to examine the possible reduction in freeboard, the resultant displacement has to be decomposed in to horizontal and vertical displacements. Fig. 5.97 to 5.100 shows the crest width involvement during Newmark deformation analysis.

Table 5.7: Stability after Earthquake using Quake/W stress (Slope/W) for El Centro MCE

Description	**Factor of safety**
Downstream Slope	1.059
Upstream Slope	3.229

Table 5.8**:** Newmark Deformation Analysis result Using Slope/W for El Centro MCE

Parameters	Dam Crest Condition			
	Downstream Slope			Upstream Slope
	100% crest	50 % Crest	0 % Crest	100% crest
Resultant displacement (m)	0.5445	3.1374	0.82514	0.01252
Base angle(^{o})	23.36	24.9	26.59	19.79
Horizontal displacement(m)	0.4998	2.846	0.7378	0.01177
Vertical displacement(m)	0.2158	1.32	0.369	0.004
Yield acceleration(g)	0.08684	0.0439	0.13395	0.46357
Average acceleration(g)	5×10^{-5}	5×10^{-5}	5×10^{-5}	$2*10^{-5}$

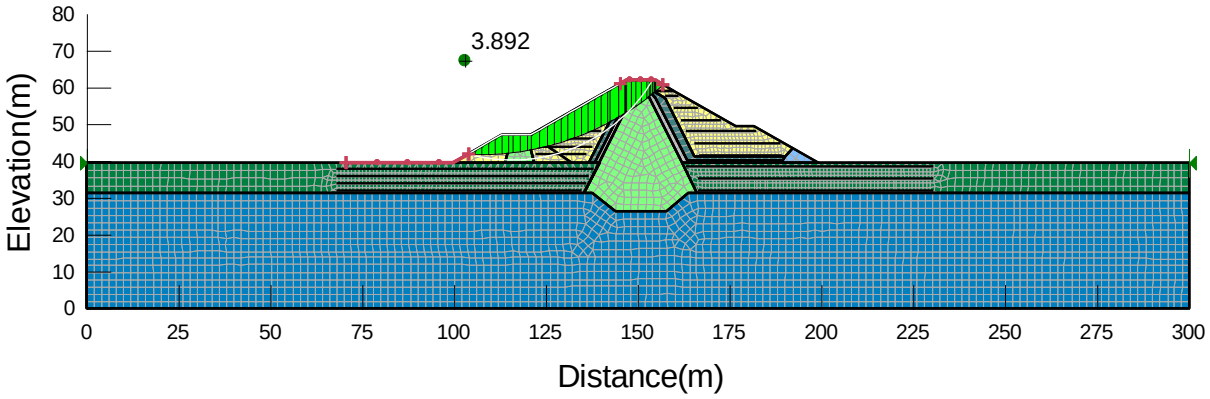

Fig. 5.97: Slip surface involving 100 % crest width from Newmark deformation analysis for Elcentro earthquake loading corresponding to MCE

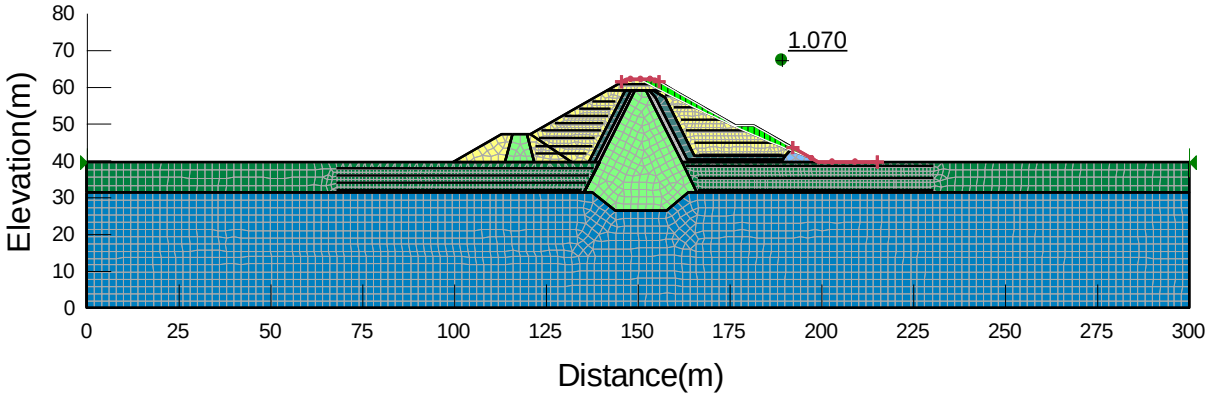

Fig. 5.98: Slip surface involving 50 % crest width from Newmark deformation analysis for downstream slope (Elcentro earthquake loading corresponding to MCE)

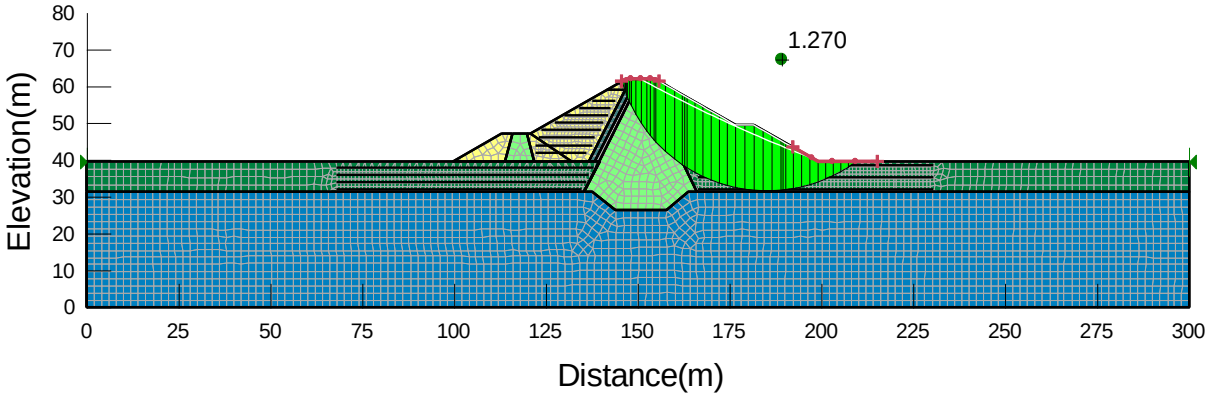

Fig. 5.99: Slip surface involving 100 % crest width from Newmark deformation analysis for downstream slope (El Centro earthquake loading corresponding to MCE)

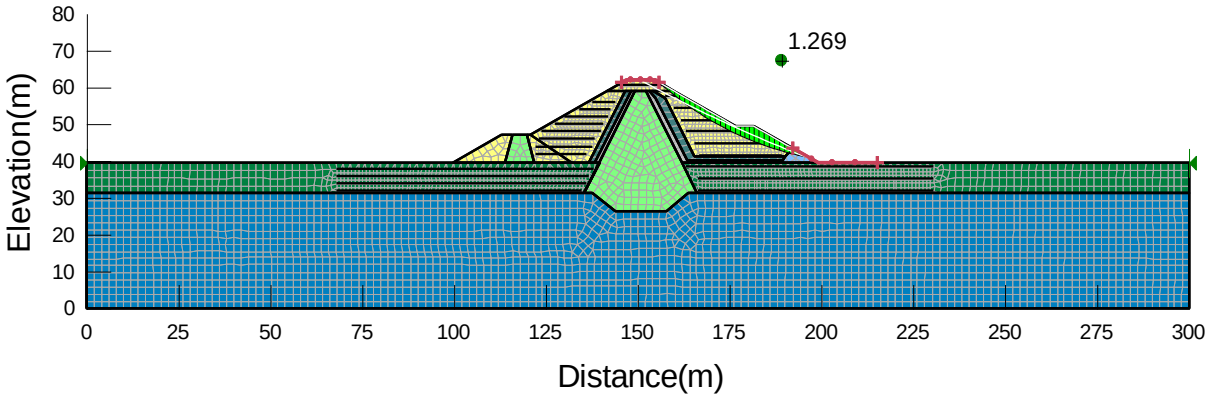

Fig. 5.100: Slip surface involving 0% crest width from Newmark deformation analysis for downstream slope (El Centro earthquake loading corresponding to MCE)

From Table 5.8, we can deduce that a maximum vertical displacement of 1.32m has been found for 50% crest width. The vertical displacement is less than the available free board of the dam (3.1m) which is acceptable and the dam can continue its function after the earthquake has stopped.

6 Conclusion and recommendation

6.1 Conclusions

6.1.1 Static analysis

From the above analysis, the following conclusions can be made

Downstream slope for long term steady state seepage condition

1. Factor of safety is decreasing with increase in spacing between geotextile layers. Considering the optimized section, reinforcement has increased the factor of safety by 21 to 55%.
2. By providing the geotextile layers at spacing 3.2m,the downstream slopes of a dam can be made steeper up to 1.75H:1V. Fore more steeper slopes,the veritcal spacing between geotextile layers is required to be reduced up to 2m.
3. The length of the geotextile layers required for reinforceing the downstream slope is found to be in the range of 6m to 30m.
4. Offset from downstream slope are found to be in the range of 0m to 42m depending upon the location of geotextile layers.

Upstream Slope for sudden drawdown loading condition

5. Considering the optimized section, the factor of safety has been improved by 51 to 74%.
6. By providing the geotextile layers at spacing of 2.0m, the upstream slopes of a dam can be made steeper up to 1.75H: 1V. The spacing can be up to 3.2m for gentler slopes
7. The length of the geotextile layers required for reinforcing the upstream slope is found to be in the range of 8m to 16m.
8. Offset from upstream slope are found to be in the range of 0m to 20m depending upon the location of geotextile layers.

General

The economic analysis of the optimized reinforced section shows 70% save of cash than the unreinforced section

6.1.2 Dynamic analysis

The dynamic analysis for statically optimized section has been carried out. Accordingly, the following conclusions can be drawn from the analysis result.

1. The post-earthquake stability analysis gives a factor of safety 1.059 for downstream slope and 3.229 for upstream slope which is greater than unity.
2. Liquefaction susceptibility study shows that there is no material zone which is expected to liquefy in the dam. Hence, there is no fear against liquefaction failure of the dam.
3. Newmark post-earthquake deformation analysis result shows that the maximum vertical displacement is found to be 1.32m which is well below a freeboard of 3.1m. Hence, the dam can function properly after the earthquake.
4. Since geotextile is thin and placed horizontally in the embankment, it has no any contribution to liquefaction prevention.

6.2 Recommendations

1. Even if the earth fill dam under this study is located in a rift valley zone which is seismically active area, the technique can be implemented with high margin of safety in other non-seismic areas of the country.
2. This technique is particularly useful for high earth dams and will result in lesser construction cost as well as construction time.
3. Even though its positive effect has been observed against seismic loading, anti-seismic effect of geotextile has not been directly studied in this study. Hence, a separate study shall be made to know the effect of geotextile reinforcement in response to earthquake loading.

7 References

Ambraseys N. N. Engineering seismology," Earthquake Engineering and Structural Dynamics" [Book Section] // " Earthquake Engineering and Structural Dynamics". - 1988. - Vol. 17.

Anonymous. Definition of geotechnical engineering [Article] // Ground engieenring magazine. - 1999. - 11 : Vol. 32. - p. 39.

ASTM American Society of Testing Materials [Report]. - D4439.

Atkinson J The Mechanic of Soils and Foundation.", 2nd Edn. Taylor & Francis, New [Book]. - New York : Taylor & Francis, 2007. - 2nd Edition.

Bishop A. W. and Morgenstern N. Stability Coefficients for Earth Slopes [Journal] // Journal of Geotechnical Engineering. - 1960. - 10(4). - pp. 164 -169.

Bonaparte R., Holtz R. D. and Giroud J. P. Soil reinforcement design using geotextiles and geogrids [Report] : Special Technical publications 952 / Geotextile Testing and the Design Engineer ; ASTM. - 1987. - pp. 26-39.

Burland J. B. Closing Session Discussions, Proceedings of the First International Conference on unsaturated Soil Conference [Conference] // Proceedings of the First International Conference on unsaturated Soil Conference. - Paris : A.A.Balkema, 1996. - Vol. 3. - p. 1562.

Burland J. B. Nash Lecture: The Teaching of Soil Mechanics – a Personal view [Conference] // 9th ECSMFE. - Dublin : [s.n.], 1987. - Vol. 3. - pp. 1427 - 1447.

Byrne P. M., Jitno H. and Salgado R. [Conference] // Proceedings,10th world conference on earthquake engineering. - Madrid : [s.n.], 1992. - Vol. 3. - pp. 1407-1412.

Christopher B. R. and Holtz R. D. Geotextiles Engineering Manual [Conference]. - Washington,DC : National Highway Institute, FHWA, 1985. - Vols. Contract DTFH61-80-C-00094..

Das B. M. Principles of soil dynamics [Book]. - [s.l.] : Brooks/Cole, 1993.

DeAlba P., Chan C. K. and Seed H. B. Determination of soil liquefaction characterstics by large scale laboratory tests [Report] = Report EERC 75 - 25 / Earthquake engineering center ; University of California. - Berkeley : [s.n.], 1975. - EERC 75 - 25.

DeAlba P., Seed H. B. and Chan C. K. Sand liquefation in large scale simple shear tests [Journal] // Geotechnical engineering. - [s.l.] : ASCE, 1976. - GT9 : Vol. 102. - pp. 909 - 927.

Duncan J. B. State of the art - static stability and deformation analysis in Stability andPerformance of slope and embankment [Journal] // ASCE Geotechnical Special Publication. - [s.l.] : ASCE, 1992. - 31. - pp. 222 - 266.

Duncan J. M. State of the art: limit equilibrium and finite element analysis of slopes [Journal] // Journal of Geotechnical Engineering. - [s.l.] : ASCE, 1996a. - 7 : Vol. 122. - pp. 577 - 597.

Duncan J. M. State of the Art: Limit Equilibrium and Finite Element Analysis of Slopes [Journal] // Journal of Geotechnical Engineering . - 2005. - pp. 577 - 596.

Duncan J. Michael and Wright Stephen G. Soil Strength and Slope Stability [Book]. - USA : JOHN WILEY & SONS, INC., 2005.

Fell Robin [et al.] Geotechnical engineering of dams [Book Section]. - London : Taylor and Francis group plc, 2005.

Fellenius W. Calculation of the Stability of Earth Dams [Journal] // proceeding of the second of Congress of Large Dams. - 1936. - 4. - pp. 445 - 463.

FHWA Mechanically Stabilized Earth Walls and Reinforced Soil Slopes [Report] / Department of Transportation ; Federal highways Adminstration. - Washington DC : FHWA, 2000. - Report FHWA-NHI-00-043,.

Fowler J. Theoretical design considerations for fabric - reinforced embankments [Conference] // Second International Conference on Geotextiles. - Las Vegas : [s.n.], 1982. - Vol. 3. - pp. 665 - 670.

Fredlund D. G. and Krahn J. Comparison of slope stability methods of analysis. Canadian [Journal] // Canadian Geotechnical Journa. - 1977. - 3 : Vol. 14. - pp. 429 - 439.

Ghaffari H. Assessment of Slope Stability in Embankment Dams Using ANN,M.Sc Thesis [Report] / Mahadad Azad university. - Iran : Ghaffari, H. (2010), "Assessment of Slope Stability in Embankment Dams Using ANN.", M. Sc., 2010.

Haliburton T. A., Lawmaster J. D. and McGuffey V. E. Use of Engineering Fabric in Transportation Related Applications [Report] : final report under Contract NO.DTFH - 80 - C-0094 / FHWA,National Highway Institute. - Washington, D.C. : [s.n.], 1982.

Hamada M. [et al.] Study on liquefaction induced permanent ground displacements [Report] : Report for the Association for development earthquake prediction. - 1986.

Hasani H. and Mamizadeh J. Stability of Slope and Seepage Analysis in Earth Fill dam using numerical models [Journal] // World Applied Sciences Journal. - [s.l.] : IDOSI publications, 2013. - 19 : Vol. 21. - pp. 1398 - 1402.

Hoek E. and Bray J. W. Rock Slope Engineering – Appendix 3 [Book]. - [s.l.] : Published for the institute of Mining and Metallurgy, 1974. - pp. 352-354.

Hoek E. and Bray J. W. [Book Section] // Rock Slope engineering - Appendix 3. - [s.l.] : Institute of Mining and metallurgy, 1974.

Idriss I. M. Response of soft soil sites during earthquakes, [Conference] // Proceedings,Memorial symposium to honor proffessor Harry Bolton Seed. - Berkeley,California : [s.n.], 1990. - Vol. II.

IFAI [Article] // Geosynthetics magazine . - [s.l.] : Industrial Fabrics Association International , 2012.

Ishibashi I. and Zhang X. Unified Dynamic shear moduli and damping ratios of sand and clay [Journal] // Soils and founations. - 1993. - 1 : Vol. 33. - pp. 182 - 191.

Ishihara K. Stability of natural deposits during earthquakes [Conference] // 11 th international conference on soil mechanics and foundation engineering. - 1985. - Vol. 1. - pp. 321 - 376.

Ishihara K. Post earthquake failure of a tailings dam due to liquefaction of the pond deposit [Conference] // Internation conference on case histories in geotechnical engineering . - [s.l.] : University of Missouri, 1984. - Vol. 3. - pp. 1129 - 1143.

Janbu N. Application of Composite Slip Surfaces For Stability Analysis [Journal] // Proceedings of the European Conference on the Stability of Earth Slopes. - Stockholm : [s.n.], 1954. - 3. - pp. 39-43.

Jasen R. B. The concrete face rock fill dam- performance of Cogoti dam under seismic loading [Journal] = Discussion of a paper presented at ASCE symposium on concrete face rock fill dams // ASCE Journal of geotechnical engineering division. - [s.l.] : ASCE, 1987.

Koerner Robert M. Designing with Geosynthetics [Book]. - New Jersy : Prentice Hall, 2005.

Kramer Steven L. Geotechnical Earthquake Engineering [Book]. - New Jersy : Prentice- Hall ,Upper Saddle River, 1996.

Krhan J. Seepage modeling with Seep/W : An engineering methodology [Book]. - [s.l.] : GEO-SLOPE International Ltd, 2007.

Lee K. L. and Albaisa A. Earthquake induced settlements in saturated sands [Journal] // Journal of the soil mechanics and foundation division. - [s.l.] : ASCE, 1974. - Vol. 100. - pp. 387 - 403. - GT4.

Leshchinsky D. and Boedeker R. H. Geosynthetic reinforced soil structures [Journal] // Journal of Geotechnical engineering . - [s.l.] : ASCE, 1989. - 10 : Vol. 115. - pp. 1459-1478.

Malla S. [et al.] Seismic analysis and safety assessment of earthfill dam founded on alluvium soil [Report] / Commission Internationale. - Barcelona : Des grands barrages , 2005.

Marcuson W. F. III Defnition of terms related to liquefaction [Journal] // Journal of geotechnical engineering division. - [s.l.] : ASCE, 1978. - 9 : Vol. 104. - pp. 1197-1200.

Marcuson W. F. III, Handala P. F. and Ledbetter R. H. Evaluation and use of residual strength in seismic safety analysis of embankments [Journal] // Earhquake Spectra. - 1990. - 3 : Vol. 6. - pp. 529 - 572.

Messele H. Haile Critical Assessment of Site Effect Parameters for Strong Ground Motion Prediction [Report] : Doctoral thesis / Tokyo Institute of technology. - Tokyo : [s.n.], 1996.

Messele Haile and Hadush Seged Earthquake induced liquefaction analysis of tendaho earth fill dam [Journal]. - Addis Ababa : Ethiopian civil engineers and archticets association, 2006. - Vol. 29.

Morgenstern N. R. and Price V. E. The Analysis of the Stability of General Slip Surfaces [Journal] // Journal of Geotechnical Engineering. - 1965. - 1. - pp. 79 - 93.

Morgenstern N. R. The evaluation of slope stability - a 25 year perspective. In stability and performance of slopes and embankments [Journal] // Geotechnical special publication. - [s.l.] : ASCE, 1992. - 31.

National Research Council Groundwater models:Scientific and regulatory applications [Report]. - Wasington D.C. : National academy press, 1990.

Newmark N. M. Effects of earthquakes on dams and embankments, Rankine Lecture [Journal] // Geotechnique. - 1965. - 2 : Vol. 15.

Petterson K. E. The Early History of Circular Sliding Surfaces [Journal]. - [s.l.] : Geotechnique, 1955. - Vol. 5. - pp. 275-296.

QUAKE/W Dynamic modeling with QUAKE/W 2007 : an engineering methodology [Book]. - [s.l.] : Geo - Slope International ltd, 2010.

Romo M. P. and Resendiz D. Computed and observed deformations of two embankment dams under earthquake loading in dams and earthquakes [Book Section] // Book of dams and Earthquake. - [s.l.] : Institute of civil engineers, 1981.

Rowe R. K. and Soderman K. L. An approximate method for estimating the stability of geotextile - reinforced embankments [Journal] // Canadian Geotechnical Journal. - 1985. - Vol. 22. - pp. 392-398.

Schmertmann G. R. [et al.] Design Charts for geogrid-reinforced soil slopes [Conference] // Proceedings from geosynthetics. - New Orleans : [s.n.], 1987. - Vol. 1. - pp. 108-120.

Seed H. B. [et al.] Representation of irregular stress time historeis by equivalent uniform stress series in liquefaction analyses [Book]. - Berkeley : Earthquake Engineering REsearch Center,University of California, 1975. - Vols. EERC75-29.

Seed H. B. and Idriss I. M. Simplified Procedure for evaluating soil liquefaction potential [Journal] // Journal of the soil mechanics and foundation Division,. - ASCE : [s.n.], 1971. - SM9 : Vol. 107. - pp. 1249 - 1274.

Seed H. B., Tokimatsu K. and Harder L. The influence of SPT procedures in evaluating soil liquefaction resistance evaluations [Journal] // Journal of geotechnical engineering. - Berkley : [s.n.], 1975. - 12 : Vol. 111. - pp. 701-712.

Seed H. B. [et al.] Moduli and damping factors for dynamic analysis of cohesionless soils [Journal] // Journal of geotechnical engineering,ASCE . - [s.l.] : ASCE, 1986. - Vol. 112. - pp. 1016 - 1032. - GT11.

Seed H. B. and Harder Variation of correction factor Ka with initial /normal stress ratio [Conference]. - [s.l.] : BiTech Publishers Ltd, 1990. - Vol. 2. - p. 364.

Seed H. B. and Idriss I. M. Soil moduli and damping factors for dynamic response anayses [Report] / Earthquake engineering research center ; University of California. - Berkeley : [s.n.], 1970a. - Report no. EERC/70-10.

Seed H. B. Considerations in the earthquake - resistant design of earth and rockfill dams [Journal] // Geotechnique. - 1979. - 3 : Vol. 29. - pp. 215 - 263.

Seed H. B., Mori K. and Chan C. K. Influence of seismic history on the liquefaction characterstics of sands [Report] / Earthquake engineering research center ; University of California. - Berkeley : University of California , 1975. - EERC 75 - 25.

Seep/W Seepage modeling with Seep/W 2007:An engineering methodology [Book]. - [s.l.] : Geo-Slope international ltd, 2008.

Siddappa G. Effect of Earthquake onembankment dams [Conference] // Proceeding of innovative dam and levee design and construction. - USA : the united states society of dams, 2012.

SIGMA/W Stress- deformation modelling with SIGMA/W 2007: An engineering methodology [Book]. - Canada : Geo- slope international ltd, 2010.

Sivakumar Babu G. L. and Amit Srivastava Remediation of Upstream Slope of An Impounding Reservoir Using Soil Reinforcing Technique [Conference] // Slop Proceedings of Indian Geotechnical Conference. - Kochi : [s.n.], 2011. - pp. 589-592..

Sivakumar Babu, G L; Amit Srivastava Remediation of Upstream Slope of an impounding Reservoir Using Soil Reinforcing Technique [Book]. - Kochi : Proceedings of Indian Geotechnical Conference, 2011.

Slope/W Stability Modeling with Slope/W: An egineering methodology [Book]. - [s.l.] : Geo-Slope International ltd, 2008.

Spencer E. A Method of Analysis of Embankments Assuming Parallel Interslice Forces [Journal] // Journal of Geotechnical Engineering. - 1967. - 17. - pp. 11 - 26.

Sun J. I., Golesorkhi R. and Seed H. B. Dynamic moduli and damping ratios for cohesive soils [Report] / Earthquake engineering research center ; University of California. - Berkeley : [s.n.], 1988. - p. 42. - UCB/EERC-88/15.

Tarbuck E. J. and Frederick K. L. Earth:An introduction to physical Geology [Journal]. - New Jersy : Prentice Hall, 1996.

Terzaghi K. Mechanics of landslides [Journal]. - [s.l.] : Geological society of America, 1950. - Vol. Engineering geology volume.

USCOLD Observed performance of dams during earthquakes [Report] / Committee of earthqukaes. - Denver,USA : [s.n.], 2000.

USNRC Liquefaction of soils during earthquakes [Report] / United States National Research Council. - Washington DC : National academy press, 1985.

USNRC United States National Research Council (USNRC. Liquefaction of Soils during Earthquakes, [Report]. - Washington, DC : National Academy Press, 1985.

Vanapalli S. K. [et al.] Model for the pridiction of shear strength with respect to soil suction [Journal] // Canadian Geotechnical journal. - 1996. - Vol. 33. - pp. 379 - 392.

Wang W. Some findings in soil liquefaction. - Beijing : Water Conservancy and Hydroelectric Power Sientific Research Institute , 1979.

Wong W. Earthquake damages to earth dams and levees in relation to soil liquefaction and weakness in soft clays [Conference] // International conference on case histories in geotechnical engineering. - 1984. - Vol. 1. - pp. 511- 521.

WWDSE Final Detail Design Report of Gidabo Earth Fill dam [Report]. - Addis Ababa : WWDSE, 2009.

WWDSE Geological and Geotechnical Invetigation final feasibility report [Report]. - Addis Ababa : Unpublished, 2008.

Youd T. L. and Hoose S. N. Liquefaction susceptibility and geologic setting [Conference] // 6th World Conference on Earthquake Engineering. - New Delhi : [s.n.], 1977. - Vol. 3. - pp. 2189-2194.

Youd T. L. and Idriss I. M. Liquefaction resistance of soils:Summary report from the 1996 NCEER and 1998 NCEER/NSF workshops on evaluation of liquefaction resistance of soils [Journal] // Journal of Geotechnical and Geoenvironmental engineering . - October 2001. - Vol. 817.

Youd T. L. Mapping of earthquake-induced liquefaction for seismic zonation [Conference] // 4th International Conference on Seismic Zonation. - [s.l.] : Earthquake Engineering Research Institute,Stanford University, 1991. - Vol. 1. - pp. 111-147.

Youd,T.L et al The Borah peak ,"idaho earthquake of october 28,1983 liquefaction" [Conference] // Earthquake spectra. - Vol. 2. - pp. 71 -89.

Zhu Ya Lin and kong Xian jing The Anti-seismic Effect of Geogrid Reinforced on High Earth-rockfill Dams [Journal] // Electronic journal of geotechnical engineering. - 2009. - Vol. 14. - pp. 1-13.

Zornberg J. G., Sitar N. and Mitchell J. K. Limit equilibrium as basis for design of geosynthetic reinforced slopes [Journal] // Journal of Geotechnical and Geoenvironmental Engieering. - [s.l.] : ASCE, 1989a. - 8 : Vol. 124. - pp. 684 - 698.

Zornberg J. G., Sitar N. and Mitchell J. K. Limit equilibrium as basis for designs of geosynthetic reinforced slopes [Journal] // Journal of Geotechnical and Geoenvironmental Engineering. - [s.l.] : ASCE, 1198a. - 8 : Vol. 124. - pp. 684-698.

Appendix A: Earthquake records

Appendix A-I: The 1940 El Centro Record a) Horizontal b) Vertical

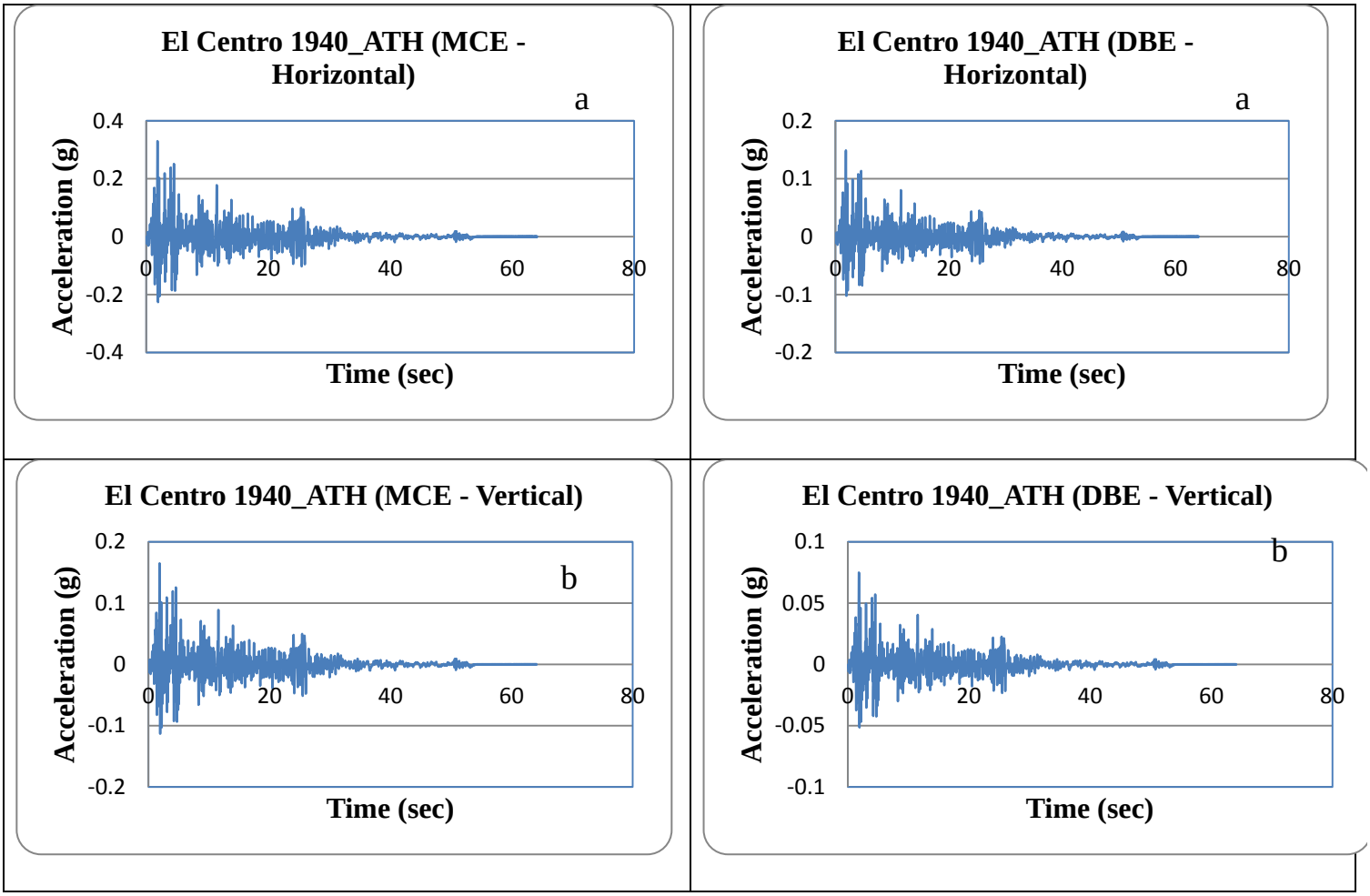

Appendix A-II: The 1995 Kobe JMA Record (Japan) a) Horizontal b) Vertical

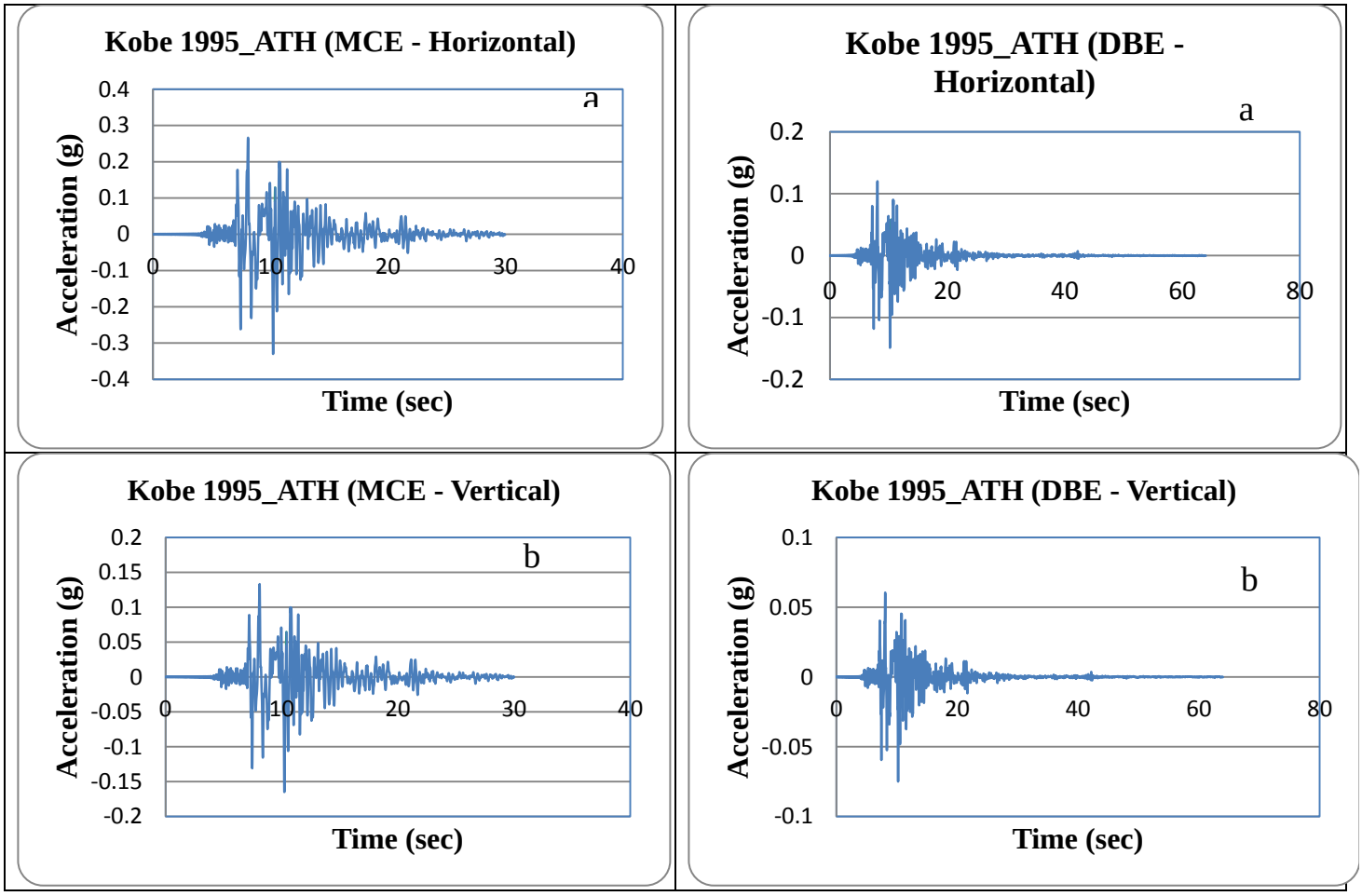

Appendix A-III: The 1968 Hachinohe record (Japan) a) Horizontal b) Vertical

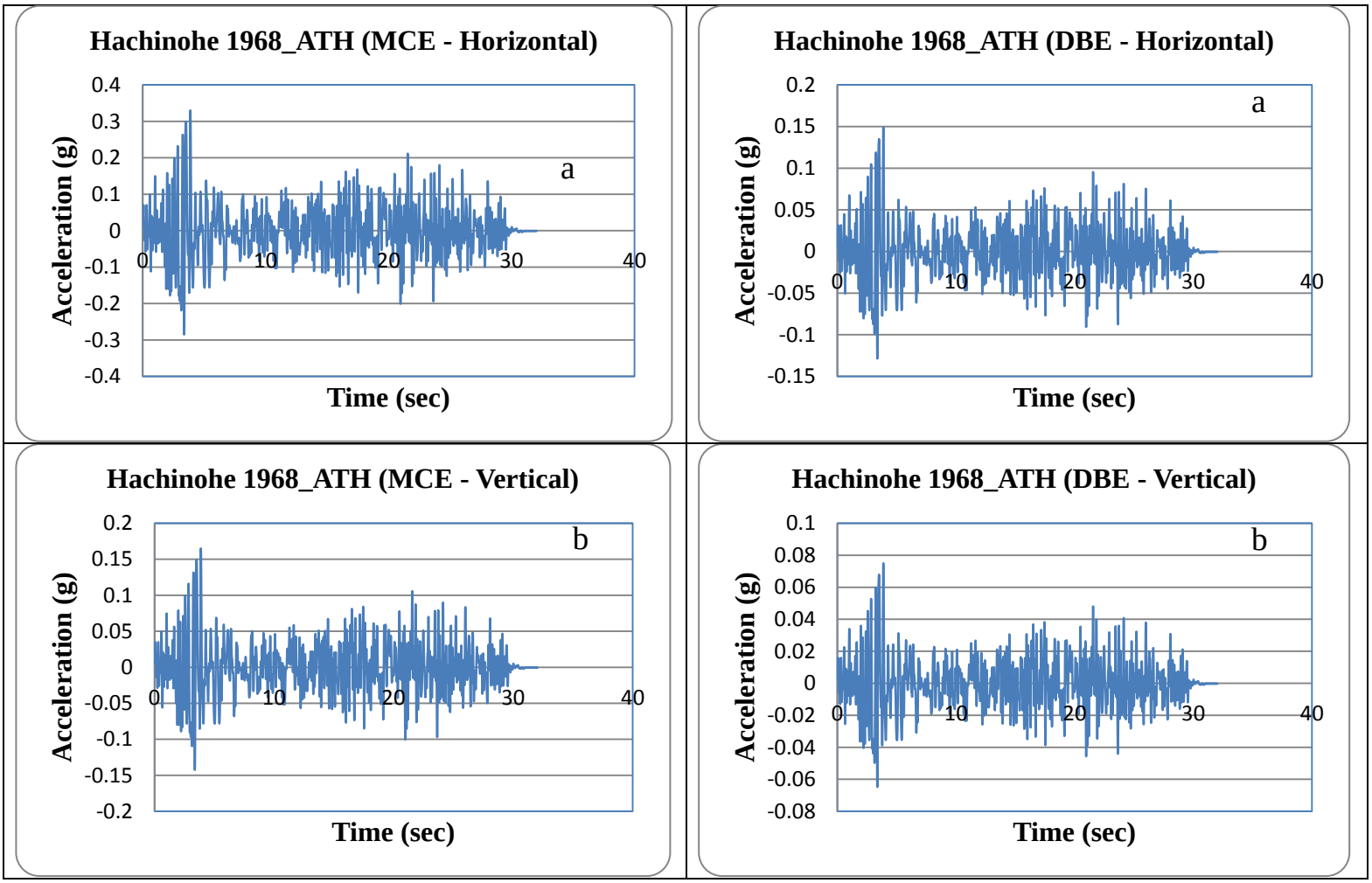

Appendix B: The 1995 Kobe JMA Record (Japan) dynamic analysis result

Appendix C-I: Acceleration response at the dam crest

MCE horizontal and vertical	DBE horizontal and vertical
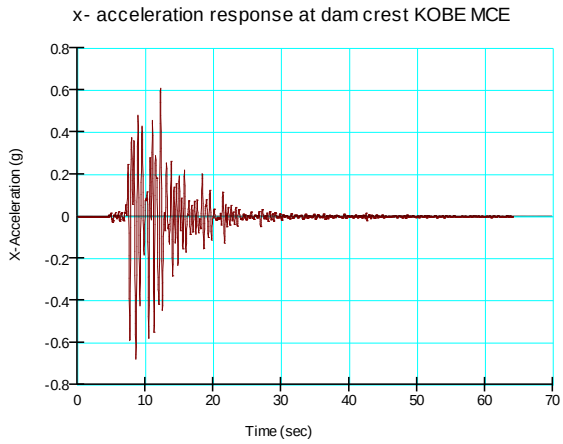	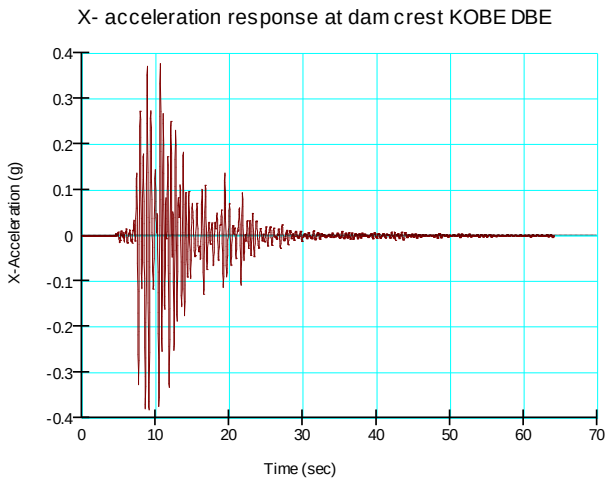
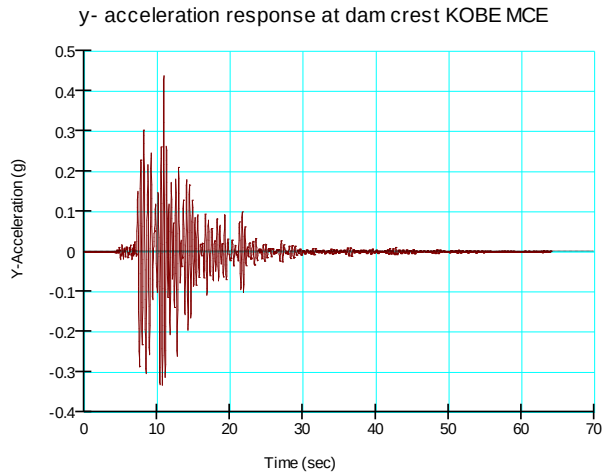	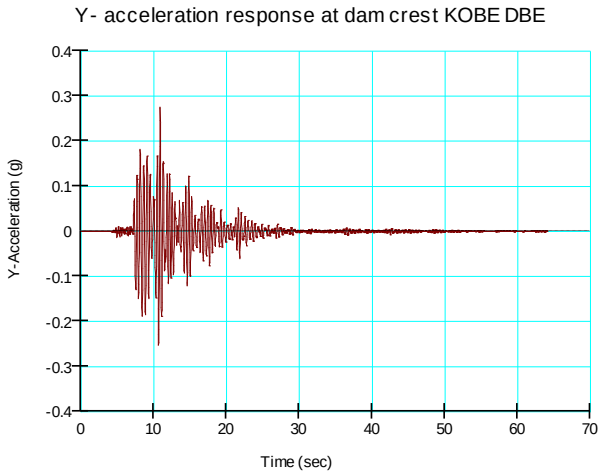

Table B1: Acceleration response at crest of the dam for KOBE earthquake record

Description	PGA		x- acceleration	y-acceleration	Remark
	Horizontal	Vertical			
MCE	0.33	0.165	0.677	0.439	Amplification
DBE	0.15	0.075	0.389	0.276	Amplification

Appendix B-II: Spectral response at the dam crest

Horizontal spectral response at dam crest corresponding to MCE (KOBE)

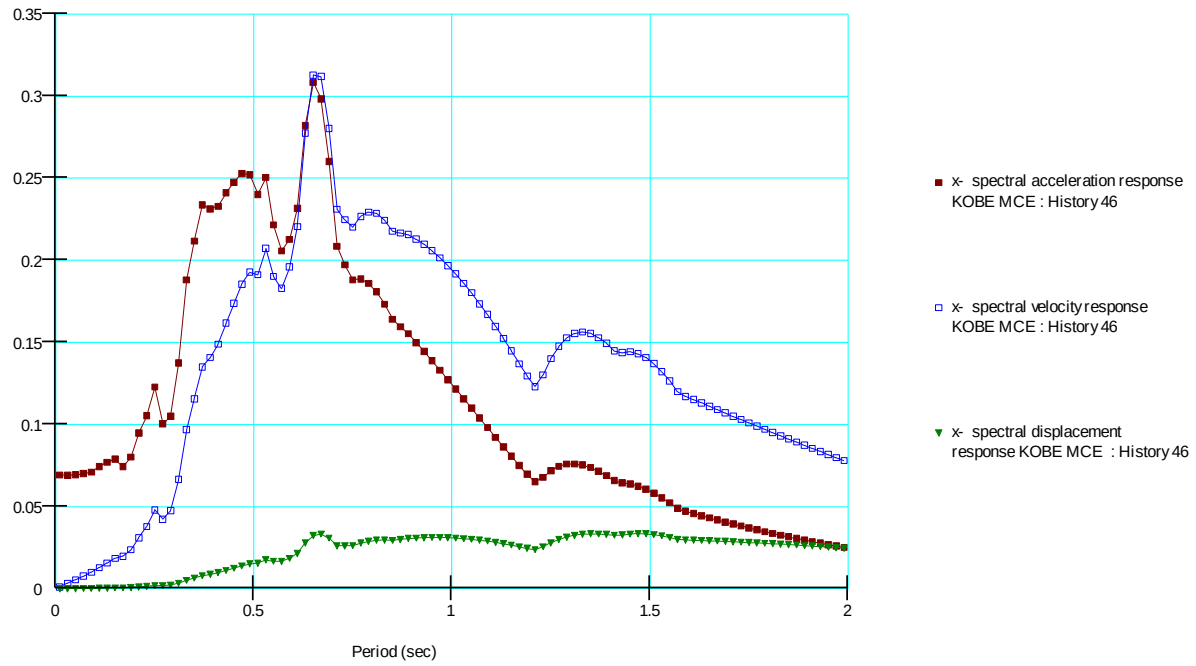

Vertical spectral response at dam crest corresponding to MCE (KOBE)

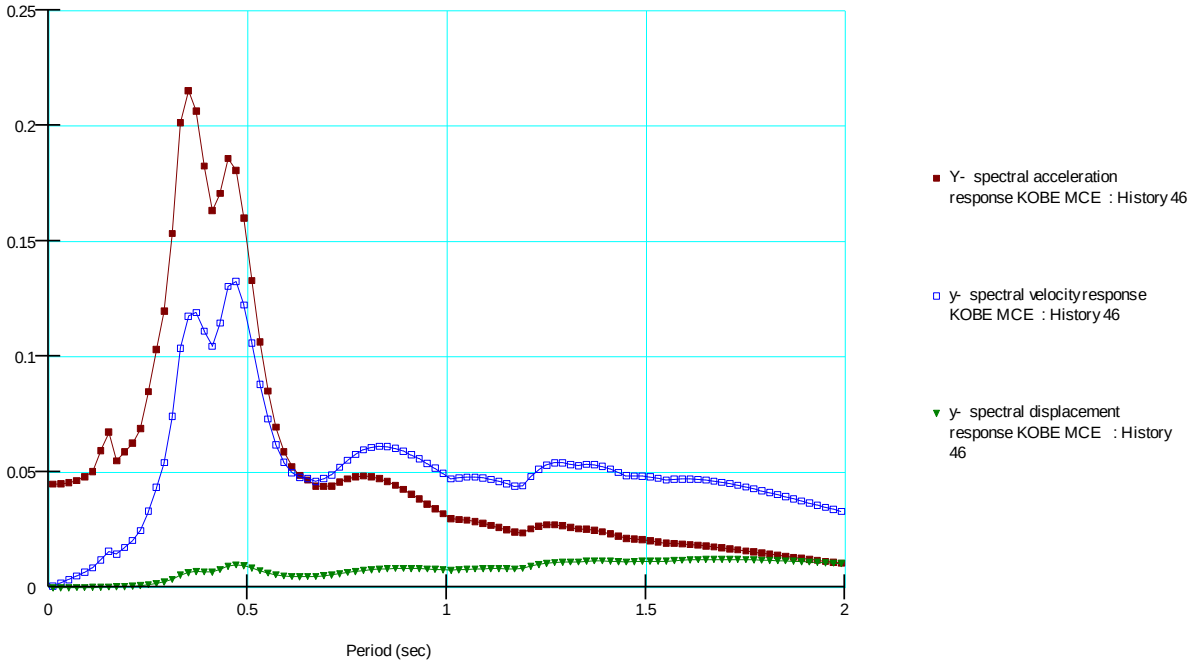

Horizontal spectral response at dam crest corresponding to DBE_KOBE

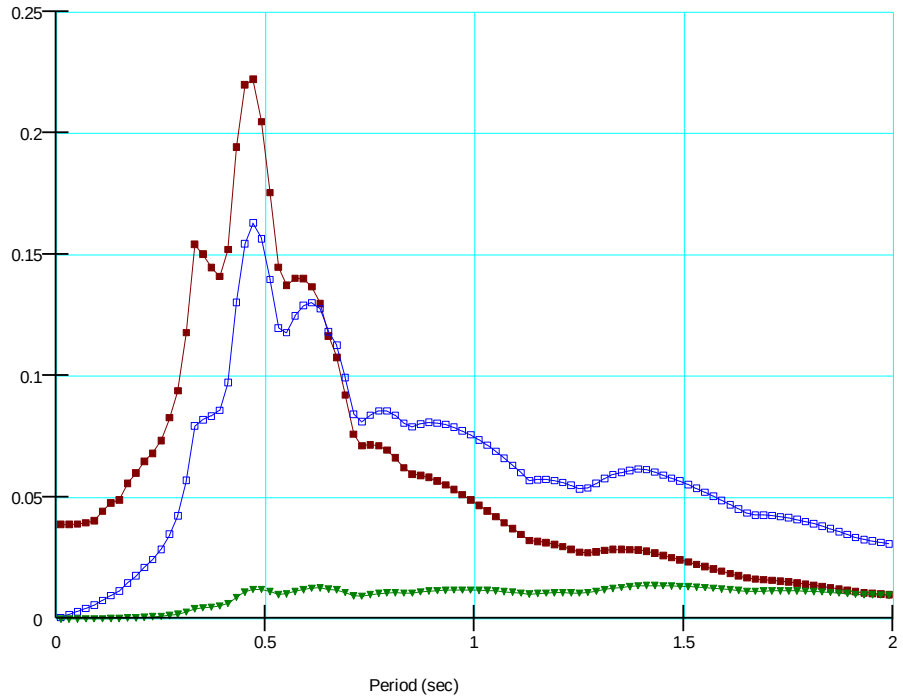

Vertical spectral response at dam crest corresponding to DBE_KOBE

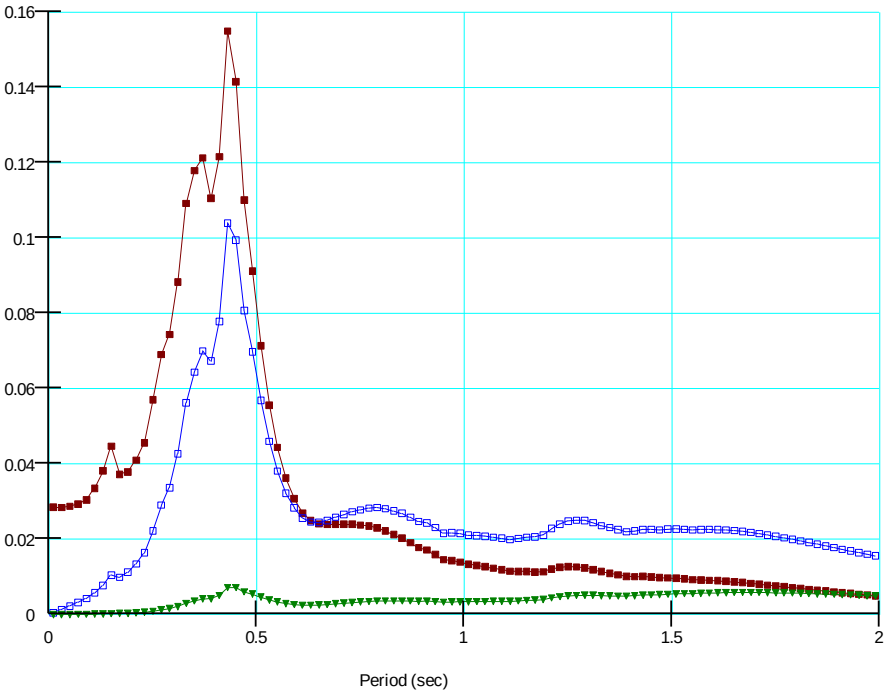

Appendix B-III: Post Earthquake Stability

Upstream slope stability corresponding to MCE

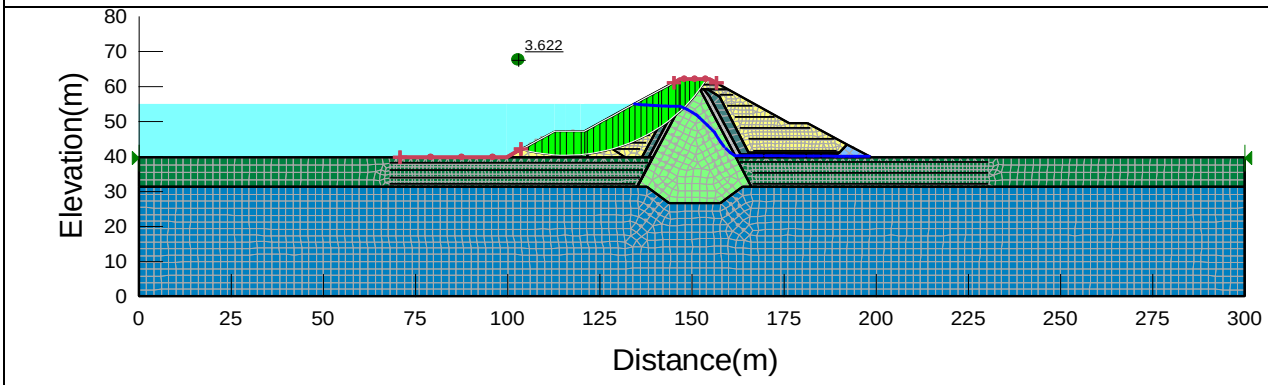

Downstream slope stability corresponding to MCE

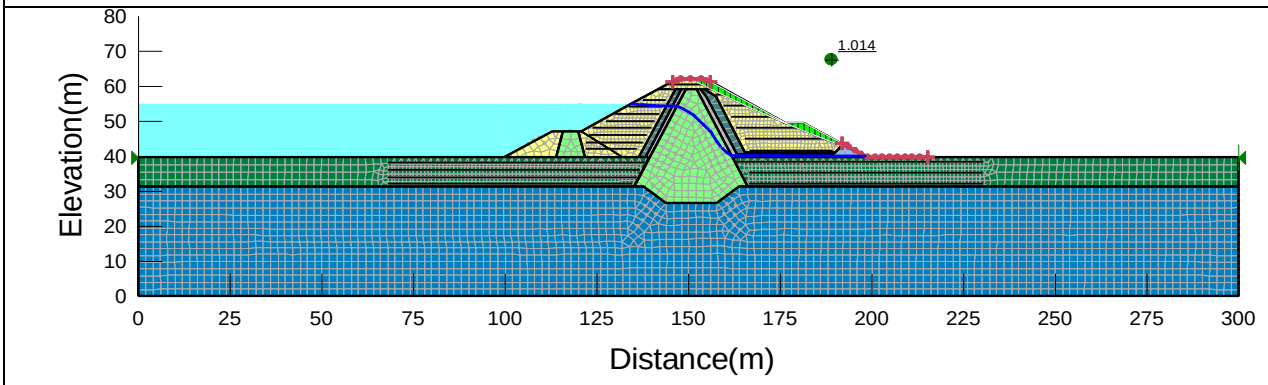

Upstream slope stability corresponding to DBE

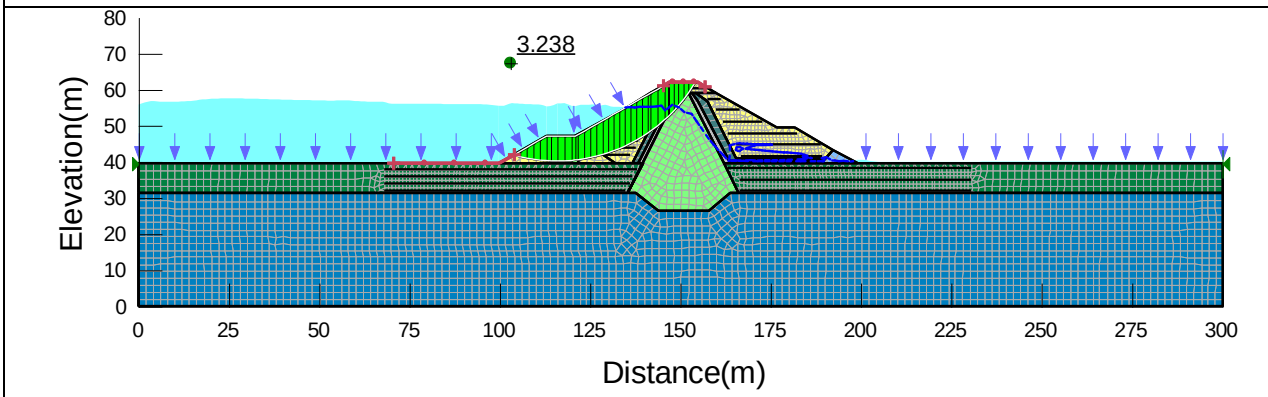

Downstream slope stability corresponding to DBE

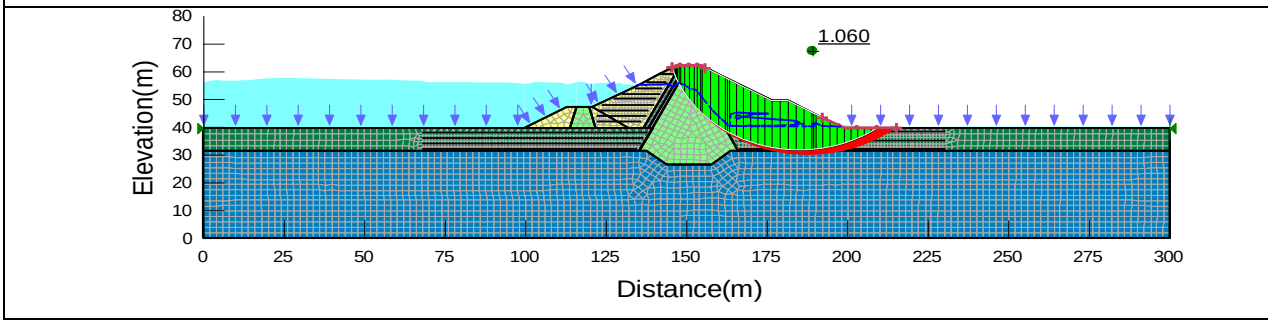

Appendix B-IV: Permanent Deformation

Table B2: Stability after Earthquake using Quake/W stress (Slope/W) for KOBE ATH

Description	Factor of safety	
PGA	MCE	DBE
Downstream Slope	1.014	1.06
Upstream Slope	3.622	3.238

Table B3: Newmark Deformation Analysis result Using Slope/W for KOBE_ MCE

Parameters	Dam Crest Condition			
	Downstream Slope			Upstream Slope
	>50% crest	50 % Crest	0 % Crest	>50% crest
Resultant displacement (m)	1.6962	0.59192	0.5658	0.01732
Base angle(^{o})	24.63	23.04	26.57	21.8
Horizontal displacement(m)	1.542	0.545	0.506	0.01608
Vertical displacement(m)	0.707	0.2317	0.253	0.0064
Yield acceleration(g)	0.04425	0.16677	0.13419	0.38168
Average acceleration(g)	0.0083	0.00026	0.00121	-3*10-5

Table B4: Newmark Deformation Analysis result Using Slope/W for KOBE_ DBE

Parameters	Dam Crest Condition			
	Downstream Slope			Upstream Slope
	>50% crest	100 % Crest	0 % Crest	No deformation result
Resultant displacement (m)	0.2453	0.045788	0.61857	
Base angle(^{o})	23	18.7	26.5	
Horizontal displacement(m)	0.2257	0.0433	0.555	
Vertical displacement(m)	0.0958	0.0146	0.276	
Yield acceleration(g)	0.10947	0.09853	0.03173	
Average acceleration(g)	0.0009	-0.00028	0.00041	

Appendix C: The 1968 Hachinohe record (Japan) dynamic analysis result

Appendix C-I: Acceleration response at dam crest

MCE horizontal and vertical	DBE horizontal and vertical
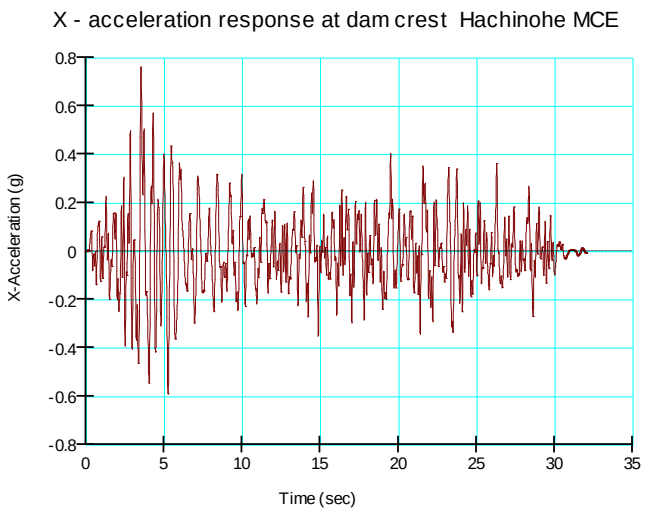	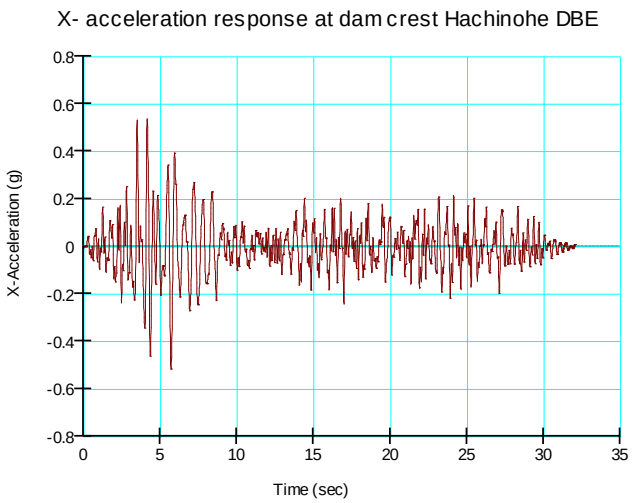
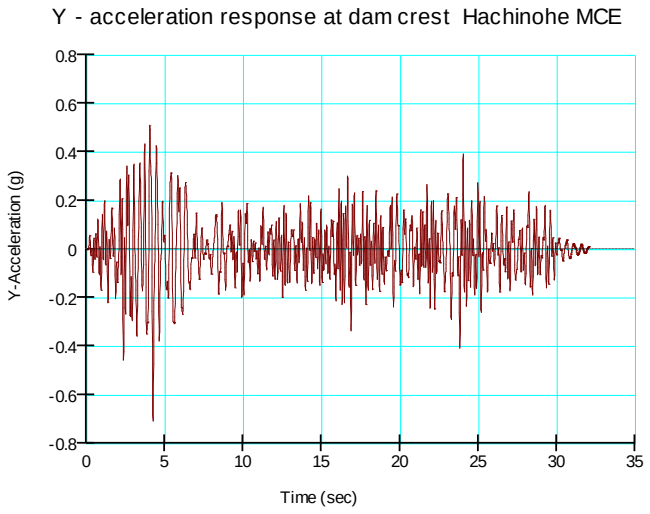	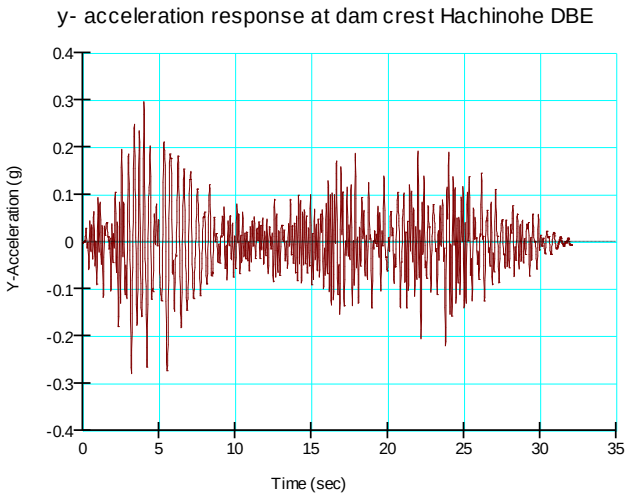

Table C1: Acceleration response at crest of the dam for HACHINOHE earthquake record

Description	PGA		x- acceleration	y-acceleration	Remark
	Horizontal	Vertical			
MCE	0.33	0.165	0.763	0.684	Amplification
DBE	0.15	0.075	0.533	0.295	Amplification

Appendix C-II: Spectral response at the dam crest

Horizontal spectral response at dam crest corresponding to MCE

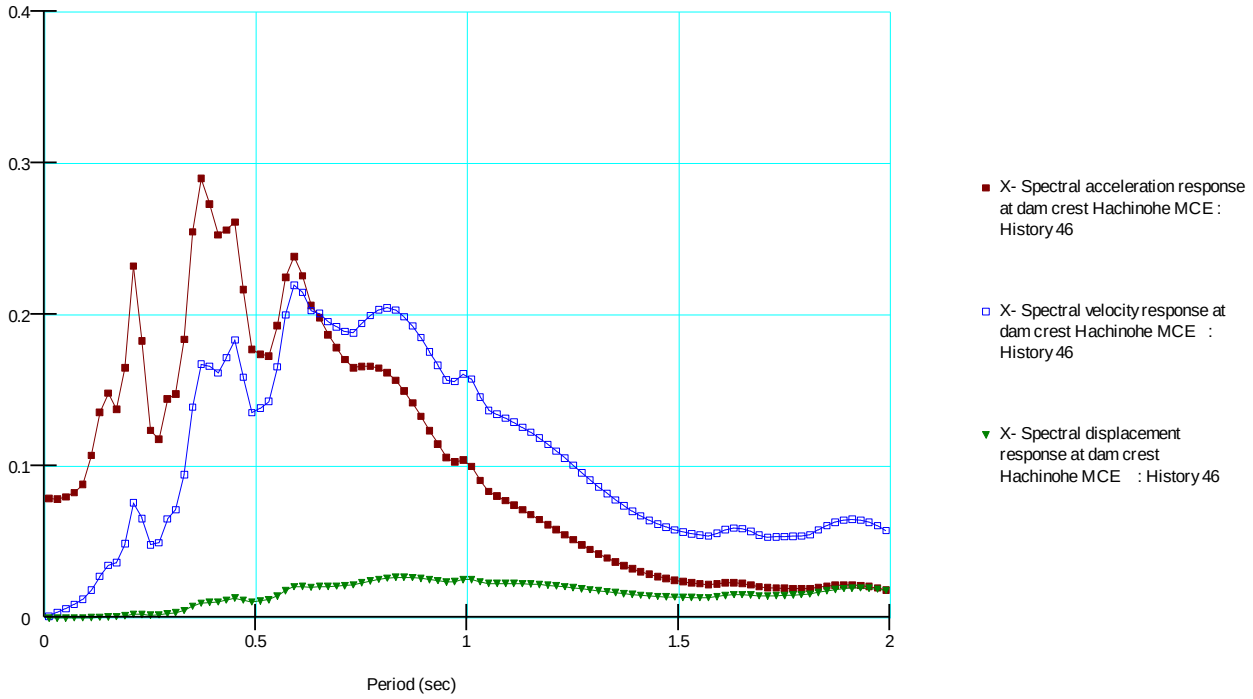

Vertical spectral response at dam crest corresponding to MCE

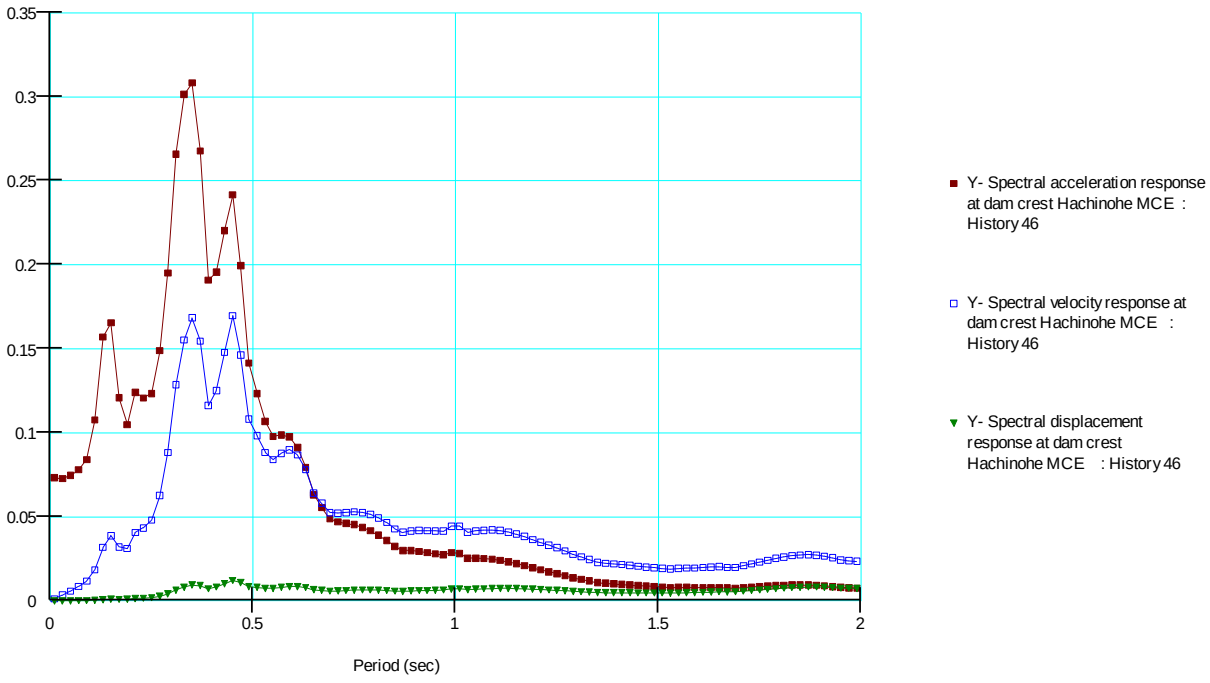

Horizontal spectral response at dam crest corresponding to DBE

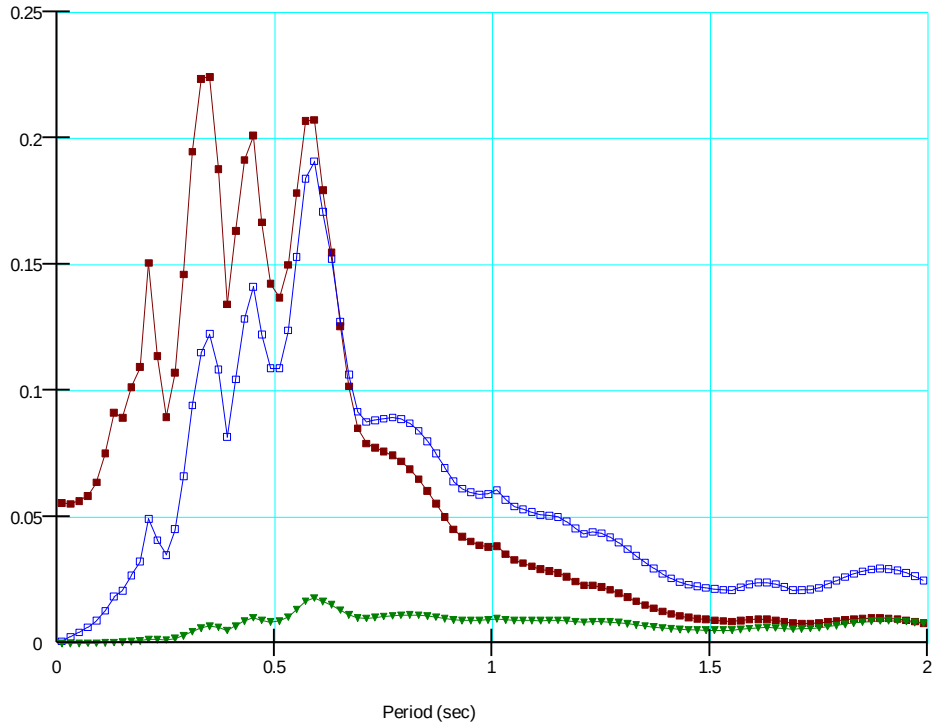

Vertical spectral response at dam crest corresponding to DBE

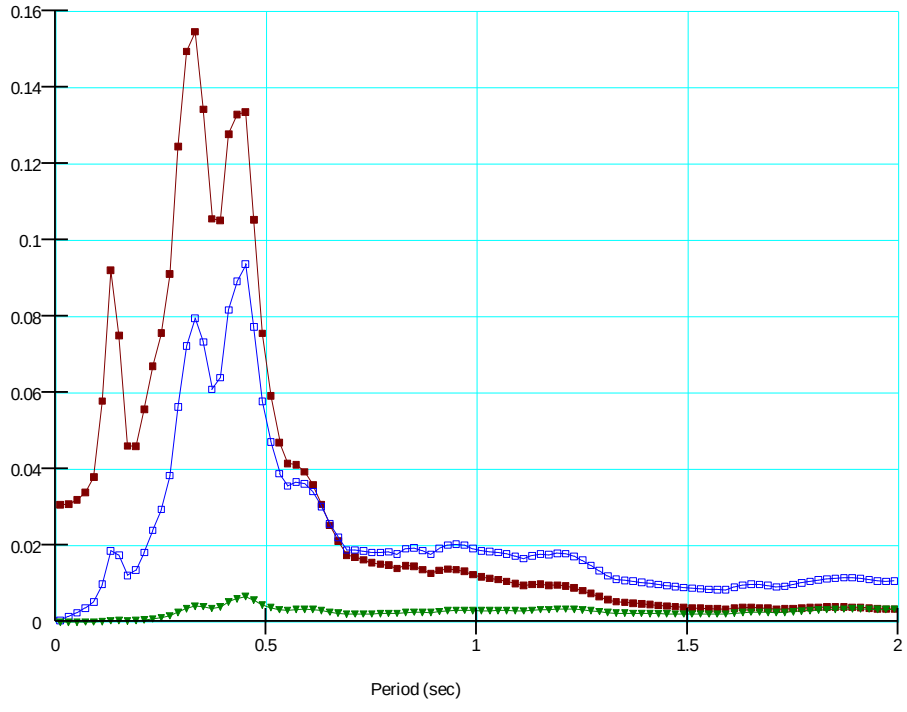

Appendix C-III: Post Earthquake Stability

Upstream slope stability corresponding to MCE

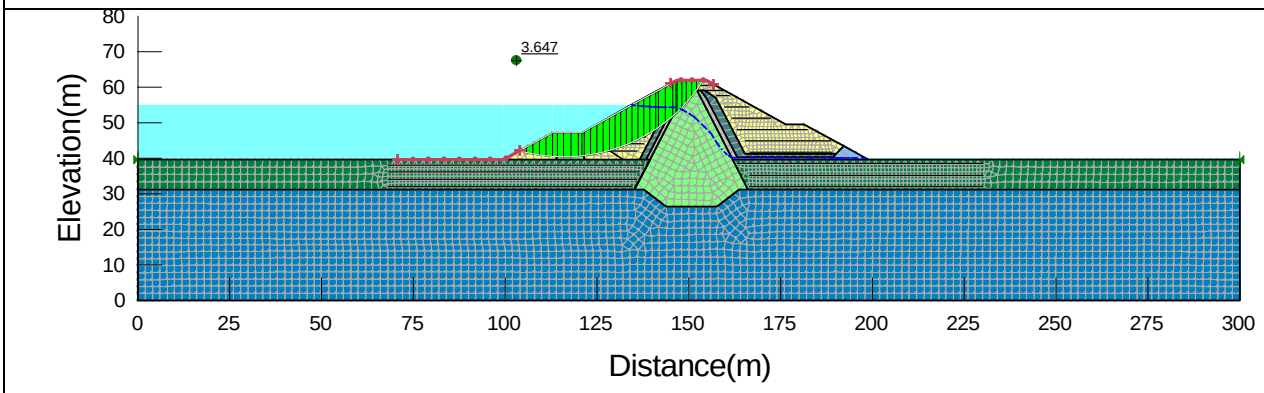

downstream slope stability corresponding to MCE

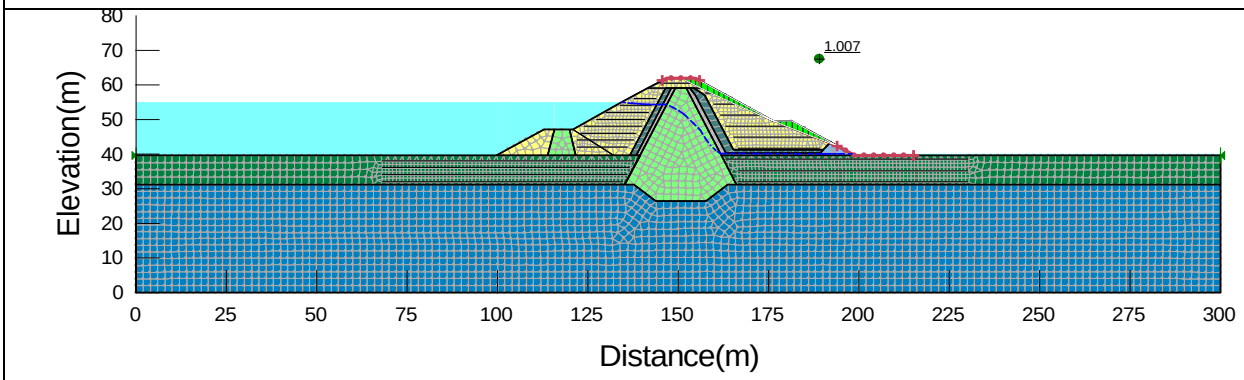

Upstream slope stability corresponding to DBE

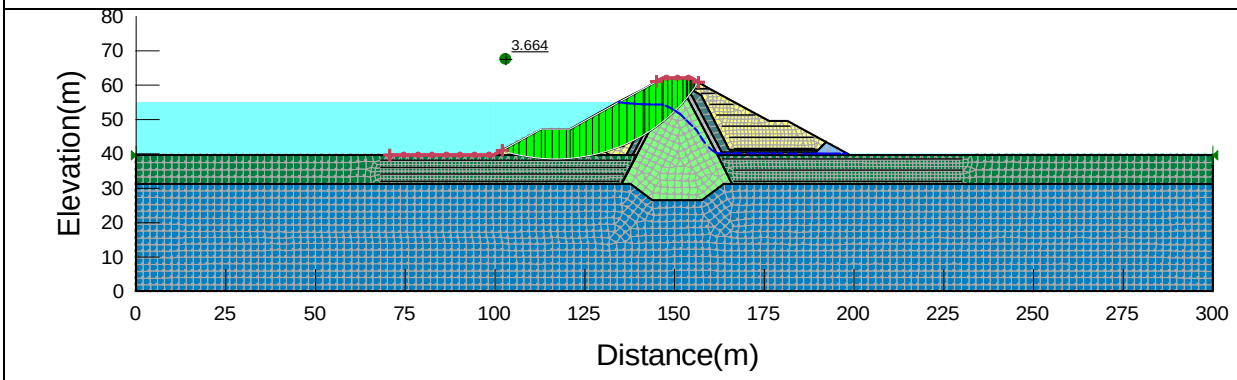

downstream slope stability corresponding to DBE

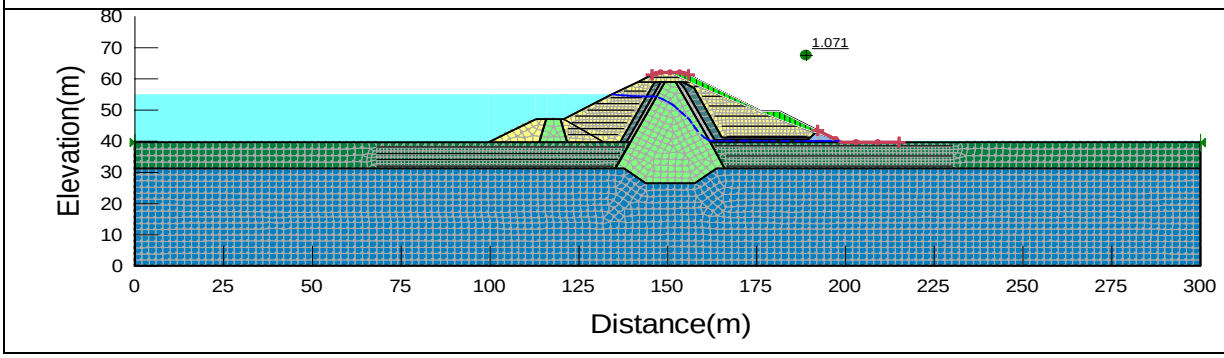

Appendix C-IV: Permanent Deformation

Table C2: Stability after Earthquake using Quake/W stress (Slope/W) for HACHINOHE_ATH

Description	Factor of safety	
PGA	MCE	DBE
Downstream Slope	1.007	1.071
Upstream Slope	3.647	3.664

Table C3: Newmark Deformation Analysis result Using Slope/W for HACHINOHE_ MCE

Parameters	Dam Crest Condition			
	Downstream Slope			Upstream Slope
	≥50% crest	100 % Crest	0 % Crest	100% crest
Resultant displacement (m)	3.8591	0.7244	1.1496	0.016044
Base angle(^{o})	24.18	22.95	26.50	21.4
Horizontal displacement(m)	3.52	0.667	1.029	0.0149
Vertical displacement(m)	1.58	0.282	0.513	0.0061
Yield acceleration(g)	0.04423	0.0868	0.09348	0.3843
Average acceleration(g)	0.01339	0.01058	0.01159	0.0014

Table C4: Newmark Deformation Analysis result Using Slope/W for HACHINOHE_ DBE

Parameters	Dam Crest Condition			
	Downstream Slope			Upstream Slope
	≥50% crest	100 % Crest	0 % Crest	No deformation result
Resultant displacement (m)	1.5183	0.1999	0.3573	
Base angle(^{o})	24.95	22.7	26.79	
Horizontal displacement(m)	1.377	0.184	0.3189	
Vertical displacement(m)	0.630	0.077	0.161	
Yield acceleration(g)	0.04423	0.0868	0.09348	
Average acceleration(g)	-0.00953	-0.00448	0.00582	